2020-03

Geological and hydro-geochemical assessment of fluorine around mount Meru, northern Tanzania

Makoba, Edikafubeni Edson

NM-AIST

GEOLOGICAL AND HYDRO-GEOCHEMICAL ASSESSMENT OF FLUORINE AROUND MOUNT MERU, NORTHERN TANZANIA

Edikafubeni Edson Makoba

A Dissertation Submitted in Partial Fulfilment of the Requirements for the Degree of Doctor of Philosophy in Hydrology and Water Resources Engineering of the Nelson Mandela African Institution of Science and Technology

Arusha, Tanzania

March, 2020

ABSTRACT

Areas around Mt. Meru are among the areas in Tanzania where climate change, population growth and high fluoride levels in much of the water sources lower availability of water for domestic and agricultural uses. Therefore, a study was conducted to review Holocene climatic records in relation to fluoride variation, assess fluorine source rocks and minerals, its dispersion patterns and hydrological characteristics of the aquifers in relation to the quality of water around Mt. Meru. Holocene climatic records indicated high concentration of fluoride in glacier at Mt. Kilimanjaro during dry phases (eg. 8.2 and 4.0 ka) and early Holocene, most likely derived from dried shallow lakes. High fluorine concentrations were obtained in rocks (mean= 0.39%, n=68) and soils (mean= 0.35%, n=32) with maximum values of 1.91% and 1.78% respectively. F was high in andesitic rocks (mean= 0.71%, n= 13) relative to other weakly fractionated rocks suggesting incompatibility of F in early stages of fractional crystallization. It was also high, about 3 folds in rocks relative to equivalent soils. The main contributing minerals in the order of decreasing are sphene, hornblende, apatite and biotite. Rock-equivalent soils relationship indicated that rock texture is the main factor controlling the release of fluorine from rocks to soils with more ions dissolved in groundwater in areas dominated by the relatively soluble materials (lahars). Mobility of fluorine in soils and water was found to be largely controlled by soil type, soil chemistry and groundwater movement. The dominant water type was found to be Na-K-HCO_3 with high Na^+ and K^+ being largely released from nepheline and clinopyroxene minerals. Overall, excluding highest fluoride values in leeward lakes (mean=567 mg/l, n=3), fluoride was also high in other water sources (mean=10 mg/l, n=97). Lowest values were in windward springs (mean=1.3 mg/l, n=21). The quality of water for domestic and agriculture uses was moderate in the order of springs > streams > boreholes > dug wells > lakes. Resistivity survey revealed freshwater aquifers characterized by the resistivity between 35 and 60 Ωm hosted in weathered mafic volcanic rocks, tuffs and breccias and aquifers of low groundwater quality exhibiting resistivity between 15 and 25 Ωm hosted in lahars. It is further revealed that there is a strong negative correlation between aquifer resistivity with both Electrical Conductivity and fluoride in the corresponding groundwater. Groundwater Potential Index Map which serves as a guide for further groundwater development has been developed using integrated data. It is recommended to conduct leaching experiments and microprobe analysis for fluoride bearing minerals, assessing mobility of fluoride from soil to plants, levels in plants and livestock, protection and conservation of water sources.

DECLARATION

I, Edikafubeni Edson Makoba, do hereby declare to the Senate of Nelson Mandela African Institution of Science and Technology that this dissertation is my own original work and that it has neither been submitted nor being concurrently submitted for degree award in any other institution.

_____ _____

Edikafubeni Edson Makoba **Date**

Name and signature of candidate

The above declaration is confirmed

Prof. Alfred N. N. Muzuka (Posthumous)

Name of supervisor

_____ _____

Dr. Revocatus Machunda **Date**

Name and signature of supervisor

COPYRIGHT

CERTIFICATION

This is to certify that the dissertation entitled, "Geological and Hydro-geochemical Assessment of Fluorine around Mount Meru, Northern Tanzania" submitted by Edikafubeni Edson Makoba (P110/T13) in partial fulfillment of the requirements for the award of Doctor of Philosophy in Hydrology and Water Resources Engineering (HWRE) of Nelson Mandela African Institution of Science and Technology (NM-AIST), Tanzania is an authentic work carried out by him under my guidance.

Prof. Alfred N. N. Muzuka (Posthumous)

Name of supervisor

_____ _____

Dr. Revocatus Machunda **Date**

Name and signature of supervisor

ACKNOWLEDGEMENT

To accomplish this work, different people, Institution and Organizations have contributed in one way or another. I gratefully acknowledge the support of all those who have assisted me in this study. I would like to recognize both individual and Institutional contributions.

First, I acknowledge the hand of God Almighty through Jesus Christ, my Lord and Saviour who empowered me throughout the entire period of my PhD study. I am very grateful to my supervisor the late Professor Alfred N. N. Muzuka (Posthumous), for his tireless supervision, support, guidance, encouragement and motivation throughout the entire period of my PhD study. His valuable criticisms, comments and advices helped to shape this dissertation and the related manuscripts. He was ready to support me at any time, really, he deserves my sincere thanks.

My sincere gratitude is extended to the management of the Nelson Mandela Institution of Science and technology (NM-AIST) for supports, encouragements, advices and tolerance throughout the entire period of my PhD study. Special thanks to Professor Karoli N. Njau, the former Dean of the School of Materials, Energy, Water and Environmental Sciences (MEWES), Dr. Revocatus Machunda, the Dean of the School of Materials, Energy, Water and Environmental Sciences (MEWES), Dr. Kelvin Mtei, Dr. Hans Komakech and all members of staff in the department of Water, Environmental Sciences and Engineering (MEWES) for their advice and encouragement. Ideas and supports from NM-AIST Laboratory scientists and technicians (Mr. Wilson Mahene, Mr. Justine Lwekolamu and Mr. Paul Sanga) are also appreciated. My sincere gratitude is further extended to financial supporters; the Government of Tanzania through Tanzania Commission of Science and Technology (COSTECH) and VLIR Project through Nelson Mandela African Institution of Science and Technology (NM-AIST).

I wish to extend my special sincere thanks to Mr. Jovine Malago who was MSc. student in the field of Hydrology and Water Resources Engineering. Parts of our works were closely related and therefore we worked together as a team in some specific areas which are related to water (water sampling, fluoride analysis in water and data processing). Through this team work, we managed to publish two articles which are related to fluoride levels and distribution in water systems. With this person, I will not forget the day when we faced Buffalo within Arusha National Park. It is real unforgettable day throughout the entire period of my PhD study.

I appreciate strong support from those who assisted me in one way or another in field and laboratory works. In this group, I start with Mr. Desdery Kimolo from the Ministry of Water and Livestock Development, Mr. Alex Moshi, driver from Nelson Mandela African Institution of Science and Technology and Mr. Braisson Habibu for their assistance in fieldwork. I extend my sincere thanks to other Institution and Organization for their support in this study. These include Tanzania National Parks (TANAPA), Tanzania Wildlife Research (TAWIRI) and Arusha National Park for granting me a permit to conduct research work in Arumeru district including Arusha National Park. Others are Geological survey of Tanzania (GST) for enabling me to conduct geo-laboratory works under the kind assistance of Mr. Mohamed Zengo, Mr. Agustine Tengia, Mr. Camilius Kamana, Mr. Samwel Ibrahim and Mr. Ronald Kishaka. University of Dar es salaam, Geology Department assisted me to conduct petrographic work under the kind assistance of Dr. Elisante Mshiu and Dr. Ronald Massawe. Sincere thanks to Dr. Ronald Massawe for his strong encouragement, criticism and contribution particularly in the mineralogical and geochemical parts of my PhD study. Last in this institutional section, my sincere thanks go to Ngurudoto Defluoridation Water Research Laboratory (NDWRL) and Southern and Eastern African Mineral Centre (SEAMIC) for enabling me to conduct water analyses.

I wish to thank my colleague at the Nelson Mandela African Institution of Science and Technology, both who were studying and those who are studying. This group is represented by Dr. Eliapenda E. Mariki, Dr. Talam Kibona, Dr. Antony Funga, Dr. Emmy Lema, Dr. Ceven Shemsanga, Dr. Nyamboge Chacha, Dr. Hyandye Canute, Mr. Avin Rujweka and Mr. Paschal Chrisogoni. Their contribution in this work is highly valuable.

Finally, my sincere thanks go to my wife (Stella Jeremiah), my children (Frank Makoba, Edista Makoba and Evelyne Makoba), my brothers (Muganyizi Makoba, Atumaini Makoba, Agidius Makoba and Dr. Josephat Makoba), my sisters (Edikednes Makoba, Geistida Makoba, Jockless Makoba, Vedia Makoba and Evitha Makoba) and my uncle (Mr. Benezeth Rutha and Mr. Shadrack Kajehe). Their support is highly appreciated.

DEDICATION

This work is dedicated to the family of Edson Makoba Lutare, my wife (Stella), and my children (Frank, Edista and Evelyne).

TABLE OF CONTENTS

LIST OF TABLES

LIST OF FIGURES

LIST OF APPENDICES

LIST OF ABBREVIATIONS

BIT	Branched Isoprenoid Tetraether
CBE	Cation-anion Balance Error
COSTECH	Commission for Science and Technology, Tanzania
CPX	Clinopyroxene
DO	Dissolved Oxygen
EAM	Eastern Arc Mountains
EARS	East Africa Rift System
EC	Electrical conductivity
ED-XRF	Energy Dispersive X-ray Fluorescence
ENSO	El Niño Southern Oscillation
FISE	Fluoride Ion Selective Electrode
GMWL	Global Meteoric Waterline
GST	Geological Society of Tanzania
GWPIM	Groundwater Potential Index Map
ICP – OES	Inductively Coupled Plasma Optical Emission Spectrometer
IPCC	Intergovernmental Panel on Climate change
ITCZ	Intertropical convergence zone
KR	Kelley's ratio
LGM	Last Glacial maximum
LIA	Little Ice Age
LOI	Loss on Ignition
MAR	Magnesium Adsorption Ratio
MDGs	Millennium Development Goals
MWP	Medieval Warm Period

NDWRL	Ngurudoto Defluoridation Water Research Laboratory
PBWB	Pangani Basin Water Board
RSC	Residual sodium carbonate
SAR	Sodium Adsorption Ratio
SDG	Sustainable Development Goal
SEAMIC	Southern and Eastern African Mineral Centre
SST	Surface sea temperature
TAS	Total Alkali versus Silica
TDS	Total Dissolved Solids
TISAB	Total Ionic Strength Adjustment Buffer
TN	Total Nitrogen
TOC	Total organic carbon
UNICEF	United Nations Children's Fund
UNOCHA	United Nations Office for the coordination of Humanitarian Affairs
VES	Vertical Electrical Soundings
VSMOW	Vienna Standard Mean Oceanic Water
WHO	World Health Organization
YD:	Young Dryas

CHAPTER ONE

INTRODUCTION

1.1 Background

The 2030 Sustainable Development Goal (SDG) No. 6 is to ensure availability and sustainable management of water and sanitation for all people (UNICEF, 2017). Its subsections 6.4-6.6 focus on global reduction of the number of people suffering from water scarcity, implementation of integrated water resources management at all levels, protection and conservation of all aspects of freshwater sources (UNICEF, 2017). It is estimated that about 11% of the population globally have no access to safe and clean water with a large number of people living in Sub- Saharan Africa and Ocenia (UNICEF, 2015)

. In sub-Saharan Africa, only 20% of the Millennium Development Goal Target No.7C of reducing to half the number of people without access to safe drinking water by 2015 was achieved (UNICEF, 2015). Population growth, poverty and economic instability among countries have been pointed out to be causative factors towards not achieving this goal (UNICEF, 2015). Majority of population in these areas continue to depend largely on rivers, lakes, ponds and irrigation canals as their major sources of drinking water (UNICEF, 2015, 2017). Some of these sources are polluted naturally and most of them are vulnerable to anthropogenic pollution.

Tanzania is among the developing countries facing economic water scarcity (UNOCHA, 2010). It depends largely on surface water for domestic and irrigation purposes. In 2015, Tanzania was still among the few countries with lowest coverage in accessing an improved drinking water sources and sanitation (UNICEF, 2015). In recent years, population growth, climate change and surface water contamination through natural and anthropogenic activities have lowered the availability of surface water leading to rapid increase in the use of alternative water sources such as groundwater (Kashaigili, 2010; Elisante & Muzuka, 2015). For instance, since 1997, there have been rapid increase in boreholes and dug wells particularly in areas with rapid population growth such as Dar es salaam city (Mjemah *et al*., 2012).

Natural contamination by fluoride is strongly affecting water quality particularly in areas with water scarcity such as central to north regions of Tanzania (Nanyaro *et al*., 1984; Ghiglieri *et al*., 2010, 2012; Thole, 2013; Malago *et al*., 2017). Fluoride in much of the water sources is

high above the recommended World Health Organization standards of 1.5 mg/l (WHO, 2008) as well as the national standard of 4 mg/l (TBS, 2007). According to Thole (2013), 30% of groundwater sources in Tanzania which are used for domestic purposes have fluoride above the recommended WHO standard. High fluoride levels up to 690 mg/l have been reported in various water sources around Mt. Meru (Nanyaro *et al*., 1984; Ghiglieri *et al*., 2010, 2012; Thole, 2013; Malago *et al*., 2017).

Fluoride is linked with geological setting particularly igneous complexes (Nanyaro *et al*., 1984; McCaffrey, 1998; Chae *et al*., 2006; Pittalis *et al*., 2010; Rango *et al*., 2010; Naseem *et al*., 2010; Hallet *et al*., 2015). As it is for other major world fluoride provinces such as the East Africa Rift System, the volcanic belts of western United State, New Zealand, France, Algeria and Tunisia, and crystalline basement rocks of granitic composition in India and Sri Lanka (Edmunds & Smedley, 2005), fluoride in Tanzania is also concentrated in volcanic province, mainly areas associated with the East Africa Rift Valley, particularly northern Tanzania and the granitoid areas in the Tanzania craton (Kaseva, 2006; Thole, 2013 & Malago *et al*., 2017). Thus, according to Malago *et al*. (2017), the regions with high mean fluoride concentrations (in mg/l) with the sampled number (n) are Arusha (13.5, n=122), Manyara (8, n=09), Kilimanjaro (7.4, n=19) and Singida (3.7, n=80).

Arumeru district, northern Tanzania is one among the areas studded by volcanic materials derived mainly from Mt. Meru. Local geology vary considerably where various rock groups such as lahars of different ages, nephelinitic to phonolitic lavas, mantling ashes, basaltic lava, tuffs, breccias, pyroclastic and ashes, and basic to alkaline parasitic cones have been documented (Wilkinson *et al*., 1983, 1986; Nanyaro *et al*., 1984; Roberts, 2002; Dawson, 2008; Ghiglieri *et al*., 2010, 2012). Some of the works (Nanyaro *et al*., 1984; Ghiglieri *et al*., 2010, 2012) documented the general groups of lahars and mantling ash as the possible source of fluoride in Arumeru waters. With the consideration that within the igneous group, fluorine varies intensively (McCaffrey, 1998), there is no any detailed study which has been conducted in the areas to assess the specific fluorine bearing rocks. Also, from the literature, there are several fluorine bearing minerals. The major ones are fluorite (CaF_2), mica (biotite) $K(Mg,Fe)_3AlSi_3O_{10}(F,OH)_2$, hornblende ($Ca_2(Mg,Fe)_4Al(Si_7Al)O_{22}(OH,F)_2$), apatite [$Ca_5(PO_4)_3(Cl,F,OH)$], cryolite ($Na_3AlF_6$) and topaz [$Al_2F_2(SiO_4)$] (Chae *et al*., 2006; Naseem *et al*., 2010). There are other minor fluorine bearing minerals which are likely to be the principal source of fluorine at local scale. Therefore, apart from fluorine bearing rocks, intensive assessment of the specific fluorine bearing minerals is also required.

There is large spatial variation of F^- in Arumeru waters (Nanyaro *et al*., 1984; Ghiglieri *et al*., 2010, 2012; Pittalis *et al*., 2010; Malago *et al*., 2017) which is likely to be controlled by weathering and mobility of fluoride. There is no any detailed study in the study area which is integrating rocks, soil and water as an attempt to evaluate the observed spatial distribution. However, it is well known that weathering and mobility assessments require integration of many factors including levels of F in these materials, rock types, texture, pH conditions, soil types, soil organic matter, climatic factors (water, temp) (Easterbrook, 1999; Wang *et al*. 2002; Deverel *et al*., 2012). To some extent, it is difficult to incorporate all factors effectively in assessing weathering and mobility of F but to large extent, immediate vicinity sampling technique involving rocks, soil and water can lead to a general understanding on fluoride mobility and hence spatial distribution of fluorine/fluoride in rocks, soil and water systems.

In Arumeru district, climate and geology is largely controlled by Mt. Meru which is the second highest Mountain in Tanzania (4565 m above sea level). The mountain, divides the district into two climatic zones; windward and leeward sides creating variations in hydrological and hydrogeological processes. Several geological and hydrological studies have been conducted within the area (Nanyaro *et al*., 1984; Roberts, 2002; Dawson, 2008; Ghiglieri *et al*., 2010, 2012), however, there are limited data set (rocks, soil and water) for the whole district that could integrate all data from the windward to leeward sides for detailed study of water-rock interaction processes.

Water demands for both domestic and agricultural purposes in Arumeru district is increasing with time due to population growth and climate changes (Istituto Oikos, 2011; Vye-Brown *et al*., 2014). Because of high rate of water abstraction for irrigation, all streams from upper Kikuletwa are disconnected from that of Pangani basin. In attempt to reduce water problem, local people have been constructing shallow hand dug wells (depth < 20 m) particularly in the areas lacking surface water sources. Apart from natural fluoride contamination which is threatening much of the water sources in the district, the wells are vulnerable to anthropogenic contamination because they are not well protected from surface inflow, constructed in congested areas and some are located in agricultural areas where application of fertilizers and manure is a common practice. Furthermore, some of these wells are utilized as drinking water sources without testing the quality and some are utilized for irrigation without testing their suitability for irrigation purposes.

Groundwater chemistry changes seasonally or in long-term depending on the variation of precipitation and temperature which accounts for rocks dissolution, evaporation and dilution processes (Healy & Cook, 2002; Varni *et al*., 2013; Lutz *et al*., 2015). This is also true for small lakes such as Duluti and Momella in the study areas as well as streams. Also, groundwater levels fluctuate largely in response to rainfall (Lutz *et al*., 2015). Therefore, in geological context, the current groundwater level, quantity and quality is temporal being a function of the recent temperature and rainfall trends. The areas such as Mt. Meru which experiences intensive annual variation of rainfall and temperature between the windward and leeward sides is likely to be characterized by aquifers with different characteristics in terms of quality and depth to groundwater water levels. High groundwater recharge and shallow potential aquifers are expected in areas experiencing high rainfall and low temperature (windward side) relative to leeward side. Therefore, there is a need of assessing groundwater potentiality in the southern part of Mt. Meru which is also among the areas facing water shortage, despite of relatively high rainfall on the slope of Mt. Meru. Owing to susceptibility of aquifers to fluoride contamination, general characterization in terms of both quality and quantity is important.

Based on the facts that: (a) Climate reconstruction at local scale might be biased because of limited data and complex tele-connectivity between the land, ocean and atmosphere (b) Global documentation of the climatic variability is biased with more works being conducted in northern mid to high latitudes (Mann, 2007; Mann *et al*., 2008) (c) Low documentation of climate records in tropics with tropical east Africa being poorly represented, there is a need of reviewing the most recent climatic records (Holocene) in Tanzania so as to relate the temperature and rainfall patterns with the current groundwater characteristics (level, quality and quantity) around Mt. Meru.

Therefore, this dissertation is structured as follows: Chapter 1 is the general introduction and Chapter 2 deals with reconstruction of Holocene climate records in Tanzania with emphasize on rainfall and temperature fluctuations. Chapter 3 focusses on geological works; volcanic rock genesis and characterization, fluorine source rocks and water-rock interaction processes. Chapter 4 deals with hydrogeochemical characterization of all water sources in the study areas and water quality for domestic and agricultural purposes. Chapter 5 focusses on delineation of potential groundwater zones and aquifer characterization whereas Chapter 6 is the general discussion, linking all chapters with the connected major findings.

1.2 Statement of Research Problem

Within the study area, groundwater and surface water pollution by high fluoride is known for a long time (Nanyaro *et al*., 1984). Due to high consumption of waters which are rich in fluoride, generally above the Tanzania's minimum standard of 4 mg/l, dental and skeletal fluorisis are common in the study area (Malago *et al*., 2017). In Meru districts, there are limited hydrogeological works which are restricted in some specific areas (Pittalis, 2010; Ghiglieri *et al*., 2012; Elisante & Muzuka, 2015). Most of these studies do not link properly geology with fluoride in water sources; they are largely focusing on fluoride distribution in water sources (Ghiglieri *et al*., 2010; Elisante & Muzuka, 2015). Such studies indicated that there is a wide variation in fluoride in water sources. The reasons for such variation, the sources of fluorine (fluorine bearing rocks and minerals) and its mobility are not clearly kown. Also, as there are distinctive zones with fresh groundwater (Ghiglieri *et al*., 2010; Malago *et al*., 2017), there is need of detailed assessment of the aquifer characteristics so as to delineate potential groundwater zones in Meru district. Furtheremore, climate is one among the important factors which control groundwater quantity and quality (Healy & Cook, 2002). The recent climate records (eg. Holocene) that could also be used to assess the current groundwater quality and quantity in Meru district are poorly known at local scale and Tanzania at large.

1.3 Rationale of the Study

There is an increase in groundwater utilisation (domestic and agriculture) within the study area due to population growth and climate change. Thus, the rate of constructing wells in agricultural area and areas lacking potable surface water sources is also increasing. Vulnerability to contamination is high through both natural (eg. Fluoride) and anthropogenic as most of the wells particularly hand dug wells are constructed in congested areas. For instance, according to Elisante & Muzuka (2016a), groundwater in some congested areas within the study area is contaminated by nitrate. However, their study was limited in a specific area and could not cover the northern and some southern parts of Mt. Meru. Few researches focusing on groundwater have been conducted in the leeward side (Ghiglieri *et al*., 2010, 2012; Pittalis, 2010). The southern side of Mt. Meru particularly areas away from mountain where local people also suffer from shortage of domestic water remained poorly researched. According to these limited researches, there are zones with acceptable/low fluoride content within the area which need to be properly identified. However, groundwater

quality and quantity as well as groundwater level fluctuations which are controlled by precipitation and temperature can vary seasonally or in log-terms depending on changes in climate (Healy & Cook, 2002; Varni *et al*., 2013; Lutz *et al*., 2015). Such climatic data at local scale and Tanzanania in general are poorly known.

In recent years, technology has led to clear evidences that relate health problems and fluoride in drinking water and the links between fluoride occurrence and geology (Edmunds & Smedley, 2005). In Meru fluoritic zone, there are various successful defluoridation techniques (Mwakabona *et al*., 2014; Said & Machunda, 2014; Lukiko *et al*., 2016). Despite these techniques, some of the residents within the district are still lacking potable water due to limited information on water quality and fluoride removal techniques. In the study area, there have been few reviews on the hydro-geochemistry of fluoride. For instance, Nanyaro *et al*. (1984) and Ghiglieri *et al*. (2010, 2012) found that there is large spatial variation of fluorine contamination probably contributed by the debris avalanche deposits and mantling ash. Yet, the specific sources of fluoride and processes of fluorine contamination and the link with the heterogeneity of lithologies have not been systematically studied. Therefore, this study focuses on water-rock interaction processes by assessing fluoride variation in the Holcene period in Tanzania, link fluoride with geology, delineate and characterize aquifers based on the water quality.

1.4 Objectives of the study

1.4.1 General objective

The general objective of this study was to assess sources of fluorine, its dispersion patterns and hydrological characteristics of the aquifers in relation to the quality of water in the study area.

1.4.2 Specific objectives

(i) To reconstruct Holocene climate records in Tanzania with emphasize on rainfall and temperature variation as the tools for controlling groundwater levels, quality and quantity.

(ii) To characterize Mt. Meru volcanic rocks geochemically for assessment of fluorine sources (F-bearing rocks and minerals).

(iii) To establish primary factors governing fluoride release from parent materials, its mobility/dispersion and distribution in rocks, soils and water systems.

(iv) To characterize geochemically all water sources in the study area and assess their suitability for domestic and agricultural purposes.

(v) To delineate potential groundwater zones in the south- eastern part of study the area and characterize the aquifers in terms of quantity and quality with emphasise on fluoride.

1.5 Research questions

(i) How did the rainfall and temperature fluctuate in the Holocene period in Tanzania?

(ii) What are the geochemical characteristics of Mt. Meru volcanic rocks in relation to fluorine bearing rocks and minerals?

(iii) What are the primary factors governing the release of fluorine from parent materials, its mobility/dispersion and distribution in rocks, soils and water systems?

(iv) How do water sources differ geochemically and what is its implication to domestic and agriculture uses?

(v) What are the characteristics of the aquifers in term of quantity and quality and how are they distributed?

1.6 Significance of the study

Review of Holocene climate change in Tanzania will provide insight on the current groundwater availability, groundwater levels, quantity and quality. It will also add information on prediction of future climate of which the country and global at large are threatened by short periods of heavy rainfall and droughts. Furthermore, the data can be of great use in tracing long term trends of natural contaminant such as fluoride levels in the study areas.

The study will lead to updated geological maps (rocks and soils) showing spatial distribution of fluorine in the study area. These maps in conjunction with hydro-geochemical and hydro-geophysical data will aid on pinpointing potential surface and spring water sources, and delineation of potential areas for locating groundwater boreholes for domestic purposes. Owing to rapid increase in population in Arumeru and Arusha city, such information will be important in addition of water resources to Meru District Council and Arusha Urban Water Supply and Sanitation Authority (AUWSA) which are currently facing water shortage. Information on fluoride level in various water sources at local scale will be important to local communities, which are highly affected by dental and skeletal fluorisis. Parallel to these lines,

and as implementation of the 2030 SDG No.6, the study will enhance public awareness on water quality for both domestic and agriculture purposes within the study area. It will assist the stakeholder, policy makers and the government to protect groundwater zones and conserve water sources with low and acceptable fluoride level. Finally, the scarce water resources within the area will be managed in sustainable ways based on sound scientific information derived from the study.

1.7 Delineation of the Study

This study is basically the water-rock interaction study. Thus, it was delineated based on geological, hydrological and climatic creteria so as to study water-rock interaction processes with emphasize on fluorine. Mt. Meru volcanic complex is the center of volcanic materials which are rich in fluorine (Nanyaro *et al*., 1984). In geological persepective, the mountain is active and different phases of such matrials cover the slopes of the mountains and the surrounding areas (Nanyaro *et al*., 1984; Vye-Brown *et al*., 2014). Also, Mt. Meru controls climatic condition in Meru district creating leeward and windward sides with different climatic conditions which control weathering and hydrological patterns. Thus, the study area covers Meru fluoritic zones; northern and southern sides of Mt. Meru and areas away from Mt. Meru towards the contact with metamorphic rocks. The study is the continuation of available limited geological and hydrogeological works (Nanyaro *et al*., 1984; Roberts, 2002; Dawson, 2008; Ghiglieri *et al*., 2010, 2012; Istituto Oikos, 2011; Vye-Brown *et al*., 2014). Most of the works in this study are centered on the south and eastern slopes of Mt. Meru which is the hydrologeological zone with numerous streams and groundwater sources for easy assessment of water-rock interaction processes.

CHAPTER TWO

A REVIEW OF THE LATE PLEISTOCENE-HOLOCENE CLIMATIC AND PALEOECOLOGICAL RECORDS IN TANZANIA[1]

Abstract

Climate change is not well addressed in the developing countries such as Tanzania. Therefore, this chapter focuses on reconstruction of the late Pleistocene to Holocene records for addressing climate change in Tanzania with emphasize on fluoride vriation. Integrated proxies from terrestrial and marine environment of Tanzania have been reviewed. In late Pleistocene, during the Last Glacial Maximum (LGM), Tanzania experienced aridity as the other areas in the tropics. This was followed by the humid high precipitation period, highly pronounced between 9-6 ka. This period was interrupted by a brief dry Younger Dryas (YD) ~13.0-11.5 ka and a cool dry event at 8.2 ka. Other remarkable events are the cool event in the mid Holocene at 5.2 ka and the global dry event at 4.0 ka. Glacier record from Mount Kilimanjaro showed that these cool and dry periods were associated with high concentration of fluoride relative to other periods, which is likely to be derived from dried shallow lakes. There is a general decrease in precipitation from 5 ka to present with the aridity being pronounced between 3-2 ka and 1.2-0.5 ka. Increased temperature in the the 20th century is likely to cause changes in hydrological circle leading to the increase in heavy rainfall and drought periods. Through this study, it is revealed that works are limited, concentrated in some specific areas with different climatic conditions. Therefore, close spaced sampling, with high resolution multi-proxy records and studies on temporal variation of fluoride are required to enhance palaeoclimate reconstruction in Tanzania.

[1] Published in the International Journal of Sciencec: Basic and Applied Research (IJSBR) (2019) Vo.44, No .2, pp 166-192.

2.1 Background

On the geological time scale, climate has been changing from glacial to interglacial conditions because of alteration of sun's energy reaching the earth surface (Dansgaard *et al*., 1993; Petit *et al*., 1999; Trauth *et al*., 2005; Kiage & Liu 2006; IPCC, 2007; Jouzel *et al*., 2007; Tiwari & Ramesh 2007; Tierney *et al*., 2008). Records of such climatic changes have been preserved in various forms including ice sheet/caps, marine and lacustrine sediments, coral reefs, cave deposits (stalagmite and stalactites), swamps, bogs, and soils.

Various physical, chemical and biological parameters or proxies have been used to document past climatic and ecological changes on global scale (Meyers, 1997; Henderson, 2002; Vincens *et al*., 2003, 2005; Kiage & Liu, 2006; Brncic *et al*., 2009). For example, pollen records from various deposits such as marine and lake sediments, swamps, peat bogs, and soils can provide detailed records of past paleoecological and climatic changes (Liu & Colinvaux, 1988; Maley & Brenac, 1998; DeMenocal *et al*., 2000; Gasse, 2000; Salzmann, 2000; Peyron *et al*.,2000; Wooller *et al*., 2000; Behling, 2002; Salzmann *et al*., 2002; Darbyshire *et al*., 2003; Lamb *et al*., 2003; Behling *et al*., 2004). Apart from pollen, other proxies such as charcoal (Burney, 1987a; 1987b; Whitlock & Millspaugh, 1996; Long *et al*., 1998), phytoliths (Piperno, 1988; Mworia-Maitima, 1997; Piperno & Pearsall, 1998), diatoms (Gasse *et al*., 1997; Barker *et al*., 2001, 2011), grass cuticles (Mworia-Maitima, 1997; Wooller *et al*., 2000), stromatolite (Cohen *et al*., 1997), Ostracode (Alin & Cohen, 2003) have proven to be very useful in paleoenvironmental reconstruction. Apart from biogenic proxies, other proxies used include stable isotopes of oxygen, carbon (inorganic and organic), nitrogen and hydrogen preserved in corals, sedimentary organic matter and carbonate (Talbot & Lærdal, 2000; Lundblad & Holmgren 2005; Muzuka *et al*., 2006; Mumbi *et al*., 2008; Barker *et al*., 2011, 2013).

Global documentation of the climatic variability using these proxies is biased with highest work being conducted in northern mid to high latitudes (Mann, 2007 & Mann *et al*., 2008). In the tropics, documentation is low with tropical east Africa being poorly represented. A review of late Quaternary climatic change in East Africa was carried out by Kiage & Liu (2006) using pollen, diatoms, microscopic charcoal and lake level records with the associated proxies. Results showed that in the late Pleistocene towards LGM, East Africa was cool with remarkable prolonged episodes of aridity. This was followed by warm and moist condition in early to mid-Holocene with the pronounced sharp dry events at 8.3, 5.2 and 4 ka and a

general decrease in precipitation in the late Holocene (Weldeab *et al*., 2014; Shanahan *et al*., 2015; Verschuren *et al*., 2009). In inferring these climatic changes, ice cores were found to be superior with the higher temporal resolution records relative to other proxies (Kiage & Liu, 2006). Furthermore, Kiage & Liu (2006) observed that the use of higher resolution palynological approach in conjunction with multi-proxies is needed to reconcile properly the Holocene climate changes, which are influenced by both natural and anthropogenic processes.

Other proxies used are seismic reflection data (Cohen *et al*., 1997; Scholz *et al*., 1998; Abbot *et al*., 2000; Verschuren *et al*., 2009; Moernaut *et al*., 2010). This technique provides distinct seismic stratigraphic layers which are powerful in long term climatic reconstruction. Through the delineated layers, important information for palaeoecological reconstruction such as layer thicknesses, lake level fluctuations, desiccation periods are obtained. Also, the C/N ratio of organic matter (OM) in river and oceanic basins in conjunction with stable isotopes has been useful in inferring the relative proportion of various sources and thus changes in vegetation cover which reflects changes in precipitation over the catchment areas (Muzuka & Nyandwi, 2002).

Tanzania is largely depending on seasonal rainfall for food production and availability of both surface and groundwater resources. Also, the major lakes of Tanzania of which their productivity depends on water quality which change seasonally or in long-term responding to variation in rainfall and temperature (Tierney, 2010), play an important role in national economy as well as local people livelihood particularly through fisheries. Despite of these importances, the roles of climate to national and local people economy have not been addressed effectively and they are poorly known particularly at local scale.

Much of the climate works have been done in some lakes (Tanganyika, Victoria, Malawi, Rukwa, Challa, Massoko), Indian Ocean, Mt. Kilimanjaro and Eastern Arc Mountains (EAM) (Table 1). These works have not been integrated together for effective reconstruction of past climate and prediction of future climate. Also, it is not clear whether the available records (proxies) are well distributed in the relevant sources within the country. Conflicting climate records may arise either through the use of different proxies or from one geographic position to the other within the country. Despite that multi-proxies have been used, though information on the consistence of the available climate records is poorly known.

Although climate has been changing since the formation of the Earth, this review paper focused on ecological and hydrological changes in terrestrial and marine environments of Tanzania during the Late Pleistocene-Holocene periods. Because of the lack of local scale historical records in Tanzania and complex tele-connectivity between land, atmosphere and ocean, this review is partly supported by regional climatic records so as to strengthen our climate reconstruction. It is basically intending to put together the available Holocene climatic records as an attempt to address effects of climate change to national and local people economy. This is important in development of national strategic plans for mitigating climate change impacts such as food shortage, water scarcity and floods. In future, these impacts are expected; resulting from abrupt short periods of heavy rainfall and droughts as the feedback response of the current global warming.

2.2 Paleoenvironmental and Paleoclimatic reconstruction in Tanzania

Few workers have used the stable isotopes of organic carbon and nitrogen separately or in combination to infer paleoclimatic and paleoecological changes in Tanzania (Muzuka *et al*., 2004, 2006). The δ-values of organic carbon for various cores collected from Lake Tanganyika, Empakai and in the Tanzanian continental margin have showed a systematic down core decrease with a minimum value at around 8.2 ka. The trend has been interpreted to represent changes in the type of vegetation cover in response to deterioration in climatic conditions. Also, stable isotopes composition of organic carbon incorporated within the silica frustules of diatom algae in the lake Challa sediments in combination with $\delta^{13}C$ of bulk sediment total organic carbon (TOC), biomarker $\delta^{13}C_n$-C_{31}, percentages of biogenic silica (% BSi), total organic carbon (TOC), total nitrogen (TN) and the TOC/TN ratio have been used to infer history of carbon cycle in lake Challa (Barker *et al*., 2013). Results of this work are reinforced by results of previous works obtained using oxygen isotope values determined on diatom silica ($\delta^{18}O_{diatom}$) in Lake Challa (Barker *et al*., 2011). Deuterium/hydrogen ratio of higher plant leaf waxes (δD_{wax}), seismic record of inferred lake level fluctuations and the Branched and Isoprenoidal Tetraether (BIT) index proxy record changes in hydrology within the Challa basin, δD_{wax}, as a proxy for the isotopic composition of precipitation (δD_p) is interpreted as a tracer of large-scale atmospheric circulation (Barker *et al*., 2011).

Other proxies used include fossil and living stromatolites which have been used to infer lake levels, paleoenvironmental history and palaeohydrology (Hillaire-Marcel *et al*., 1986; Casanova & Hillaire-Marcel 1992; Cohen *et al*., 1997; Alin & Cohen, 2003). However, they

have been used to infer paleohydrology (through ^{13}C and ^{18}O analyses of stromatolitic carbonates), paleoenvironments (from their growth morphology), and chronology (through direct ^{14}C dating). For instance, in Lake Tanganyika, these proxies indicted that the total amplitude of lake-level fluctuations has been small for the past 3000 years (»20 m). Lake levels were 5–10 m below present between ca. 800 B.C. and A.D. 400) (Cohen *et al*., 1997) with minor low stand that correlates with generally low lake levels in East Africa between 3000 and 2000 yrs ago (Casanova & Hillaire-Marcel, 1992).

Stromatolites were further used to infer palaeohydrological history of Lake Natron (Hillaire-Marcel *et al*., 1986). It was found that there are three generations of stromalites with the younger one corresponding to early Holocene humid period. During this period, the lake Natron water level was high about 60m above the modern level (Hillaire-Marcel *et al*., 1986). Unlike other lake proxies, stromatolites were found to be closely related to highstands (Hillaire-Marcel *et al*., 1986) and therefore powerful in inferring lake level fluctuations. The early Holocene highstand inferred using stromatolite is in close agreement with other proxies from lake Challa such as BIT Index and δD_{wax} Vs VSMOW (Tierney *et al*., 2011).

Records showed predominantly arid conditions throughout the past 2500 years, interrupted by relatively brief episodes of higher precipitation and lake levels. According to the work by Alin & Cohen (2003) on Lake Tanganyika, the most pronounced low lake level occurred at ~200-0 BC, with other remarkable low lake levels between ~200-500 AD, ~700-850 AD, the Medieval Warm Period (MWP; ~1050-1250 AD) and the latter part of the Little Ice Age (LIA; ~1550-1850 AD). Furthermore, Lake Tanganyika level records suggest the most pronounced wet intervals to be centered on ~500 AD, ~1500 AD, and ~1870 AD (Alin & Cohen, 2003). Over longer period, the seismic reflection data from Lake Challa have shown three events of low lake stand during the late Pleistocene-Holocene period (Moernaut *et al*., 2010).

The past climatic changes can be inferred using wind intensity. Wind intensity variation is reconstructed using the lake productivity–that upwelling which favour diatom bloom by bringing the nutrients from the deeper part of the lake to the surface is favoured by strong wind. Due to this fact, lamination encountered in cores from the Lakes such as Challa (Wolf *et al*., 2011) and Malawi (Johnson *et al*., 2001) is the result of alternation of diatom-rich sediment deposited in the windy/dry period (light layer) and diatom–poor sediments (dark layer) deposited during the rainy period. Also, periods of anoxic condition are inferred using

laminations which are not disturbed supported by oxygen composition. With consideration of sedimentation rate factor, the thicknesses of these layers based on laminations were used also as a proxy to infer specific summer or rainy period. Calcite-rich sediments in the cores are used to infer period of high temperature. Furthermore, in Lake sediments, the concentration of soluble elements such as K, Ca, Mg, Ba tend to increase with increasing precipitation (Felton *et al*., 2007) and therefore useful in reconstruction of palaeohydrology in the related catchment. Common proxies that have been used to infer palaeoclimate in Tanzania are presented in Table 1.

Table 1: Common proxies that have been used to infer palaeoclimate in Tanzana

Zone	Proxies	Authors
Lake Tanganyika	Stromatolites	Casanova & Hillaire-Marcel (1992) and Cohen *et al*. (1997)
	δD_{wax} in combination with the Branched and Isoprenoid Tetraether (BIT) index of soil bacterial	Tierney *et al*. (2011)
	Seismic reflection (Acoustic impedance)	Cohen *et al*. (1997)
	Elemental geochemistry-soluble elements and sedimentological records	Felton *et al*. (2007)
	Stable isotopes of carbon and nitrogen, contents of OC and nitrogen	Muzuka & Nyandwi (2002)
	Ostracode	Alin & Cohen (2003)
	Sedimentological data	Cohen *et al*. (2006)
	Diatom and Pollen	Stager *et al*. (2009)
	Pollen	Felton *et al*. (2007)
Lake Malawi	$\delta^{18}O_{diatom}$	Barker *et al*. (2007)
	Pollen	DeBusk (1997, 1998)
	Lignin phenols, plant leaf wax carbon isotopes, TOC	Castañeda *et al*. (2009, 2011)
	Seismic reflection (Acoustic impedance)	Branchu *et al*. (2005) and Lyons *et al*. (2011)
	Diatom	Stone *et al*. (2011)
	Terrestrial and aquatic biomarkers (diatom, cyanobacteria etc), $\delta^{13}C_{TOC}$	Castañeda *et al*. (2011)
	Elemental geochemistry (Sedimentary calcite, TOC, Si:Ti, Rb:K ratios)	Brown (2010)
Lake Victoria	Seismic reflection (Acoustic impedance)	Scholz *et al*. (1998)
	Stable isotopes of carbon and nitrogen, contents of OC and nitrogen	Talbot & Lærdal (2000)
	Pollen	Stager *et al*. (2005)
Lakes Massoko, Mbaka	Diatom and cyanobacteria	Barker *et al*. (2000, 2003)
	Charcoal	Thevenon *et al*. (2003)
	Pollen	Vincens *et al*. (2003)
	Stable isotope of Oxygen and Hydrogen	Delalande *et al*. (2008)

	Pollen, Magnetic susceptibility	Garcin *et al*. (2006)
Lake Empakai Crater	Stable isotopes of carbon and nitrogen, contents of OC and nitrogen	Muzuka *et al*. (2004)
	Ostracode, Chironomids, Diatoms, Pollen	Ryner *et al*. (2007)
Lake Natron	Stromatolites	Hillaire-Marcel *et al*. (1986)
Coastal and Island caves	Stalagmite and Stalactite ($\delta^{18}O$, $\delta^{13}C$)	Lundblad & Holmgren (2005)
Western Indian Ocean	Corals	Grumet *et al*. (2000) and Kayanne *et al*. (2006)
	Foraminifera	Romahn *et al*. (2014) and Kuhnert *et al*. (2014)
Lake Challa	$\delta^{18}O$, $\delta^{13}C$	Barker *et al*. (2011, 2013)
	δD_{wax} in combination with the Branched and Isoprenoid Tetraether (BIT) index of soil bacterial	Verschuren *et al*. (2009)
	Seismic reflection (Acoustic impedance)	Verschuren *et al*. (2009) and Moernaut *et al*. (2010)
	^{14}C and ^{210}Pb-dating and $\delta^{13}C$	Blaaw *et al*. (2011)
	Stable isotopes of carbon and nitrogen, contents of OC and nitrogen	Barker *et al*. (2013)
Lakes Magat (Ngorongoro Crater),	Stable isotopes of carbon and nitrogen, contents of OC and nitrogen	Muzuka (2006)
Lake Duluti	Diatom and Pollen	Öberg *et al*. (2013)
Lake Rukwa	Diatom	Barker *et al*. (2002)
	Pollen	Vincens *et al*. (2005)
Mt. Kilimanjaro	Oxygen and Hydrogen Isotopes in Ice cores	Thompson *et al*. (2002) and Barker *et el*. (2011)
Mt.Udzungwa	Stable isotopes of carbon and nitrogen, contents of OC and nitrogen, Spores, Macrofossil, Pollen	Mumbi *et al*. (2008)
Mt.Uluguru	Charcoal, Pollen	Finch *et al*. (2009)

Oxygen-isotope results ($\delta^{18}O$) of authigenic (e.g. marls, micritie) and biogenic (ostracods, bivalves) carbonates, biogenic silica, and sulfates materials provide a unique source of hydrological and paleohydrological data for saline-lake studies. The stable isotope composition of saline-lake carbonates ($\delta^{18}O_{Carbonate}$) is primarily a reflection of the isotopic composition of the lake water at the point of precipitation. The isotopic composition of the lake water will in turn reflect several interconnecting factors including atmospheric temperature and the hydrological balance of the lake catchment. During periods of increased evaporation and/or decreased precipitation, $\delta^{18}O_{Lake}$ will become enriched in ^{18}O as the lighter ^{16}O is preferentially lost to the atmosphere. With the transition to a pluvial phase, increasing lake volume will result in a decrease in $\delta^{18}O_{Lake}$ as the input of isotopically lighter water sources (atmospheric, groundwater, and fluvial) exceeds the loss of lighter isotopes through evaporation. Such information has been useful in palaeohydrological reconstruction of saline lakes in Tanzania (Barker *et al*., 2002). For instance, in Lake Rukwa, the present salinity is the results of decrease in precipitation and increase in evaporation in the late Holocene (DeMenocal *et al*., 2000). The decrease in precipitation is supported by sharp changes of biogenic and terrestrial sediments in marine parts of subtropical Africa from the end of humid phase to present (DeMenocal *et al*., 2000).

Carbon and oxygen isotopes of foraminifera fossils and Mg/Ca ratios were used to assess deglacial SST variability in the western Indian Ocean (Romahn *et al*., 2014). It was found that the variability was mainly controlled by Antarctic air temperature, with Southern Ocean Intermediate Waters as the subsurface pathway to the equatorial Indian Ocean (Romahn *et al*., 2014). Similarly, the carbon and oxygen stable isotope ($\delta^{13}C$ and $\delta^{18}O$) of planktonic foraminifera have been used to reconstruct paleoecology (Kuhnert *et al*., 2014). Records from foraminifera inferred a warm period in early to mid-Holocene relative to late mid Holocene (Kuhnert *et al*., 2014). Records in corals have been used to infer changes in recent climatic condition. Coral records in the western Indian Ocean showed shifts in ENSO teleconnectivity of the Western and Central Indian Ocean on multi-decadal time-scales (Zinke *et al*., 2004).

2.3 Study Approach

To reconstruct the Holocene climatic changes in terrestrial and marine environments in Tanzania, major focus has been on lakes, Indian Ocean and eastern arc mountains. These are potential areas with historical records for climate reconstruction. Data are missing in other areas such as small lakes and sedimentary basins. As a result, the used records are

concentrated in some specific areas (Fig. 1). Lakes have been used as a major archive because most of them are sensitive to climate change (Zinke *et al*., 2009). For example, lake level fluctuations, changes in water chemistry and processes have been used to reconstruct the past temperature and rainfall trends (Cohen *et al*., 1997; Nicholson, 1998, 1999; Conway, 2002; Alin & Cohen, 2003; Moernaut *et al*., 2010; Tierney *et al*., 2011; Wolf *et al*., 2011).

The available data were compiled to understand and delineate the areas with proxies for palaeoclimate reconstruction in Tanzania (Table 1 and Fig. 1). Thereafter, review focused mainly on three key areas with integrated data (multi-proxies). The first area was the lakes; these were crater lakes (Challa, Duluti, Ngorongoro, Empakai and Massoko), East Africa Rift Big Lakes (Tanganyika, Malawi and Rukwa) and Lake Victoria (Table 1 and Fig. 1). To the great extent, sediment cores from these lakes represents past-terrestrial environment of Tanzania. The second area was the mountains where vegetation as the source of many proxies (eg. pollen, charcoal) and Ice core can be obtained for palaeo-climate reconstruction. Mountains reviewed are Mt. Kilimanjaro and Easter Arc Mountains (EAM) of Tanzania comprising mainly Uluguru and Udzungwa mountains (Table 1 and Fig. 1). The third area was the marine environment represented by the continental margin of the western Indian Ocean and its corresponding coastal areas (Table 1 and Fig. 1). These are potential areas with palaeo-indicator fossils such as corals, foraminifera and diatoms. Coastal areas are potential areas with caves where geological materials mainly stalagmites and stalactites are found. These materials are the best recorders of palaeo-hydrological environment.

In general, review was based on the integrated proxies mainly stable isotopes of carbon, nitrogen and oxygen, ice core, microfossils (pollen, charcoal and diatom) and geological materials (stalagmites and stalactites). These proxies were further used to generate maps showing the general lake level fluctuations for major lakes throughout the Holocene period. For the past two centuries, a period with increased modern lake records relative to pre-1800 period, maps are generated precisely for inferring dry and rainfall periods. To strengthen the interpretation, major events from late Pleistocene to present were reviewed chronologically by integrating proxies from the same area and comparing them with other proxies in different areas.

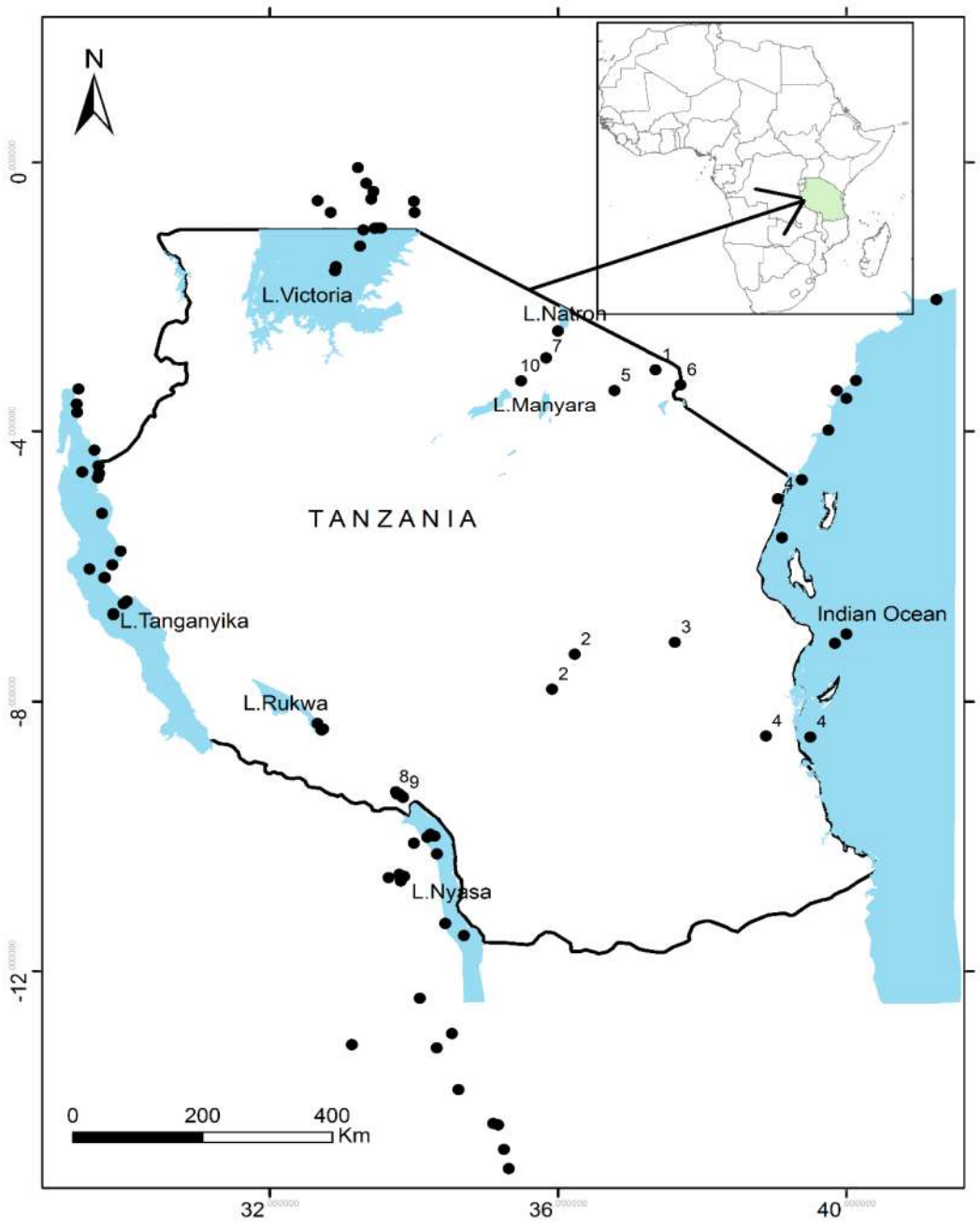

Figure 1: Distribution of the recorded proxies in Tanzania and surrounding areas.

The numbers 1-3 represent proxies on Mountains Kilimanjaro, Udzungwa and Uluguru respectively. 4- Caves along the coast and Songo songo Island where as 5-10 represent proxies on craters and small Lakes- Duluti, Challa, Empakai, Massoko, Mbaka and Ngorongoro respectively. Major water bodies are labelled in the map.

2.4 General climatic variability recorded in various localities

2.4.1 Lakes

Lake Victoria is the largest lake by area in Africa, located in East Africa bordering Tanzania, Kenya and Uganda (Fig. 1). It is characterized by two main rainy seasons with the peaks between April-May and November-December (Ssemanda & Vincens, 2002; Stager *et al*., 2005). The annual average rainfall is about 2000 mm/yr and there is no pronounced prolonged dry season in a year (Ssemanda & Vincens, 2002). As it is for most of the east Africa regions, the rainfall is controlled by ITCZ. The wind patterns (Congo humid air, southeast and northeast trade winds) converge on Lake Victoria because of pressure differences (Ssemanda & Vincens, 2002). As the lake is in the tropical zone with large surface area, water balance is mostly a function of evaporation and precipitation. Despite of having several small streams, Kagera river is the main river entering the lake and Nile river is the main river draining water from the lake.

Various works using Lake sediments have been done on Lake Victoria to infer palaeoclimate changes. These works include pollen analyses as a powerful tool for inferring palaeo-hydrological conditions (Ssemanda & Vincens, 2002), stable isotope of carbon and nitrogen with C/N ratios for accounting the sources and proportion of organic matters (Machiwa, 2010) and paleolimnological studies using sediment cores for assessing ecological changes in Lake Victoria (Verschuren *et al*., 2002). Also, diatom studies in combination with water conductivities have been useful in palaeoclimate reconstruction (Stager *et al*., 2005). Diatoms are important in inferring palaeoclimate through $\delta^{18}O$ in combination with other proxies. Their powerfulness is attributed to their sensitivity to water chemistry, particularly pH, salinity and nutrients (Barker *et al*., 2000). Furthermore, water balance models over Lake Victoria in conjunction with oral tradition records have been used in reconstruction of rainfall particularly in the last two centuries (Nicholson, 1998; Nicholson & Yin, 2001).

Lake Tanganyika is among a series of lakes in the western branch of East Africa Rift system, in the western part of Tanzania. It is an extensive structural lake, being the second deepest lakes in the word with the maximum depth of 1470 m (Burnett *et al*., 2011). As the lake is deep, upwelling of cooler water in some parts of the lake as it occurs in the Ocean is commonly forcing the nutrients from deeper parts to the surface. This mechanism enhances diatom productivity leading to preservation of silica rich sediments. Diatom study has been a significant tool in palaeclimate reconstruction (Barker *et al*., 2000, 2003, 2007, 2014; Stager

et al., 2005). The lake receives annual rainfall of about 1000 mm/yr (Burnett *et al*., 2011). However, rains are seasonally variable within the lake from north to south being controlled by changes in ITCZ, surrounding topography and the Indian Ocean (Mumbi *et al*., 2008; Burnett *et al*., 2011).

Lake Malawi is the third largest lake in Africa covering an area of about 30 000 km^2 with the maximum depth of about 785 m (Weyl *et al*., 2010). Its climate is largely controlled by ITCZ with the rainy season between October and March and a dry season between April and September (Barker *et al*., 2007). The mean annual rainfall is about 1350 mm/yr. The lake experiences high evaporation rate of about 54 km^3/yr (Weyl *et al*., 2010) leading to enrichment of $\delta^{18}O$ in lake water relative to major inputs within the catchment (Barker *et al*., 2007). In the dry season, there is cooling of surface of water influenced by the decrease in humidity and SE winds. In this season, strong lake water mixing occurs and diatoms become the dominant phytoplankton (Barker *et al*., 2007). Despite that diatom silica can undergo dissolution during early stages of diagenesis, some are permanently buried in the lake and have been used to reconstruct palaeoclimate (Barker *et al*., 2007). Apart from diatoms, various proxies such as pollen, stable isotopes, lignin phenols and plant leaf wax carbon isotopes, elemental composition as well as sedimentological data from lake Malawi have been used in palaeoclimate reconstruction (DeBusk, 1997, 1998; Branchu *et al*., 2005; Castañeda *et al*., 2009, 2011; Brown, 2010; Lyons *et al*., 2011; Stone *et al*., 2011).

Lake Rukwa is among the four largest Lakes in Tanzania with surface area of about 4000 km^2 (Barker *et al*., 2002), situated between Lakes Tanganyika and Malawi. Due to uncertainties in age estimation and the fact that the big catchment of large Lakes such as Rukwa (78 200 Km^2) exhibits different climatic conditions, it has been difficult to define precisely the transitional climatic boundaries (Barker *et al*., 2002). Present climate indicates that the average rainfall is about 995 mm/yr with the rainy season between November and April followed by the extended dry period between May and October (Barker *et al*., 2002). In this area evaporation goes up to 2000 mm/yr exceeding precipitation for most of the months.

Lake Massoko is the Crater Lake within the Rungwe Volcanic province in southwest Tanzania, situated between Lakes Rukwa and Malawi. It is morphologically related to other crater lakes of Tanzania such as Duluti dominated by circular tuff-rings without any surface outlet. It is a small fresh water lake with the surface area of about 0.36 km^2 and catchment areas of about 0.22 km^2 (Garcin *et al*., 2006). From the Holocene period to recent, Rungwe

area is characterized by tectonism associated with volcanism with the last volcanic eruption at Mt. Kiejo in the 18th century (Garcin *et al*., 2006). The Rungwe volcanic materials overly the high grade metamorphic rocks (Precambrian formation as basement), karoo sediments (Permian to Triassic) and Neogene sediments.

The current regional climate of Rungwe is controlled by the Inter Tropical Convergence Zone (ITCZ) leading to rainy season between November and April averaging at 1200 mm/yr (Garcin *et al*., 2006) and the dry period from May to October. The climate over Lake Makoko area differs from regional climate due to orographic features: the mean monthly temperature is 25 °C (Garcin *et al*., 2006) favouring high evaporation from the Lake and the Lake is surrounded by mountains which favour wind convergence leading to high precipitation over this area. As a result, the lake receives high rainfall averaging at 2400 mm/yr and since its formation about 50 million years ago, lake levels have been fluctuating depending on rainfall intensity without any dry period. This is contrary to most of the low land lakes in tropical Africa (Garcin *et al*., 2006).

The core results integrating dating and litho-correlation indicate strong variability of sediments deposition from 45 ka (Early period of lake formation) to 11.7 ka (Last Glacial Period) and low depositional variation from Holocene to present (Garcin *et al*., 2006). Thus, from the beginning of Holocene to present day, the lake is exhibiting more stable climatic condition compared to pre-Holocene period (Glacial period) and this stability influences the present Lake - hydrological conditions.

Lake Emakat is the volcanic crater lake within Empakaai crater in the eastern branch of East Africa rift system, northern part of Tanzania. The area receives low rainfall averaging at 600 mm/yr in the western part and intermediate rainfall of about 1000 mm/yr in the highland eastern parts of the crater (Ryner *et al*., 2007). The rainfall period is generally between November and May with maximum precipitation between March and May. The daily mean temperature is between 15-22 °C with more cold condition up to negative values during the night (Ryner *et al*., 2007).

The water input to Lake Emakat is by precipitation and few streams from the crater. Lake level and water chemistry of the lake has been changing due to variation in climatic conditions. Climate change studies by Muzuka *et al*. (2004) & Ryner *et al*. (2007) using carbon and nitrogen isotopes, magnetic susceptibility of sediment cores, microfossil assemblages and elemental compositions have been used to infer hydrological and ecological

changes within the catchment from Holocene to present. Ryner (2007) indicated that the lake exhibited a general high lake level between 12.7 - 10.3 ka and thereafter a decreased precipitation which led to abrupt transition of lake water from fresh to alkaline at 9.7 ka. This is in close agreement with an abrupt climatic change at 8.7 ka inferred using stable isotope of organic carbon and nitrogen (Muzuka *et al*., 2004). The cores were characterized by enrichment of both ^{15}N and ^{13}C prior to 8.7 ka and depletion of these post 8.7 ka suggesting climatic changes from wetter to dryer conditions (Muzuka *et al*., 2004).

Lake Challa is among the crater lakes in eastern branch of East Africa Rift System located on the eastern slope of Mt. Kilimanjaro surrounded by savanna vegetation (Barker *et al*., 2011; Nelson *et al*., 2012). The basin is composed of volcanic materials mainly trachy-basalt being underlying calcareous tuffaceous sediments (Wolff *et al*., 2014). As other lakes in Tanzania such as Tanganyika, Malawi and Rukwa, the local climate is highly controlled by ITCZ. It is characterized by two rainy seasons; October to December and March to May with an average annual rainfall of about 600 mm (Wolff *et al*., 2014). As it is a tropical semi–arid region with annual mean temperature of about 25 °C (Nelson *et al*., 2012), evaporation over the lake area (1700 mm/yr), exceeds precipitation (Nelson *et al*., 2012; Wolff *et al*., 2014). Thus, the lake water is likely derived from groundwater that is recharged by percolation process from the heavy rains on the highlands of Mt. Kilimanjaro.

Unlike most of the lakes in East Africa, Palaeo-reconstruction over Lake Challa is favoured by conducive preservation conditions at the sediment-water interface where water stratification and anoxic environment have persisted for the past 25 ka (Barker *et al*., 2011, 2013; Wolff *et al*., 2014). For this reason, more researches using integrated proxies have been done at Lake Challa to reconstruct the East Africa tropical climate. For instance, Verschuren *et al*. (2009) and Moernaut *et al*. (2010) used seismic reflection whereas, Barker *et al*. (2013) and Wolff *et al*. (2014) used elemental composition, textural and structure of sediments to infer palaeoclimate through seasonal changes in deposition of sediments. Blaaw *et al*. (2011) used dating techniques (^{14}C and ^{210}Pb-lake sediments) and the obtained ages were integrated with other proxies to reconstruct palaeoclimate.

2.4.2 Mountains

Ice retreats at the top of Mt. Kilimanjaro have been reported by many researchers (Thompson *et al*., 2002, 2011; Kaser *et al*., 2010). Isotope data of oxygen and hydrogen are used to define the degree at which the water molecules have undergone evaporation. As evaporation increase, the divergence from the Global Meteoric Waterline (GMWL) also increases. Oxygen and hydrogen isotopic data from the Ice core drilled on Mt. Kilimanjaro lies close to the GMW line suggesting that evaporation is not the main cause of Ice melting. Ice core results indicated that different ice field over Mt. Kilimanjaro are characterized by different ages with some ice being expanding and contacting through Holocene (Kaser *et al*., 2010). However, the annual mass balance is negative. Thus, these isotopes have been powerful in inferring palaeoclimate (Thompson *et al*., 2002; Barker *et al*., 2011). It is further noted that the beginning of current ice retreat on Mt. Kilimanjaro coincided with global warming (Thompson *et al*., 2011) and ice retreat is therefore a factor of temperature and not hydrological changes.

The Eastern Arc Mountains (EAM) of Tanzania which is comprised of faulted blocks and isolated mountains is characterized by high grade metamorphic rocks. It covers an area of about 5400 km^2 with the highest peak at Uluguru south (2600 m) (Mumbi *et al*., 2008). Like other areas of Tanzania, the rainfall over the EAM is controlled by ITCZ. It is high in the side facing the Indian Ocean compared to the western part but the overall average is about 1700 mm/yr (Mumbi *et al*., 2008).

The biodiversity in the Eastern Arc Mountains of Tanzania (plants and animals) is high to the extent of providing ecological data for palaeo- climate reconstruction. The forest over this area is believed to have retained moist since the last glaciations (Mumbi *et al*., 2008; Finch *et al*., 2009). In attempt to reconstruct palaeo-climate of these mountains, ecological stability of the forest was tested using a combination of pollen, charcoal, spores, macrofossils and stable isotope proxies (Mumbi *et al*., 2008; Finch *et al*., 2014). Results inferred the cool and dry conditions associated with high ecological stability in the late LGM to the start of Holocene period. High stability during this aridity period is linked to the influence of Indian Ocean in maintaining moist forest cover (Mumbi *et al*., 2008). Vegetation change in EAM occurred in late Holocene and this was attributed to climatic warming and anthropogenic activities related to food demand (agricultural expansion), wood, charcoal and medicinal plant demands (deforestation), pastoralism and hunting. The increase in such activities is supported by

abundance of coprophilous fungi and algal bloom together with neurospora spores as an indicator of fire activities (Mumbi *et al*., 2008).

2.4.3 Continental margin of Indian Ocean

The climate of continental margin of the western Indian Ocean is largely controlled by the Asian monsoon. The monsoon is the result of pressure gradient resulting from differential heating between the Indian Ocean and the land (Himalaya Mountains). The monsoon is not easily predicted; sometimes there is delay or failure because of the complex tele-connectivity involving the Indian Ocean and the atmosphere through the Oceanic currents, sea surface temperature and atmospheric circulations. The delays or failure of monsoon have been causing severe impacts in agriculture, health and economy at large due to unexpected rain and draught periods. Areas such as East Africa and India have been significantly affected (Grumet *et al*., 2000).

Corals are common in the equatorial continental margin of the western Indian Ocean. They are commonly used in inferring palaeo-climate because of their fast growth rate with life span of about 100 - 400 yrs (Zinke *et al*., 2005). Their strength in palaeo-reconstruction is also favoured by their sensitivity to salinity, river input and sea surface temperature. A combination of these gives a clear insight on the past climatic changes on precipitation and temperature patterns. However, they are restricted in tropical climate and their records through skeletons enable short- term palaeoclimate reconstruction generally up to few centuries (Lundblad & Holmgren, 2005). A study by Zinke *et al*. (2009) indicated 350 yrs as the maximum period of which land rainfall and surface air temperature can be reconstructed effectively using corals and therefore concluded that corals are not suitable for palaeoclimate reconstruction for the past centuries. Decadal climate variabilities influenced by regional hydrologic changes have been inferred using corals from the western part of the Indian Ocean (Cole *et al*., 2000; Zinke *et al*., 2004, 2008, 2009). Cole *et al*. (2000) pointed out that changes in surface sea temperature, currents and atmospheric convergent zones coupled with El Niño-Southern Oscillation (ENSO) variability are the main factors accounting for climate variability in the western parts of the Indian Ocean. Therefore, because of the above coral-limitations in reconstruction of paleoclimate, corals have been used together with stalagmites and stalactites to infer Holocene ecological changes in Tanzania.

In Tanzania, there are stalagmite and stalactite in the caves along the coastal areas. These geological formations have been useful in inferring tropical climate changes (Holmgren *et al*.

1997; Lundblad & Holmgren, 2005). Changes in $\delta^{13}C$ in stalagmite may reflect changes in vegetation cover and hence changes in hydrological condition (Lundblad & Holmgren, 2005). Changes from C_3 plants (mainly trees) to C_4 plants (mainly grassland) reflect largely changes from a period of high precipitation to a period of low precipitation. Variation of $\delta^{18}O$ in stalagmite may reflect changes in temperature and or rainfall. The $\delta^{18}O$ values during the formation of stalagmite in the cave will largely depend on the prevailing temperature in the cave and the temperature of the solution which is a factor of the outside temperature, the source and paths of precipitations.

For the case of precipitation, both, the routes/paths and amount effect play a significant role in variation of $\delta^{18}O$ in stalagmite. This is based on the fact that during evaporation of seawater, lighter isotope will be incorporated quickly in vapour phase leading to depletion of ^{18}O in vapour and enrichment of ^{18}O in Oceanic water. As water vapour move away from the ocean, depletion of ^{18}O continues and as results rains along the coast are more enriched with ^{18}O relative to the rains away from the coast. In the same areas, amount effects account for variation in $\delta^{18}O$; as it starts to rain, the drops will be enriched with ^{18}O and as it continues to rain, depletion of heavy isotope along with enrichment of light isotope continues progressively.

In attempt to reconstruct palaeoclimate, stalagmites were collected along the coast of Tanzania and $\delta^{13}C$ and $\delta^{18}O$ showed millennial scale fluctuations suggesting variation in CO_2 level likely to be caused by changes in temperature (Lundblad & Holmgren, 2005). However, the effectiveness of stalagmite in palaeoclimate reconstruction was found to be low because most of them were porous with detrital sediments leading to unreliable U-series dating (Lundblad & Holmgren, 2005). Using foraminiferal Mg/Ca ratio from the tropical western Indian Ocean and $\delta^{18}O$ from the sediment core off northern Tanzania, it was possible to infer two palaeotemperature phases in the Holocene period. The first phase (~7.8–5.6 ka) was inferred as a warm phase and the second phase (5.6–4.2 ka) was inferred as cool phase with the temperatures dropped by 2 °C relative to the first phase (Kuhnert *et al*., 2014).

2.5 Paleoclimatic major events of the Late Pleistocene to present

2.5.1 Late Pleistocene-Early Holocene

(i) Last Glacial Maximum (LGM)

Africa was dry during the Last Glacial Maximum (LGM) (Lærdal *et al*., 2002, Muzuka & Nyandwi, 2002; Barker & Gasse, 2003; Barker *et al*., 2003; Felton *et al*., 2007; Tierney *et al*., 2008; & Barker *et al*., 2011). In this period, most of the East African lakes were characterized by low lake levels and the basins were dominated by savanna vegetation compared to wood vegetation (Tierney *et al*., 2008; Burnett *et al*., 2011; Finch *et al*., 2014). Aridity was severe such that Lake Victoria was completely dry (Stager *et al*., 1997) and Lake Massoko was completely saline (Barker *et al*., 2003).

In Lake Tanganyika where water level has been changing in response to climate change over the entire period, the Lake level dropped more than 350 m during the LGM period (Felton *et al*., 2007; Burnett *et al*., 2011). The work by Felton *et al*. (2007) in Lake Tanganyika using elemental geochemistry and textural changes in sediments suggested aridity period between 16 and 15 ka. This is in agreement with low diatom productivity between 17 and 10 ka of which hydrological changes are linked with changes in ITCZ (Burnett *et al*., 2011).

In Lake Malawi, lacustrine records provided evidences of dry condition during LGM concomitant with other lake records in northern and southern equatorial Africa (Crul, 1997; Barker *et al*., 2007; Powers *et al*., 2005; Scholz *et al*., 2011; Stone *et al*., 2011). Furthermore, lake level records derived from benthic diatom assemblages, seismic reflection data and geochemical analyses of endogenic calcite showed low lake level and hence aridity during LGM (Castañeda *et al*., 2007). For instance, drop in lake level to about 100 m was inferred using diatom records and seismic data between 23-19 ka (Stone *et al*., 2011). This is in agreement with the works by Lyons *et al*. (2011) which indicated a significant drop of lake level to about 75 -100 m below the modern levels during LGM. Furthermore, according to Barker *et al*. (2007), a pronounced dry period is inferred through enrichment of $\delta^{18}O_{diatom}$ between 17.8 -14.5 ka. However, some workers have indicated less intense Glacial maximum conditions. For example, the work of DeBusk (1998) using pollens showed widespread montane forest in the Lake Malawi catchment basin. This is in close agreement with a study by Scholz *et al*. (2011a, b) which revealed a general high lake level between 60 ka to present relative to the period between 145-60 ka.

(ii) African Humid Period

Last Glacial Maximum (LGM) was followed by the African Humid Period (AHP) between 14-5.5 ka, being culminated in Holocene between 9 and 6 ka (DeMenocal *et al*., 2000). During AHP, the known Sahara Desert in Africa was nearly covered by vegetation mainly shrubs and grasses and various Lakes existed in the sub-tropical areas of Northern Africa. Some of the Lakes with saline water during this time such as Lake Rukwa were characterized by freshwater during the humid period due to high precipitation (Barker *et al*., 2002). In Lake Rukwa, the transition from fresh to saline water is evidenced by change in diatom species composition from freshwater to saline water diatom species as well as the fluctuations of pH and conductivity inferred using diatoms (Barker *et al*., 2002).

Integrated proxies in Lake Empakai indicate a period of high lake level with freshwater between 14.8 to 12.3 ka being well pronounced between 14.8 -14.4 ka and 13.2 - 12.3 ka (Muzuka *et al*., 2004). From Lake Challa, a lake that has been responding well to climate changes, the $\delta^{18}O_{diatom}$ were relatively low (average = -38.2°/$_{\infty}$) from the late Pleistocene to early Holocene (15-9 ka) suggesting a reduced aridity with high precipitation (Nelson *et al*., 2012). In Lake Tanganyika, the humid period is indicated by a significant drop of $\delta^{13}C$ between 19-9 ka associated with changes in vegetation from C_4 to C_3 types and increase in C/N ratio (Burnett *et al*., 2011).

(iii) Young Dryas

Humid period was interrupted by the cool and dry short-lived period of Young Dryas (YD) around 12 ka (DeMenocal *et al*., 2000; Garcin *et al*., 2006; Muzuka *et al*., 2006; Barker *et al*., 2007, 2011; Ryner *et al*., 2007; Tierney *et al*., 2008; Verschuren *et al*., 2009). It was terminated abruptly, completed within tens to hundreds of years (DeMenocal *et al*., 2000; Barker *et al*., 2011). Geological evidences indicate that termination of the humid period was immediately followed by change in African climate to more arid condition and decline in lake levels for major Lakes. The work of DeMenocal *et al.* (2000) on marine core, off Cap Blanc, Mauritania has shown sharp increase in eolian sediments between 13.4-12.3 suggesting the YD period. In this period, most east African lakes are known to have experienced low lake levels (Verschuren *et al*., 2009).

In Tanzania, the Younger Dryas event has been documented widely using integrated proxies particularly in Lake Tanganyika (Tierney *et al*., 2008, ~ 12 ka), Lake Malawi (Barker *et al*., 2007, 12.5-11.8 ka), Lake Victoria (Talbot & Lærdal, 2000), Lake Challa (Verschuren *et al*.,

2009, 13.3-11.7 ka), Lake Massoko (Garcin *et al*., 2006, 12.8-11.6 ka) and other smaller lakes (Muzuka *et al*., 2006; Barker *et al*., 2007; Ryner *et al*., 2007; Barker *et al*., 2011). In Lake Malawi, the YD is reflected by high $\delta^{18}O_{diatom}$ (+39.7‰) at 12.5 ka suggesting very dry condition (Barker *et al*., 2007). In Lake Massoko, it is well reflected by the sharp decline in magnetic susceptibility (Garcin *et al*., 2006). Furthermore, branched isoprenoid tetraether (BIT) record in Lake Challa sediments shows that drought encompassing the YD in equatorial East Africa lasted from13.3 to 11.7 cal. Kyr BP, with most intense aridity during 12.4 –12.8 cal. kyr BP (Tierney *et al*., 2011). Hydrological changes during YD period are linked to changes in earth orbital oscillations (DeMenocal *et al*., 2000) leading to the changes in ITCZ (Garcin *et al*., 2006).

2.5.2 Early-Mid Holocene Period

(i) Early Holocene Period

Towards the beginning of Early Holocene, Tanzania was characterized by high precipitation (DeMenocal *et al*., 2000; Muzuka *et al*., 2004; Felton *et al*., 2007; Verschuren *et al*., 2009; Nelson *et al*., 2012; Weldeab *et al*., 2014; DeMonocal, 2015; Shanahan *et al*., 2015). In this period, the lake levels for most of the eastern Africa lakes were above the present levels (Barker *et al*., 2011). In Lake Tanganyika, around 10 ka, high precipitation is evidenced by increase in soluble components in lake sediments represented by Be/Al, Ni/Al, Cr/Al, Fe/Al ratios (Felton *et al*., 2007) and depletion of $\delta D_{leaf\ wax}$ relative to late Holocene values (Tierney *et al*., 2008). In Lake Emakat, the early Holocene high precipitation is evidenced by the increase in C_3 vegetation type with depleted $\delta^{13}C$ value averaging at -27 ‰ compared to -12 ‰ of the C_4 plant types (Muzuka *et al*., 2004) whereas in Lake Massoko, it is inferred through diatom by low water conductivity between 13.1 to 8.5 ka (Barker *et al*., 2003). In Lake Challa it is reflected by high Lake level supported by elevated BIT index and depletion of δD_{wax} vs VSMOW (Fig. 2). The high precipitation in this period is linked/related to the increase in Northern Hemisphere precession leading to strengthening of summer and winter monsoon (Tierney *et al*., 2008).

According to the work by Ryner *et al*. (2007) in northern Tanzania, within the early Holocene period, there was a short period between ~10.3-9.7 ka with decreased precipitation followed by abrupt transition from fresh water to high salinity and alkalinity in Lake Empakai. This is closely in agreement with the study by Muzuka *et al*. (2004) in the same lake which indicated abrupt climate change around 8.7 ka and the study by Nelson *et al*. (2012) in Lake Challa

which indicated an increase in $\delta^{18}O_{diatom}$ around 9 ka. Furthermore, as pollen can be transported a long distance (Schüler, 2014), decrease in precipitation in this particular period is supported by the decrease in pollen over lake Challa as noted by Nelson *et al*. (2012) as a result of reduced vegetation cover over Mt. Kilimanjaro.

(ii) The 8.2 ka event

Despite the fact that the early Holocene was a period of high precipitation (Muzuka & Nyandwi, 2002; Barker *et al*., 2003), a short period of dry event about 8-8.2 ka has been inferred (Stager & Mayewski, 1997; Lærdal *et al*., 2002; Powers *et al*., 2005; Blaaw *et al*., 2011). Records from many lakes in Tanzania show that at around 8 ka, the area experienced climatic reorganization in concomitant with global observations (Gasse, 2000; Felton *et al*., 2007). Such a record has been preserved in the Kilimanjaro ice field through high concentration of Na^+ and F^- at around 8.3 ka suggesting decline in regional lake levels (Thompson *et al*., 2002). This is in close agreement with the relative high water conductivity in Lake Massoko as inferred from diatoms between 8.5-7.8 ka, suggesting dry condition in this particular period (Barker *et al*., 2003). Generally, the 8.2 ka event has been recorded in both lacustrine and marine environments in Northern Hemisphere and has been referred to be a cooling event which resulted from meltwater outflow into the North Atlantic Ocean and a slowdown of North Atlantic Deep Water formation (Rohling & Pälike, 2005; Barker *et al*., 2007; Zalasiewicz & Williams, 2009).

(iii) Mid Holocene

Mid Holocene is recognised as a humid period in equatorial East Africa (Verschuren *et al*., 2009) with high precipitation reflected by high lake levels in major Lakes of Tanzania - Victoria, Tanganyika and Rukwa (Muzuka & Nyandwi, 2002; Ssemmanda & Vincens, 2002). In Lake Victoria, this is supported by the pollen data which indicate abundance of Moraceae/Urticaceae between 7.1- 6.5 ka suggesting humid condition around Lake Victoria catchments (Ssemmanda & Vincens, 2002). However, the available data indicate a general progressive decrease in precipitation from mid-Holocene to present in Tanzania likely to be attributed to the intensity variation of the monsoon winds. For instance, diatom records from Lake Victoria and $\delta^{13}C$ values for the core in Lake Tanganyika indicated a general decrease in precipitation from mid-Holocene to present (Muzuka & Nyandwi, 2002). In Lake Tanganyika, aridity has been interpreted through a down-core decrease in $\delta^{13}C$ which indicate changes from the dominance of C_4 to C_3 vegetation types (Muzuka & Nyandwi, 2002). In

Lake Challa aridity is reflected by high $\delta^{18}O$ values averaging at 40.3‰ from 5 ka to present (Nelson *et al*., 2012).

2.5.3 Mid Holocene-Present

(i) Mid Holocene 6-4.1 ka, with the 5.2 ka event

The period from 6-4.1 ka was wet relative to the present climatic condition and dry relative to early Holocene with pronounced cooling episodes (Thompson *et al*., 2002). High precipitation (high lake level stands) was inferred over Lake Victoria between 6.5 – 4.1 ka (Ssemmanda & Vincens, 2002) and water levels were maximum in the basins such as Ziway-Shala in the main Ethiopia rift system (Thompson *et al*., 2002). From the Indian Ocean, off northern Tanzania, foraminiferal Mg/Ca ratio and $\delta^{18}O$ from sediment cores inferred a cool period between ~5.6-4.2 ka with the temperature decreased to about 2 °C relative to the preceded early to mid-Holocene period (Kuhnert *et al.,* 2014). From the ice core retrieved from Mt. Kilimanjaro, a cool climatic condition is reflected by depletion of ^{18}O at about 6.5 ka with maximum depletion at about 5.2 ka (Thompson *et al*., 2002, 2011). The 5.2 ka event is in agreement with Greenland Ice core where in both cores, the cooling event is reflected by the decline in lake levels, CH_4 concentration as well as the vegetation cover (Thomson *et al*., 2002). The cooling event is also reflected in northern Africa to Arabia (Thompson *et al*., 2002). Thus, it is likely that the event was influenced by regional climatic forcings. In general, precipitation in this period was found to be relatively lower than the precipitations in the Early Holocene (Thompson *et al*., 2002).

(ii) The 4.0 ka event

Global climatic data particularly from Northern Africa, China and Southern America suggest another climatic event around 4-4.5 ka. This event was associated with the decrease in precipitation leading to low lake levels. On Mt. Kilimanjaro, this period is evidenced by decrease in ice cover and thick dust deposit at around 4 ka (Thompson *et al*., 2002, 2011; Tierney *et al*., 2011). On this mountain, the event is shown in Fig. 2 where the dust histories and $\delta^{18}O$ values are compared with other proxy records. The same event is recorded in the nearly crater lake (Lake Challa) where it is reflected by depletion of δD_{wax} (Tierney *et al*., 2011; Fig. 2). This was a regional event as the thick dust deposit was also recognised in other parts of the world such as the Gulf of Oman, the eastern parts of Mediterranean Sea around 4.2 ka (Tierney *et al*., 2011).

From marine cores (eg. Core from Indus Delta and Gulf of Oman), the dry event is reflected by sharp peaks of carbonates (short period of high carbonates) (Thompson *et al*., 2011). In China, it is reflected by a sudden decrease in pollen concentrations around 3.95-4.45 ka (Thompson *et al*., 2011). In Southern America, it is evidenced by high $\delta\ ^{18}O$ in Amazon fan from planktonic foraminifera suggesting the decrease in river flow. Furthermore, dry condition is recognised in other lakes of Africa such as Lakes Tilo in Ethiopia, Bahr-El-Ghazal, Ziway-Shala, and Abhe in the Northeast of Africa (Tierney *et al*., 2011). The 4.0 ka dry event is likely to have been caused by strong changes in solar activity influencing changes in systems such as deep ocean circulation and El Niño-Southern Oscillation (ENSO) (Tierney *et al*., 2011; Thompson *et al*., 2011).

(ii) 3-2 ka event

The 3-2 ka period is recognised as the dry period characterized by low stands for most of East Africa Lakes (Cohen *et al*., 1997). In Lake Tanganyika, low precipitation period is supported by stromatolitic data (^{14}C dates, $\delta^{18}O$, $\delta^{13}C$) coupled with elemental geochemical and sedimentological data which indicated a low lake levels about 5-10 m below the present lake level and enrichment of $^{18}O_{stromatolite}$ around 800 BC to 400 A.D (2.8-1.6 ka) (Cohen *et al*., 1997). This is in close agreement with both stromatolite records which indicated maximum aridity at 2.5 ka (Casanova & Hillaire-Marcel, 1992) and ostracode records where a low stand period was inferred between 2.2-2 ka (Alin & Cohen, 2003).

The 3-2 ka dry period is in close agreement with the charcoal studies in Lake Victoria which indicated the relative dry period between 3-2 ka (Thevenon *et al*., 2003) and the work by Barker *et al*. (2011), specified this low stand period for Lake Victoria to be between 2.7 and 2.4 ka. In Lake Massoko catchments, there was a decline in vegetation cover around 3.45 -2.8 ka (Vincens *et al*., 2003). The 3-2 ka dry condition is further supported by other proxies from other areas. For instance, studies in other Lakes of Africa (eg. Lake Bosumtwi – Ghana, Lake Turkana- Kenya) suggest more dry condition around 3 ka (Shanahan *et al*., 2015) and some of the lakes such as Lake Naivasha were completely dry around this period (Barker *et al*., 2013).

Aridity in this period was not as intensive as the aridity in the LGM (Fig. 2). In the Eastern Arc Mountains (EAM), $\delta^{13}C$ values suggest high proportion of C_3 plant materials compared to the LGM C_3 proportions (Finch *et al*., 2014) probably owing to increased precipitation. There is clear evidence that from 3.5 ka to present, there is an increase in human activities

which are affecting ecological stability of Eastern Arc Mountains (EAM). For instance, the abundance of fungi which are associated with herbvores such as pleospora and Sordalia between 3.5 ka to present reflects the increased cattle over the area (Finch *et al*., 2009). Also, the Neuspora records particularly in the past 2000 yrs indicate the increase in fire burning activities over the EAM (Finch *et al*., 2009).

(iii) 2-1.7 ka

The available records in East Africa indicate a transition from the dry to wet period. Ssemmanda & Vincens (2002) reported the wet period in Turkana basin, Kenya. This is closely in agreement with a 2 ka event inferred using $\delta^{13}C_{diatom}$ over Lake Challa where the $\delta^{13}C_{diatom}$ values were totally depleted relative to the pre and post 2 ka values (Barker *et al*., 2013). Contrary to this, records from the same lake (Lake Challa) indicate that the period from 2.0–1.7 ka is among the drought periods that match properly with other Eastern Africa droughts (Verschuren *et al*., 2009). This is further supported by records over lake Edward and most of the east Africa Lakes where a short period from 1.8 to 1.7 ka was inferred as the aridity period (Lærdal *et al*., 2002).

(iv) 1.7-1.2 ka

This is recognised as a period of high precipitation in equatorial East Africa with the peak around 1.5 ka (Alin & Cohen, 2003; Verschuren, 2009). In Lake Massoko, this is evidenced by expansion of vegetation cover in Lake Massoko catchment's from 1.65 to 1.2 ka (Vincens *et al*., 2003). This is further supported by wet condition inferred through diatom records at 1.7 ka in Lake Massoko (Barker *et al*., 2000, 2003).

In Lake Tanganyika, this period is marked by high stand through ostracode records (Alin & Cohen, 2003). In this lake, Stager *et al*. (2009), through sedimentary time series, diatom and pollen records inferred this wetter period in a specific interval between 1.7 and 1.4 ka. As the peak of early summer isolation are associated with high rainfall, the high precipitation in this period (as well as the period at ~11.5ka) is explained as the outcome of maximum early summer insulation in either north or south of the tropics over these periods (Verschuren *et al*., 2009).

(v) Medieval Warm Period (1.2-0.5 ka)

A combination of proxies such as pollen, diatom and magnetic susceptibility indicate that this period was characterized by a dry climatic condition (Vincens *et al*., 2003). In Lake Massoko, this is supported by diatoms records which suggest dry period between 1.0-0.5 ka (Barker *et al*., 2000) and the decrease in vegetation cover (woodland type) from 1.1-0.6 ka (Thevenon *et al*., 2003; Vincens *et al*., 2003). In Lake Tanganyika, this is supported by the low lake level between the eighth and fourteenth centuries (1.2-0.6 ka) which corresponds to the low Nile River discharge over this period (Cohen *et al*., 1997). This is in agreement with the ostracode abundance records in Lake Tanganyika which revealed low stands between 1.2-1.15 ka and 0.95-0.75 ka (Alin & Cohen, 2003). In Lake Victoria, diatom records suggest minima lake levels in this period, specifically between 0.82-0.76 ka, 0.68-0.66 ka and 0.64-0.62 ka (Stager *et al*., 2005). In Lake Duluti, northwest of Tanzania, a dry climatic condition was inferred using pollen and diatom records between ~0.97-0.54 ka (Öberg *et al*., 2013). However, very short wetter periods are suggested within this period. For instance, Tierney *et al*. (2011) interpreted a wetter condition between 1-0.9 ka using δD_{wax} data from Lake Challa and Stager *et al*. (2009) interpreted such condition between 1.15-0.9 ka and 0.7-0.55 ka using sedimentary time series, pollen and diatom records from lakeTanganyika.

(vi) Little Ice Age (0.5 -0.15 ka)

Little Ice Age (LIA) was cool and dry with some episodes of wet conditions (Stager *et al*., 2005; Tierney *et al*., 2011). Aridity during the LIA was inferred between 0.5 and 0.35 ka using sedimentary time series, diatom and pollen records of Lake Tanganyika (Stager *et al*., 2009). Also, in the same lake, short brief periods of low lake levels are recognised using ostracode records around 0.42, 0.27 and 0.2 ka (Alin & Cohen, 2003). In Lake Duluti, a brief low lake level is inferred using pollen and diatom records between ~0.41-0.37 ka (Öberg *et al*., 2013) while in Lake Victoria short periods of low stands which are concomitant with the short dry periods in Lake Tanganyika were inferred between 0.37-0.34 and 0.22-0.15 ka (Stager *et al*., 2005).

Episodes of high precipitation are evidenced by the dominance of terrigeneous sediments with low biogenic silica concentration in most of the lakes (Johnson *et al*., 2001). In Lake Tanganyika, this is supported by the relative high lake level stands from the 14^{th} to19th century (Cohen *et al*., 1997) with the remarkable high stands inferred using ostracode abundances at 0.5 and 0.13 ka (Alin & Cohen, 2003), pollen and diatom records between

0.35-0.2 ka (Stager *et al*., 2009). The Tanganyika high lake levels in the 19th century compare well with the relative increase in Nile River discharge suggesting high precipitation in the corresponding catchments (Cohen *et al*., 1997). In Lake Victoria, high precipitation was inferred using water conductivities and shallow water diatoms as proxies with the highest peaks around 0.5 ka and 0.3-0.25 ka (Stager *et al*., 2005). In Lake Massoko, it is evidenced by the increase in sedimentation rate with high content of terrigeneous sediments from 0.5 ka (Thevon *et al*., 2003). Generally, the available data in Tanzania indicate that there was high variability of rainfall during the LIA with early period characterized by high precipitation relative to the late period.

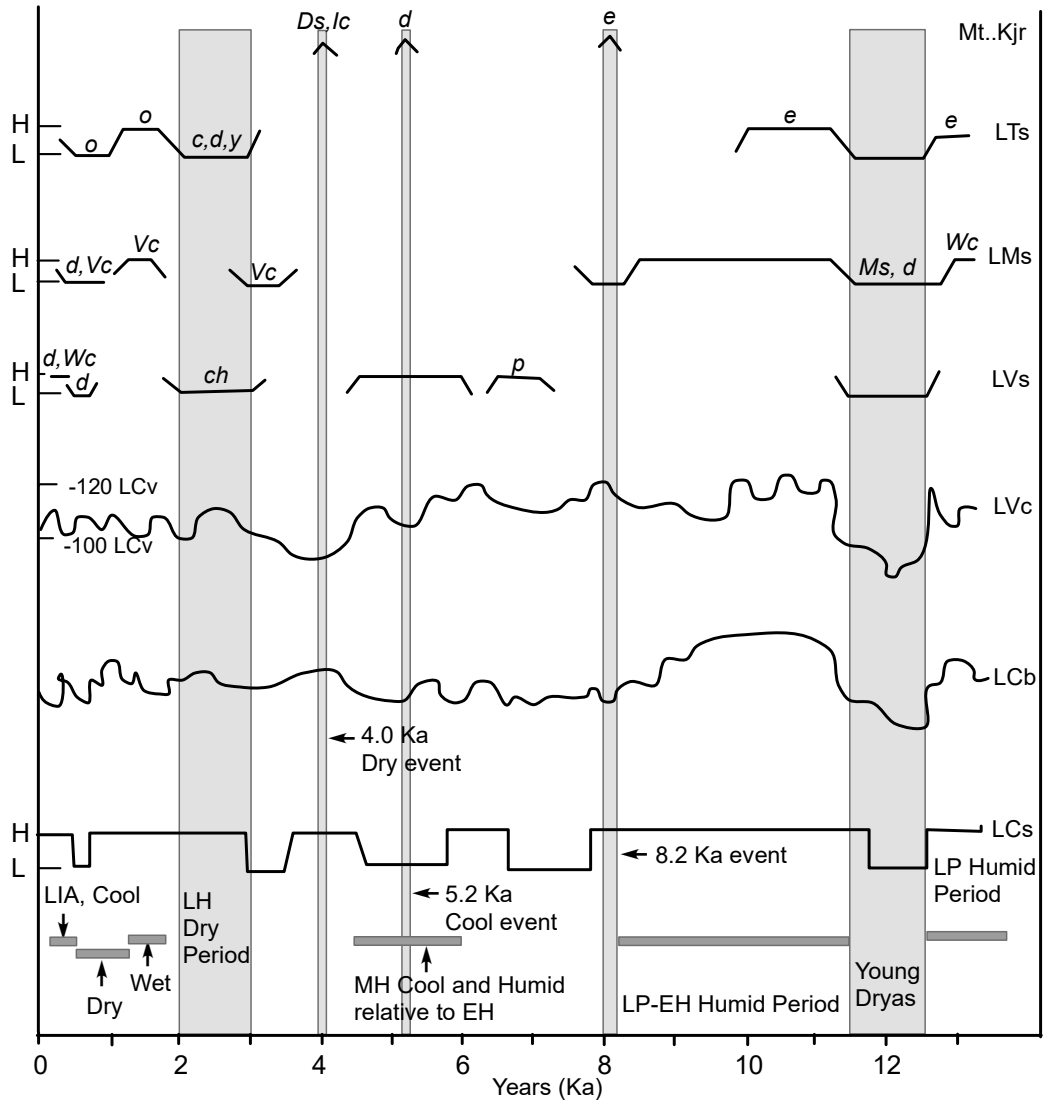

Figure 2: Relative lake levels variation from late Pleistocene to Holocene reconstructed using integrated proxies with "H" as high stand and "L" as low stand (left)

The light gray indicates the major abrupt climatic event inferred using both lake levels and Ice core at Mt. Kilimanjaro. LCs, LCb, LCv are Lake Challa lake level fluctuation, BIT Index and δDwax Vs VSMOW respectively as modified from Tierney *et al*., 2011. LVs, LMs and LTs (right) are the relative lake level fluctuations for lakes Victoria, Massoko and Tanganyika respectively. Mt. Kjr is Mt. Kilimanjaro abrupt event records. The symbols in specific segments indicate the common proxies used where c: δ13C or 14C dates Ch: charcoal, d: δ18O, Ds: dust cover, e: elemental geochemistry, Ic: Ice cover, Ms: magnetic susceptibility, o: ostracode records, p: pollen, Vc: vegetation cover, Wc: water conductivity and y: sediment textural changes.

(vii) Period from 1800-1900

In the nineteenth century (also a part of LIA), the first half was characterized by low precipitation relative to the second half of the century and this is evidenced by low lake levels for most of the lakes in East Africa (Zinke *et al*., 2009). In 1830s, integration of recorded data (history of indigenous people, European explorers and settlers) around Lake Victoria in all bordering countries indicated that the drought was so intensive to the extent of forcing migration of local people (Nicholson, 1998). The Lake began to rise slowly around 1850s in response to increased precipitation that led to expansion of vegetation cover in East Africa (Nicholson, 1998).

Around 1870s, precipitation was also low leading to low stands for most of the lakes in East Africa (Verschuren *et al*., 1999). In this period, water level in Lake Rukwa was completely low as evidenced by Livingstone's servant who encountered salt residue at the bottom of the former lake (Nicholson, 1999). From the mid of 1870s to 1900, most of the East Africa Lakes were characterized by high lake levels (Zinke *et al*., 2009) suggesting increased precipitations. However, some brief periods of droughts occurred in 1880s (Nicholson, 1998). In the period from 1870s to 1900, Catholic missionaries at Buganda measured levels of Lake Victoria frequently and therefore data are based on modern gauge measurements (Nicholson, 1998). Such data indicated that in the late 19th century, the main precipitation peak over Lake Victoria was around 1890s (Nicholson, 1998). This peak is also reflected in all major lakes of Tanzania (Fig. 3). This is supported by Conway (2002), where records indicated the period between 1895 and 1897 as the main peak of precipitation over Lake Victoria and 1898 as the year peak in Lake Tanganyika.

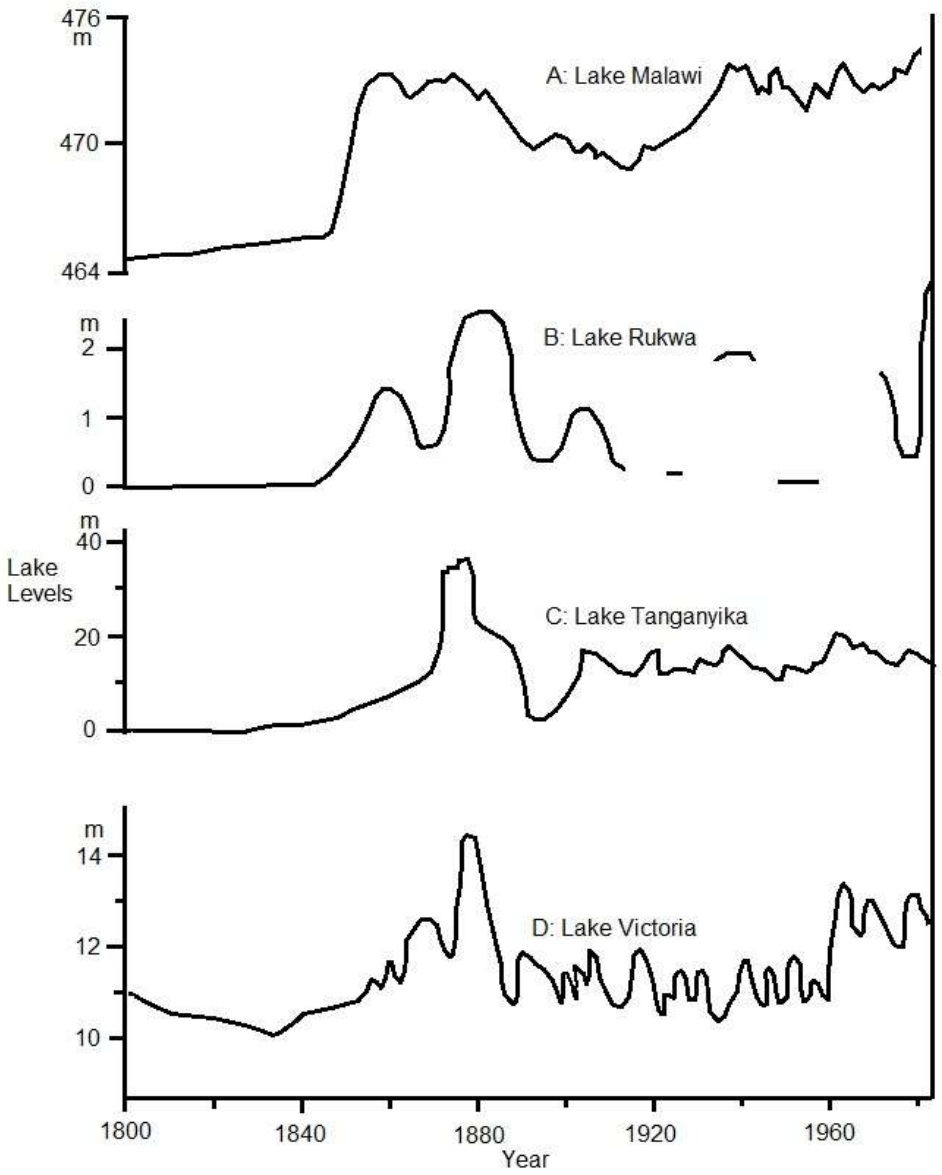

Figure 3: Lake levels fluctuations of major lakes in Tanzania from the 1800 to 1980

Lake Victoria- it is redrawn from Nicholson, 1998 where data source are historical data (pre-1900) and modern measurements (post 1900). For Lake Tanganyika, it is redrawn from Nicholson, 1999 and source of data are historical and geographical information (pre-1900), early rainfall records (1902-1921) and modern records (post-1921). The scale is in meters above modern gauge height. For Lake Rukwa, it is redrawn from Nicholson, 1999 and data source are historical and geographical information (pre-1840), proxy data (1840-1960) and modern lake records (post 1970). Lake Malawi-redrawn from Nicholson, 1998 and data source are historical and geographical information (pre-1845), proxy data (1845-1896) and modern lake records (post 1896).

(viii) Period from 1900 – Present

The twentieth century was characterized by variable precipitation with increased temperature. From the beginning of the century to around 1920, the high precipitation was recorded through high lake levels in East Africa (Zinke *et al*., 2009). In Lake Victoria, the major peaks in the early 20th century were recorded between 1903-1907 and 1916-1918 through gauge measurements (Conway, 2002). From 1920s to 1960s, most of the major lakes of Tanzania were at low levels characterized by minor fluctuations (Fig. 3). Remarkable low precipitation period was recorded between 1940 -1950 evidenced by low stands in most of the lakes in East Africa (Zinke *et al*., 2009).

The 1960s precipitation was a high rainfall event in East Africa and extended across the Indian Ocean (Stager *et al*., 2005; Zinke *et al*., 2009). In Tanzania, lake levels responded immediately after the 1960s precipitations. This is well reflected in Fig.3 particularly through Lakes Victoria and Tanganyika. In Lake Victoria, the peak was reached in 1964 (Conway, 2002) whereas in Lake Tanganyika it was reached in 1965 (Nicholson *et al*., 1999). As the rains started early in 1960s, the peaks suggest that the high rainfall period persisted for not less than 5 years. Despite of having other peaks in Lake Victoria towards the end of the 20th century, particularly in 1978-79, 1990-91 and 1997-98, the 1960$_s$ precipitation is recorded as the highest peak of the century in Lake Victoria (Stager *et al*., 2005).

The 1997-98 high precipitation event has been documented in many locations in East Africa (Conway, 2002; Kayanne *et al*., 2006; Zinke *et al*., 2009). The East Africa lakes and streams responded to this precipitation. Stream flooding associated with major economic impacts such as infrastructure destruction occurred in all eastern Africa countries including the countries in the Horn of Africa. This event together with the 1960s event was related to changes in ENSO with the strong SST anomalies being developed in Indian Ocean causing unusual SST gradient (in reverse ways) that led to disruption of the normal wind trends.

2.6 El Niño and La Niña

El Niño and La Niña result from variation in temperature between the ocean and atmosphere in the east-central Equatorial Pacific. It is basically a deviation from the normal surface sea temperature. Both events; El Niño and La Niña which are the warm and cold events of ENSO respectively occur irregularly creating small to large scale impact on weather and climate. Globally, ENSO events have been known to control inter-annual climate variability in many countries (WHO, 1999; Cole *et al*., 2000; Moy *et al*., 2002). Holocene climate records

indicate that frequency of occurrence of El Niño which is commonly associated with extreme events such as flood and drought is 2-8 yrs (Moy *et al*., 2002). This is in agreement with WHO report (WHO, 1999) which indicated El Niño frequency interval of 2-7 yrs. However, each event exhibit unique characteristics in terms of duration and intensity (WHO, 1999). For instance, East Africa records from 1975 indicate that El Niño was strong in 1982/83, 1997/98 and 2014/15 (UNOCHA, 2016). This frequency of occurrence of strong El Niño (recurrence interval of about 15 years) is high compared to La Niña which was strong in 1988/89 (UNOCHA, 2016) in the last 42 yrs.

2.7 Holocene Fluoride Variation in Ice Cores

Water chemistry is dynamic being controlled largely by anthropogenic activities and climatic variability of precipitation and temperature (Varni *et al*., 2013; Lutz *et al*., 2015). Fluoride is among the natural contaminant in water systems which varies with climatic conditions (Opdyke *et al*., 1993; De Angelis & Legrand, 1994; Thompson *et al*., 2002). Arid to semiarid areas of northern Africa and Eastern Africa particularly countries crossed by East Africa Rift system are among the areas with high fluoride in water systems (Ali *et al*., 2016; Malago *et al*., 2017). As discussed previously, there has been transition from freshwater to saline water and vice-versa in various lakes of Tanzania particularly small lakes throughout the Holocene period. To what extent fluoride was concentrated in sediments and ice cores with changes in climate conditions and its implication is discussed in this section using the available limited data.

Lake sediments and ice cores are likely places where preservation of fluoride signals in response to climatic changes are expected to take place. The Holocene record of fluoride variation in Tanzania has only been documented from the Mt. Kilimanjaro ice core (Fig. 4). Because fluoride has affected human kind and animals, it is important to find out the levels of fluoride over time and estimate its contribution to current levels in lacustrine environments, particularly in the lift lakes.

The Kilimanjaro ice core record showed a general declining trend with time with some enrichment of fluorine during the dry phases such as the 8.2, 5.2, 4 and 2.2 ka dry events (Thompson *et al*., 2002) (Figs. 2 and 4). High levels of fluorine during the dry events could be a result of deposition of dust from lake surfaces that previously had trona deposits (Kaseva, 2006). The general decrease in F from early Holocene to late Holocene (Fig. 4)

suggest that an increase in precipitation and warming during early Holocene could have reduced availability of dust.

However, a study by De Angelis & Legrand (1994) using Greenland firn and ice core revealed that volcanic events have great influences in regulating F through rock composition and gas emissions. Their study indicated that the peak fluoride values correspond with the major volcanic events. Such volcanic activities (active and dormant) are common in Tanzania, along the East Africa Rift System, releasing alkaline volcanic materials rich in fluorine and volcanic ashes with gases such as HF particularly in the northern parts around Mt. Kilimanjaro, Meru and Oldoinyolengai. However, existing records do not show any major volcanic eruption during the Holocene thus, precluding the possibility of volcanic eruption as a cause of the observed variation in fluoride distribution in the two ice cores from Mount Kilimanjaro.

Based on the above facts, elevated F in Kilimanjaro Ice core around 8.2 ka may indicate high input of F from dust materials (trona) as explained previously or addition of F through dust and ashes which could have been triggered by local volcanic activities around Mt. Kilimanjaro and Meru, northern Tanzania. Although there is limited Holocene historical records of volcanic activities over these mountains, emission of gases and volcanic materials rich in F have been documented as the source of high fluoride in water systems in surrounding areas (Nanyaro *et al*., 1984; Ghiglieri *et al*., 2010, 2012). High fluoride in ice core around 8.2 ka was concomitant with decline in lake levels in other lakes of Tanzania as well as in the northern Hemisphere (Thompson *et al*., 2002; Barker *et al*., 2003, 2007; Rohling & Pälike, 2005; Zalasiewicz & Williams, 2009). In northern Tanzania, one among the areas dominated by fluorine rich materials, decline in lake levels could have been accompanied by enrichment of F^- in lakes resulting from evaporation-crystallization circles as F^- tends to concentrate in lakes in the rainy period through runoff and precipitate as trona in the dry periods (Kaseva, 2006).

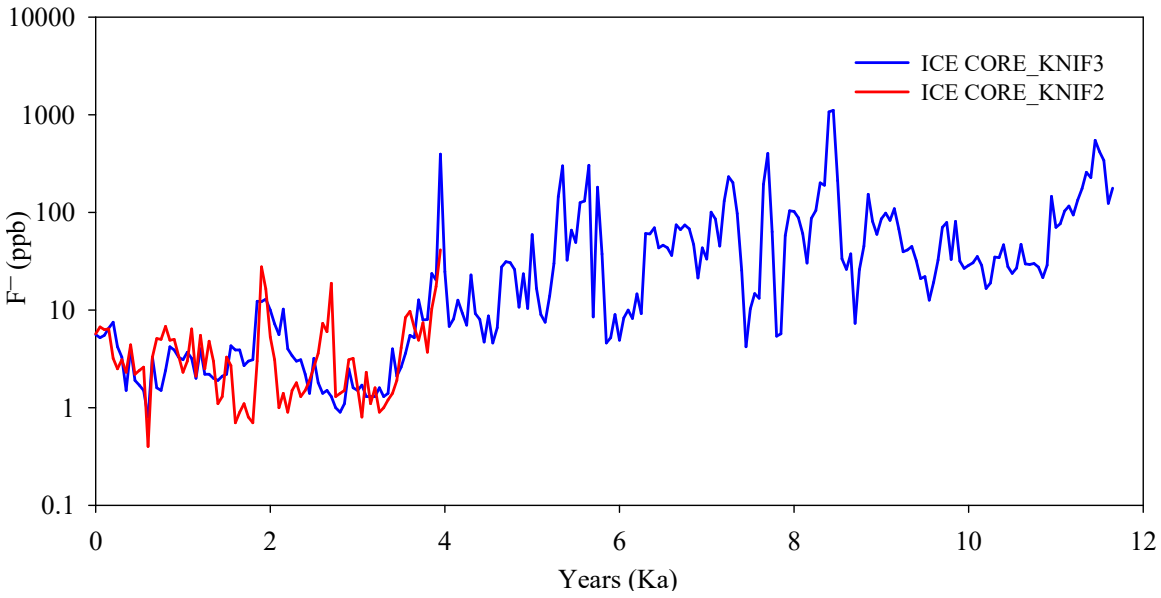

Figure 4**: Fluoride variation in the Holocene period. Data are from Mt. Kilimanjaro Ice core (After Thompson, 2002)**

From 4 ka to present, records from Kilimanjaro ice core indicate that there is decrease in F relative to post 4 ka Holocene period (Thompson *et al*., 2002) which could be attributed to changes in temperature and precipitation as discussed previously. However, it was intermittently high between 3-2 Ka (Fig. 4) due to aridity in this period probably influenced by addition of F through dust as discussed previously. In general, it is hypothesized that decrease in F from 4 ka to present is likely to be controlled periodically by short dry-wet periods. That, in dry period, there is formation of trona which is rich in F as discussed previously. For instance, under the current global increase in temperature, within a period of about 33 yrs only (1984-2017), fluoride in Lake Momella, northern Tanzania varied from 690 mg/l (Nanyaro *et al*., 1984) to 1410 mg/l (Malago *et al*., 2017). However, there are no intra F records in this period that could provide the general trends as well as the relationship with weather and climatic conditions. Such findings are in close agreement with the recent study by Jirsa *et al*. (2013) in Lakes Nakuru and Bogoria, Kenya, which showed enrichment of F during the low lake levels. Thus, for proper evaluation of fluoride with climate, timing of volcanic events need to be integrated with other climatological factors.

2.8 Conclusions and Recommendations

Limited terrestrial and marine proxies in Tanzania have been used to reconstruct palaeoclimate from the late Pleistocene to present. The major pronounced events were found to be linked with global events. The first event was the Last Glacial Maximum (LGM) in the late Pleistocene. This was the period of extensive aridity in the late Pleistocene-present records with some shallow Lakes such as Victoria being completely dry. This period was followed by the humid period with high precipitation which continued to early Holocene but being interrupted by a brief cool and dry Young Dryas (YD) period around 13-11.5 ka. The early Holocene was generally marked by high precipitation with a brief cool and dry period at 8.2 ka. The mid Holocene between 8-4.5 ka was a cool period with high rainfall but relatively lower than early Holocene precipitations. This period was interrupted by a brief cooling event at 5.2 ka. The termination of the humid mid-Holocene period was marked by the global dry event at 4 ka.

Integrated proxies showed a general decrease in precipitation from the Late Holocene to present with the pronounced aridity between 3-2 ka and 1.2-0.5 ka. Remarkable high precipitation in the late Holocene was recorded between 1.7-1.2 ka, LIA-a cool period (~0.5-0.1 ka) and the late period of the 20th century. In the 20th century, a century with increased temperature, Tanzania and East Africa in general experienced high precipitation in the early and late periods of the century with low precipitation in the mid of the century around 1940-1960s. The 1960s and 1997/98 rainfall were recorded as the major high precipitation events in late period of the 20th century. Between these two events, there is a general decline in Lake levels and hence, low rainfall with exception of few periods between 1978-79, 1982/83 and 1990-91. The 1960s and 1998 events are related to changes in ENSO.

Record in the variation of fluoride concentration during the Holocene period is scanty. The available record from Mount Kilimanjaro showed higher levels of fluoride levels during the early Holocene relative to late Holocene and this could be attributed to reduction in dusty availability. Peak fluoride values were found to correspond with dry events (8.2 and 4 ka) indicating that cool and dry conditions are associated with formation of F-rich trona lake deposits which are sources of dust.

By integrating the Holocene proxies, it is likely that the heat and moisture budget responsible for precipitation as well as temperature patterns are linked with the Northern Hemisphere Insolation. Thus, the hydrological circle linking the Indian Ocean SST with the atmosphere

which connects the high and low latitudes accounts for rainfall variations in Tanzania. However, the ITCZ plays its role by modifying the intensity of seasonal winds. It is still difficult to predict accurately the future climate changes in Tanzania due to insufficient records with high resolution. High resolution records from the Indian Ocean, major lakes and eastern arc mountains in conjunction with records from small lakes and river basins are needed for proper reconstruction of palaeoclimate in Tanzania. Because of different climatic zones in Tanzania, the available data which are concentrated in specific areas and are not well distributed do not fully represent the whole country. There is a need of more palaeoclimate studies which are widely distributed based on climatic zones. Potential areas that are not well researched include small lakes; these are very sensitive to climate changes, river basins, tropical and equatorial forests. Geographically, more palaeoclimate studies are needed in the central parts of Tanzania, a climate zone which is very poorly represented. In relation to fluoride, research works are still needed on fluoride during the Holocene. Studies should focus on the temporal variation of fluoride and how former deposits could cause concentration of fluoride in groundwater and lakes. In general, there is a need of promoting climate change studies using multi-proxies in Tanzania for projection of future climate and resolving existing conflicting records such as the records during the Little Ice Age and records from the Eastern Arc Mountains.

CHAPTER THREE

GEOCHEMICAL EVALUATION OF VOLCANOGENIC MATERIALS AROUND MT. MERU AREA, NORTHERN TANZANIA: IMPLICATIONS FOR FLUORINE SOURCE, MOBILITY AND CONTAMINATION OF GROUNDWATER SYSTEMS[2]

Abstract

Water-rock interaction study involving rocks, soil and water was undertaken to assess the possible source of high fluoride concentration, its mobility and eventually contamination of groundwater systems in Arumeru district. Results indicated that magmatic rocks are cogenetic, subalkaline to alkaline in nature that ranges from mostly silica under saturated to silica saturated. Volcanic rocks are weakly to moderately fractionated with variable compositions that span from foidite to andesite. Petrographic examination indicated the presence of at least four minerals that are known to incorporate fluorine (F) in their lattice structures. In order of decreasing abundance, these minerals include: sphene, hornblende, apatite, and biotite. These results indicated that fluorine occurs in all rock types in varying amount that ranges from 251 to 19 122 mg/Kg (mean = 3921 mg/Kg, n=68) and that andesitic rocks contain the highest amount than the other rock types (mean = 7133 mg/Kg, n=13). This may suggest that F is largely incorporated during late crystallization process. Based on rocks and equivalent soils, fluorine was higher in rocks than equivalent soils at the ratio of 3:1. In general, distribution of F is largely controlled by parent material, texture of the parent material, geomorphology and soil types. Overall, unlike the springs where short water-rock contact time limits dissolution of fluorine, the amount of fluoride in well waters correlated well with fluorine in the rocks and/or soils proximal to the well. In leeward Momella lakes where fluoride is above 1000 mg/l, fluorine results in surrounding rocks (mean=2759 mg/Kg, n=3) and soils (mean=4590 mg/Kg, n=2) suggest other mechanisms for enrichment of fluoride in those lakes. Further studies on fluoride enrichment in leeward lakes, leaching experiment for all rock groups and microprobe analyses of the suggested fluorine bearing minerals are recommended.

[2]This manuscript is under review in the Journal of African Earth Sciences (Elsevier). Manuscript ID: AES6760

3.1 Introduction

Fluoride as a natural pollutant in water lowers the quality of water for domestic purpose in many countries. It can therefore be considered as one among the bottlenecks for the country not achieving the Millennium Development Goals (MDGs), particularly goal No.7, which focused on provision of adequate and safe water to people (UNICEF, 2015). Globally, major fluoride provinces are associated with geological settings, with igneous rocks as the major source (Nanyaro *et al*., 1984; McCaffrey, 1998; Chae *et al*., 2006; Pittalis *et al*., 2010; Rango *et al*., 2010; Naseem *et al*., 2012; Hallet *et al*., 2015; Ali *et al*., 2016). The major provinces are the geothermal zones and the rift zones associated with volcanic activities such as the East Africa Rift System (EARS), the volcanic belts such as the western United States, New Zealand, France, Algeria and Tunisia. Others include crystalline basement rocks of granitic composition such as the basement aquifers of India and Sri Lanka, and the sedimentary aquifers in the semi-arid regions such as La Pampa Province of central Argentina (Edmunds & Smedley, 2005).

The EARS is associated with many volcanic activities including the active volcanoes on Mt. Oldoinyo Lengai, northern Tanzania, resulting from continental break-up. All the countries which are linked with the EARS (e.g. Tanzania, Kenya, Uganda and Ethiopia) are facing dental and skeletal fluorosis, particularly in the areas around the rift valley (Gaciri & Davies, 1993; Pittalis *et al*., 2010; Rango *et al*., 2010; Thole, 2013). Arumeru District of Arusha, Tanzania is among those areas that are studded by volcanic materials derived mainly from active Mt. Meru. These materials have been documented as the main source of high fluoride in groundwater system in this area (Nanyaro *et al*., 1984; Ghiglier *et al*., 2010, 2012).

Within volcanic rocks, fluorine bearing suites vary significantly. For instance, Ghiglieri *et al*. (2012) reported high fluorine from pyroclastic and ash materials. Rango *et al*. (2010) pointed out felsic rocks (commonly rhyolite) as the source of fluorine while studies by Chae *et al*. (2006) and Naseem *et al*. (2010) indicated that the intrusive equivalent of rhyolite (granites) are the main source of fluorine in groundwater systems. In Tanzania, these granites are known to be the source of fluoride in waters within and around the Tanzania Craton which is out of the EARS. Review of fluorine source summarized by McCaffrey (1998) indicates that fluorine is more favored in alkaline and granitic rocks than intermediate to mafic rocks. Continental rift rocks are generally alkaline in nature (Gaciri & Davies, 1993; Peccerillo *et al*., 2007; Pittalis *et al*., 2010; Ghiglieri *et al*., 2012) but have not been assessed intensively

for their fluorine content. The most common fluoride-bearing minerals in igneous systems include fluorite (CaF_2), micas [$K(Mg,Fe)_3AlSi_3O_{10}(F,OH)_2$], hornblende [$Ca_2(Mg,Fe)_4Al(Si_7Al)O_{22}(OH,F)_2$], apatite [$Ca_5(PO_4)_3(Cl,F,OH)$], cryolite ($Na_3AlF_6$), topaz [$Al_2F_2(SiO_4)$] (Chae *et al*., 2006, Naseem *et al*., 2012). However, since there are other many fluoride bearing minerals which not common but can accommodate high F (e.g titanite: $CaTi[SiO_4](O,OH,F)$) (Hallet *et al*., 2015), systematic petrographic is required for effectively assessment of fluorine bearing minerals along the East Africa rift system. This should be done systematically with consideration that there are other F addition mechanisms other than minerals such as exsolution of fluids/vapor phase from magmas that are rich in volatiles such as SO_2, HCl, H_2O-vapor, halides (including F) etc.

Most researches in Arumeru fluoritic zone and East Africa in general, have been largely focusing on fluoride content in water systems and its effect in the community (Nanyaro *et al*., 1984; Gaciri & Davies, 1993; Malago *et al*., 2017), but few studies have attempted to establish the relationships between fluoride content of groundwater and that of the surrounding rocks and/or soils. A study by Ghiglieri *et al.* (2012) partially indicated the relationship between high fluoride in water and fluorine content in rocks. Their study was restricted in the northern part of Mt. Meru and the findings suggest that volcanic ashes are the major source of fluorine. Similar studies have not been done in the southern part of Mt. Meru where fluoride is also a critical problem. Also, the rock groups identified by Ghiglieri *et al.* (2012) are general rock groups; their study could not focus on specific rock type and its implication to fluorine generation. Furthermore, the work of Roberts (2002), which reported on geochemical and volcanogenical evolution of Mt. Meru did not address the issue of fluoride. In general, despite of large spatial variation of fluoride in Arumeru district and East Africa in general (Nanyaro *et al*., 1984; Gaciri & Davies 1993; Fawell *et al*., 2006; Kaseva 2006; Ghiglieri *et al*., 2010, 2012; Pittalis, 2010; Thole 2013, Vye-Brown *et al*., 2014; Malago *et al*., 2017) and very high fluoride (up to thousands mg/l) in lake Momella and 50-80_s mg/l in some dug wells (Malago *et al*., 2017), there is no detailed study that has been conducted in the region specifically to assess sources of fluoride. Source rocks, fluoride bearing minerals, mineral distribution in relation to rock genesis are poorly known.

Weathering processes control the release of fluorine from parent rocks to soils. The processes are primarily controlled by parent rock composition, texture, and temperature and moisture content/available water (Easterbrook, 1999). In areas such as Arumeru district where rock types and texture, temperature and precipitation vary significantly (Wilkinson *et al*., 1983,

1986; Roberts, 2002), these factors become important in assessing the release of F from these rocks. Mobility of elements within the soils and from soils to groundwater is a complex process controlled by many factors. These include soil type, soil texture, soil pH, organic matter content, metal oxides and the concentration of a particular element (McCaffrey, 1998; Smedley & Kinniburgh, 2002; Wang *et al*., 2002; Deverel *et al*., 2012). For instance, F^- can be partially removed from the solution by clay minerals (Senior & Sloto, 2006). Therefore, detailed and effective evaluation of F^- mobility becomes difficult in areas with intensive variation of the mentioned controlling factors. However, sampling of rocks, soil and water which are close to each other can lead to a general understanding on fluoride mobility. In Arumeru district, the observed large spatial variation of F^- is likely to be controlled by the factors affecting mobility of elements as discussed previously. There is no any study that integrates rocks, soil and water as an attempt to evaluate fluoride mobility in the area.

From the above point of view, the specific sources of fluoride and processes of fluorine mobility and contamination and the link with the heterogeneity of lithologies have not been systematically studied. Therefore, the general aim of this study was to undertake geochemical evaluation of the rocks and associated soils as an attempt to assess fluorine sources and its mobility from rocks-soil-groundwater system. Specifically, the study aimed to: 1) infer rock genesis and the associated magmatic processes; 2) examine possible rocks associated with fluorine, and identify fluorine-bearing minerals and their distribution; and 3) assess mobility of fluorine from rocks-soils-groundwater.

3.2 Methodology

3.2.1 Study area

The study area is about 2500 km^2 in Arumeru district, northern Tanzania (Fig. 5). It is basically a part of eastern branch of East Africa Rift Valley with the active Mt. Meru (4565 m a.s.l), being one of the active volcanic mountains dividing the major part of the area into windward and leeward sides. The other covered part is the low altitude zone (~900 m a.s.l), the southern part of the study area (Makiba, Bwawani and Mbuguni) (Fig. 5). Mt. Meru plays major role in controlling and regulating climatic condition of the area. The windward side exhibits high rainfall (~1000 mm/yr) whereas the leeward side and the low altitude areas exhibit low rainfall generally less than 500 mm/yr (Oettli & Camberlin, 2005). Steep slope over Mt. Meru cause high temperature gradient which decreases rapidly with altitude.

Generally, the mean temperature in a year varies between 20 to 29 ˚C within the district (Ghiglieri *et al*., 2010).

Geologically, the area is part of volcanic provinces along the EARS with Mt. Meru as a major source of volcanic materials. Volcanic activities at Mt. Meru have led to accumulation of different volcanic materials in the study areas over time, with the latest materials representing the l910 volcanic eruption (Wilkinson *et al*., 1983, 1986; Roberts, 2002; Ghiglieri *et al*., 2010, Vye-Brown *et al*., 2014). The geology is complex, and materials are too erratic probably of explosive nature of volcanic activities. For this reason, many researchers (Wilkinson *et al*., 1983, 1986; Nanyaro *et al*., 1984; Roberts, 2002; Dawson, 2008; Ghiglieri *et al*., 2010; 2012), with most of the works focusing on fluoride in water systems, documented different volcanic materials largely based on volcanic groups. The major units identified and documented by Wilkinson (1983) include lahars of various ages and groups, nephelinitic to phonolitic lavas, basaltic lava, pyroclastic ashes and scoria, volcanic tuffs and breccias, and parasitic cones of basic to alkaline lava (Fig. 5). Recent sediments are represented by alluvial sediments, lake deposits and calcareous sediments being controlled by the morphology and drainage network (Fig. 5).

Soil distribution in the area is controlled by the rock types and the morphology. Reddish brown soils derived from undifferentiated volcanic units dominate in the south-western part (Fig. 5). Also, based on field observations, grayish soil with variable grain size from clays to pebble size dominates in areas covered by lahars such as Leguruki- Kingori -Kikatiti-Maroroni, whereas transported soils (clays to sands) dominates in flat and low altitude areas such as Makiba-Bwawani and Mbuguni. Transported soil (clay and organic matter rich sediments) occur in small patches in depression areas.

Local communities in Arumeru district are affected by dental and skeletal fluorosis as a result of high fluoride levels in drinking water, which are beyond the recommended Tanzania standard of 4 mg/l and also above the recommended WHO standard of 1.5 mg/l (WHO, 2008). Fluoride in water system is largely a result of dissolution of fluorine rich rocks (Nanyaro *et al*., 1984; McCaffrey, 1998; Chae *et al*., 2006; Rango *et al*., 2010; Naseem *et al*., 2012; Hallet *et al*., 2015; Ali *et al*., 2016). Thus, high level of fluoride in the study area is an indication of high fluorine in source materials. However, dissolution is highly controlled by integrated factors including temperature, moisture content, structure and texture of the rocks and soils. Therefore, for effective evaluation of fluorine source rocks, dissolution and

mobility to groundwater system, factors like rainfall and temperature variation, land morphology, rock and soil properties need to be evaluated and integrated together.

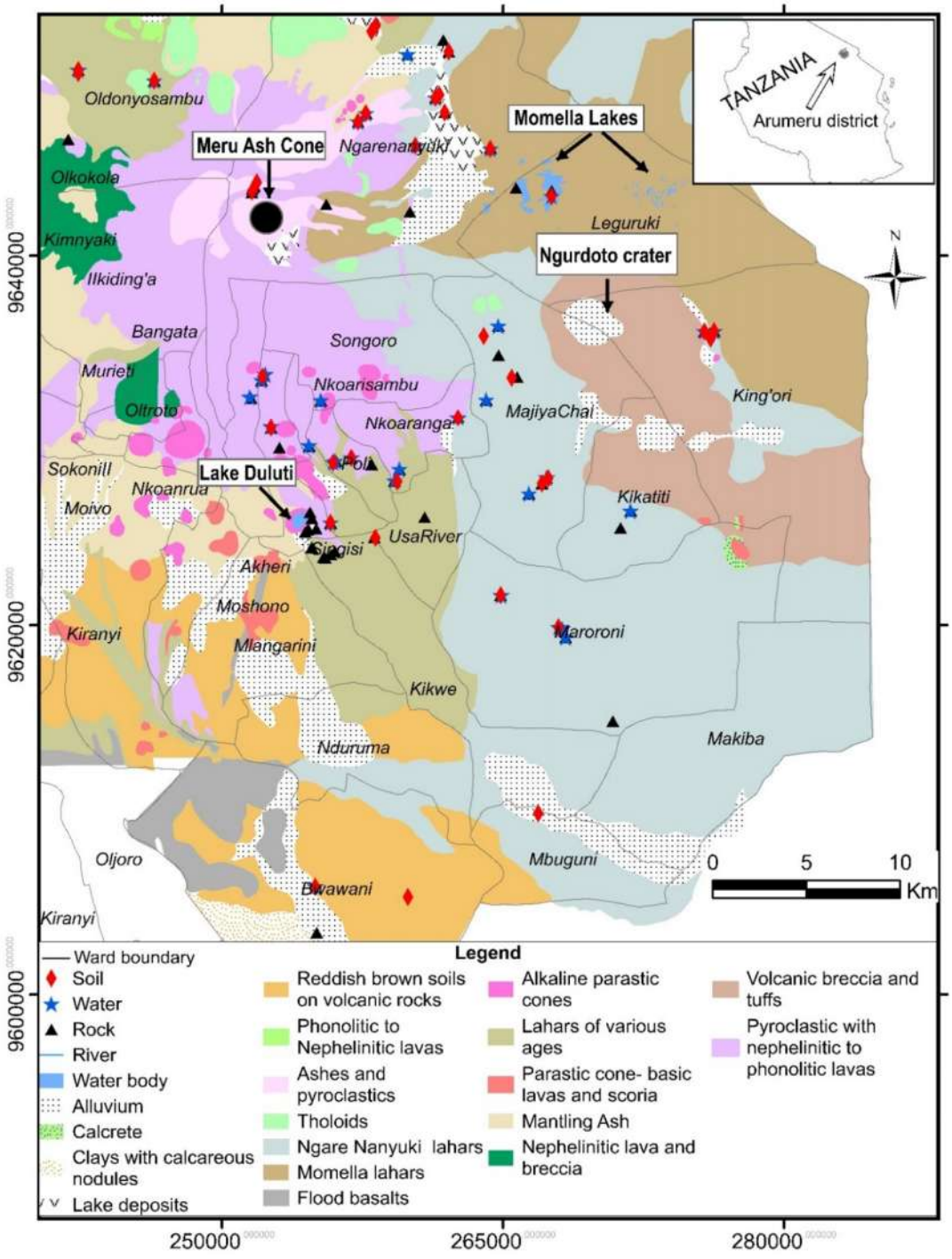

Figure 5: Simplified geology map of Arumeru District showing the location of rocks, soils and water samples taken for rock characterization and assessment of fluorine dispersion mechanisms in the study area (modified after Wilkinson, 1983).

3.2.2 Fieldwork

A total of 67 rock samples, 32 soil samples and 34 water samples presented in Fig. 5 were collected in 2015. In order to get representative rock samples that will address the desired objectives, sampling criteria was governed by rock type, rock group (lava flow or lahars) and proximal groundwater sources (dug wells, springs and boreholes). The target was to collect fresh samples as possible, its equivalent weathered samples and soils but in most cases depending on the field conditions, rocks and equivalent soils or residual soils were sampled. In few cases where different rocks were outcropping at the same point, more than one sample was collected to get the representative of each rock types. Each rock sample was represented by 3 to 5 Kg, enough for geochemical and petrographic analyses.

Most of the soil samples were collected at a depth of about 30 cm from the surface which is the recommended depth for assessing dispersion of element from the regolith (Miller & Donahue, 1990). Selection of soil sampling locations was based on criteria and priorities such as: residual soils proximal to its source/parent rock, the availability of groundwater sources, and type of soils. However, few soil samples were only collected in areas where the above criteria were not met. The considered soil types/groups with the number in brackets were the residual soils (25) for assessing their interaction with water and parent rocks, typical alluvial soils (2) taken as deposits on river banks, lacustrine soils (2) representing interaction with lake water, and transported soils (2) mostly composed of very fine sediments with organic matter representing the composition of transported materials. About 3 Kg of each soil sample was collected, dried and sieved before taken to laboratory for geochemical analysis.

Collection of water samples aimed to assess mobility and dispersion of fluorine from rocks and soils to groundwater system. As a result, groundwater samples (mostly springs and wells) were highly considered in this sampling. The number of springs were 20; 13 from the windward side and 7 from the leeward side. The total number of wells was 12 and the stagnant water bodies were represented by 2 lake samples.

To assess rock genesis, 25 rock samples (37% of all samples) that were found to represent lava flow were considered. To assess water-rock interaction that is based on fluorine mobility and dispersions, all samples were categorized into 5 groups as: Group 1 (rocks and equivalent soils, 8 paired samples), group 2 (soil and proximal groundwater sources; 6 paired samples), group 3 (rocks and proximal groundwater sources, 13 paired samples), group 4

(rocks and proximal/immediate spring water sources; 20 paired samples and group 5 (rocks, equivalent soils and groundwater, 5 tripled samples).

3.2.3 Analytical work

Analytical work in this study involved whole-rock geochemical analyses, analyses of soils and water samples, petrographic examination of representative samples. In these analyses, much emphasis was put on total F content on each material.

(i) Geochemical analysis of rocks and soils

Analyses of rocks and soils were carried out at the Geological Survey of Tanzania (GST), Dodoma using X-ray fluorescence spectrometry (XRF) method. Analyses were specifically on whole-rock geochemical parameters (SiO_2, TiO_2, Al_2O_3, Fe_2O_3, MnO, MgO, CaO, K_2O, ZnO, BaO, P_2O_5 and Loss on Ignition (L.O.I)) and trace elements (F, Cl, S, V, W, Sr, Rb, Cu, Cr, Y, U, Pb, As, Ni, Nb and Ag). LOI was conducted using standard procedures by heating about 1g of the powdered sample for one hour at 950 ˚C. Measurements of other analytes with exception of fluorine were done with the aid of Energy Dispersive X-Ray Fluorescence (ED-XRF) using pressed powder without binder technique. Accuracy and precision were checked using the standard reference materials and duplicates. At least one out of every 12 samples (1:12 ratio) was used as duplicate. For the major oxides, results were estimated to better than 10% indicating that analysis was generally fair.Unfortunately, fluorine which was among the main target elements could not be detected using XRF. This could be attributed to its low atomic number as the method is suitable for elements with high atomic number (Alloway, 1995). Therefore, a special method as described below was used to determine total fluorine in rocks and soils.

(ii) Total fluorine analysis in rocks and soils

All rock and soil samples (99 in total) were analyzed for total fluorine. Sample preparation was carried out at GST, Dodoma and final measurements were done at the Nelson Mandela African Institution of Science and Technology (NM-AIST). The powdered rocks and soils (~80 microns) samples used in XRF, were used for total fluorine analyses. In general, there is no specific method for determining total fluorine in rocks; several analytical methods are available and are largely depending on the chemistry of the rocks. In this study, a modification of the method developed by Ingram (1970) was used. This method has been applied successfully in determination of total fluorine in rocks (Hallet, 2012).

About 0.2 g of each sample was weighed and then mixed thoroughly with 1 g of Na_2CO_3 and 0.2 g of ZnO in a platinum crucible and then placed in a furnace at 950 ˚C for 90 minutes. The crucibles were then removed from the furnace and immediately upon cooling the samples were transferred to a Teflon beaker (200 ml). The crucibles were washed effectively with de-ionized water into the beaker. To ensure no any sample materials left on crucibles, the latter were further rinsed in the Teflon beaker by using de-ionized water, which was then covered by plastic lid and subjected to hot plate where heating took place slowly for 11 hrs. These beakers were then removed from the hot plate and all crucibles were washed thoroughly with de-ionized water. Thereafter, the solutions were passed through a 40 µm filter paper into 200 ml volumetric flask. The filter papers were then washed down with 0.1M Na_2CO_3 solution followed by addition of 2 ml of 50% HCl. The obtained final solution was shaken well; the volume was measured and recorded accurately. Data quality assessment was conducted by using the duplicate samples where one sample out of 15 samples was used as a duplicate sample.

Fluoride analyses were done at the NM-AIST laboratory using the Fluoride Ion Selective Electrode (FISE) by extracting 10 ml from the prepared rock and soil solutions. Fluoride standards of 1 mg/l and 10 mg/l were used to calibrate the instruments and accuracy of calibration was tested using water sample with known concentration and the solution that were used in calibration. For each sample, 5 ml of the solution was mixed with 5 ml of Total Ionic Strength Adjustment Buffer (TISAB II) with CDTA for measurements. For more accuracy, two portions from each solution were prepared and the average results were recorded. Sample weight and volume of the solutions were used to calculate total fluorine in each sample of which the results can be expressed in mass per unit mass or percentage. Fluoride in water was analyzed immediately within 3 days after sample collection using similar procedures as for the solutions from rocks and soils.

(iii) Petrography

Out of 67 rock samples, 19 samples were selected for petrographic examination based on amount of fluorine in rocks, rock types and physical texture. This petrographic study focused mainly on (a) identifying mineralogical compositions of the rocks and fluorine bearing minerals (all 19 samples were used) and (b) mineralogical composition and rock texture for inferring the general history of volcanic rocks and associated magmatic processes (5 rock samples which represent lava flow were used). Thin section preparations were done at GST

and mineralogical study was conducted at the Department of Geology, University of Dar es salaam.

3.3 Result

3.3.1 Chemical composition of the rocks

Chemical compositions of individual rocks are presented in Appendices 2 and 3. In this section, chemical composition of the rocks is presented in two sets that differentiate lava flow from other materials such as lahars and well materials. Composition of lava flows (n=25) which represent pure volcanic rocks is presented in Fig. 6 whereas chemical composition of other rock materials (n=42) is presented in Fig. 7. Plot of pure volcanic rocks (lava flows) on total alkalis versus Si diagram indicate that the rocks exhibit variable compositions ranging from silica under-saturated (e.g., foidite) to silica saturated such as basalt, andesite and one sample with a dacitic affinity (Fig. 8). To some extent all rocks have been affected by hydrothermal alteration. Alteration is high in lahars and well materials as reflected by high Loss on Ignition (LOI) which is 3.5% (Fig. 7). LOI is relatively low in lava flows with the mean value of 1.65% (Fig. 6).

Lava flows were further characterized using Harker diagrams (Figs. 9-11). When plotted on Harker diagrams that involve CaO, TiO_2 and Fe_2O_3 versus SiO_2, these rocks exhibit a negative correlation at 95% confidence level, consistent with fractional crystallization of ferromagnesian minerals (Fig. 9). Only a scatter plot of SiO_2 vs Al_2O_3 showed a reverse trend (positive correlation) which is also supporting fractional crystallization sequence (Fig. 9f). The alkali-element values (K and Na) are generally scattered (Figs. 9a,b). Such scattering is considered as a result of alkali-element leaching and resulting micaceous/clay alteration. A scatter plot of SiO_2 vs trace elements As, V and Sr displayed a significant decreasing trend (Fig. 10a, c, d) while Rb correlated positively with SiO_2 (Fig. 10b) at 95% confidence level. Inter-element plots of TiO_2 vs selected major oxides (CaO, Fe_2O_3) and trace elements (As, Cu, V and Y) displayed significant positive correlations at 95% confidence level (Fig. 11).

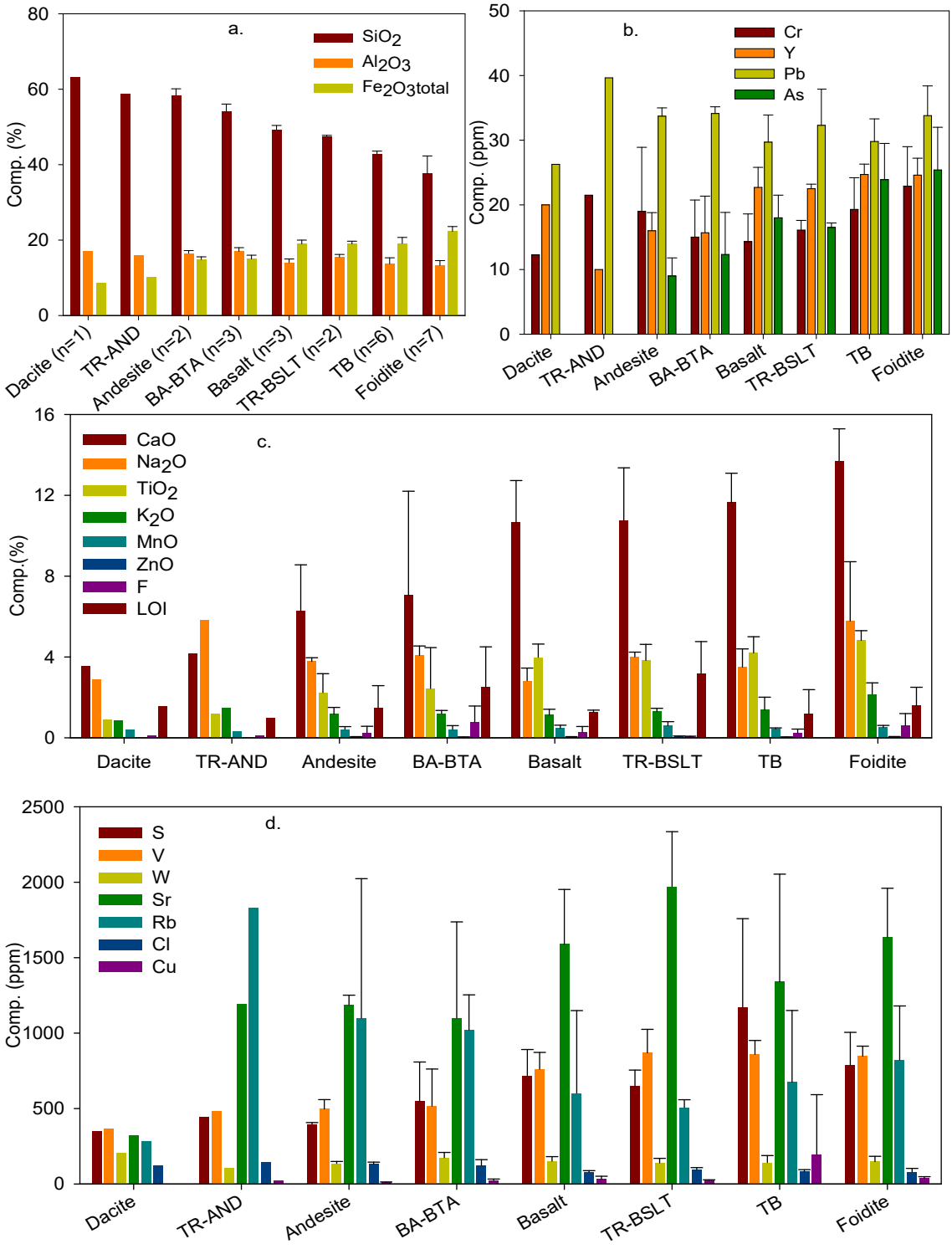

Figure 6**:** Major and trace element composition of volcanic rocks (lava flows) around Meru volcanic complex. TR-AND: Trachy-andesite, BA-BTA: Basaltic andesite to basaltic trachy-andesite, TR-BSLT: Trachy-basalt, TB: Tephrite basanite

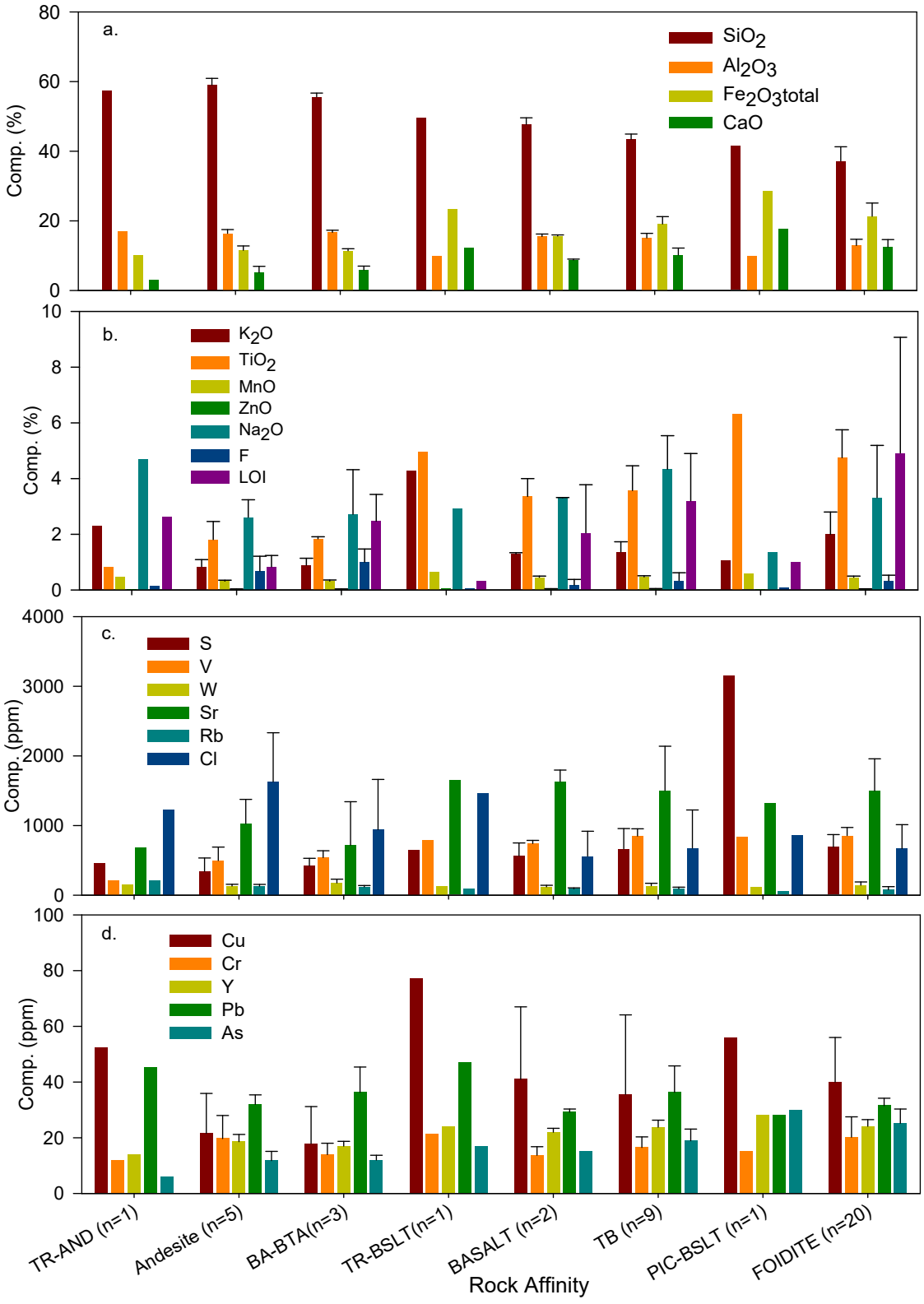

Figure 7: Major and trace element composition of Volcanic materials (lahars and well materials) around Meru volcanic complex. Abbreviations are as stated in Fig. 6.

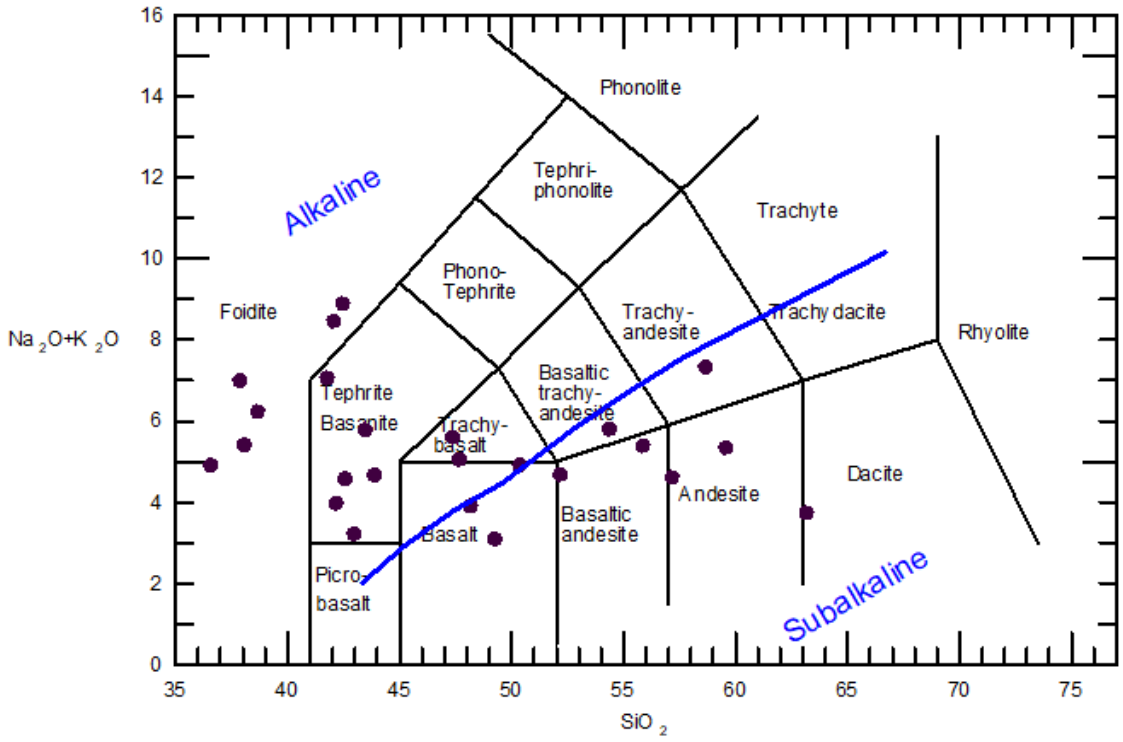

Figure 8: Total alkali versus silica (TAS) diagram used to discriminate volcanic rocks at the study area (After Le Bas. 1986) with a line dividing alkaline and subalkaline fields (After Irvine and Baragar, 1971).

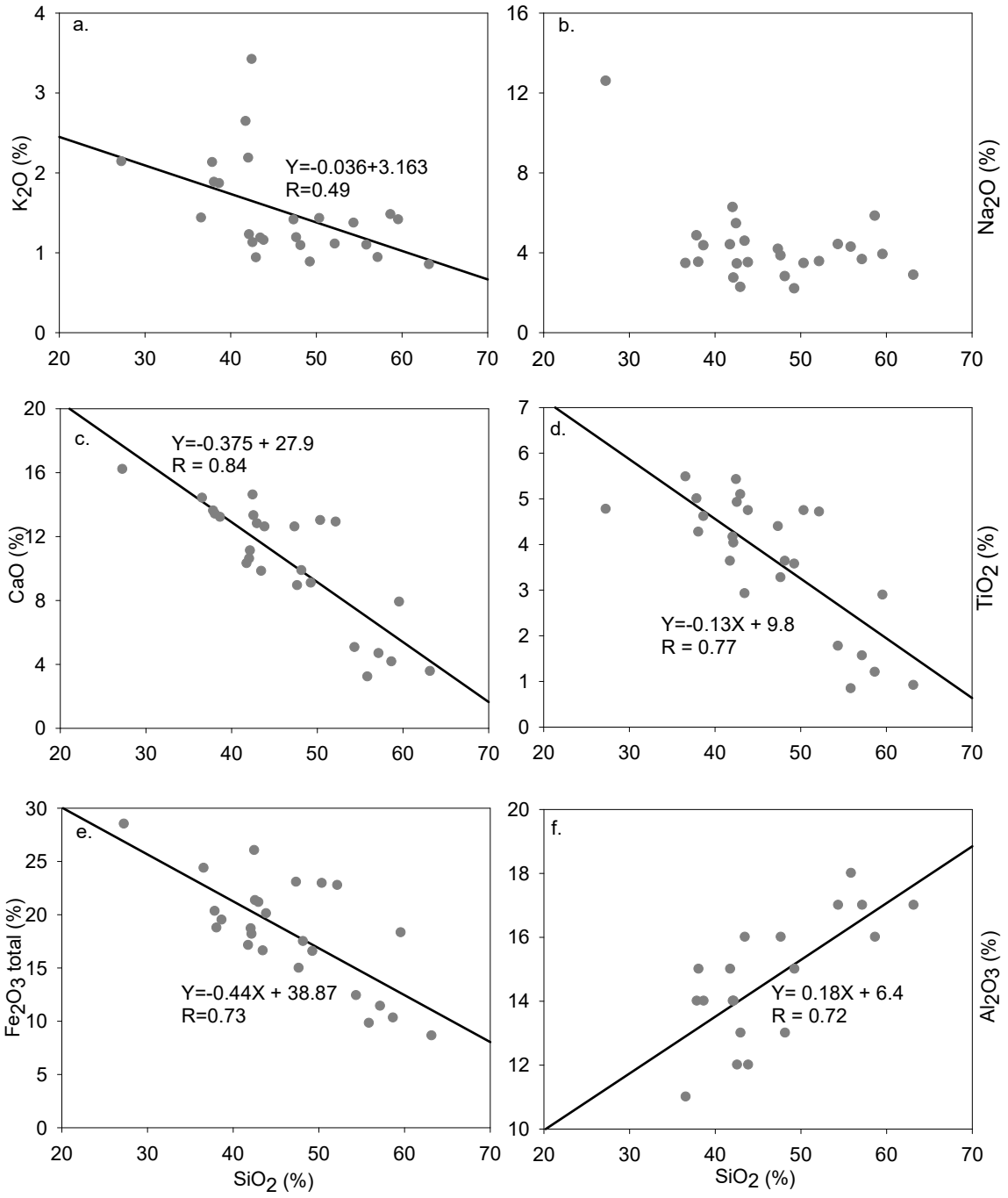

Figure 9: Harker diagrams showing relationships between SiO_2 and other major oxides for volcanic rocks (lava flow) from Arumeru area

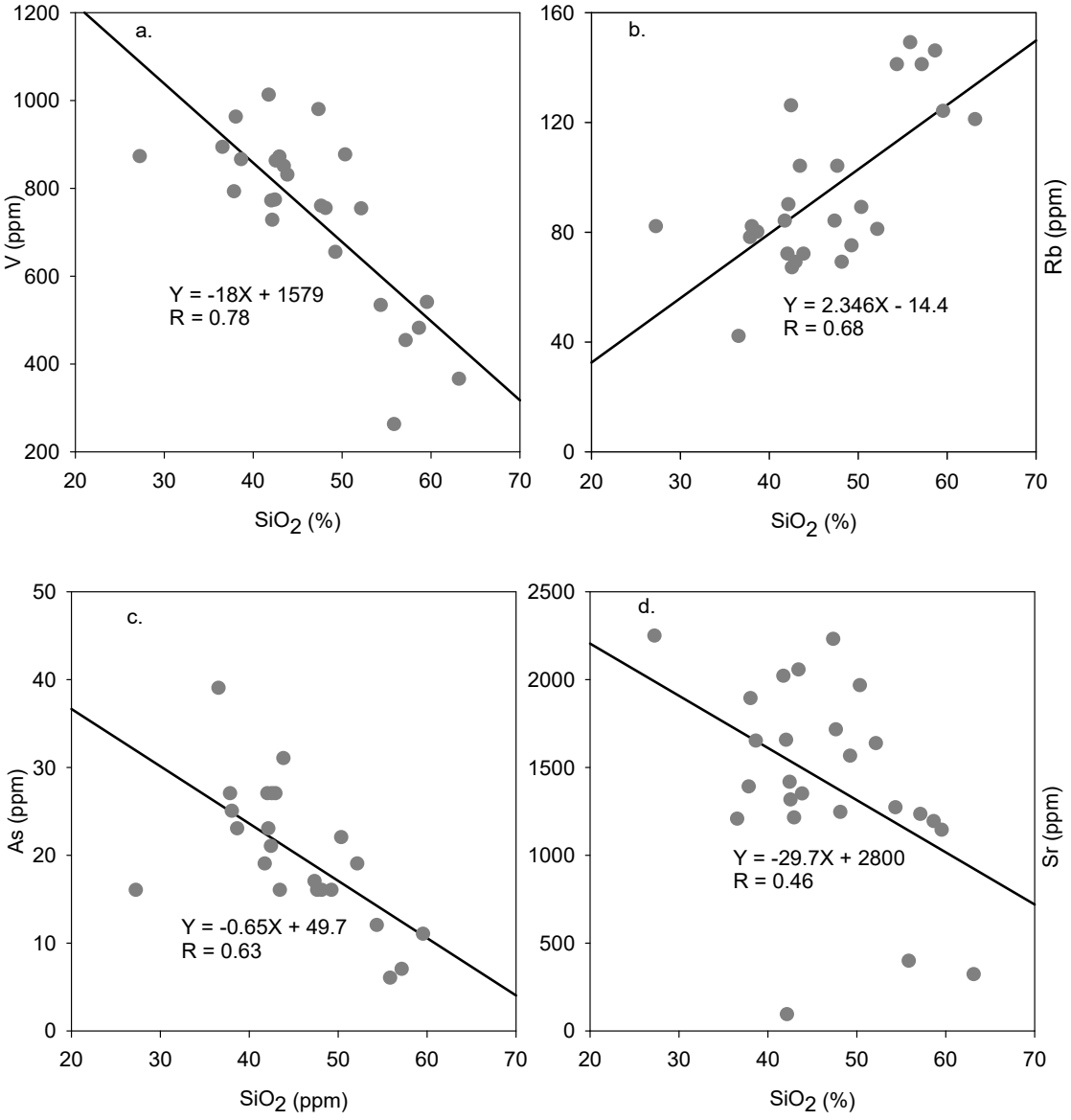

Figure 10: Harker diagrams showing relationships between SiO_2 with selected trace elements for volcanic rocks (lava flow) around Meru volcanic complex

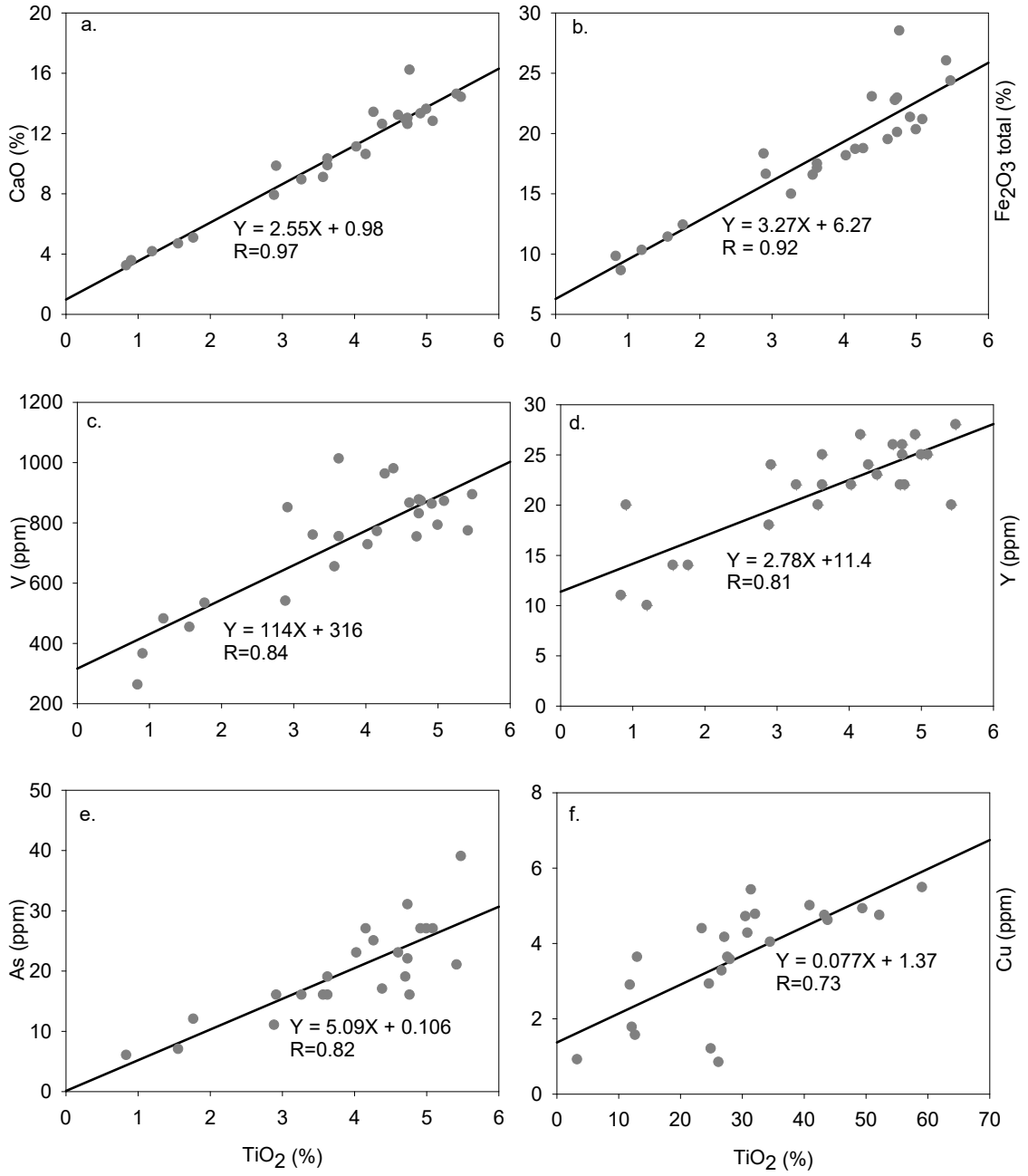

Figure 11: Scatter plots of TiO_2 vs selected major oxides (CaO, Fe_2O_3) and trace element (V, Y, As and Cu) for volcanic rocks (lava flow) around Meru volcanic complex

All rocks (lahars and lava flows) were further assessed using inter-element plots (Figs. 12 and 13). Fe_2O_3 displayed significant positive correlation (R=0.63-0.9) with both major oxides (CaO and MnO) and trace elements (As and V) while correlating negatively (R= -0.73 to -0.92) with Al_2O_3 and Rb (Fig. 12). Arsenic showed significant correlations with some of the oxides and trace elements at 95% confidence level. It showed positive correlation with CaO

(R = 0.83) (Fig. 13a). Although the data points are slightly scattered, As showed also a positive linear relationship (R = 0.63-0.75) with the trace elements V, Y and Ni (Fig. 13b-d) while correlating negatively with Rb (R = -0.77) (Fig. 13e). Apart from As, trace elements V and Y showed a strong positive correlation (R = 0.82) (Fig. 13f).

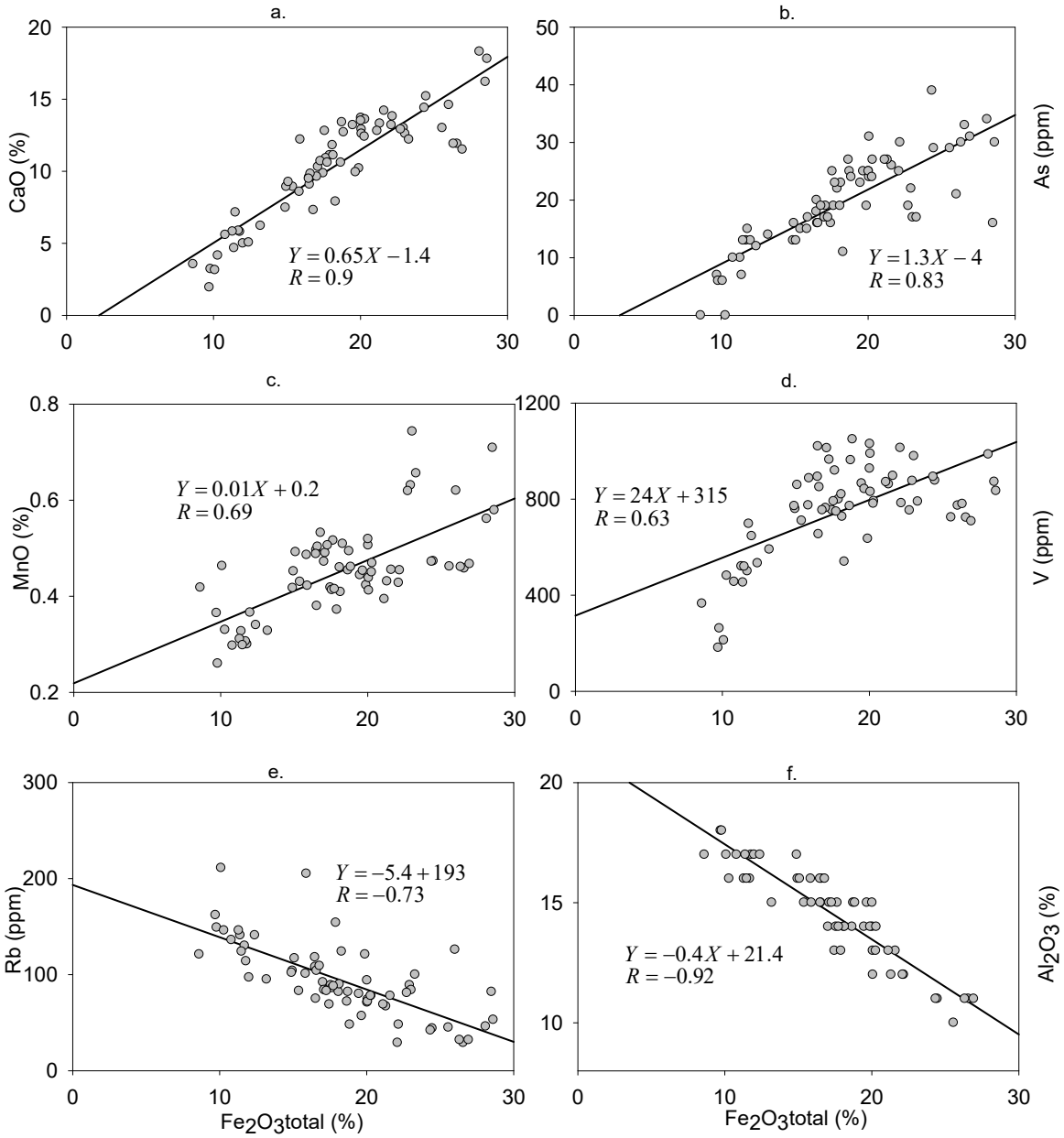

Figure 12: Scatter plots of Fe_2O_3 vs selected oxides (CaO, Al_2O_3 and MnO) and trace elements (As, Rb and V) for samples from Arumeru area.

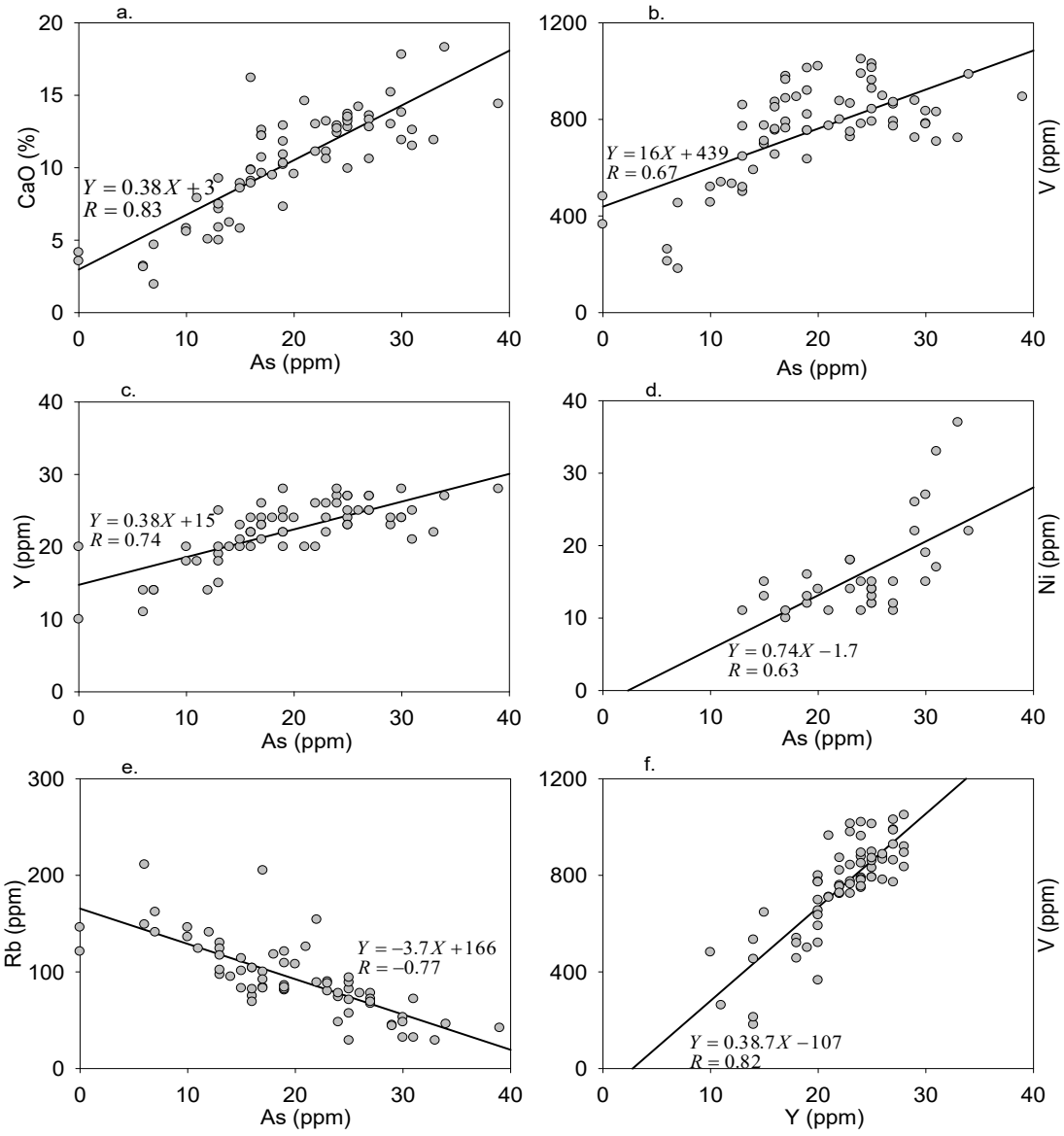

Figure 13: Scatter plots of As vs CaO and trace elements (V, Y, Rb and Ni) for rock samples from Arumeru area as shown from a-e. "f" shows positive correlation between Y and V

3.3.2 Chemical composition of the soils

Chemical composition of the soil results is presented in Fig. 14 and the individual soil compositions are presented in Appendix 4. Overall, soils showed high concentrations of SiO_2, Al_2O_3 and Fe_2O_3 with the mean values of 31%, 27% and 13.6% respectively. Also, soils exhibited high Loss on Ignition (LOI) averaging at about 13.5%. Inter-chemical variation in soils indicated that lacustrine soils had high concentration of K_2O and Na_2O relative to other

soil types (Fig. 14b). While the mean concentrations of K_2O and Na_2O in lacustrine soils were 2.48 and 5.05%wt respectively, the average concentration of these oxides in all soils were 1.43 and 2.95 %wt respectively. These oxides were generally low in residual soils relative to other soil types (Fig. 14b). Fluorine was found to be high in transported soils (mean =0.74%, n=3) and low in alluvial soils (mean=0.12%, n=2) (Fig. 14b).

Inter-elements scatter plots of residual soils indicated that there are limited linear correlations among elements and/or oxides. Fe_2O_3 was found to be the only oxide which displayed significant positive correlation at 95% confidence level with other major oxides (e.g., CaO and TiO_2) and trace elements (e.g., As and V) (Fig. 15a-d). In this diagram, the plot of Fe_2O_3 vs As indicated strong positive correlation (R = 0.85) (Fig. 15b) while other plots displayed a linear positive correlation with R ranging between 0.65-0.69 (Fig. 15a, c, d). MnO correlated positively with ZnO and TiO_2 (Fig. 15f-g), whereas Na_2O displayed a positive correlation with K_2O (Fig. 15e). For all trace elements in soils, only As and V showed a linear relationship (R = 0.64) (Fig. 15h).

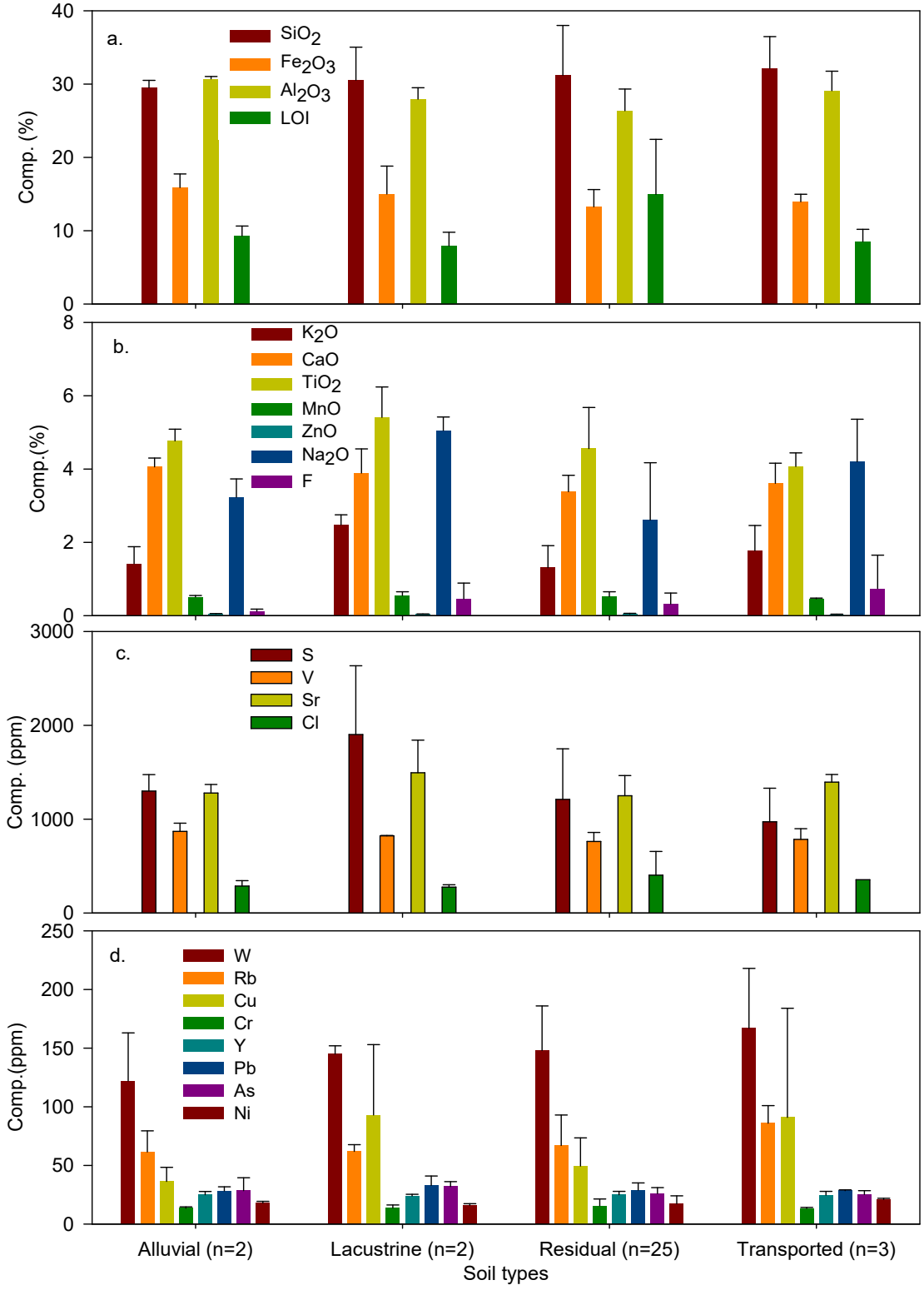

Figure 14: Chemical composition of the soils around Meru volcanic complex

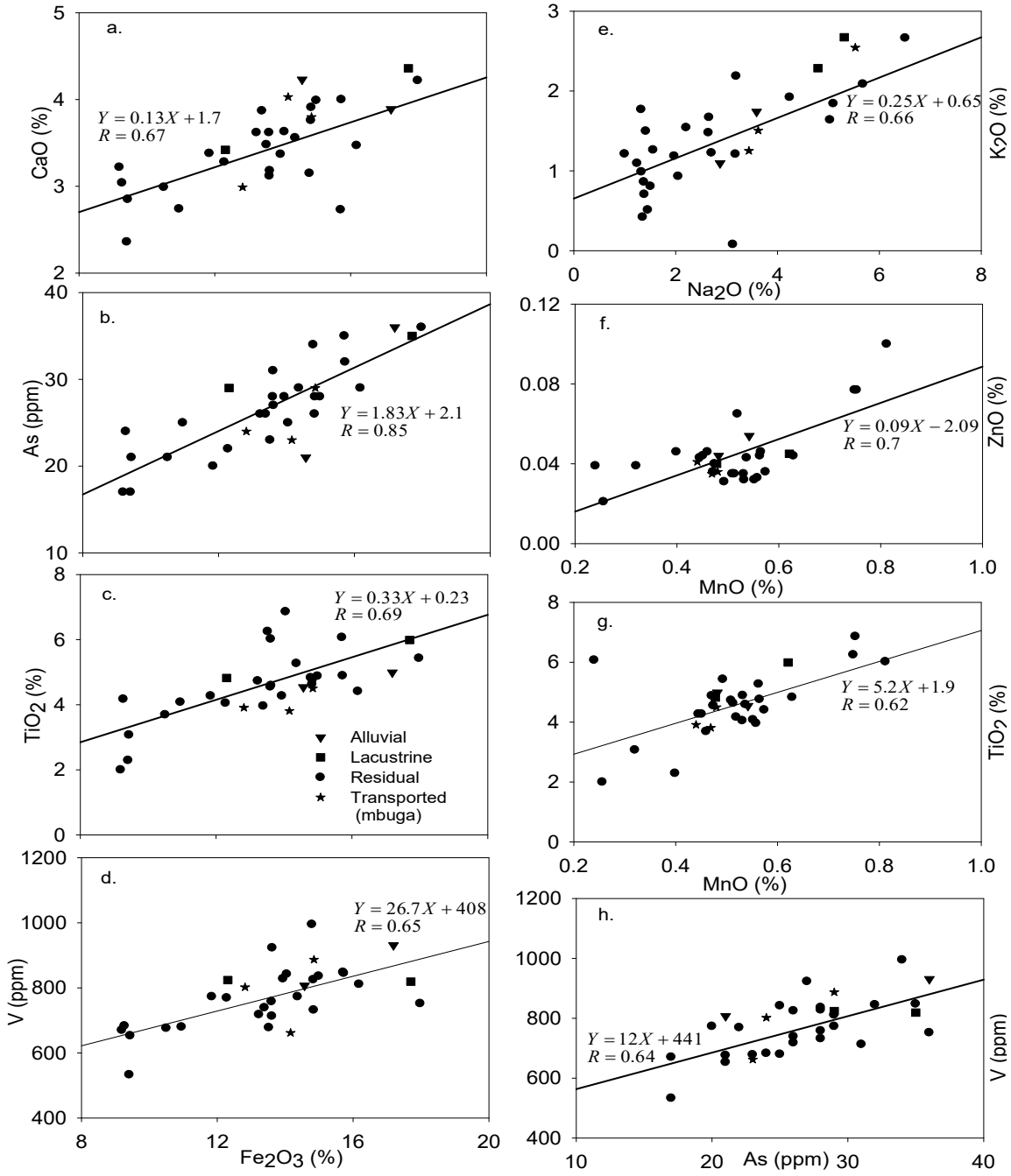

Figure 15: Inter-element scatter plot in residual soils showing correlation among various parameters. X-axis is the same for all left-hand side figures and the legend in (c.) applies to all figures (a-h).

3.3.3 Major geochemical differences in soils and rocks

Overall, soils had low SiO_2 content (mean = 31.1% wt) relative to the rocks (mean = 44.8%). Other oxides such as Al_2O_3 and CaO displayed remarkably high compositional difference between soils and rocks. The average Al_2O_3 in soil is 27% which is nearly twice the average Al_2O_3 in rocks (14.5% wt), whereas the average CaO in soils is 3.5% wt which is very low compared to the average of 10.4% wt in rocks. Loss on Ignition was extremely high in soil (mean = 13.5%) relative to rocks (mean = 2.82%). Overall, the average concentration of trace elements (V, As, Rb, Sr, W, Cr, Y, Cu and Pb) in rocks and residual soils remained nearly uniforms.

3.3.4 Fluoride results in water samples

Fluoride results from water samples collected from sources such as lakes, springs and wells are presented in Table 2. Overall, these water samples were collected purposely to assess water-rock interaction in relation to fluoride and the results indicated fluoride concentrations ranging between 0.5 – 1402 mg/l (Table 2) with the median value of 4.57 mg/l. The extremely high fluoride value (1402 mg/l) was obtained in Lake Big Momella. In these water sources, the order of increasing fluoride was windward spring (median = 1.12 mg/l, n=13) < leeward springs (median = 7.75 mg/l), n=7) < wells (median= 19.47 mg/l, n=12) < lakes (median = 717.27 mg/l, n=2).

Table 2: Fluoride results in the collected water samples for assessing water-rock-soil interaction processes in Arumeru area

Sample_ID	Water_Source	Proximal_rock ID	Proximal_soil ID	Fluoride_Water (mg/l)
ARW_08	Lake	MR_19	ARS_08	32.53
ARW_90	Lake	MR-56	ARS-31	1402
ARW_01	Leeward spring	MR_11	ARS_01	4.12
ARW_02	Leeward spring	MR_12	ARS_02	5.19
ARW_03	Leeward spring	MR_13	NS	9.73
ARW_05	Leeward spring	MR_16	ARS_04	7.75
ARW_06	Leeward spring	MR_17	ARS_06	4.66
ARW_11	Leeward spring	MR_20	ARS_11	15.33
ARW_14	Leeward spring	MR_23	ARS_13	14.00
ARW_27	Windward spring	MR_29	ARS_19	4.48
ARW_28	Windward spring	MR_30	NS	0.99
ARW_30	Windward spring	MR_31	NS	1.04
ARW_67	Windward spring	MR-41	NS	0.921
ARW_68	Windward spring	MR_42	ARS_27	1.12
ARW_69	Windward spring	MR_43	NS	0.67
ARW_70	Windward spring	MR-44	NS	1.63
ARW_71	Windward spring	MR-45	NS	0.807
ARW_74	Windward spring	MR-47, MR-48	ARS_28	2
ARW_75	Windward spring	MR-47, MR-48	ARS_28	2.25
ARW_83	Windward spring	MR-52	NS	1.22
ARW_87	Windward spring	MR-54	ARS-30	25.2
ARW_97	Spring	MR_59	NS	0.51
ARW_46	Well	MR_33	ARS_24	24.43
ARW_16	Well	MR_24	ARS_14	3.10
ARW_19	Well	MR_25	ARS_16	22.40
ARW_21	Well	MR_26	NS	8.48
ARW_25	Well	MR_28	NS	28.10
ARW_40	Well	NR	ARS-22	1.50
ARW_47	Well	MR_34	NS	23.67
ARW_48	Well	MR_35	NS	51.63
ARW_52	Well	NR	ARS_25	84.00
ARW_57	Well	MR_38; MR_39	NS	16.53
ARW_77	Well	MR-048B	ARS-28B	0.958
ARW_79	Well	MR-050	NS	4.43

NR: No proximal rock, NS-No proximal soil

3.3.5 Petrography

In order to elucidate the relationship between volcanic rocks and the existence of fluoride in the groundwater system in Arumeru area, field observations during mapping (Table 3) and 19 standard thin sections prepared from hand samples obtained from these rocks were integrated together. Thin sections were investigated by petrographic microscope to observe variations in texture (matrix and phenocryst size) and mineralogy (major and accessory phases), and the results are presented in Table 4.

The mineralogy of these rocks generally consists of porphyritic and fine-grained nepheline, clinopyroxene, plagioclase, sanidine, sphene, amphibole, Fe-Ti oxides, and biotite with subordinate microcline, apatite, zircon, and calcite). Two photomicrographs (Figs. 16 and 17) are used to describe these samples. Volcanic rock (lava flow) are represented by Fig. 16, largely focusing on rock genesis and magmatic process while lahars and well materials are represented by Fig. 17, largely focusing on fluorine bearing minerals.

In lava flows, the dominant major rock-forming minerals were subhedral to euhedral nepheline, clinopyroxene, sanidineand plagioclase crystals, which account for more than 80% of the phenocrysts (~100 μm to < 2.5 mm in length) in most samples (Fig. 16).Unlike other major rock forming minerals, sanidine occurrence is restricted only in intermediate rocks (andesite to dacite) (Table 4; Fig. 16a-d), suggesting that magmas for these rocks erupted and cooled rapidly to preserve such high temperature-minerals. Fluorine bearing phenocryst mineral in these samples is sphene that account for about 5% and occurs in a wide range of size from fine crystals (Fig. 16a) to mega crystals (Fig. 16c). These samples exhibit porphyritic, seriate and trachytic textures (Fig. 16). Porphyritic texture is well pronounced in Fig. 16e, f with nepheline and clinopyroxene as the dominant mega phenocrysts. Seriate and trachytic textures are well reflected in Fig. 16a-d, the latter suggests magma flow during crystallization. There is also zoning in some pyroxene crystals which provide evidence for periods of crystal growth that was accompanied by changing physicochemical conditions brought in by magma replenishment.

The wells and lahar materials exhibit porphyritic texture, lacking seriate and trachytic textures (Fig. 17). The dominant phenocrysts are clinopyroxene crystals. The selected samples had high fluorine content (>1.4 %) with sphene, amphibole, biotite and apatite as fluorine bearing minerals (Fig. 17). Sphene is the dominant fluorine bearing mineral in these samples accounting for 5 to 10 % of the phenocrysts and < 1.5 mm in length (Fig. 17).

Amphiboles and biotite occurred in few samples, which account for less than 3 % of all phenocrysts (Fig. 17c, d). Apatite occurs commonly as an inclusion in pyroxene crystals (Fig. 17a, e) and few phenocrysts may contain deep embayment. Remnants of these fluorine bearing minerals particularly amphibole and sphene are also present in groundmass (Table 4; Figs. 16-3.17). Lahars contain other accessory minerals such as opaque phases (Fe- and/or Fe-Ti-bearing phases) that can account for 5 % in few samples, zircon as an inclusion and/or in groundmass, calcite and microcline. Microcline occurs in some few volcanoclastic samples (Fig. 17f).

Unlike sphene in lahar and well materials, some of the other fluorine bearing mineral such as biotite and amphiboles have been partially altered. Due to such alteration, some biotite crystals have been partially or completely replaced by Fe- and/or Fe-Ti-bearing phases. Hornblende indicates a replacement texture around its rims or a complete replacement by Fe-oxides as a result of decrease pressure on surface after eruption.

Table 3: Arumeru rocks description based on field observations. Rock name is derived from both field observation and geochemistry

Rock_ID	Sampled area	Field occurrence	Rock description	Rock name
MR-01	Nelson Mandela	Outrcopping as thrown materials (explosive eruption)	Massive intermediate volcanic materials with porhyritic texture, dominance of feldispathoid minerals	Basaltic Andesite
MR-02	Nelson Mandela	Lahar	Lahar materials dominated by trachytic materials and subrounded pebbles of diffenrent compostion	Andesite
MR-03	Romana	Outcropping as thrown materials (explosive materials)	Intermediate to mafic volcanic with aphanitic texture	Andesite
MR-04	Nambala	Small outcrop, scattered	Mafic, porphyritic texture with elongated pyroxene crystals	Foidite
MR-05	Emmy pub	Small outcrop (spot)	Very hard, aphanitic, intermediate volcanic rock	Basaltic trachandesite
MR-06	Emmy pub	Small outcrop (spot)	Very hard, aphanitic, mafic volcanic rock	Tephrite Basanite
MR-07	Lake Duluti_East	Lava flow-rings/layered	Volcanoclastic lahar materials	Foidite
MR-08	Lake Duluti_East	Lahars in form of rings/layers	Volcanoclastic lahar materials	Foidite
MR-09	Lake Duluti_East	Lahars in form of rings/layers	Volcanoclastic lahar materials	Foidite
MR-10	Tengeru LITI	Lava flow	Massive, mafic volcanic with weak amygdoloidal texture	Foidite
MR-11	Kisimiri chini	Lava flow	Extensive massive volcanic rock	Foidite
MR-12	Kisimiri-Uzunguni street	Lava flow	Massive, basaltic stuff	Basalt
MR-13	Kimosomo-Kyamang'ata	Lahar on the river bed	Weathered lahar matrials	Foidite
MR-14	Kimosomo-Kyamang'ata	Small outcrop at the hill	Mafic fresh sample with elongated mafic mineals	Tephrite Basanite
MR-15	Kimosomo-Kyamang'ata	Lahar on the river cut	Slightly weathered, dominance of feldspathoid minerals	Foidite
MR-16	Burebure	Lava flow, very extensive outcrop	Mafic, massive volcanic	Foidite
MR-17	Mwakey	Lava flow, hill coverage	Amygdoloidal lava	Foidite
MR-18	Ngarenayuki-Close to centre	Lahar on top of small hill	Dominance of framents with different composition	Foidite
MR-19	Momella-Lake Mlolozi	Scattered, small outcropping formation	Amygdoloidal lava	Foidite
MR-20	Oldonyosambu-Lemou	Lahars on river bed	Lahar underlying basaltic materials on the river bed	Foidite
MR-21	Upper Oldonyosambu	Lahar on river bed, about 20 m depth	Aggromerate, different composition	Trachyandesite
MR-22	Upper Oldonyosambu	Big outcrop on the river floor	Porthyritic, Felsic with feldsparthoid mega- crystalls	Andesite
MR-23	Oldonyowas	Hill dominated by lahar materials	Pumice to amygdoloidal lava	Tephrite Basanite

Table 3 continued

MR-24	King'oli	Well materials-Laha from the surface to bottom(~8m)	Lahar(lapilli/Aggromerate)	Tephrite Basanite
MR-25	Miundombinu	Well materials (Lahar)	Fragments of different composition	Foidite
MR-26	Maji ya Chai_Kati	Well materials (lahar)	Fragments of various composition Including porphyritic basalt, trachyte, basalt	Tephrite Basanite
MR-27	Maji ya Chai	Presence of Lahar and basaltic flow	Fragments of different composition	Foidite
MR-28	Maji ya Chai	Well materials, taken at a depth of about 5m	Basalts to Amygdoloidal lava materilas	Foidite
MR-29	Maji ya Chai_Mto Kati	Quarry volcanic materials	Massive, mafic volcanic material	Foidite
MR-30	Ngareselo intake	Well exposed basaltic materials	Massive, aphanitic basalt	Basalt
MR-31	USA_NAIC2	Small outcropping basaltic materials	Massive, aphanitic basalt	Tephrite Basanite
MR-32	Bwawani	Layered, weathered sedimentary unit along the road cut	Precipitated Calcareous materials	Calcareous mudstone
MR-33A	Marororoni_Magadini	Scattered, small outcropping formation. Dominance of lahars	Aggromerate	Foidite
MR-33B	Marororoni_Magadini	Not common, small outcroping formation	Very hard, aphanitic, basaltic formation	Basaltic Andesite
MR-34	Marororoni_Magadini	Well materilas	Lahars, dominance of aggromerates	Foidite
MR-35	Makiba_Maroronl	Intercalation of Lahar and basaltic outcrop	Lahars, dominance of basaltic fragments	Tephrite Basanite
MR-36	Makiba_Maroroni	Parastic cone- intermediate volcanics	Porphyritic, dominance of coarse feldspathoid crystals	Basaltic Andesite
MR-37	Kikatiti	Big massive volcanic rock	Lahar dominated by fragments of porphyritic basalt	Foidite
MR-38	Kikatiti	Well materials-Lahars and pyroclastic materials	Mafic volcanic	Basalt
MR-39	Kikatiti	Not common, small outcroping formation	Very hard, aphanitic, felsic to intermediate composition	Dacite
MR-40	Nkoarisambu	Massive volcanic formation along the the river cut underlying lahar materials	Porphyritic, intermediate to mafic volcanics, dominance of coarse feldspathoid and pyroxene crystals	Foidite
MR-41	Nkoarisambu	Massive volcanic formation along the the river cut underlying lahar materials	Porphyritic, dominance of coarse feldspathoid crystals	Tephrite Basanite
MR-42	Nkoarisambu_Mbola	Exposed along the river cut	Porphyritic, feldspathoid crystals	Foidite
MR-43	Mburukuu	Massive volcanic formation along the the river cut	mafic, aphanitic	Trachybasalt
MR-44	Poli	At the water fall,outcrop extends to more than 30 m from the surface (depth). Pure lava flow	aphanitic,intermediate to mafic volcanic	Trachyandesite

Table 3 continued

MR-45	Poli	River bed volcanic material, about 20 m below the surface	aphanitic, intermediate composition	Andesite
MR-46	Poli	Not common, small outcroping formation	Porphyritic, very coarse felspathoid crystals	Andesite
MR-47	Poli	Spots	Intermediate to mafic volcanic formation	Basaltic Andesite
MR-48	Poli	Spots	Phaneretic texture, dominance of feldspathoid crystals	Basaltic trachy andessite
MR-48B	Ndatu	Well materials	Pyroclastic, and lahars-felsic to mafic composition	Andesite
MR-49	Makumira-Kalamu	At the spring point	Massive, lava flow-mafic composition	Basalt
MR-50	Ng'ong'ong'are	Lahars	Dominance of basaltic fragments	Picro basalt
MR-51	USA-Mandela road, Mkidoma river	Lahars on the river bed	Dominance of fragments with coarse feldsparthoid crystals	Andesite
MR-52	CDTI	Lava flow, big outcrop at the spring source	Massive, mafic volcanics	Foidite
MR-52B	Arusha Ntional park	On the river bed, surrounding areas are covered by lahars	Basaltic stuff	Tephrite Basanite
MR-53	Arusha National park	On the river bed, massive exposed basaltic materials (Lava flow)	Aphanitic, mafic volcanic	Foidite
MR-54	Arusha National park_Makisolo	Lava flow	Aphanitic, mafic composition	Tephrite Basanite
MR-55	Lake Small Momella	As spot at the hill close to the Lake	Aphanitic, mafic volcanic	Tephrite Basanite
MR-56	Big Momella lake	Typical lahars	Different fragments	Foidite
MR-57	Lake Duluti_E	Like tuff ring on the eastern wall of the lake	Layered, aphanitic, mafic volcanic	Foidite
MR-58	Serana hotel	Lahar	Fragments with variable composition	Foidite
MR-59	USHIRI-Songoro	Lava flow at the spring source	Massive, aphanitic, mafic composition	Tephrite Basanite
MR-60	Arusha N. Park-Bufallo zone	Extensive lahars (~200m, up the hill)	Diffent fragments	Tephrite Basanite
MR-61	Arusha N. Park-Bufallo zone	Lava flow	Basaltic stuff	Tephrite Basanite
MR-62	Arusha N. Park_ Rhyino station	Ashes and pyroclasic materials towards the top of Mt. Meru	Dominace of sands, ashes and pyroclasic maaterials	Basalt
MR-63	Arusha N. Park_ Rhyino station	Pumice,occupy small area relative to other pyroclastics	Vescular texture	Trachy-basalt
MR-64	Arusha N. Park_ Rhyino station	Tuffaceos materials	Reddish/Oxidized tuff materials	Tephrite Basanite
MR-65	Arusha N. Park- Rhyino - top of Mt.Meru	Basaltic flow towards the top of Mt. Meru overlying lahars, ashes and pyrocaltic materials	Fresh, massive baltic stuff	Trachy-basalt

Table 4: Mineralogical and textural descriptions of rock samples based on petrographic examination

Microscopic Results														**Field and Hand specimen description**	**Rock affinity**
Minerals (% Phenocrysts)													G.mass (%)	Texture	
S/ID	Neph	CPX	Ilm/Mag	Sph	Apat	Hbld	Biot	Plag	Sanid	Microcl.	Calc	Zirc			
MR-01	10	15	2	3	x	20	10	x	x	1	x	x	40	Porphyritic. Highly altered groundmass with remnants of pyroxene, biotite, hornblende and feldspathoids.	Big massive outcrop with K-Feldsparmega crystals	Basaltic andesite in composition
MR-04	30	20	10	10	x	1	x	x	x	x	x	1	30	Porphyritic. Altered groundmass with remnants of zircon, sphene and Fe-Ti oxides	Dark with some elongated mafic minerals	Nephelinite/Foidite
MR-05*	x	50	15	5	x	x	x	x	x	x	x	x	30	Porphyritic. Altered groundmass with remnants of plagioclase, sphene and Fe-Ti oxides	Occurring as thrusted dark outcrop	Basaltic trachyandesite
MR-14*	x	30	20	1	x	x	x	x	x	x	x	x	50	Porphyritic dominated by phenocrysts of pyroxene	Dark with some elongated mafic minerals	Tephrite Basanite
MR-15	30	30	8	2	x	x	x	x	x	x	x	x	30	Needle like crystals of cpx. Red stains around cpx crystals, may suggest replacement by oxides of iron (commonly haematite).	Lahar materials	Nephelinite/Foidite
MR-21	40	5	x	x	x	x	x	40	5	x	x	x	10	Trachytic texture, needle likecrystals of plag and sanidine	River cut big lahar outcrop with fragments of different	Trachyandesite

Microscopic Results															Field and Hand specimen description	Rock affinity
Minerals (% Phenocrysts)													G.mass (%)	Texture		
															composition	
MR-22	35	5	x	x	x	2	x	20	x	x	x	x	40	Trachytic texture, fine crystals of amphibole in groundmass	River cut, felsic volcanic materials	Andesite
MR-24	30	25	2	2	1	x	x	x	x	x	<1	1	40	Porphyritic texture with apatite inclusion in CPX crystals	Amygdaloidal lava	Tephrite Basanite
MR-35	15	35	4	4	1	x	x	x	x	x	x	x	40	Porphyritic. Biotite replacement by Fe-Ti oxides	Lahar materials	Tephrite Basanite
MR-39*	x	4	1	1	x	5	4	30	30	x	x	x	25	Intergrowth texture (sanidine and CPX), trachytic texture, replacement of hornblende by Fe-Ti oxides	Greenish gray, hard and rare rock among the collected samples outcropping as a small rock	Dacite
MR-44*	x	5	5	2	x	x	x	40	45	x	x	x	-	Trachytic to seriate texture with very few mega crystals of sphene.	Big massive outcrop -30 m surface to river floor	Trachyandesite
MR-48	5	10	2	2	1	5	x	10	5	5	x	x	55	Porphyritic. Apatite inclusion in CPX crystals	Intermediate volcanic rocks with felsic mega crystals	Basaltic trachyandesite
MR-48B	x	20	2	10	x	x	x	10	x	x	x	x	60	Groundmass is dominated by plagioclase crystals	Lahar materials	Andesite
MR-50	5	35	5	4	x	x	1	x	x	x	x	x	50	Porphyritic texture	Lahar materials	Picro basalt
MR-51	5	10	1	1	x	x	x	10	5	x	x	x	70	Porphyritic texture	Lahar, intermediate volcanic rock	Andesite

Microscopic Results															
Minerals (% Phenocrysts)													G.mass (%)	Texture	**Field and Hand specimen description**	**Rock affinity**
MR-52	15	15	10	x	x	x	x	10	x	x	x	x	50	Porphyritic.Remnants of Fe-Ti oxides, CPX and nepheline in groundmass	Massive mafic volcanic rock	Nephelinite/Foidite
MR-54	10	20	3	2	x	x	x	20	x	x	x	x	45	Trachytic texture (elongated plagioclase crystals)	Massive mafic volcanic rock	Tephrite basanite
MR-58	25	30	5	5	x	x	x	5	x	x	x	x	30	Porphyritic. Chemical zoning in CPX crystals	Lahar materials	Nephelinite/Foidite
MR-65*	40	30	8	2	x	x	1	x	x	x	x	x	20	Porphyritic. Euhedral nephelinitic crystals	Basaltic lava flows overlying lahar/ashes towards the top of Mt.Meru	Trachy-basalt

Note: *Abbreviation: *Lava flows, Neph: nepheline, CPX: Clinopyroxene, Ilm/Mag: ilmenite/magnetite, sph: sphene, Apat: apatite, Hbld: hornblende, Plag: plagioclase, Biot: biotite, Sanid: sanidine, Microc: microcline, calc: calicite, zirc: zircon and "x": not seen*

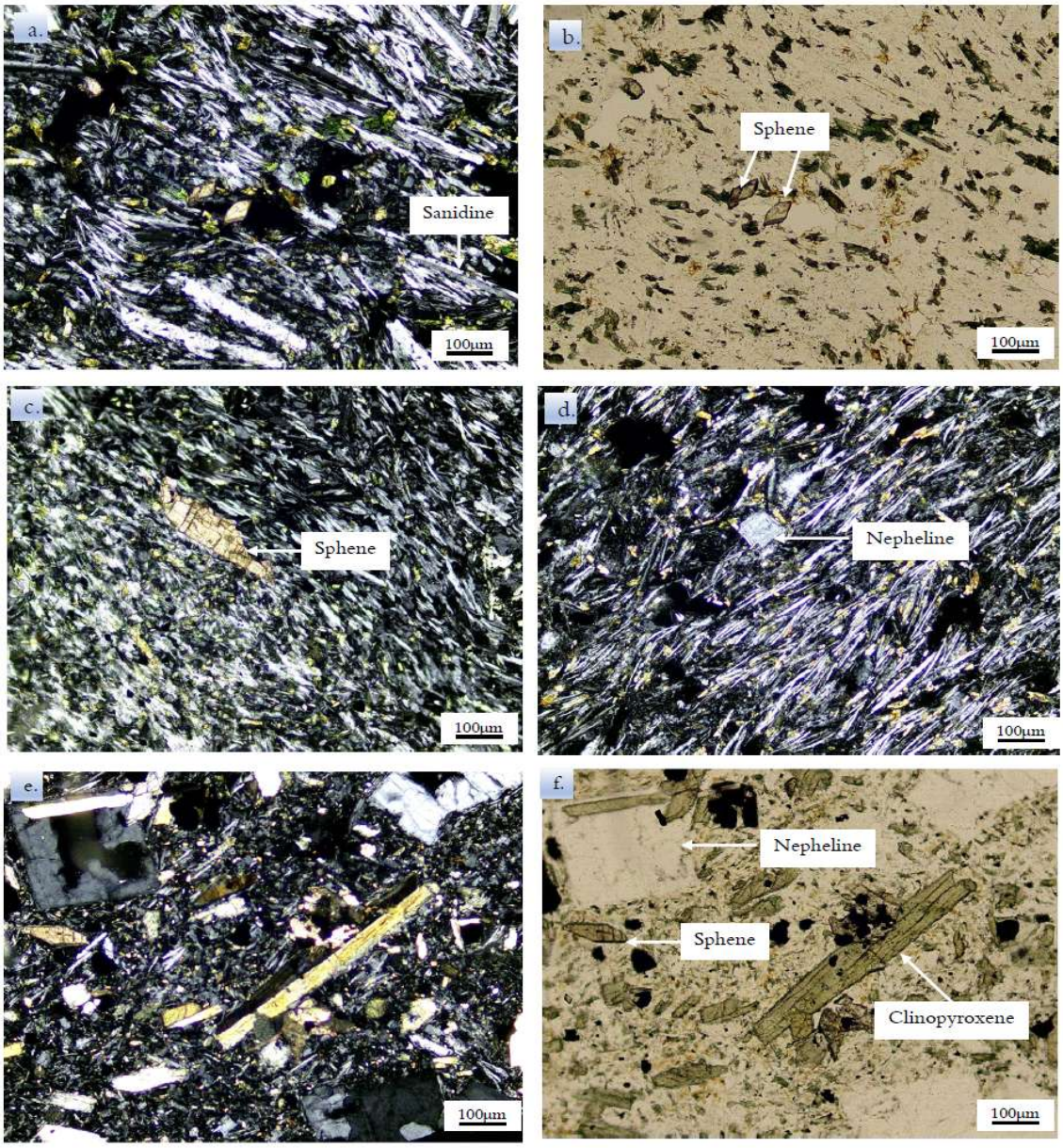

Figure 16: Photomicrographs of volcanic rock samples which represent lava flow.

Two samples “a” and “e” (cross polarized) are presented with their corresponding plain polarized (bandf) and the remaining (c and d) are cross polarized. Samples “a” to “d”are samples of andesitic affinity exhibitingtrachytic texture (and or seriate texture) with plagioclase and sanidine as the dominant coarse crystals. Fine crystals include amphibole/pyroxene while few mega-crystals are sphene and nepheline. Sample “e’ exhibits basaltic affinity with porphyritic texture (clinopyroxene and nepheline as the dominant phenocrysts).

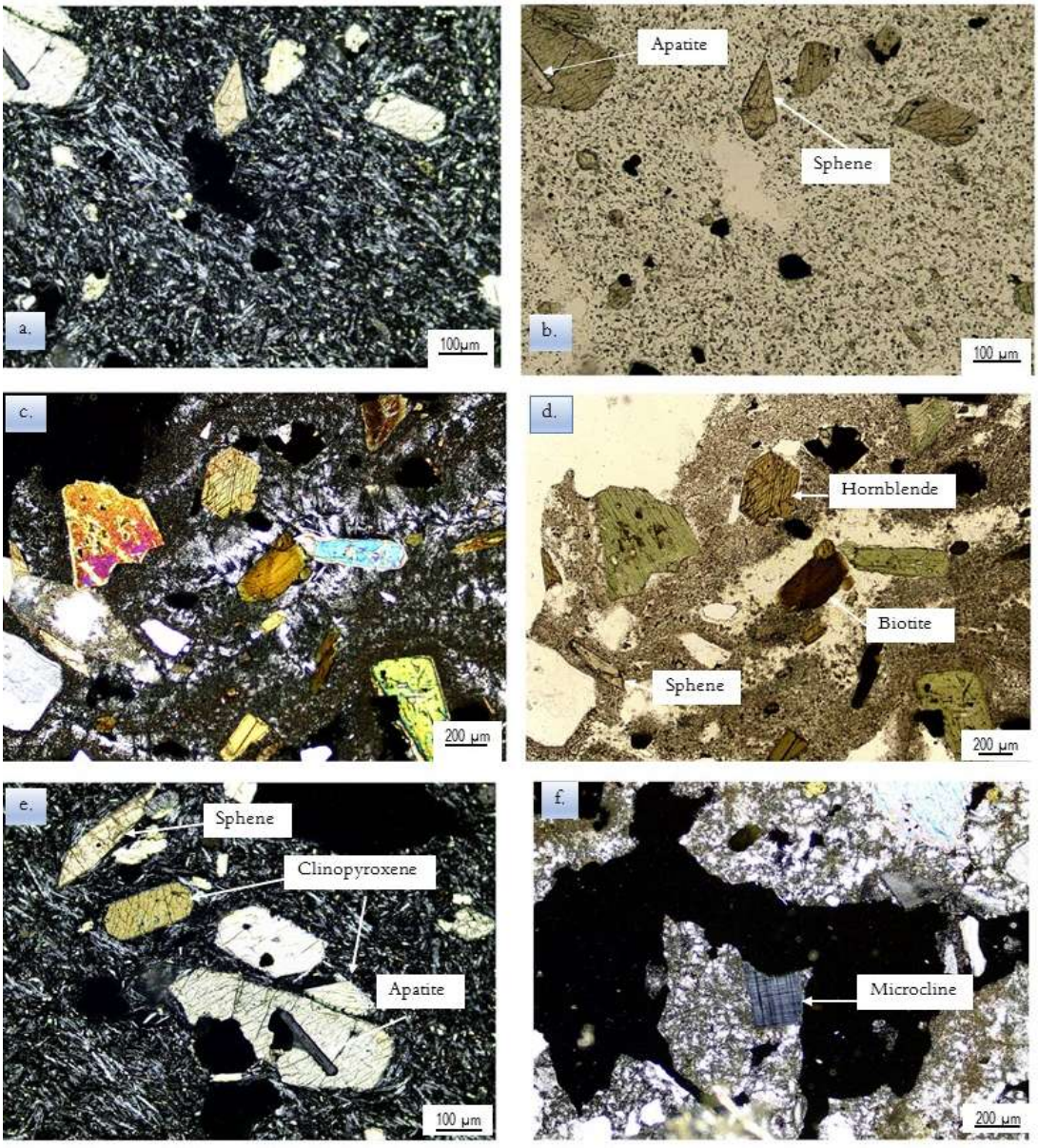

Figure 17: Photomicrographs of volcanic materials with high fluorine content (>1.4 %).

Two samples “a” and “c” (cross polarized) are presented with their corresponding plain polarized (b and d) and the remaining (e and f) are cross polarized. (a, c, e and f) are cross-polarized, whereas (b and d) areplane-polarized. Apatite occurs as inclusion in pyroxene (e) and other fluorine bearing minerals (biotite, hornblende and sphene) are common as phenocrysts. Sample “f”represent occurrence of microcline in lahar materials with andesitic affinity suggesting crustal contamination.

3.3.6 Fluorine distribution among rock types

The average fluorine in 67 sampled rocks was 3.92 g/Kg (0.392 %) and its distribution is as shown in Fig. 18a. Based on this distribution, the lowest values were obtained in dacite (0.93 g/Kg), picro basalt (0.85 g/Kg) and trachy-basalt (0.55 g/Kg) (Fig. 18a). However, the number of sampled rocks was low relative to other rock groups (Fig. 18a). The high fluorine values greater than 5 g/Kg were obtained in andesite, basaltic andesite to basaltic trachyandesite (Fig. 18a).

Out of 67 sampled rocks, 19 samples had fluorine values above 5 g/Kg (0.5 %). The distribution of these 19 samples with the average fluorine values is shown in Fig. 18b. In this diagram, it is clear that andesite and basaltic andesite to basaltic trachyandesite had high fluorine values relative to all other rock types. 83 % of all sampled basaltic andesite to basaltic trachyandesite had fluorine value above 5 g/t, with an average of 10.61 g/Kg. Also, 42.8 % of all sampled andesite had fluorine values above 5g/t with an average of 10.24 g/Kg (Fig. 18b). Based on the number of samples in these two groups, it can be generalized that andesitic rocks, which are mostly porphyritic have high fluorine content relative to all other rock types.

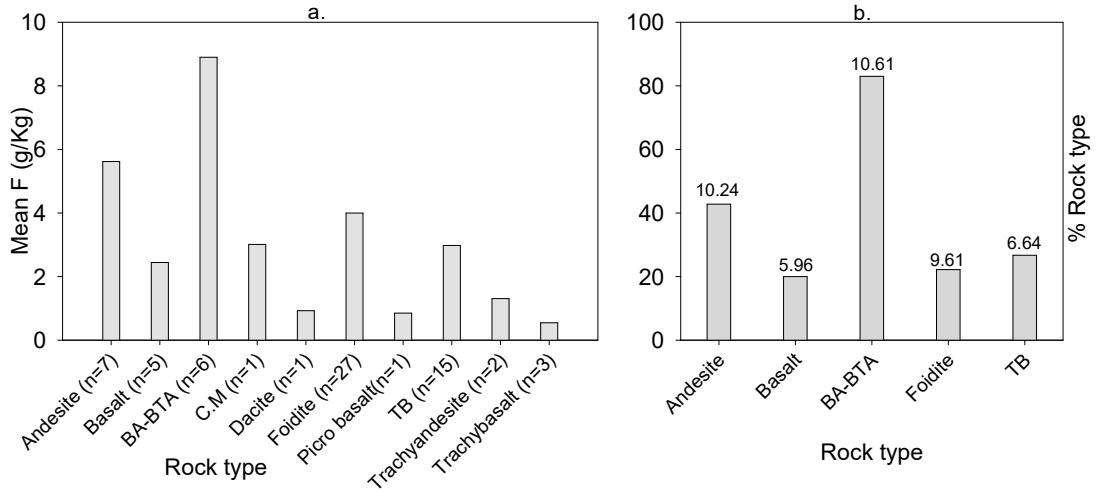

Figure 18: Mean fluorine in the sampled rocks (b). Percentage of rock types with fluorine > 5 g/Kg and the labelled values are the mean fluorine in g/Kg

Note that BA-BTA=Basaltic andesite to basaltic trachyandesite, CM=Calcareous mudstone, TB= Tephrite basanite

3.3.7 Spatial distribution of fluorine in rocks

Generally, fluorine distribution is random, and in most cases, two or more different rocks sampled from the same location are characterized by different fluoride content (Fig. 19). The distribution of rock groups as shown in Fig. 19 does not control spatial distribution of fluorine. However, it is weakly reflected that rocks towards the top Mt. Meru exhibit generally low fluorine content relative to rocks on the foot of Mt. Meru (USA River-Songoro) (Fig. 19). Some areas such as Maji ya Chai, Kikatiti and Maroroni have been reported to have high fluoride in groundwater (Nanyaro *et al*., 1984; Kaseva, 2006; Malago *et al*., 2017). In these areas, fluorine is relatively low in rocks (Fig. 19). Furthermore, rocks with high fluorine content generally above 7000 mg/Kg are locally distributed in some of the areas with fresh groundwater (Nelson Mandela AIST, author's unpublished data). Despite the fact that extremely high fluorine-rich rocks are generally not observed in the leeward side (Ngarenanyuki-Oldonyosambu), the obtained values are generally high (3000 - 7000 mg/Kg as the dominant group) to the extent of reflecting high fluoride in groundwater.

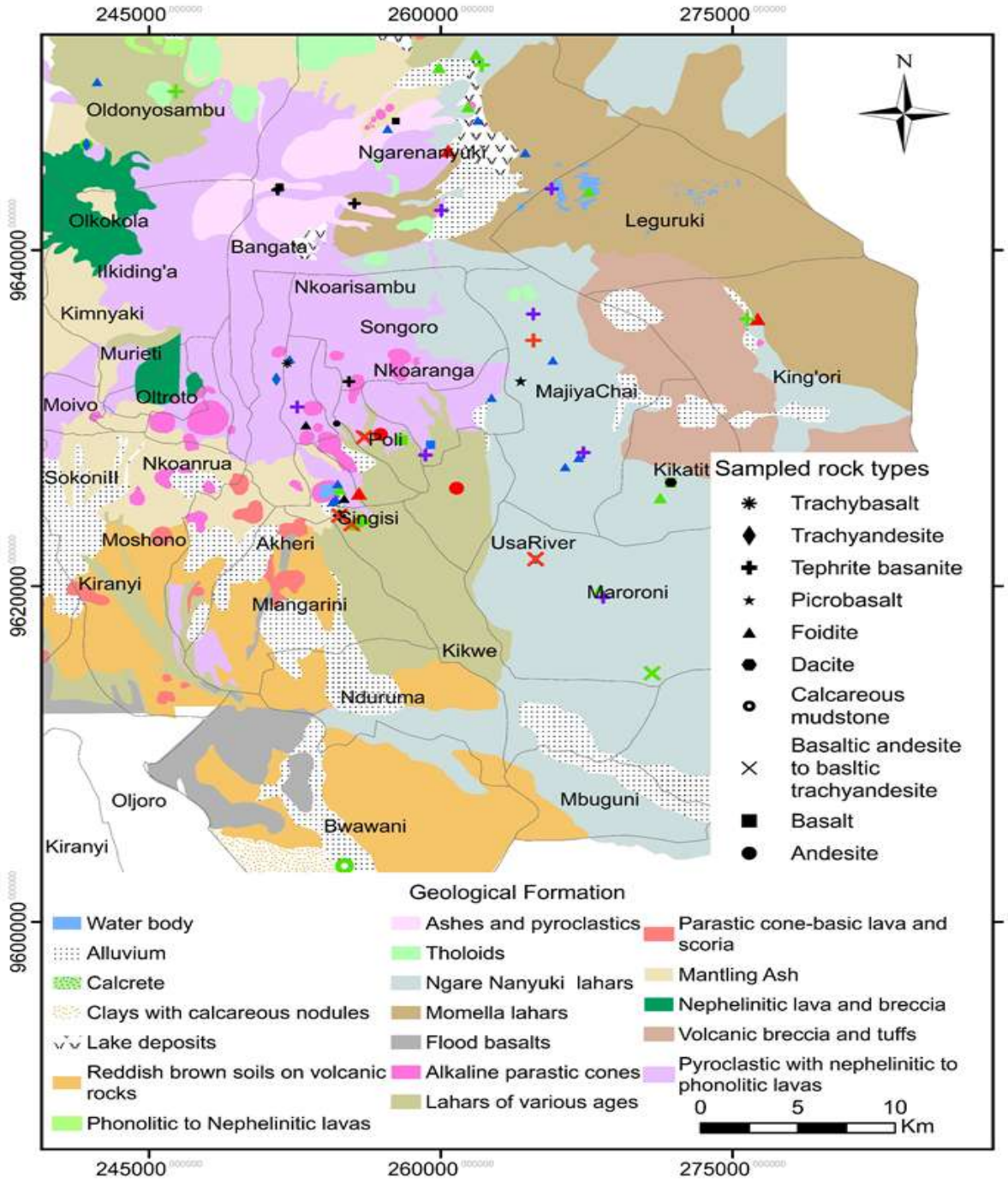

Figure 19: Fluoride distribution based on specific rock types and geological formation.

Colour represents specific range of fluorine values in g/Kg as black (252-1000), blue (1001-3000), green (3001-7000) and red (7001-19125)

3.3.8 Fluorine distribution in soils

The average fluorine in 32 soil samples was 3526 mg/Kg which is slightly lower relative to that in rocks (3920 mg/Kg). The distribution of fluorine in soils indicated that transported soils, locally known as mbuga (soil rich in clays and organic matter) has high fluorine concentration than other groups (average = 7382 mg/Kg; Fig. 20). This group includes the highest value in soils of 17848 mg/Kg. Typical alluvial soils (sandy soil) had the lowest fluorine concentration averaging 1190 mg/Kg (Fig. 20). However, number of samples in these two groups was low to the extent of not representing effectively the two groups of soils. Lacustrine soils had also high fluorine content with high contribution from the soil around Lake Small Momella (7653 mg/Kg) which is the second highest fluorine value in soils. Fluorine concentration in residual soils which is the dominant soil group was intermediate averaging at 3165 mg/Kg (Fig. 20).

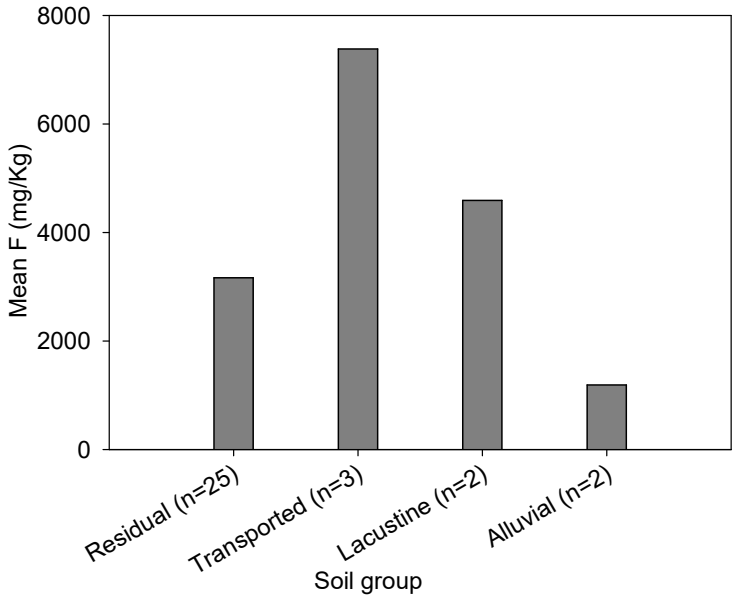

Figure 20: Mean fluorine in different soil groups

3.3.9 Spatial distribution of fluorine in soils

Spatial distribution of fluorine in soils is not directly controlled by the spatial distribution of fluorine in rocks. In some cases, the soils with high fluorine were associated with rocks rich in fluorine (e.g. Singisi, Lake Momella and Ngarenanyuki to Oldonyosambu) (Figs. 19 and 21). In other cases, areas such as Songoro and towards the top of Mt. Meru (Fig. 21), soils had high fluorine concentrations relative to the surrounding rocks (Fig. 19). Soils in the low flat land areas of Makiba-Bwawani Mbuguni had relatively low fluorine concentration (Fig.

21). Therefore, with exception of few cases such as transported soil at Maroroni (Fig. 21), it can roughly be generalized that the concentration of fluorine in soils decreases with increasing distance from the summit (volcanic centers) (Fig. 21).

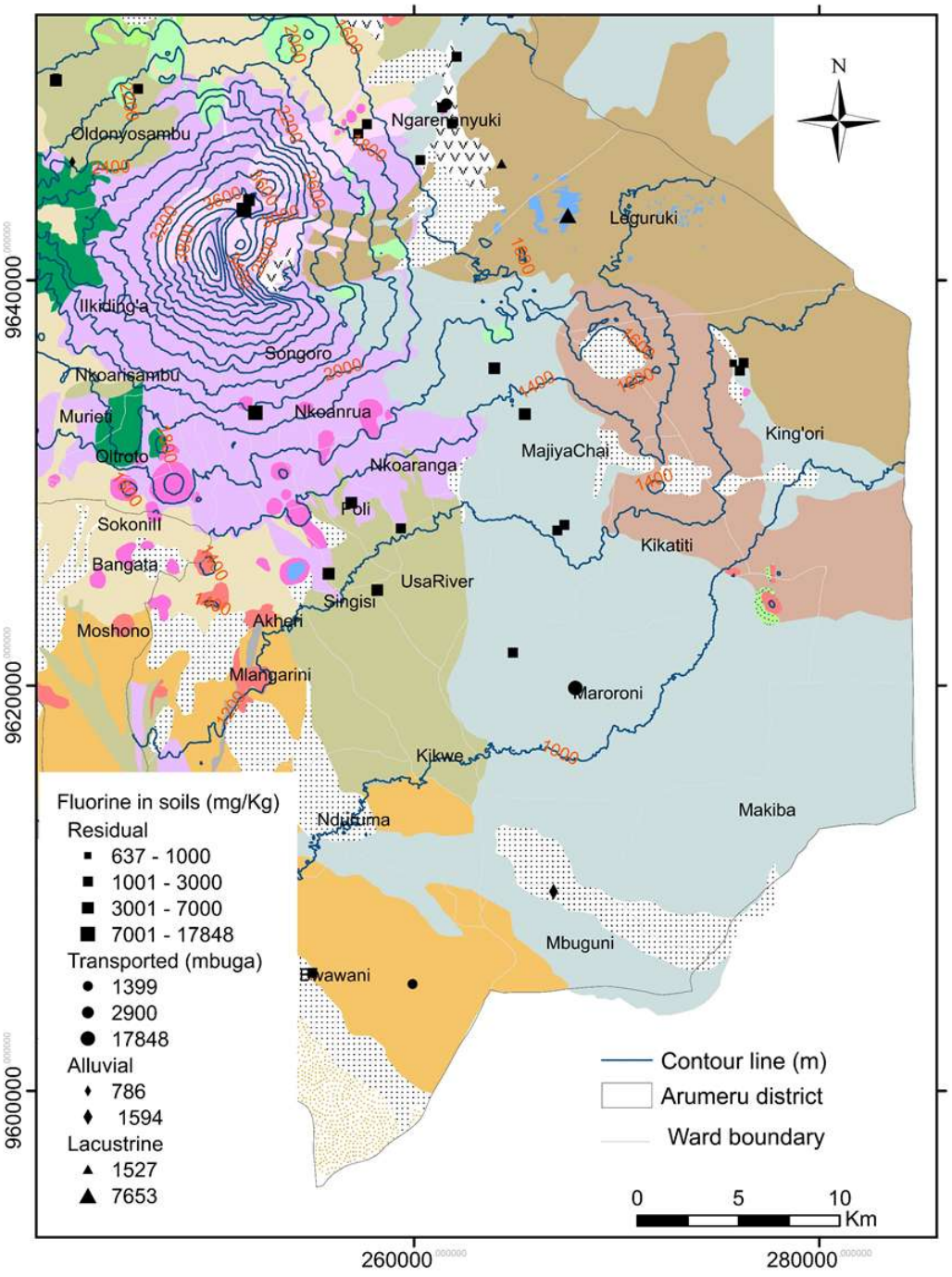

Figure 21: Spatial distribution of fluorine in soils in relation to geology and altitude. Geological legend is as in Fig. 19

3.3.10 Dispersion and mobility of fluoride

This section integrates results of rocks, soil and water so as to come up with a summary of data for assessing fluorine mobility from rocks, soil and eventually groundwater system. Based on detailed field work, results of 5 different cases integrating these three components (rock, soils and water) with fluorine/fluoride as a major focus are presented.

(i) Case 1: Rocks and their residual soils

Textural and chemical variation of 8 rocks (and others) used in this case are presented in Table 3. Results indicated that the amount of fluorine is high in rocks than equivalent soils (residual soils) (Fig. 22). However, there is exceptional case such as MR-18 where fluorine content in soil is higher than rocks (Fig. 22). On average, the amount of fluorine in rocks is three times than the amount of fluorine in soils.

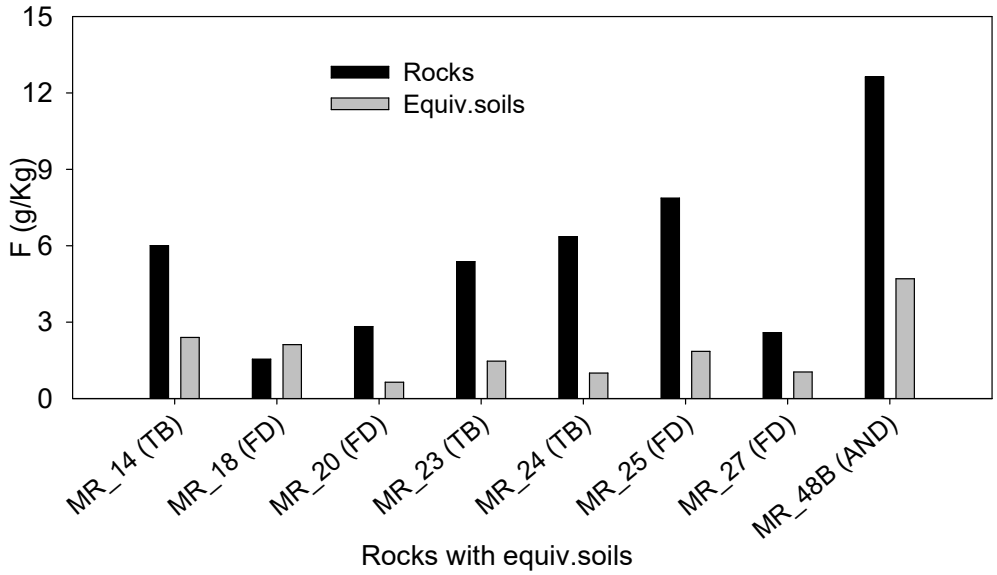

Figure 22: Fluorine concentration in rocks and their residual soils. Note that TB: Tephrite basanite, FD: Foidite, AND: Andesite

To examine fluorine mobility and dispersion mechanisms from rocks to soils, other elemental compositions were considered as shown in Figs. 23 and 24. Overall, considering the major oxides, the decrease in fluorine from rocks to equivalent soils, is associated with the decrease in SiO_2, CaO and Fe_2O_3, (Fig. 23b, f and h). Despite that Na_2O and K_2O did not show directly an increase or decrease trends from rocks to equivalents soils, there is a general increase in K_2O and a decrease in Na_2O from rocks to equivalent soils (Fig. 23c, d). The concentration

of TiO_2 remains nearly the same in rocks and their equivalent soils (Fig. 23g) whereas Al_2O_3, MnO and ZnO increased from rocks to equivalent soils (Fig. 23e, i and j).

The trace element behavior in rocks and their equivalent soils are shown in Fig. 24. In this group of trace elements, Cu is the only element which showed a clear increasing trend from rocks to equivalent soils (Fig. 24a) while V, Sr, Cr and Cl showed a general reverse trend which is similar to fluorine trend with the concentrations decreasing from rocks to equivalent soils (Fig. 24). For other trace elements (Pb, As, Rb, Y and W), their concentrations fluctuated in narrow ranges without showing a remarkable increase or decrease trend (Fig. 24).

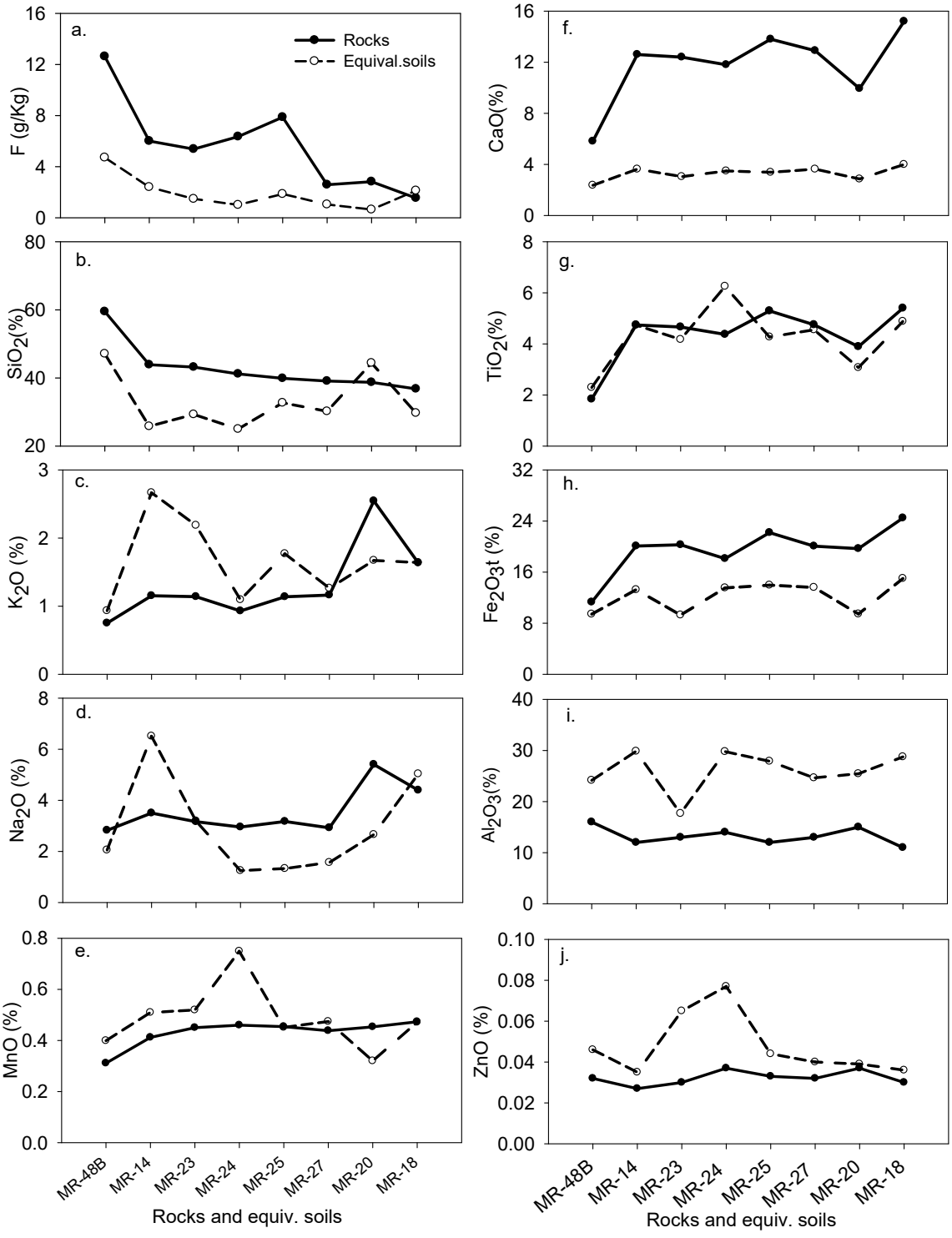

Figure 23: Fluorine and major oxides trends in rocks and their equivalent soils. The rock arrangement in all figures is similar as arranged in the bottom figures (e and j) and the legend in "a" applies to all Figures.

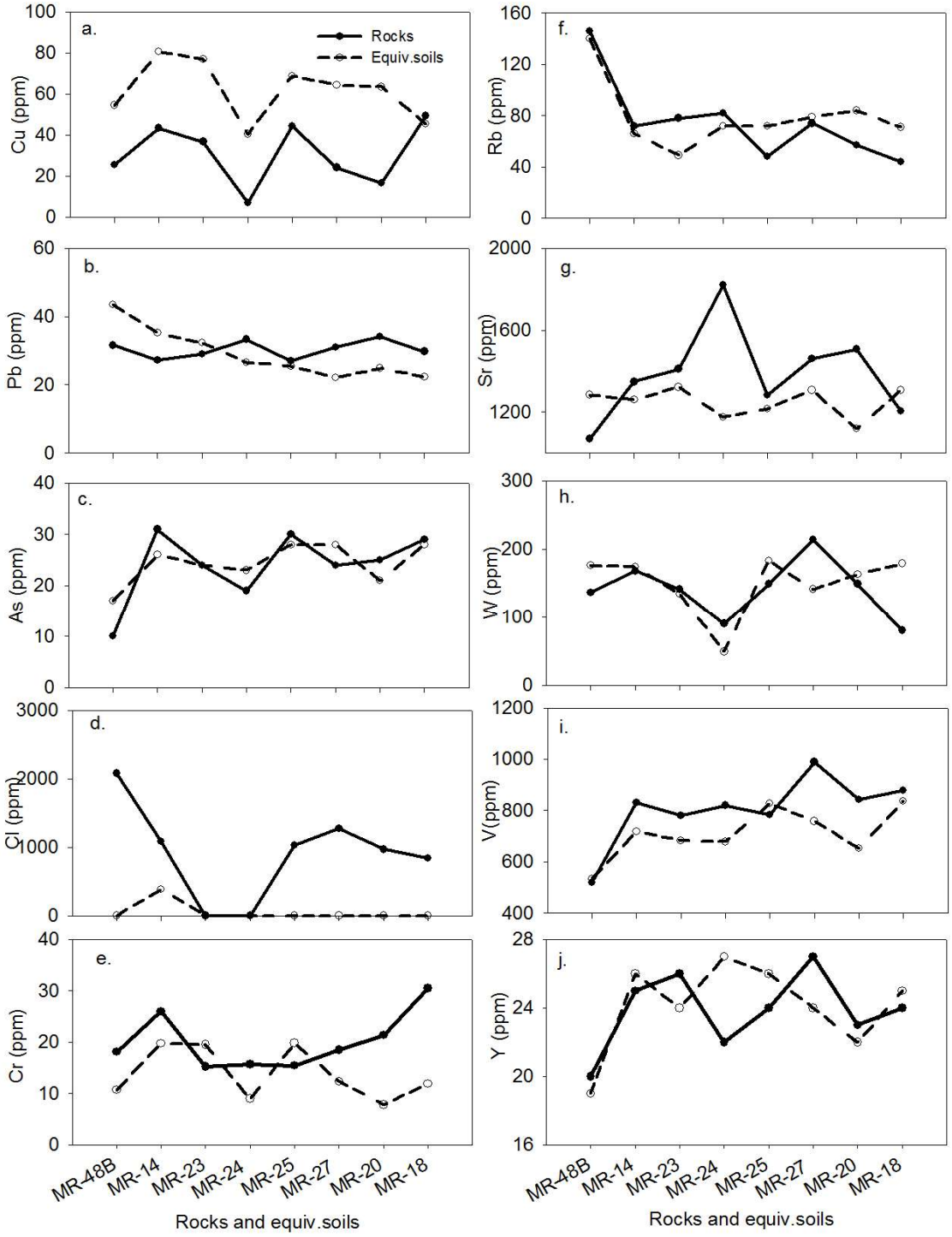

Figure 24: Trace elements trends in rocks and their residual soils. The rock arrangement in all figures is similar as arranged in the bottom figures (e and j) and the legend in "a" applies to all Figures.

(ii) Case 2: Soils and proximal groundwater water sources

Relationship between fluorine in residual soils and fluoride in the immediate (proximal) groundwater sources is presented in Fig. 25. However, one soil sample (ARS-25, transported soil) which had also its proximal water source is not presented in this Figure because of extremely high fluorine in both soils and vicinity water of 17.8 g/Kg and 84 mg/l.

Two residual soils presented in Fig. 25 (ARS-11 and ARS-13) were sampled in the leeward side (Oldonyosambu) with springs as the proximal groundwater source. Geomorphological condition supported that the soils are derived from the rocks where the springs are emerging. In this case, fluorine in soils (mean = 1.05 g/Kg) does not reflect properly the high fluoride in the proximal water sources of 14-15.3 mg/l, if the relationship obtained between mbuga soil and its proximal water source is considered. Soil samples (ASR-14 to 28B) presented in Fig. 25 were associated with well water. With exception of ARS-16 in this group, soils had low fluorine concentrations which do not match/relate with the high fluoride concentrations in the proximal groundwater source (Fig. 25). Overall, there is no clear relationship between fluorine in soils and proximal groundwater sources although some specific samples (ARS-13, 16 and 25) showed a positive relationship (Fig. 25).

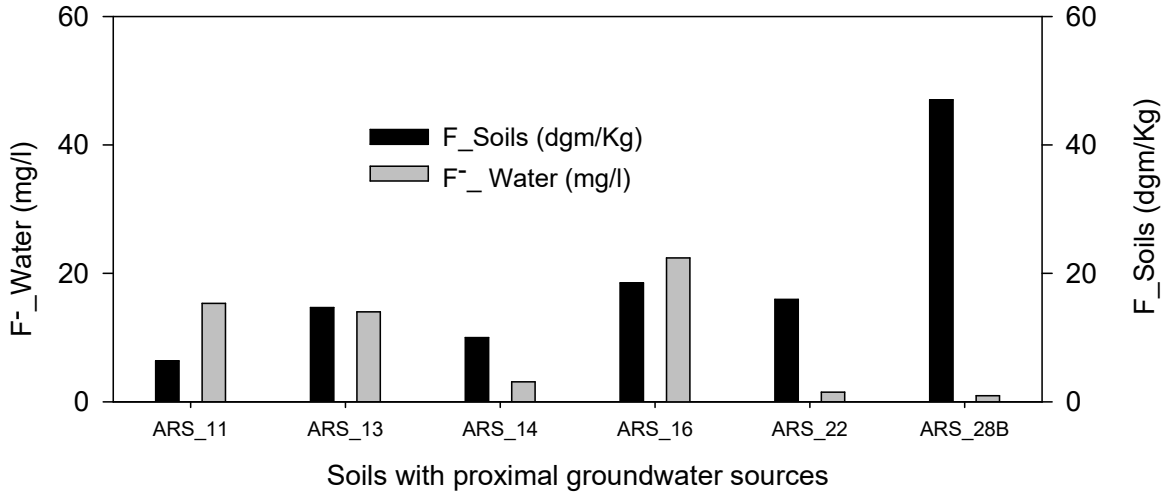

Figure 25: Relationship between fluoride concentration in soils and proximal groundwater sources with exceptional of one sample with high fluorine in both soil (178 dgm/Kg) and its vicinity water source (84 mg/l).

(iii) Case 3: Rocks and proximal groundwater sources

The relationship between rocks and vicinity groundwater sources is presented in Fig. 22. Basically, 61.5% of the rocks (MR_48B, 38, 25, 28, 34, 24, 26 and 35) are direct materials from the recent drilled dug wells and the remaining are rocks from the proximal groundwater sources. General textural variation in these rocks is also shown in Table 3. Overall, there is a direct relationship between fluorine in rocks and fluoride in the vicinity groundwater sources (Fig. 26). However, there are two exceptional cases lacking fluorine proportionality in the two sources (MR-35 and MR-48B) as shown Fig. 26.

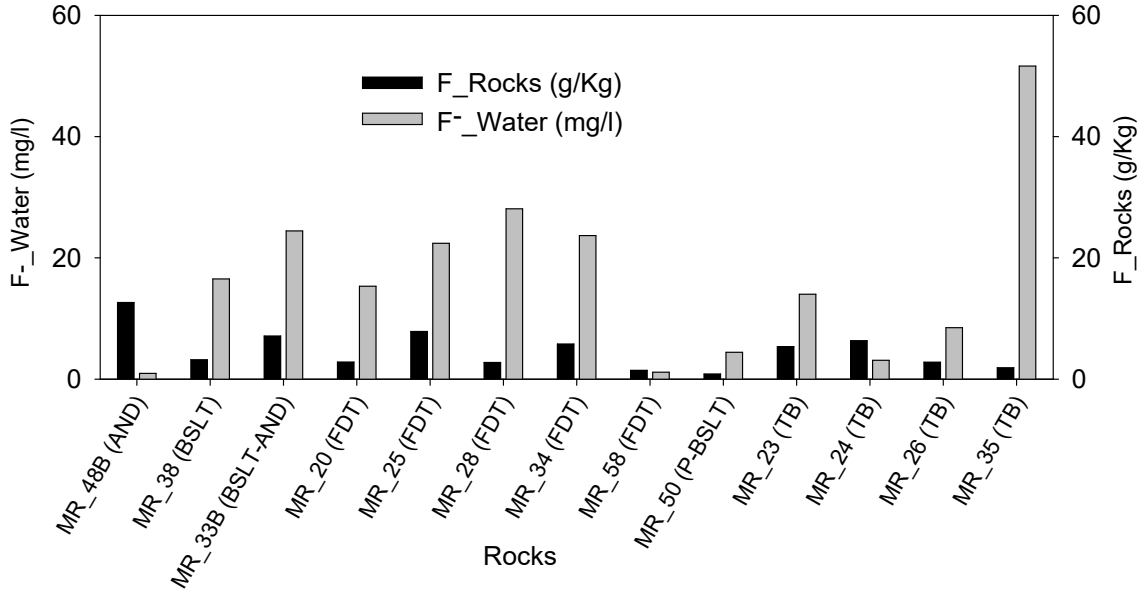

Figure 26: Relationship between fluorine in rocks and fluoride in the vicinity groundwater sources (wells) presented by histogram (a) and scatter plot (b). Note that "AND": Andesite, "BSLT": Basalt, "BSLT-AND": Basaltic andesite, "FDT": Foidite, "P-BSLT": Picrobasalt, "TB": Tephrite basanite.

(iv) Case 4: Rocks- equivalent soils-groundwater

Samples (rocks, soil and water) in Fig. 27 are presented with confidence that they are inter-linking, representing fluoride variation from rocks-soil-groundwater at the specific locations. Results showed that fluorine in rocks and equivalent soils are related to the amount of fluoride in the associated groundwater source as presented in Fig. 27. However, there is only one exceptional case (MR-48B) where fluorine content in rock and equivalent soil compare

well with other samples (proportionality) but the fluoride content in water is not in agreement with the proportionality reflected in other samples (Fig. 27).

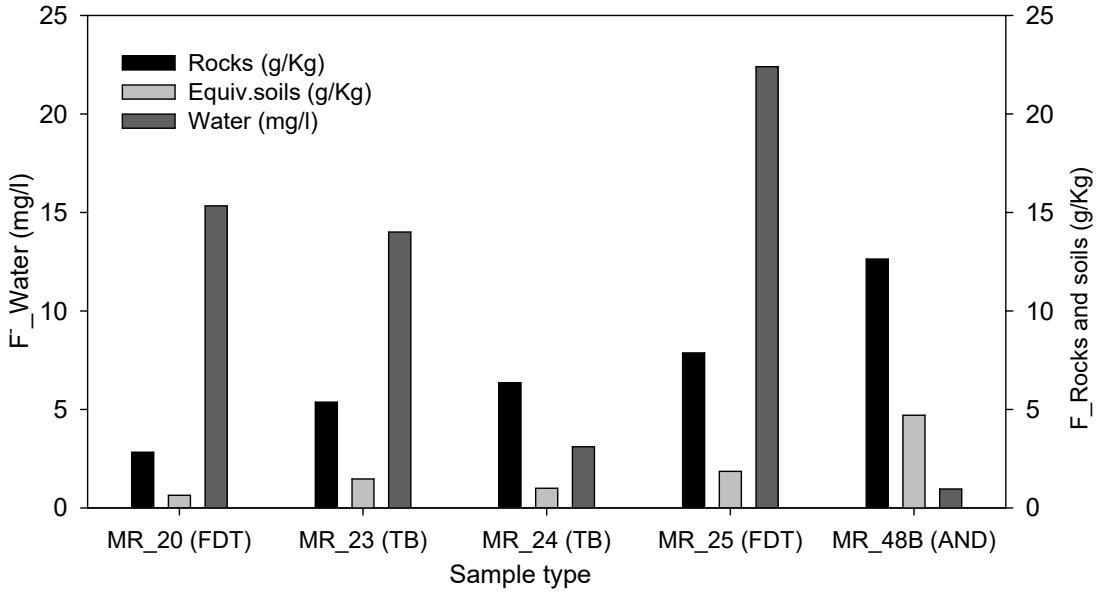

Figure 27: Fluorine variation from rocks-equivalent soils-groundwater system. The capital letters in brackets abbreviate the rock types as defined in Fig. 22.

(v) Case 5: Rocks and spring water sources

Fluoride in spring water sources does not reflect fluorine content in the associated rocks. Overall, fluorine content in rocks is randomly distributed in the leeward and windward sides of Mt. Meru but fluoride content in leeward spring sources was generally high relative to fluoride in the windward springs (Fig. 28). However, exceptional case is recognized at MR-54 (Fig. 28) where the windward spring is characterized by high fluoride (25.2 mg/l).

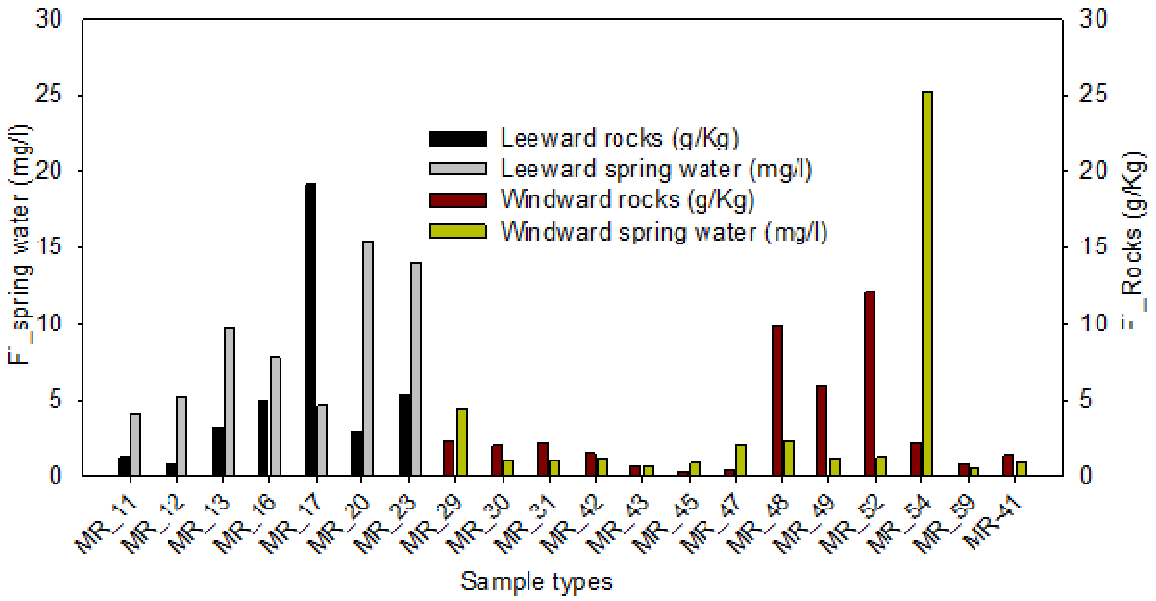

Figure 28: Relationship between fluoride in spring water sources and fluorine in the proximal rocks for the windward and leeward sides of Mt. Meru.

3.4 Discussion

3.4.1 Petrogenesis of Arumeru volcanic rocks

Geochemical data coupled with petrographic examination of lava flows were used to infer rock history and associated magmatic processes. The observed porphyritic texture in most of the Arumeru volcanic rocks reflect at least two contrasting stages of magma solidification, one in the magma chamber below surface resulting in the development of early phenocrystic crystals of various phases. This was followed by a rapid emplacement and cooling at the earth's surface, resulting in the development of fine-grained groundmass. Some phenocrysts (e.g. clinopyroxene) exhibit chemical zoning which suggests a variation in physicochemical conditions in magma chamber possibly brought in by magma replenishment. It is evident from rocks that volcanic activities at Arumeru area were accompanied by fluids (e.g., CO_2, H_2O-vapour, etc) emission. Gas emission such as CO_2 has been reported elsewhere along the EARS (Vye-Brown, 2014).

The absence of felsic rocks and limited andesitic to dacitic rocks indicate that the magma was not highly fractionated. These rocks are mostly silica under-saturated (felspathoids-bearing such as nepheline and leucite) with few silica saturated suits. The poor-silica system is further supported by the abundance of nepheline minerals which are typical the silica under-saturated minerals. The presence of sanidine in the rare intermediate rocks in the study area (andesite to

dacite), suggests that these rocks crystallized at high temperature conditions followed by eruption and rapid quenching during emplacement at surface. Alignment of minerals in one direction in some rock samples indicates the lava flow direction during the solidification of groundmass. Presence of this texture in some specific samples suggests that such rocks were formed from lava flow. However, most of the rocks exhibited different mineral orientations and in some cases crystals were broken suggesting explosive eruptions. Explosive style of volcanism is further supported by the way the rocks are randomly distributed in the study area and the presence of sanidine crystals. Such findings on the style of volcanism concur with the observation by most of the researchers along the East Africa Rift system (Roberts, 2002; Rango *et al*., 2010; Vye-Brown *et al.,* 2014).

The linear relationships shown by most of the major oxides vs SiO_2 variation diagrams for lava flows (Fig. 9) suggest a cogenetic relationship. Different trends observed in this study suggest fractionation processes. For the highly fractionated rift rocks, Na_2O and K_2O in felsic rocks generally increase with increasing SiO_2 (Peccerillo *et al*., 2007). For the Arumeru rocks which are not highly fractionated, the overall scattering of oxides of the highly mobile elements (Na_2O and K_2O) could be attributed to hydrothermal alteration as evidenced by high LOI in most of the rocks. The decrease in total Fe_2O_3, CaO, TiO_2 with SiO_2 (Fig. 9) is consistent with fractional crystallization of early and high temperature ferro-magnesian minerals (Tiepolo *et al*., 2002; Deverel *et al*., 2012). Ferro-magnesium minerls such as pyroxene, hornblende, biotite as well as Fe- and/or Ti-bearing oxides (e.g., Ilmenite, rutile and magnetite) and sphene were common in the sampled rocks (Table 4). This relationship is also supported by the strong positive correlation coefficient of 0.92 to 0.97 indicated by Fe_2O_3, and CaO when plotted vs TiO_2 (Fig. 11). The reverse trend exhibited by Al_2O_3 (i.e., increase with increasing SiO_2) suggest that Al was incompatible in most of the early high temperature minerals discussed above and consequently became enriched in the residual magma.

Positive relationship between SiO_2 and the trace element such as Rb (Fig. 10), explain the incompatibility of this element in early crystallizing minerals. Rubidium commonly substitutes for K but no K-bearing minerals crystallized in early stages of magma evolution, as a result, its enrichment is consistent with fractionation sequence. This also explains high Ba content in the andesitic to dacitic rocks while generally absent in foidite to basaltic rocks. The negative trend displayed by trace elements As, Ni and V when potted vs SiO_2 (Fig. 10) indicates their compatibility during fractional crystallization of early phases. For instance, a

study by Tiepolo *et al*. (2002) indicated high compatibility of Sr, V and Y in titanite crystals which is also abundant in the Arumeru volcanic rocks. The observed positive correlation between TiO_2 with V, Y and Y with V (Figs. 11 and 13) is due to the compatibility of these trace elements in titanite crystals. Also, according to Deverel *et al*. (2012), arsenic can easily be incorporated in Fe and Ti-oxides minerals while V has a tendency of replacing Fe in Fe-oxide minerals. Generally, compatibility explain the positive correlations of trace elements such as As with Ni, Y, V, F_2O_3, TiO_2 and CaO (Figs. 11 to 13) of which all are favored in high temperature minerals in early stages of fractional crystallization. This fact is well supported by the negative correlation between As and Rb (Fig. 13), whereas the latter is favored in the intermediate to low temperature minerals as discussed previously.

Pseudomorphs of early phenocrysts observed in some of these rocks particularly lahars and well materials result from hydrothermal alteration at or near the earth surfaces. This includes replacement of hornblende and biotite by Fe-oxides resulting mainly from the instability nature of these phases at near surface conditions. Hornblende phenocryst commonly dehydrates to Fe-oxides plus pyroxene due to pressure release upon eruption and this is exhibited by a dark rim around or a complete replacement of these crystals (Table 4; Fig. 17). Such alteration processes are likely to be accompanied by the release of species like F from these biotite and hornblende crystals.

Unaltered minerals (from fresh rocks) as observed in the rocks overlying lahar near the top of Mt. Meru are likely to represent the most recent volcanic eruption, probably of 1910 as reported by Roberts (2002). In this regard, such rocks represent the youngest sampled rock materials over Mt. Meru. However, weathering rates in this area is low due to low temperature and rainfall towards the top of Mt. Meru relative to low land areas. Thus, chronologically, the rocks at the top of the mountain and low land areas can be grouped together.

3.4.2 Fluorine sources and distribution

Among major and accessory minerals identified in the volcanic rocks at Arumeru area, the fluoride bearing minerals include apatite: $Ca_5(PO_4)_3(OH, F, Cl)$, hornblende: $Ca_2(Mg, Fe)_4Al(Si_7Al)O_{22}(OH,F)_2$, biotite: $K(Mg,Fe)_3AlSi_3O_{10}(F,OH)_2$ and titanite: $CaTi[SiO_4](O,OH,F)$. The relationship between these minerals and fluoride content in groundwater is new information along the East Africa system, although it has been reported

elsewhere but outside EARS (Hallet *et al*., 2015). In this section, these minerals are discussed separately for the purpose of assessing fluorine contribution from each mineral.

Apatite: This is an accessory mineral in these volcanic rocks that occurs as an inclusion in CPX crystals and/or interstitial phase in the fine-grained groundmass. It is encountered in only three samples: (MR-20: nephelinite, MR-24: tephrite basanite and MR-48: porphyritic basaltic trachyandesite) in minor amount (~1%). However, the possibility that it's present as a groundmass constituent in other rocks/samples cannot be precluded due to its fine-grained nature. The amount of fluorine obtained from whole rock geochemical data for these samples are 2.83, 6.35 and 9.9 g/Kg, respectively. This amount is relatively high, so apatite may contribute significant amount of fluorine.

Hornblende: It was detected in only 5 samples but in high amount compared to apatite. With respect to general composition (phenocrysts and groundmass), estimated amount was 20 % in MR-01: porphyritic basaltic andesite, 1% in MR-04: nephelinite, 2% in MR-22: andesite, 5% in MR-39: dacite and 5% in MR-48: porphyritic basaltic trachyandesite. Geochemical data indicates that fluorine composition for these rocks is quiet variable that ranges from 14.7, to 4.14, to 6.21, to 0.93 and 9.9 g/Kg, respectively. These results suggest that hornblende is the source of fluorine particularly in the porphyritic basaltic to andesitic rocks. Contribution of fluorine from other minerals such as sphene in the same rocks cannot be ignored. Hydrothermal alteration exhibited by some of these rocks, which resulted into replacement of some of these minerals (e.g., hornblende) by Fe-oxides (e.g. MR-39) could explain low fluorine content in such rocks.

Biotite: It is present in minor amounts in only 4 samples examined in this study. With exception of sample MR-01 that contains hornblende up to 20%, other three samples had low fluorine between 0.25 and 0.93 g/Kg. Minor amounts of biotite in these rocks and the obtained fluorine values from the samples containing biotite, may suggest that biotite has low contribution in the observed high fluorine values from Arumeru rocks.

Sphene: This is the abundant accessory mineral in most of the rocks. It was encountered in 16 samples out of 19 (79 %) in variable amounts ranging between 1 and 10% (Table 4). The average fluorine in this group was found to be 6.07 g/Kg which is high relative to the average fluorine values in all 68 samples (~3.92 g/Kg). Furthermore, most of the highest fluorine values such as 16.04, 14.71, 12.63 and 11.87 g/Kg are in this group. Scrutinizing this group

using integrated three factors (mean F, elevated F and abundance of sphene), reveal that sphene can be a major source of fluorine in rocks around Meru volcanic complex.

In general, petrographic examination has revealed four fluorine bearing minerals do exist in the volcanic rocks in Arumeru area, which can contribute to total fluorine in these rocks. The sequence of contribution from these minerals, in decreasing order is interpreted to be titanite > hornblende > apatite > biotite. Contribution from a combination of two or more of these minerals cannot be preclude, however, a microprobe analyses of similar phases is deemed necessary to fully understand the major host mineral(s). Sphene as the main contributing mineral has been reported elsewhere (Hallet *et al*., 2015) as a source of fluorine and one among the fluorine bearing minerals releasing significant amount of fluorine to groundwater. Volcanic rocks lacking phenocrysts of the four-suggested fluorine-bearing minerals, but with high fluorine as 6.21g/Kg (MR-22) and 12.07 g/Kg (MR-52) can be attributed to its texture. Fluorine bearing minerals in these rocks commonly occur as both phenocrysts and fine-grained unrecognizable groundmass constituent.

High fluorine content in andesitic rocks relative to all other rocks can be explained by fractionation processes. Fluorine tends to concentrate in liquid phase in early stages of magma fractionation and as a result, it becomes enriched in the fractionated/evolved magmas such as andesitic to rhyolitic rocks. Thus, for Mt. Meru magmatic source, high fluorine content is expected for the rocks which are highly fractionated such as dacite and rhyolite.

In this study, silica undersaturated (nepheline-bearing) rocks had the least fluorine bearing minerals and eventually low fluorine contents/values. Silica saturated contains most of the F-bearing minerals leading to high F contents. For instance, within a group of rocks with high fluorine (andesitic affinity), fluorine was as high as 16.04 g/Kg (MR-05) and 12.63 g/Kg (MR-48B), which are the rock sample lacking nepheline minerals (Table 4). This agrees with a study by Christiansen *et al*. (1983) which indicated that F is associated with enrichment of Rb; in this study Rb was found to be favored in late stages during magma fractionation as discussed previously. It is also in agreement with a study by McCaffrey & Willis (2001) which indicated that fluorine is more favored in felsic rocks than mafic rocks.

3.4.3 Spatial distribution of fluorine

Low fluorine in rocks toward the top of Mt. Meru relative to the rocks on the foot of the mountain could be attributed to the abundance of nephelinitic to phonolitic rocks toward the mountain (Fig. 19). The high fluoride in groundwater in areas with relatively low fluorine in rocks such as Maji ya Chai is due to the dominance of lahar materials (Fig. 19) which are mixed with pyroclastic materials (field observations). Apart from chemical composition, texture of such materials favors dissolution of minerals from parent materials leading to high dissolved ions including fluoride in water. Furthermore, relationship between fluorine in the sampled rocks and fluoride in the proximal groundwater source is not so direct because of the presence of rock fragments with different compositions in lahar materials. It is revealed that some samples collected from the zones with low fluoride in groundwater had high fluorine content. This can arise from: (a) The rock composition and texture which do not favor dissolution. (b) The outcropping rock which does not represent the major formation in that particular local area. (c) Movement of groundwater from free/low fluoride areas to that particular area.

General spatial distribution of fluorine in soil is largely controlled by parent materials, geomorphology and soil types. These factors have been pointed out by many researchers elsewhere (McCaffrey, 1998; Easterbrook, 1999) as the main control of fluorine distribution in soils. The high concentration of fluorine in soil towards the top of Mt. Meru (Fig. 21) could be attributed to addition of fluorine through volcanic ashes and pyroclastic materials. High fluorine in transported soils particularly near the foot of Mt. Meru is a result of accumulation of sediments derived mainly from lahar materials. Such sediments had high clay and probably organic matter contents; which they both have high capacity of retaining fluorine in soils (McCaffrey, 1998; Deverel *et al*., 2012). Low fluorine content in soils in the low land areas of Makiba - Bwawani - Mbuguni (Fig. 21) can be attributed to the decrease in volcanic materials (far from the source) and a nearly flat terrain from the foot of Mt. Meru to those areas which limits transportation of fluorine rich sediments.

3.4.4 Water-rock interaction processes

(i) Soils and parent rock relationship

In initial stages of weathering, the soil texture and chemistry can be used to infer the parent rock characteristics (Easterbrook, 1999). Therefore, the obtained geochemical residual soil results can be used to study the weathering processes and mobility behavior/dispersion of

some elements including fluorine from parent rocks to soils and within the soils. Studies on mobility of elements in soils (Easterbrook, 1999, Jianwu *et al*., 2013) indicate that CaO, Na_2O SiO_2 are generally mobile relative to oxides of Fe and Al. Their concentrations in soils are largely depending on the composition of the parent rock and the weathering intensity. However, their mobility is also governed by the factors such as temperature, water availability, pH of the soils, and organic matter (McCaffrey, 1998; Smedley & Kinniburgh, 2002; Wang *et al*., 2002). Extremely low CaO, low Na_2O and SiO_2 content in soil relative to parent rocks were largely attributed to high mobility of Ca^{2+}, Na^{+} and Si^{3+} relative to Fe^{3+} and Al^{3+}. They are mobilized easier within the soils and to groundwater soon after being released from parent rocks. This also, explains the observed high Al_2O_3 content in soils relative to parent rocks.

In this study, total F_2O_3 remained nearly uniform in rocks and soils and this could be attributed to the weathering intensity of the rocks and the resistant of Fe-bearing minerals such ilmenite and rutile to weathering (Easterbrook, 1999). Trace elements are powerful in defining the intensity of weathering with the mobile elements such as Sr being mobilized easier to groundwater soon after weathering (Jianwu *et al*., 2013). Thus, the nearly constant concentrations of trace elements in rocks and their residual soil (V, As, Rb, Sr, W, Cr, Y, Cu and Pb) concur with the argument of low weathering intensity and that the sampled Meru volcanic rocks are the outcome of recent volcanic phases.

The lakes, Mlolozi and Momella where Na_2O in lacustrine soils was as high as 4.8-5.3% wt are characterized by high Na^{+} in water ranging between 250 and 560 mg/l (Makoba & Muzuka, 2018, unpublished). Therefore, high concentrations of K_2O and Na_2O in lacustrine soil relative to residual soil suggest addition input of these components from lake waters. The positive relationship between Fe_2O_3 with CaO, TiO, As and V suggest the common source rocks and the strong positive correlation between Fe_2O_3 and As could indicate the common mineral source such as Arsenopyrite (FeAsS).

Similarities in rock materials and the ion exchange between Na^{+} and K^{+} can be used to explain the positive relationship between Na_2O and K_2O in residual soils. However, rocks similarity is not well supported by rock composition because of the lack of linearity between these two oxides in soils. In contrast, lack of linearity could be attributed to hydrothermal alteration as evidenced by high LOI. Organic matter, Fe and Mn-oxides tend to adsorb metals

in the soil (Deverel *et al*., 2012). Therefore, the positive correlation between ZnO and MnO could be largely attributed to adsorption of Zn onto MnO.

(ii) Rocks and their residual soils

Rocks and their residual (equivalent) soils are considered for assessing mobility and dispersion of fluoride from rocks to soils. High fluorine in rocks relative to their residual soils indicate that high amount of fluorine is still locked in the rocks. A direct proportionality (R = 0.77, P=0.05) between fluorine in rocks and soils (Fig. 29a) indicate that fluorine in the soil is the direct weathering product from the parent rocks. Under the assumption that there is no fluorine input on soils from ashes and pyroclastic materials and by neglecting fluorine that have been mobilized to groundwater, the amount of fluorine that have been released from rocks is estimated to be 27% only. According to Easterbrook (1999), Ca^{2+} and Na^{+} are the most mobile element while Fe^{3+} and Al^{3+} are nearly immobile. Therefore, the similar decreasing trends for fluorine and the oxides of the most mobile elements (Ca^{2+} and Na^{+}) that displayed a positive relationship (Fig. 29) suggest that some amount of fluorine have been mobilized from residual soils. This accounts for high fluoride in the transported soils as well as groundwater. However, as pointed out by Smedley & Kinniburgh (2002) that clay content and organic matter have high capacity of retaining fluorine, high clay content and possibly organic matter contribute to high fluoride in transported soils. This also accounts for low fluoride in typical alluvial soils (dry wash sands) which are dominated by relatively medium to coarse sands. The decrease in SiO_2 and Fe_2O_3 and an increase in Al_2O_3 from rocks to soils were discussed previously.

Nearly constant concentrations for the trace elements (As, Pb, Rb, Y and W) in rocks and equivalent soils suggest that weathering was not so intensive as discussed previously. Since the mobility of the elements Cr, V is always high in soils (Deverel *et al*., 2012) and Sr is one among the active elements in weathering and mobility processes (Jianwu *et al*., 2013), their low concentrations (including Cl) in soils relative to their parent rocks is strongly attributed to their mobility. The metals such as Cu, Zn and Pb are easily adsorbed by organic matter, clays through ion exchange processes, Fe and Mn-oxides (Rieuwerts, 2007; Deverel, 2012). This explains the high concentration of Cu, Zn and Mn in soils relative to their parent rocks.

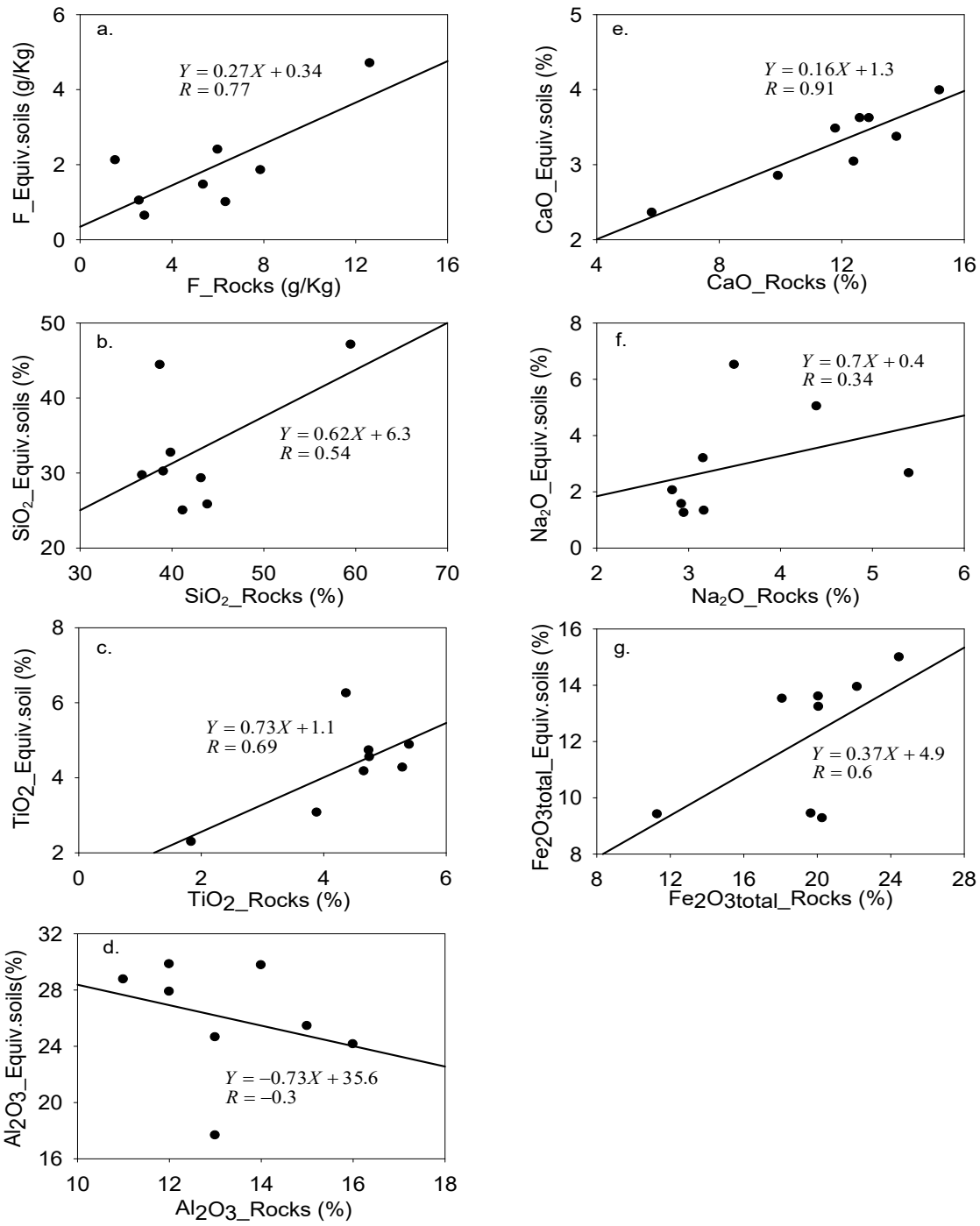

Figure 29: Scatter plots showing fluorine and major oxides trends in rocks and their residual soils

(iii) Water and rocks/soils with emphases on fluorine

Fluoride relationship between soils and proximal groundwater sources is not so direct suggesting that fluoride in groundwater sources can be attributed to a combination of

processes such as dissolution of fluorine from geological materials (e.g., rocks and soils) and fluoride that has been mobilized from other areas. For instance, high fluorine in soil collected from the dug well which was under construction on the steep slope of Mt. Meru (e.g., ARS-28B, 4703 mg/Kg) which is not reflected in the nearby water source (0.96 mg/l) may suggest that: (a) Short contact time between soil and water (b) Since the well is dominated by lahars of different composition, the soil taken was from the upper part of the well above the water table which lack direct interaction with groundwater. The observed correspondence between fluorine in soil (ARS-25, 1780 mg/Kg) and fluoride in the proximal water source (84 mg/l) for the well located in transported soil may suggest a direct dissolution of fluorine from soil to groundwater. This is well supported by the nearly flat terrain and the surrounding lahar materials which are susceptible to weathering due to their texture (loose ashes and pyroclastic materials which favor water-rock interaction).

A general direct proportionality between fluorine in rocks and fluoride in the proximal groundwater sources indicate dissolution of fluorine from the rocks. In few exceptional cases where fluoride in water is extremely high (51.6 mg/l) which does not reflect low fluorine in rocks (1872 mg/Kg) could be attributed to lahar materials that exhibit different chemical composition (Table 3). In such cases, it is possible to sample the rocks which are not/weakly contributing to fluoride in the proximal groundwater source. The association of low fluoride in water (0.96 mg/l) with high fluorine in the proximal rocks and soils (MR-48B; 12629 mg/Kg, ARS-28B; 4703 mg/Kg) could be related to groundwater movement as discussed previously. Fluorine dissolution from rocks is well supported by the samples which were selected with confidence to represent fluorine mobility from rocks-soil -groundwater at various stations.

Spatial distribution of fluorine indicated that fluorine bearing rocks are randomly distributed regardless of the type of water sources (Fig. 19). Therefore, the low fluoride in springs which is not reflected in the nearby rocks suggests short residence time between water and rocks. The short residence time could be attributed to fractured formation (Ghiglieri *et al*., 2012) and high hydraulic gradient on the slope of Mt. Meru where most of the springs are located. Difference in fluoride between the windward and leeward springs is largely attributed to climatic factors (Malago *et al*., 2017; Makoba & Muzuka, 2018, unpublished data). Extremely high fluoride in lakes does not conform with the observed fluorine values in the vicinity rocks suggesting other mechanisms for fluoride enrichment. In this study, the integrated F^- enrichment mechanisms are proposed: (a) The lakes were formed as a result of

collapse of eastern arm of Mt. Meru (Vye-Brown *et al*., 2014) of which rocks contain significant amount of fluorine as stipulated in this study. The lake formation was associated with accumulation of huge volcanic materials and water accelerated dissolution of fluorine from the rocks/mass materials; (b) There are underground springs which are feeding the lakes; these are responsible for high input of fluoride in the lakes; (c) Excessive evaporation and low precipitation in the leeward side enhance fluoride concentration in lakes. (d) There is additional input of F^- from volcanic ashes and gases. Volcanic ashes were proposed by Ghiglieri *et al*. (2012) as the main source of fluorine in the study area and the argument on fluorine enrichment through gases arises from the tendency of F to concentrate in vapor phases during magmatic processes (Christiansen *et al*., 1983).

3.5 Conclusions and Recommendations

It is revealed from lava flows that volcanic rocks around Mt. Meru are weakly to moderately fractionated, mostly silica undersaturated to minor silica saturated, which are possibly derived from a common homogeneous parent magma (i.e. cogenetic magmatic rock). Classification based silica content versus total alkali (TAS classification diagram) indicate that these rocks have variable compositions that ranges from silica-poor (foidite) to intermediate (andesitic) compositions. Harker and correlation diagrams indicated that the elements As, Sr and V were compatible in early crystallizing minerals during magma evolution processes. Trace elements specifically V and Y were highly compatible in sphene crystals suggesting that these elements were incorporated into sphene crystals. In contrast, Ba and Rb were incompatible during early stages and therefore incorporated into phases crystallizing late during magmatic evolution.

Petrographic examination indicated that clinopyroxene, nepheline and plagioclase are the dominant minerals in both lava flows and lahar materials around Mt. Meru accounting for >70% of all minerals. Other minor and accessory minerals are sphene, Fe-oxides (ilmenite and magnetite), apatite, rutile, hornblende, biotite, sanidine microcline, zircon and calcite as a secondary mineral. Generally, unlike porphyritic texture which is common in both lava flows and lahars, lava flows exhibited trachytic and seriate textures. Only few samples exhibited aphanitic textures. Some phenocrysts contain inclusions of other phases (commonly apatite). The presence of pristine phenocrysts of sanidine crystals, broken phenocrysts of some minerals suggest an explosive volcanism that was followed by rapid cooling.

All rock types contain fluorine but in varying amounts that ranges from 251 to 19 122 mg/Kg (mean = 3921mg/Kg). Petrographic examination suggests that minerals that are likely to contribute to high fluorine in rocks in decreasing order are: sphene > hornblende > apatite > biotite. Fluorine is more concentrated in rocks with andesitic affinity than in any other rock type. About 83% of the rocks with basaltic andesite to basaltic trachyandesite affinities (n = 6) and 43% of rocks with andesitic affinity (n = 7) have F above 5000 mg/Kg, with the mean values of 10610 mg/Kg and 10 240 mg/Kg, respectively. This suggests that F was largely favored in late crystallizing minerals than early crystallizing minerals. This is well supported by the dominance of fluorine bearing minerals in fractionated silica saturated rocks relative to silica under-saturated rocks.

Fluorine in soil samples ranged from 637-17848 mg/Kg (mean = 3526 mg/Kg). High fluorine content was found in transported soil (mean = 7382 mg/Kg, n = 3) and this can be attributed to accumulation of F-rich materials, high clay content and possibly organic matter. Lacustrine soils particularly around Lake Momella also had high fluorine content (7382 mg/Kg), reflecting its interaction with lake water where fluoride is as high as 1402 mg/l. Fluorine in rocks is generally randomly distributed but in soils is more controlled by its abundance in parent materials (commonly rocks), texture of the parent material, geomorphology and soil types.

The average concentration of F in rocks was found to be higher (about 3 times) than the average F in their residual (equivalent) soils. Linear correlation of F in these two materials was positive with the correlation coefficient of 0.77 (P = 0.05). Strong depletion of mobile elements particularly Ca^{2+} and depletion of trace elements Sr, Cr, V and Cl in residual soils relative to their parent rocks indicate that some amount of fluorine have been mobilized from the residual soils to groundwater. However, nearly constant concentration of trace elements As, Rb, Y and W in rocks and their residual soils suggest that weathering was not so intensive.

As it was for the case of fluoride in the soils, water-rock interaction showed that fluoride in well water is controlled by the abundance of fluorine in the rocks and soils, the rock texture and groundwater movement. However, in some few cases, particularly in the areas dominated by lahar materials, a link between fluoride in groundwater and fluorine in rocks was not well pronounced. This is attributed to difficulties in getting reliable the sample during sampling campaign that could represent chemical interaction with well waters. These data further

suggest that spring water source, particularly from the windward side are characterized by short residence time between water-rock interaction as evidenced by low fluoride which does not conform with/or reflect the amount of fluorine in the rocks proximal to water sources. This short residence time is attributed to fractured formation and high hydraulic gradient on the main recharge zone (slopes of Mt. Meru). Also, despite of high fluorine in the rocks and soils around the windward lakes, the amount of fluoride in the lakes is extremely high suggesting other sources (or enrichment mechanism) of fluoride than rocks alone. The possible mechanisms are: fluoride inputs from underground springs, excessive evaporation accompanied with low precipitation and intensive dissolution of fluorine rich materials. As a result, this study recommends leaching experiments for all rocks so as to understand fluorine release mechanisms and microprobe analyses of proposed fluorine bearing minerals to quantify and ascertain the amount of fluorine in these minerals.

CHAPTER FOUR

WATER QUALITY AND HYDRO-GEOCHEMICAL CHARACTERISTICS OF GROUNDWATER AROUND MT. MERU, NORTHERN TANZANIA[3]

Abstract

Climate change and population growth around Mt. Meru experienced lower availability of water for domestic and agricultural uses. Reduction in quantity of water is compounded by lack of information on water quality which could lead to undesired health risks and agricultural effects when such water is used for irrigation. Thus, major ions from 54 different water types (springs, streams, dug wells, boreholes, and lakes) were used to assess hydrogeochemical characteristics and suitability of water for domestic and agricultural purposes. Results showed dominance of the major cation and anion in the order of $Na^+ > K^+ > Ca^{2+} > Mg^{2+}$ and $HCO_3^- > CO_3^{2-} > Cl^- > SO_4^{2-} > NO_3^- > F^-$, respectively. It is revealed that Mt. Meru is the recharge zone. Geology, water–rock interaction time, and climatic conditions control water chemistry. Major freshwater aquifers were found to be fractured mafic volcanics, breccia, and tuff. Lahars, due to their susceptibility to weathering, were found to host groundwater of low quality. The suitability of water for domestic and irrigation purposes was moderate, in order of lakes < dug wells < boreholes < streams < springs. Fluoride was found to be the major natural contaminant affecting water quality for domestic purposes with mean value of 17.6 mg/l, while elevated Na^+ (mean = 118 mg/l), K^+(mean = 59 mg/l) and HCO_3^- (mean = 390 mg/l) relative to other ions were found to affect water quality for irrigation purposes. In some few cases, anthropogenic pollutions were recognized through NO_3^- and Cl^-. Effective utilization of the available water sources, geological and geophysical works for rock characterization and delineation of low fluoride groundwater zones are recommended.

[3] Published in the Journal of Applied Water Science (2019) 9:120

4.1 Introduction

Access and provision of safe and clean water to people, which is among human rights, has been a continued aim globally. Population growth, poverty and economic instability among countries have been pointed out to be causative factors towards not achieving goal No. 7 of the Millennium Development Goals (MDGs) particularly (UNICEF, 2015). It is estimated that about 11% of the population globally have no access to safe and clean water with a large number of people living in Sub- Saharan Africa and Ocenia (UNICEF, 2015). Majority of population in these areas continue to depend largely on rivers, lakes, ponds and irrigation canals as their major sources of drinking water (UNICEF, 2015). Some of these sources are polluted naturally and most of them are vulnerable to anthropogenic pollution.

Most of the developing countries are facing economic water scarcity (UNOCHA, 2010). Tanzania, one among the developing countries is significantly facing economic water scarcity despite of having several fresh water sources such as lakes and rivers. Water supply from these potential sources to rural and urban areas is still at low scale. In the year 2015, Tanzania was still among the few countries with lowest coverage in accessing an improved drinking water sources and sanitation (UNICEF, 2015). The water demand is currently increasing due to both population growth and climate change. Due to these factors, there is a positive trend towards utilization of groundwater as the main water source for domestic purposes. However, groundwater in the country is not yet properly explored and natural to anthropogenic contaminations continued to lower availability of water for drinking purposes. This creates urgent need for more scientific researches on groundwater in Tanzania.

Anthropogenic activities are pronounced in both urban and rural areas. In urban areas, contamination is mainly attributed to industrial activities and onsite sanitation where as in sub-urban to rural areas it is mainly caused by agriculture activities (Mohammed, 2002; Elisante & Muzuka, 2015, 2016a,b). Fluoride is one among the natural contaminants in groundwater systems which is common in volcanic regions of Tanzania. According to the fluoride groundwater survey in Tanzania, it was found that 30% of waters used for drinking exceed the recommended standard by WHO, 1.5 mg/l (Thole, 2013). The most affected areas are along the rift system, the central to Lake zone parts with fluoride being released from igneous rocks of variable alkaline to basic compositions.

Arumeru district is among the districts of Tanzania situated along the Eastern branch of the East Africa Rift System. Its climate and geology is significantly controlled by Mt. Meru

which is the second highest Mountain in Tanzania (4565 m above sea level). The mountain, divides the district into two climatic zones- windward and leeward sides creating variations in hydrological and hydrogeological processes. The mountain is active and volcanic activities have led to several phases of volcanic materials such as lahars, pyroclastic, mantling ash, phonolitic to nephelinitic materials (Dawson, 2008; Ghiglieri *et al.,* 2010; Ghiglieri *et al.,* 2012). Such materials have been related to high concentration of fluoride in groundwater above the maximum recommended standard of 1.5 mg/l (WHO, 2008). For instance, Nanyaro *et al*. (1984) reported high concentration of 690 mg/l from Lake Momella. Since then, high fluoride values have been reported in other water sources within the study area (Gaciri & Davies, 1993; Ghiglieri *et al.,* 2010, 2012). Several geological and hydrological studies have been conducted within the area (Nanyaro *et al.,* 1984; Gaciri & Davies, 1993; Dawson, 2008; Ghiglieri *et al.,* 2010, 2012) . Most of the researches were limited to fluoride (Nanyaro *et al.,* 1984), some studies were constrained in specific parts (Ghiglieri *et al.,* 2012, northern part of Mt. Meru) and most of them lacked a continuous data set for the whole district that could integrate all water types from the windward to leeward sides for detailed study of hydrogeochemical characteristics, groundwater evolution and water quality for both domestic and irrigation purposes.

There is high population growth in Arumeru district leading to rapid expansion of agricultural activities and increased water demand for domestic purposes (Istituto Oikos, 2011; Vye-Brown *et al.,* 2014). Agricultural expansion is associated with application of fertilizers and therefore likely to cause contamination in both surface and groundwater systems. In attempt to reduce water problem, local people have been drilling deep bore holes and/or constructing shallow hand dug wells particularly in the areas lacking surface water sources. Due to climate change, the rate of constructing wells in these areas has increased rapidly. Vulnerability to contamination is high as some wells are drilled close to pit latrines and cow sheds. Furthermore, according to the interview with the local people, most of the drilled hand dug wells are utilized without testing the suitability of such water for particular uses. This is obviously affecting the human health through direct or indirect consumption of such water and also likely to lower crop production. Therefore, this study aimed to characterize all water sources in the area and assess their suitability for domestic and agricultural purposes. It also intended to gather information on hydrogeological processes which integrate water types and its evolution. Through this, zones with different water types and quality and zones susceptible to rapid significant hydrogeochemical changes can be identified. Such information is also

important in Water Management Plans especially in water allocation for specific uses, protection and conservation of water resources and in locating future potential boreholes for domestic purposes.

4.2 Methodology

4.2.1 Study area

The study was conducted in Arumeru district, which is located along the eastern branch of the East Africa Rift System, northern Tanzania (Fig. 30). Mount Meru divides the area into two distinctive windward and leeward zones with different climatic conditions. The windward side receives high rainfall averaging at about 1000 mm per annual (PBWB/IUCN, 2008) with most of the springs originating on the slopes of the mountain. The leeward zone receives low rainfall; the mean annual rainfall being less than 500 mm (PBWB/IUCN, 2008). There are limited springs in this side relative to windward side with Ngarenanyuki River as the only perennial stream. Most of the tributaries join the main streams on the slopes of the mountain. As a result, on the foot of the mountain and further in the lowland within the study area, access of surface water to local people becomes low, forcing them to alternative source which is groundwater. Hence, most of the boreholes and dug wells are located in these areas.

There are two groups of Lakes surrounding Mt. Meru. The first group is composed of crater lakes of Duluti and Ngurodoto in the windward side of the mountain. The second group is the Momella series lakes in the leeward side of the mountain which are believed to have been formed from the collapse of Mt. Meru (Dawson, 2008; Istituto Oikos, 2011). As the formation mechanism of the two groups of lake is different and they are subjected to slightly different climatic conditions, different hydrological and hydro-geological characteristics are expected.

Groundwater chemistry is highly controlled by the geology of the area. Mt. Meru is tectonically active with last eruption occurring in 1910 (Vye-Brown *et al.,* 2014). Various volcanic materials and probably of different eruption phases such as lahars, ashes, pyroclastic, basalts, nephelinite and phonolites have been documented in the area (Wilkinson *et al.,* 1986; Dawson, 2008; Ghiglieri *et al.,* 2010, 2012) . Also, erosion from the steep slopes of Mt. Meru, particularly from the loose lahars, ashes and pyroclastic materials has led to accumulation of alluvial sediments in the lowland areas within the study area. Thus, factors such as geology of the area, topography and climatic conditions need to be considered for effective evaluation of groundwater characteristics.

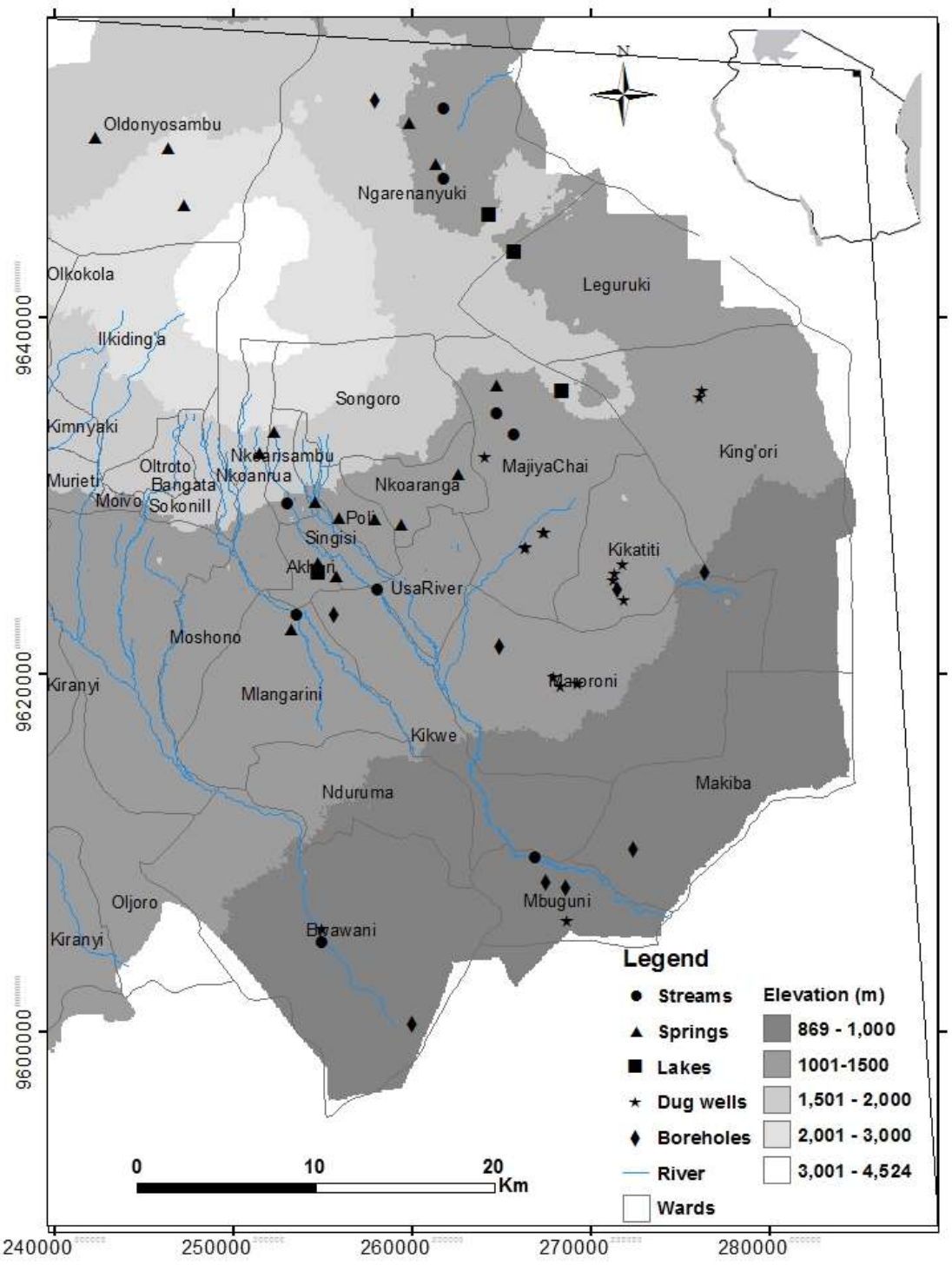

Figure 30: Location of water samples collected for assessing water quality and hydro-geochemical characteristics of groundwater in Arumeru district.

4.2.2 Fieldwork

A total of 54 water samples (16 dug wells, 10 boreholes, 4 lakes, 15 springs and 9 streams) were collected within Arumeru districts between May and August, 2015 for major ions characterization purpose. As fluoride is the critical problem in the area (Nanyaro *et al.,* 1984; Ghiglieri *et al.,* 2010, 2012; Malago *et al.,* 2017), other 45 water samples were collected specifically for detailed assessment of spatial distribution of fluoride in the area. Unlike the boreholes which were deep (~20-180m), dug wells were shallow (~5 – 30 m) being drilled for specific uses such as domestic, agriculture and washings. Regardless of the uses, samplings were conducted in dug wells with the intention of assessing water-rock interaction processes. The relevant information such as the well use, age, water level, water level fluctuation history, well-geological materials and the general local geology were accurately documented.

The sampled windward springs were 10 and the leeward springs were 5. In all cases, sampling was done systematically from the slopes of the mountain to the foot of the mountain and away from the mountain so as to have good representative samples for assessing variation in hydro-geochemical characteristics. However, most of the springs were on the slope of the Mt. Meru; only 2 springs were found to be at a distance of about 5-10 km away from the foot of Mt. Meru which is locally defined by an altitude of 1500 m above sea level (Fig. 30). Representative streams were sampled in both leeward and windward sides with consideration of important factors such tributaries joining the streams, presence of agricultural activities, ephemeral and perennial streams, stream depths and flows. These are important factors for assessing water-rock interaction processes. Stagnant water bodies were represented by 4 lake samples; 2 being crater lakes located in the windward side and two in the leeward side of Mt. Meru. In all cases, the surrounding local geology was properly documented.

During sampling, water sampling procedures were followed. All sampling precautions mainly bottle cleanness, labelling and tightness, duplicates and proper water mixing before sampling were taken in care. In-situ measurements of total dissolved solids (TDS), pH, dissolved oxygen (DO), electrical conductivity (EC), and temperature were done using the Hanna - HI 9829 Multi-parameter under appropriate daily calibration. Finally, the collected samples were filtered using 0.45 μm membrane filters. The filtered samples were collected in triplicate in 1000, 500 and 500 ml polyethylene bottles. For two bottles of 500 ml each, samples were

acidified immediately by concentrated HNO_3 and H_2SO_4 to pH < 2 and kept in cool boxes for preservation purposes before analyses of major cations. The 1000 ml bottles were not acidified and were used for immediate analyses of fluoride and major anions.

4.2.3 Analytical work

Fluoride analyses were done at the Nelson Mandela African Institution of Science and Technology (NM-AIST) laboratory using the Fluoride Ion Selective Electrode (FISE) within six days of sampling. The reagent used was the Total Ionic Strength Adjustment Buffer (TISAB II) with CDTA. The daily calibration of the instrument was done using fluoride standards of 1mg/l and 10 mg/l with the magnetic steer at 25 °C. The ratio of TISAB to field sample was 1:1 making a total of 10 ml for analyses. Various measures were taken for quality control and assurance. The FISE was first tested using both the solutions that were used in calibration and the certified drinking water bottled samples with the known fluoride concentration. Secondly, three portions of each field sample were prepared and appropriate average fluoride concentrations were recorded. Thirdly, some few water samples were taken at Ngurudoto (the near de-fluoridation water laboratory centre) for analysis and the results were compared.

(i) Major ions

The concentrations of major cations (Na^+, K^+, Ca^{2+} and Mg^{2+}) were measured using Inductive Coupled Plasma Optical Emission Spectroscopy (ICP-OES) at SEAMIC, Dar es Salaam. Titration technique was employed to determine total alkalinity and hence concentrations of HCO_3^- and CO_3^{2-}. Different techniques were used to determine concentrations of other major anions. Cl^- was determined by Argentometric titration, SO_4^{2-} was measured by turbidimetric method and NO_3^- was determined by cadmium reduction method (Spectrophotometric, Cadmium Reduction). For quality purposes, duplicates were used and some samples were cross-checked at the nearby Ngurodoto Laboratory Defluoridation Research Centre (NDLRC). Accuracy of the major analysis was checked using cation - anion balance error (CBE). Generally, CBE was found to be <10% indicating that analysis was fair.

(ii) Major parameters for Agriculture purposes

The important parameters for irrigation purposes (Residue Sodium Carbonate (RSC), Sodium percent (%Na), Sodium Adsorption Ratio (SAR), Magnesium Adsorption Ratio (MAR) and

Kelley's ratio (KR)) are summarized below with the appropriate equations (values in meq/L) which were used in evaluation of Arumeru groundwater (equations 4.1 to 4.5).

Residue Sodium Carbonate (RSC): It is an important factor in irrigation when water samples are characterized by high [(HCO_3) + CO_3)] relative to [Ca+Mg] (Bashir *et al.,* 2013). RSC was calculated using equation 4.1.

$$RSC = \left[\left(HCO_3^{-}\right) + \left(CO_3^{2-}\right)\right] - \left[\left(Ca^{2+}\right) + \left(Mg^{2+}\right)\right] \quad (4.1)$$

Sodium percent (%Na): Sodium percent is an important factor in irrigation as it relates directly to soil structure. It was calculated using equation 4.2:

$$\%Na = \left(\frac{Na^{+} + K^{+}}{Na^{+} + K^{+} + Ca^{2+} + Mg^{2+}}\right) * 100 \quad (4.2)$$

Sodium Adsorption Ratio (SAR): This is the measure of the amount of Na in water relative to Mg and Ca for irrigation purposes. It was calculated using equation 4.3 (Bashir *et al.,* 2013):

$$SAR = Na^{+} \Big/ \sqrt{\frac{Ca^{2+} + Mg^{2+}}{2}} \quad (4.3)$$

Magnesium Adsorption Ratio (MAR): Magnesium content in water is highly related to infiltration process during irrigation. The Magnesium adsorption ratio was calculated using equation 4.4:

$$MAR = 100 * \left(\frac{Mg^{2+}}{Mg^{2+} + Ca^{2+}}\right) \quad (4.4)$$

Kelley's ratio (KR): This is basically a ratio of Na+ to (Mg^{2+}+Ca^{2+}), used to evaluate the suitability of water for irrigation purpose. It was calculated using equation 4.5:

$$KR = \frac{Na^{2+}}{Ca^{2+} + Mg^{2+}} \quad (4.5)$$

4.3 Results

4.3.1 Physico-chemical parameters and major ions

Physico-chemical parameters and major ions results from Arumeru water sources are presented in Appendix 5. Statistical summary of Physico-chemical parameter results is presented in Table 5 and the corresponding summary of the major ion results is presented in Table 6.

Table 5: Statistical summary of physico-chemical parameters

Parameter	Min-Max	Mean ± SD	Median	25th Perc	75th Perc
		Boreholes (n=10)			
pH	6.78 - 8.9	8.04 ± 0.57	8.01	7.89	8.18
DO (ppm)	2.56 - 6.12	4.96 ± 0.99	5.2	4.61	5.47
EC (µS/cm)	437 - 3573	1121.8 ± 954.84	777	568.75	1093
TDS (mg/L)	219 - 1786	560.8 ± 477.28	388	284	546.5
Temp (°C)	21.85 - 26.33	25.06 ± 1.28	25.46	24.73	25.84
		Dug wells (n=16)			
pH	7.17 - 9.25	8.43 ± 0.57	8.47	8.23	8.8
DO (ppm)	0.62 - 4.53	3.28 ± 0.99	3.2	2.74	4.05
EC (µs/cm)	592 - 4844	2335.13 ±1290.28	2342	1117.75	3451.25
TDS (mg/L)	296 - 2422	1167.25 ± 644.96	1170.5	558.5	1726
Temp (°C)	22.36 - 27.04	24.32 ± 1.45	24.19	23.11	25.24
		Lakes (n= 4)			
pH	6.84 - 9.57	8.24 ± 1.12	8.28	7.86	8.66
DO (ppm)	0 - 5.37	2.65 ± 2.38	2.62	1.13	4.15
EC (µs/cm)	254 - 8715	2961.5 ± 3949.7	1438.5	445.25	3954.75
TDS (mg/L)	127 - 4357	1481.75 ± 1974.3	721.5	223	1980.25
Temp (°C)	19 - 27.84	22.15 ± 3.9	20.87	20.39	22.63
		Springs (n= 15)			
pH	6.46 - 10.91	7.77 ± 1.25	7.44	6.73	8.53
DO (ppm)	2.59 - 7.28	4.72 ± 1.3	4.60	4.01	5.70
EC (µs/cm)	137 - 1094	471.47 ± 322.22	339.00	232.50	737.00
TDS (mg/L)	69 - 547	235.73 ± 160.76	170.00	116.50	368.00
Temp (°C)	13.76 - 22.54	18.57 ± 2.57	18.00	17.43	20.16
		Streams (n= 9)			
pH	7.04 - 9.7	8.43 ± 0.91	8.41	7.70	9.32
DO (ppm)	3.75 - 6.93	5.36 ± 1.05	5.43	5.25	5.76
EC (µs/cm)	154 - 1744	691.78 ± 512.6	722.00	231.00	845.00
TDS (mg/L)	77 - 872	345.89 ± 256.2	361.00	116.00	422.00
Temp (°C)	16.46 - 22.28	19.78 ± 2.22	19.63	17.83	22.01

Table 6: Statistical summary of the major ions

Ions (mg/L)	Min-Max	Mean ± SD	Median	25th Perc	75th Perc
		Boreholes (n=10)			
Ca^{+2}	3.04 - 40.11	16.16 ± 10.72	15.16	9.52	18.18
K^{+}	15.85 - 136.89	41.61 ± 36.41	27.5	22.05	47.35
Mg^{+2}	0.79 - 9.22	3.5 ± 2.66	2.37	1.57	4.95
Na^{+}	23.52 - 376.97	104.48 ± 107.64	68.7	46.44	88.77
Cl^{-}	10 - 105	27.30 ± 28.13	20	13.5	24.75
CO_3^{-2}	0.1 - 36.5	8.4 ± 11.53	3.4	1.62	12.9
F^{-}	1.14 - 46.97	9.28 ± 14.93	2.89	2.5	4.18
HCO_3^{-}	126.9 - 1073.5	383.3± 294.21	321.6	189.39	375.95
NO_3^{-}	0.57 -37.4	14.62 ± 12.87	9.68	6.93	24.09
SO_4^{-2}	6.00 - 39.00	13.8 ± 10.10	9	8.25	15.5
		Dug wells (n=16)			
Ca^{+2}	3.22 - 82.11	17.14 ± 21.34	9.16	5.87	16.67
K^{+}	22.31 - 234.12	104.36 ± 64.13	88.71	52.79	155.59
Mg^{+2}	0.9 -37.82	4.84 ± 9.09	2.01	1.3	2.9
Na^{+}	41.6 - 488.52	207.68 ± 135.06	182.75	79.52	298.36
Cl^{-}	12 - 300	70.06 ± 69.83	43.5	30.75	100.25
CO_3^{-2}	0.3 - 145.6	35.8 ± 46.22	16.1	5.55	40.92
F^{-}	1.5 - 84	24.1 ± 22.55	19.47	7.34	34.51
HCO_3^{-}	194 - 1219.5	613.4 ± 353.46	535.9	311.37	884.11
NO_3^{-}	1.32 -198	42.27 ± 61.63	16.28	6.16	36.74
SO_4^{-2}	8.00 - 320.00	56.8 ± 76.95	31	13.75	58.75
		Lakes (n=4)			
Ca^{+2}	1.26 - 24.14	17.14 ± 10.66	21.57	16.02	22.69
K^{+}	5.1 - 409.24	139.36 ± 186.69	71.55	19.34	191.57
Mg^{+2}	3.3 - 4.92	4.32 ± 0.71	4.52	4.14	4.69
Na^{+}	12.71 - 565.43	215.52 ± 257.12	141.96	27.58	329.9
Cl^{-}	2 - 230	94.25 ± 107.23	72.5	11.75	155
CO_3^{-2}	0.1 - 1009	256.2 ± 501.88	7.9	3.23	260.81
F^{-}	0.94 - 259	73.77 ± 124.33	17.58	2.2	89.15
HCO_3^{-}	98.9 - 2889	989.6 ± 1299.81	485.2	177.43	1297.28
NO_3^{-}	1.32 -12.76	7.15 ± 4.94	7.26	4.29	10.12
SO_4^{-2}	2.00 - 300.00	88.5 ± 142.80	26	2	112.5

Table 6 continued

		Springs (n=15)			
Ca^{+2}	0.31 - 40.18	8.45 ± 10.48	3.55	2.57	11.09
K^{+}	4.55 - 47.87	18.02 ± 13.8	12.53	6.29	30.05
Mg^{+2}	0.16 - 23.65	3 ± 6.04	0.63	0.45	2.7
Na^{+}	5.89 - 119.17	39.40 ± 36.92	19.64	13.32	56.46
Cl^{-}	4.0 - 21.0	10.6 ± 5.21	9	8	12.5
CO_3^{-2}	0 -90.2	8.7 ± 22.93	0.2	0.03	5.93
F^{-}	0.81 - 25.2	6.07 ± 7.17	2.25	1.24	8.74
HCO_3^{-}	11.8 - 371.4	129.9 ± 122.57	87.5	31.95	207.87
NO_3^{-}	0.35 -18.48	8.61 ± 5.03	8.8	5.72	11.22
SO_4^{-2}	0.00 - 39	12.4 ± 12.06	8	4	19
		Surface(n=9)			
Ca^{+2}	3.35 - 26.46	9.79 ± 7.05	8.19	5.11	10.04
K^{+}	4.4 - 99.67	28.86 ± 29.29	23.4	7.68	30.66
Mg^{+2}	0.73 - 6.88	2.78 ± 1.90	2.02	0.96	2.6
Na^{+}	9.34 - 175.46	61.62 ± 55.29	41.05	13.82	85.9
Cl^{-}	6.0 - 56.0	21.33 ± 17.0	9	18	24
CO_3^{-2}	0.1 -143.7	22.9 ± 46.38	4.9	0.33	21.24
F^{-}	1.13 - 30.07	9.41 ± 10.53	2.29	1.5	18.1
HCO_3^{-}	33 - 309	164 ± 105.75	141.3	69.5	242.8
NO_3^{-}	0.35 -136.4	22.9 ± 42.86	7.92	6.6	12.32
SO_4^{-2}	2.0 - 80.0	18.3 ± 24.37	15	3	18

The pH values for all water sources ranged from 6.46 to 10.91 and averaged 8.16±0.9. The mean values were nearly uniform between 8.04±0.57 and 8.43±0.91 in borehole, dug well, stream and lake samples and slightly low in springs (7.7±1.25) as shown in Table 5. The extremely low and high pH values of 6.46 and 10.91 were obtained in springs leading to a wide range of pH values in springs relative to other water types (Fig. 31a). Classification of pH values based on three categories of nearly neutral (6.4-7.5), slightly alkaline (7.5-8.5) and alkaline (8.5-11) indicated that 53% of the springs were nearly neutral whereas most of the boreholes (70%), dug wells (56%) and lakes (50%) were slightly alkaline and most of the streams (44%) were alkaline. Intra-classification of pH within spring water type, indicated that 80% of the windward springs were under nearly neutral category whereas 40% and 60% of the leeward springs were slightly alkaline and alkaline respectively (Fig. 31b).

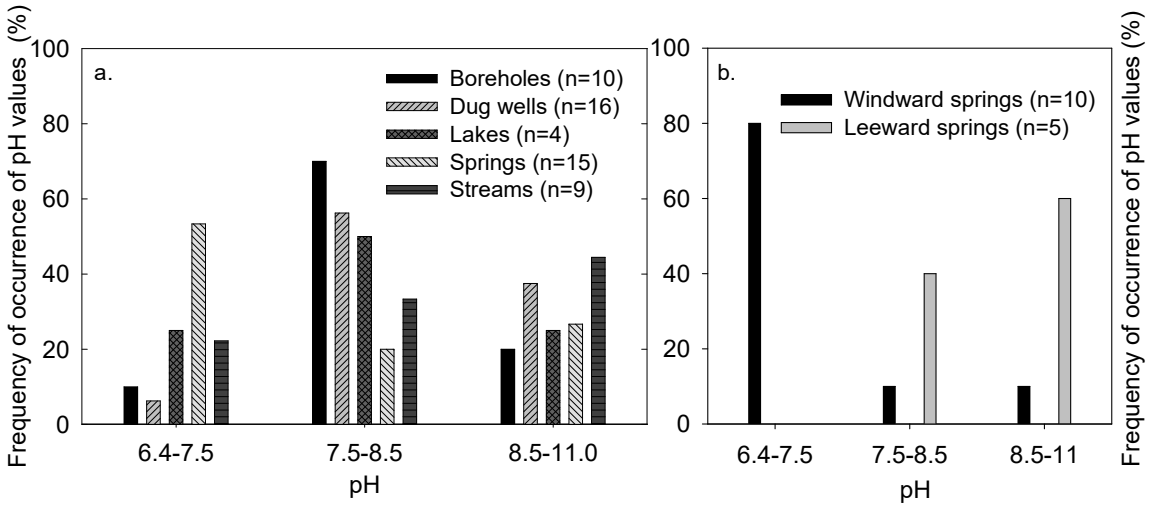

Figure 31: (a.) pH values distribution in all water types (b.) pH distribution in springs based on their position with respect to Mt. Meru

The mean dissolved oxygen (DO) in all sample types was 4.4±1.5 ppm (Table 5). Generally, it showed an increasing trend from lakes-dug wells-springs-boreholes to streams (Fig. 32a). 50% of the lakes and 62.5% of the dug wells had low DO between 0 and 3.5 ppm whereas 78% of the streams and 70% of the boreholes had high DO between 5 and 7.5 ppm (Fig. 32a). Despite the wide range of DO for all samples, there were neither stream samples with DO less than 3.5 nor dug wells with DO above 5 ppm (Fig. 32a).

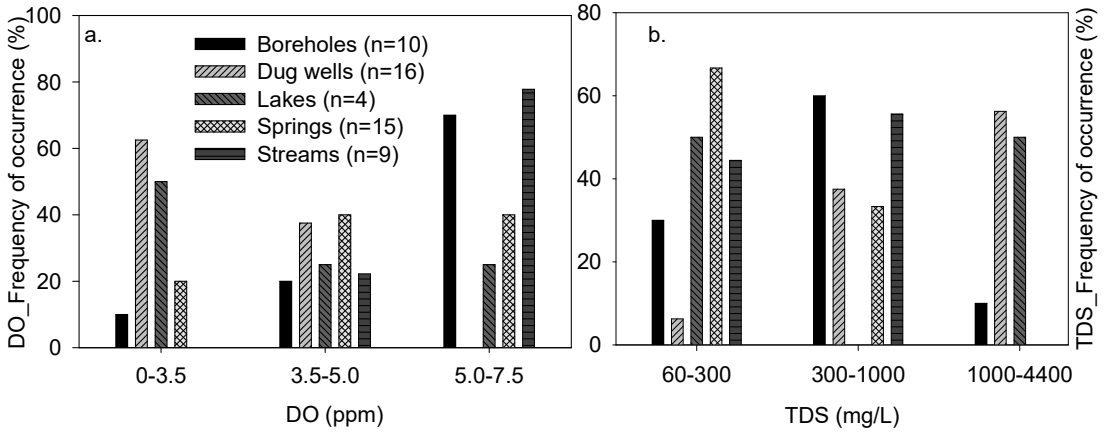

Figure 32: Physico-chemical parameter distribution in water types (a.) Dissolved oxygen (DO) (b.) Total dissolved solids (TDS).

Total Dissolved Solid (TDS) was classified into three categories as very fresh water (60-300 mg/l), fresh water (300-1000 mg/l) and brine to saline water (1000-4400 mg/l). However, the first two categories are within the recommended WHO fresh water standard of TDS<1000

(WHO, 2011). It showed a general increasing trend in the order of spring < stream < boreholes < dug wells < lakes. The low TDS category (60-300 mg/l) was dominated by springs (67%), lakes (50%) and streams (44%) (Fig. 32b). Dug wells water type was the lowest percentage in this category (6.25%) while dominating the high TDS category (100-4400 mg/l) to 56% (Fig. 32b). Streams and boreholes dominated the intermediate category (300-1000 mg/l) with the percentage of 56 and 60 respectively (Fig. 32b). While springs and streams are completely absent in the high TDS category (Fig. 32b), the lakes showed two distinct ranges of TDS); the low TDS (60-300 mg/l) comprising windward lakes (Duluti and Ngurudoto) and the high TDS (1000-4400 mg/l) comprising leeward lakes (Mlolozi and Small Momella).

Temperature in water types varied significantly from 13.76 to 27.84 °C with the mean value of 21.94 ± 3.4 °C. It was low in springs and streams with the mean values of 18.57 ± 2.57 °C and 19.78 ± 2.22 °C respectively and high in boreholes with the mean value of 25.06 ± 1.28 °C. Temperature was intermediate in Lakes (mean=22.15 ± 3.9 °C) and relatively high in dug wells (mean=24.32 ± 1.45 °C) (Table 5).

Major ion distribution: Sodium was found to be the dominant cation in all water types comprising about 61% of the total cations with the mean value of 118 mg/l. However, it showed a strong variation in different water types and within each group (Fig. 33a). The high mean value was in lakes (215.52 ± 257.12 mg/l) whereas the low values were in streams (61.62 ± 55.29 mg/l) and springs (39.40 ± 36.92 mg/l). Sodium was classified based on the WHO threshold taste of 200mg/l (WHO, 2011) into low (0-50 mg/l), intermediate (50-200mg/l) and high sodium (200-600 mg/l). Classification showed that springs (73%), streams (56%) and windward lakes (50%) dominate the low Na^+ category whereas dug wells (50%) and leeward lakes (50%) dominate the high Na^+ category. Both springs and streams were absent in the high Na^+ category (Fig. 33a).

Potassium was the second dominant cation comprising about 30% of the total cations. Its dominance pattern was found to be similar to that of Na^+, being characterized by elevated K^+ concentrations in lakes (mean=139.36 ± 186.69 mg/l) and dug wells (mean=104.36 ± 64.13 mg/l) and low concentrations in streams (mean=28.86 ± 29.29 mg/l) and springs (mean=18.02 ± 13.8 mg/l). Based on the recommended WHO maximum standard of K^+ in drinking water (12 mg/l) (WHO, 2008), 80% of all samples were above the recommended standard (Fig. 33b). Only 47% of the springs, 33% of the streams and 25% of the boreholes

were within the acceptable standard (Fig. 33b). High K^+ category group (Fig. 33b) was dominated by dug wells (37.5%) and leeward lakes (50%), lacking spring and stream sample types (Fig. 33b).

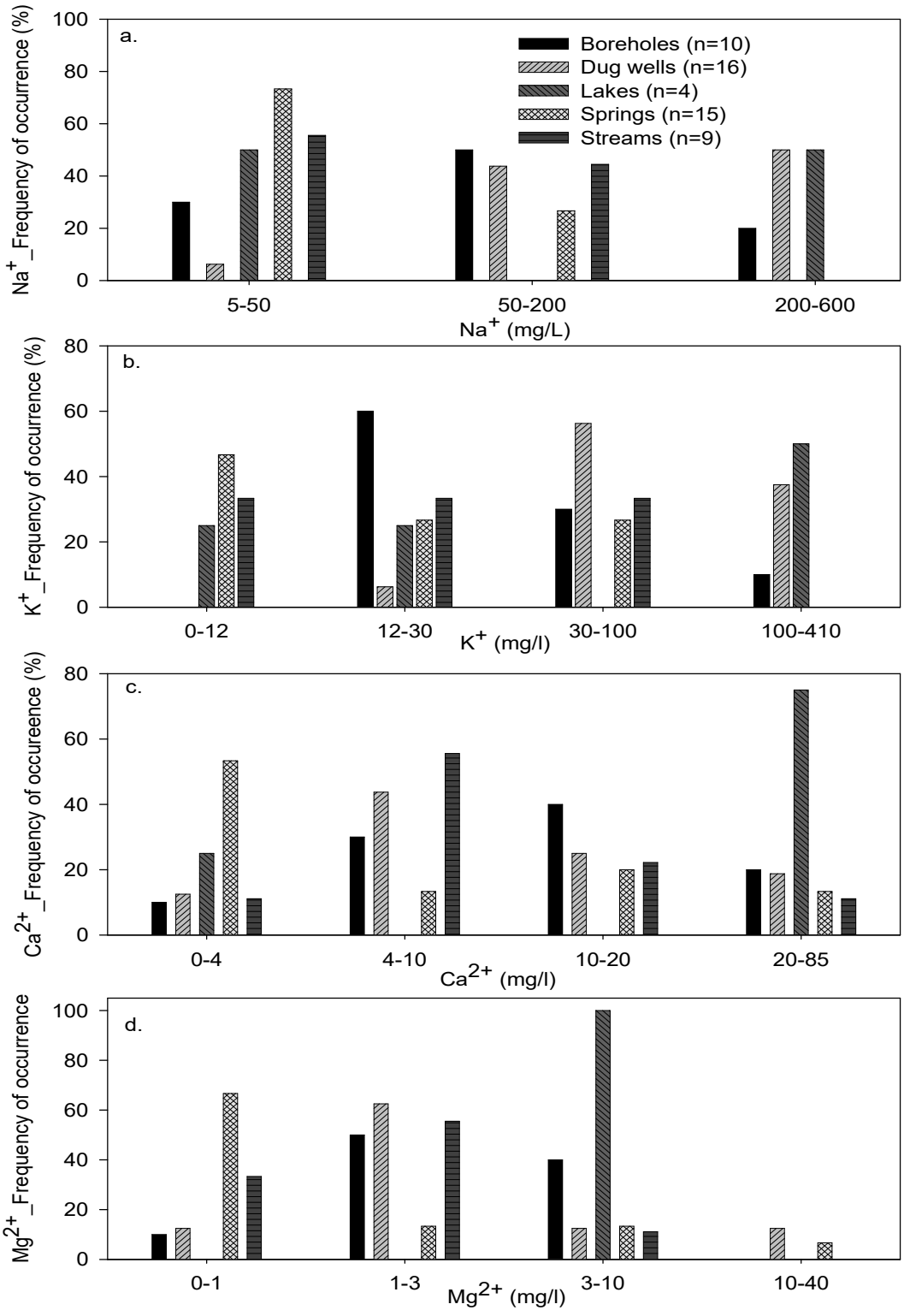

Figure 33: Major cation distribution in different water types

Calcium and magnesium were low in water samples comprising only 9% of the total cations with the mean values of 13.3±14.4 mg/l and 3.6±6.0 mg/l respectively. With exception of two dug well samples, the concentration of Ca^{2+} and Mg^{2+} in other samples were within the recommended WHO standard of 50 and 75 mg/l respectively (WHO, 2008). The mean concentrations of Ca^{2+} were nearly uniform in boreholes, dug well and lakes between 16-17.2 mg/l. Mean uniformity was also observed in spring and surface water types where the mean Ca^{2+} concentrations were slightly low, restricted between 8.4 and 9.8 mg/l. Classification of Ca^{2+} values showed the dominance of the springs (53%) in the very low Ca^{2+} category (0-4mg/l) and the dominance of lakes (75%) in the high Ca^{2+} category (20-85 mg/l) (Fig. 33c). The mean values for Mg^{2+} in different water types ranged from 2.78 mg/l (surface water) to 4.84 mg/l (dug wells) and averaged 3.7 mg/l. Despite that, dug well and the spring water types showed a wide range of Mg^{2+} concentrations, 67% of the springs had the concentration less than 1 mg/l and 62.5% of the dug wells had Mg^{2+} concentration between 1 and 3 mg/l (Fig. 33d). Unlike dug wells and springs, all lakes fell in one category with Mg^{2+} concentration between 3-10 mg/l (Fig. 33d). The cation results with the dominance pattern of $Na^{+} > K^{+} > Ca^{2+} > Mg^{2+}$ compare well with the results obtained in the northern part of the same rift system in Ethiopia (Rango *et al*., 2010). These two parameters were positively correlated (Fig. 37).

Bicarbonate was found to be the dominant anion comprising 73% of the total anions in water samples. Overall, it showed a wide range in all sample types with an increasing trend in the order of springs < streams < boreholes < dug well < lakes (Fig. 34d). Based on classification of HCO_3^- into very low (0-100 mg/l), low (100-300 mg/l), intermediate (300-1000 mg/l) and high (1000-3000 mg/l), dug wells and boreholes were absent in the very low category while springs and streams were absent in the high category (Fig. 34d). Springs had relatively low HCO_3^- with 53% and 33% in the categories of very low and low respectively (Fig. 34d). 40% and 50% of the boreholes were restricted in the low and intermediate categories respectively. However, the intermediate category was dominated by dug wells to 56.25% (Fig. 34d). Lakes exhibited a wide range of HCO_3^- concentrations varying from 98.9 mg/l (Ngurudoto crater) to 2889 mg/l (Lake Small Momella) and were uniformly distributed in four categories (Fig. 34d). In alkaline water samples, HCO_3^- occurred together with carbonates. About 70% of the samples had CO_3^{2-} concentrations varying between 1.2-1009 mg/l (mean=53±164 mg/l). However, the concentrations were less than 12 mg/l in most of the samples. Carbonates

showed a wide range of concentration in all water sample types with the dominance pattern similar to that of HCO_3^-.

In this study, fluoride was found to be among six dominant anions, comprising about 3% of total anions. It varied between 0.8-259 mg/l with mean value of 17.6 ± 37.4 mg/l. Classification of fluoride values based largely on the WHO and Tanzania standards showed that 78 % of all samples had fluoride above the recommended WHO standard of 1.5 mg/l (WHO, 2011) and 52 % had fluoride above Tanzanian standard of 4mg/l. Within the low fluoride category (0-1.5 mg/l), the dominant sample types were springs (40 %), streams (33 %) and lakes (25 %; lake Ngurudoto) while dug wells and boreholes were limited to 6.25 % and 10% respectively (Fig. 34a). Unlike the boreholes which dominated the relatively low fluoride category of 1.5-4.0 mg/l to 60 %, the dug wells had relatively high fluoride dominating the category of 20-100 mg/l to 50 % (Fig. 34a). The Leeward lakes-Small Momella and Mlolozi exhibited extremely high fluoride of 259 mg/l and 32.5 mg/l respectively being reflected in the high fluoride categories shown in Fig. 34a.

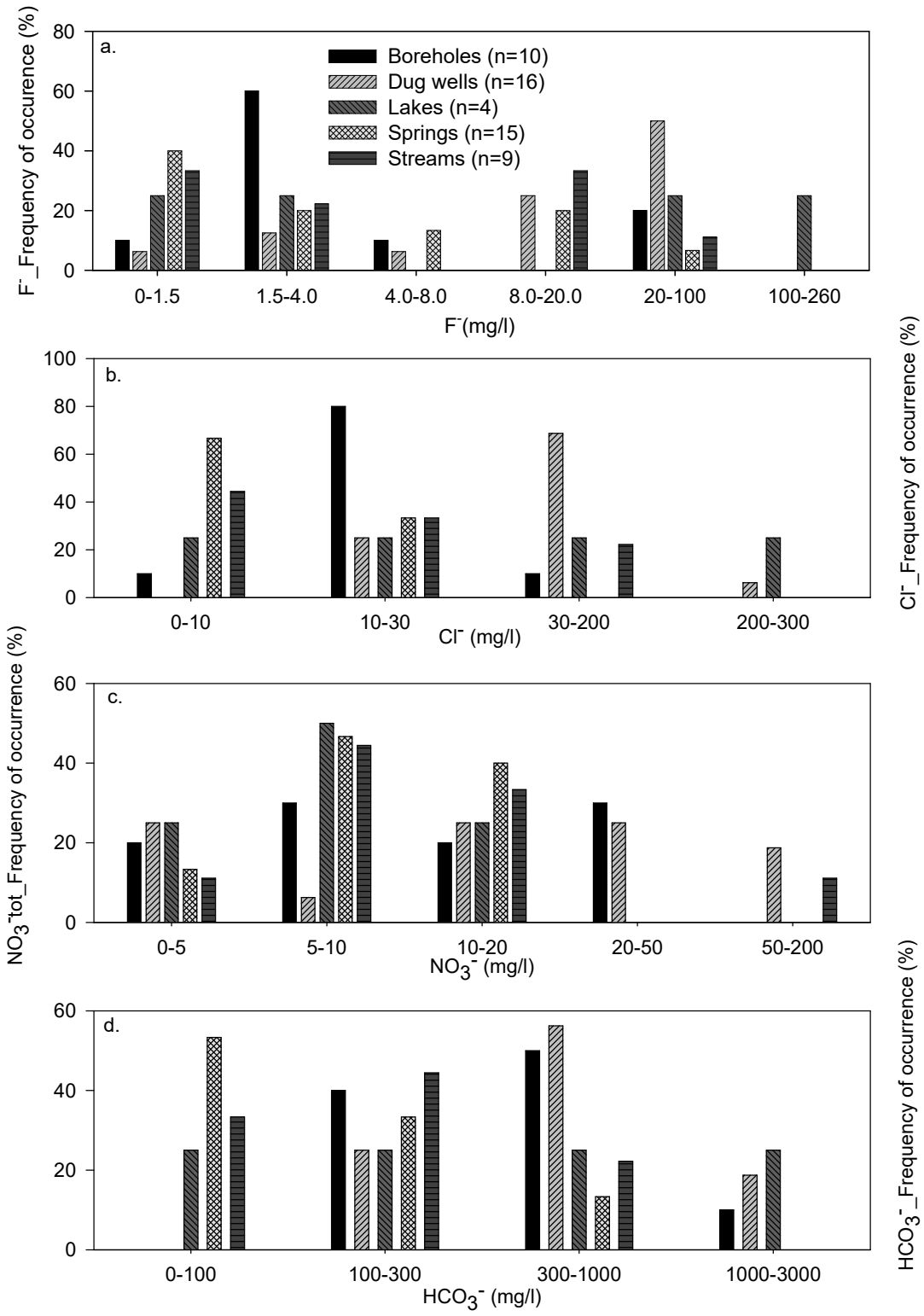

Figure 34: Major anion distribution in different water types

Chloride comprised about 7% of the total anions ranging between 2-300 mg/l with the mean value of 39.3 ± 55.2 mg/l. Based on the minimum WHO provisional standard of 250 mg/l (WHO, 2011), only one dug well sample (Cl^- =300 mg/l) was above the recommended standard. Classification of chloride into very low (0-10 mg/l), low (10-30 mg/l), intermediate (30-200 mg/l) and high (200-300 mg/l) showed the dominance of the springs (67%), boreholes (80%) and dug wells (69%) in the very low, low and intermediate categories respectively (Fig. 34b). Streams had relatively low chloride with 44.4%, 33.3% and 22.2% in the very low, low and intermediate categories respectively (Fig. 34b). The high chloride category was represented by lake Small Momella (230 mg/l) and one dug well as discussed previously.

Nitrate comprised about 4% of the total anions ranging between 0.35-198 mg/l with the mean value of 22±40 mg/l. Elevated NO_3^- values were found in dug wells (mean = 42.3 ± 61.7 mg/l) and surface water (mean = 22.9 ± 42.9 mg/l) (Table 6). NO_3^- distribution presented in Fig. 34c showed nearly uniform distribution of NO_3^- in dug wells in all categories whereas in surface water it dominates the intermediate categories represented by NO_3^- values between 5 and 20 mg/l (Fig. 34c). With the minimum WHO provisional standard of 50 mg/l for NO_3^- (WHO, 2011), two dug wells with NO_3^- concentrations of 101.2 mg/l and 198 mg/l and one surface water (NO_3^- = 136.4 mg/l) were considerably above the recommended minimum standard. These samples represent the high NO_3^- category (200-300 mg/l) (Fig. 34c). Unlike other ions, the lake samples had the lowest NO_3^- concentrations (mean = 7.15 ± 4.94 mg/l (Table 6) with 75% in the categories of low concentrations (NO_3^- < 10 mg/l) (Fig. 34c). Interestingly, based on WHO (2011), all NO_3^- concentrations in borehole, spring and lake water types were below the recommended WHO standard of 50 mg/l.

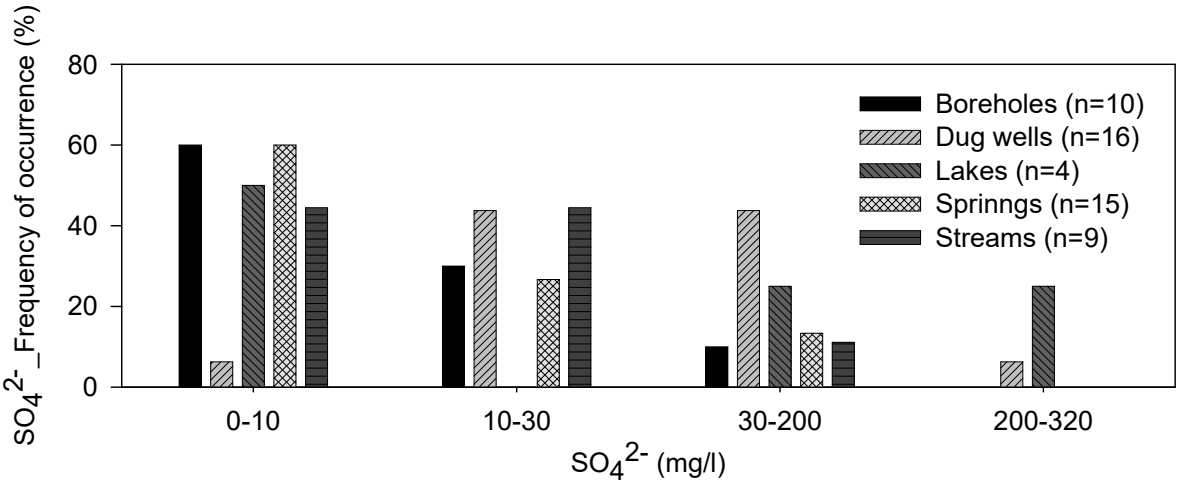

Figure 35: Distribution of SO_4^{2-} in all water types

Sulphate comprised about 6% of the total anions ranging between 0-300 mg/l with the mean value of 32.4±60 mg/l. Overall, it showed an increasing trend in the order of springs <boreholes <stream <dug wells <lakes (Table 6 and Fig. 35). In all samples, only two water types; one dug well sample (320 mg/l) and one lake sample (Lake small Momella; 300 mg/l) exceeded the minimum WHO provisional standard of 250 mg/l for SO_4^{2-} (WHO, 2011). Based on the SO_4^{2-} classification into very low (0-10 mg/l), low (10-30mg/l), intermediate (30-200 mg/l) and high (200-300 mg/l), most of the springs and boreholes fell in the very low category (Fig. 35). Despite that this category included also 50% of the lake and 44.4% of the stream samples, the percentage of dug wells was very low (6.25%) (Fig. 35). The anion results showed a dominance pattern of $HCO_3^- > CO_3^{2-} > Cl^- > SO_4^{2-} > NO_3^- > F^-$.

4.3.2 Spatial distribution of fluoride

For spatial assessment of fluoride and its relationship with geology, other 46 samples which were collected specifically for fluoride (Appendix 6) are combined with 54 samples which were analysed for major ions and the results are as presented in Fig. 36. Overall fluoride results do not differ significantly with results of 54 samples as discussed previously. Leeward lakes had the highest fluoride values (mean=567 mg/l, n=3) as shown in Fig. 36. Both leeward springs and streams exhibited elevated mean fluoride values of 7.3 mg/l (n=9) and 22.3 mg/l (n=8) respectively relative to windward springs and streams which showed low mean fluoride values of 1.32mg/l (n=21) and 4.67 mg/l (n=13) respectively. The boreholes and dug well had relatively high mean fluoride values of 8.4 mg/l (n=16) and 17.4 mg/l (n=27).

Spatial distribution of fluoride showed strong variability of fluoride in the study area (Fig. 36). Low fluoride values generally less than 1.5 mg/l are mainly associated with phonolitic to nephelinitic lava on the windward side of Mt. Meru (Fig. 36). Intermediate fluoride values general between 1.5 and 4 mg/l are concentrated on the foot of Mt. Meru (Pori-Singisi) where lahars are intercalated with nephelinitic to phonolitic lavas and alluvial sediments (Fig. 36). The intermediate values also dominate the low land areas of Makiba-Bwawani-Mbuguni being associated with interaction of weathered volcanic formation, alluvial sediments and rarely Ngarenanyuki lahars (Fig. 36). High fluoride (8-20 mg/l) dominates the areas characterized by lahars of various groups (leeward side and some parts of Maji ya Chai) and very high fluoride (20-100 mg/l) dominate the eastern part of the study area particularly Kikatiti and Maroroni wards being associated with Ngaranayuki lahars. Extremely high fluoride values (> 100 mg/l) were obtained in leeward lakes which are the areas studded by Momella lahars (Fig. 36). Overall, fluoride results indicated that there is a general relationship between fluoride and geology with high fluoride values in lahar materials relative to lava flows.

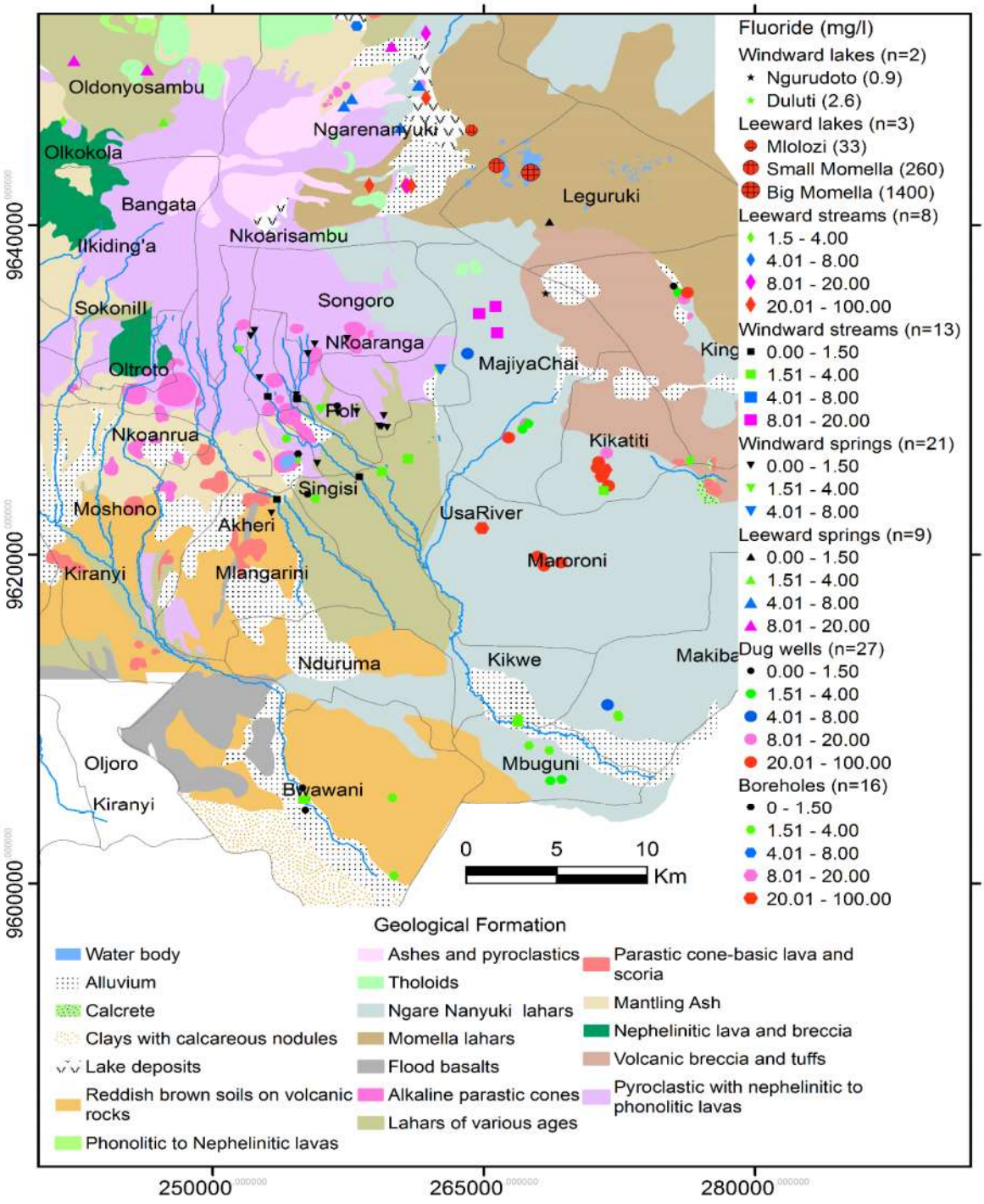

Figure 36: Relationship between geology and fluoride in Arumeru water type.

Note that 54 water samples which were analysed for major anions is combined with other 46 samples which were collected specifically for fluoride.

4.3.3 Relationship among physico-chemical parameters

Physico-chemical parameters (TDC and EC) and major ions were further assessed using correlation matrix (Table 7). Strong positive correlations (r >= 0.9) were observed between HCO_3^- with TDS and EC (r = 0.96), Na^+ (r = 0.92), K^+ and F^- (r = 0.90) (Table 3, Fig. 37-38). Such strong correlations were also observed between Cl^- and SO_4^{2-} (r = 0.90) and F^- with CO_3^{2-} (r = 0.93) (Table 7). Apart from strong positive correlation between F^- with CO_3^{2-} and HCO_3^-, F^- was also found to correlate positively with TDS (r = 0.84), EC (r = 0.84), K^+ (r = 0.72), Na^+ (r = 0.86), SO_4^{2-} (r = 0.69) and Cl^- (r = 0.73) as shown in Fig. 38. It had no significant correlation with Mg^{2+} (r = -0.06) and Ca^{2+} (r = -0.19) (Table 7 and Fig. 39). TDC and EC were found to have significant positive correlation with all major ions with exception of Mg^{2+}, Ca^{2+} and NO_3^-. Cations (Mg^{2+} and Ca^{2+}) correlated positively (r = 0.85); which is the same correlation coefficient for the other two major cations (Na^+ and K^+) (Fig. 37).

Table 7: Pearson correlation matrix for groundwater samples in Arumeru district (N=54, p=0.01)

	Na^+	**K^+**	**Mg^{2+}**	**Ca^{2+}**	***F^-***	***Cl^-***	***HCO_3^-***	**CO_3^{2-}**	**SO_4^{2-}**	**NO_3^-**	***EC***
Na^+	1.00										
K^+	0.85*	1.00									
Mg^{2+}	0.10	0.22	1.00								
Ca^{2+}	0.01	0.11	0.85*	1.00							
F^-	0.86*	0.72*	-0.06	-0.19	1.00						
Cl^-	0.77*	0.79*	0.55*	0.45*	0.73*	1.00					
HCO_3^-	0.92*	0.90*	0.08	0.00	0.90*	0.73*	1.00				
CO_3^{2-}	0.58*	0.75*	0.00	-0.11	0.93*	0.54*	0.79*	1.00			
SO_4^{2-}	0.66*	0.79*	0.53*	0.37*	0.69*	0.90*	0.66*	0.66*	1.00		
NO_3^-	0.23	0.24	-0.08	-0.08	0.03	0.09	0.16	-0.06	0.10	1.00	
EC	0.95*	0.91*	0.18	0.07	0.84*	0.83*	0.96*	0.74*	0.76*	0.18	1.00
TDS	0.95*	0.91*	0.18	0.07	0.84*	0.83*	0.96*	0.74*	0.76*	0.18	1.00

**Correlation is significant at the 0.01 level (2-tailed)*

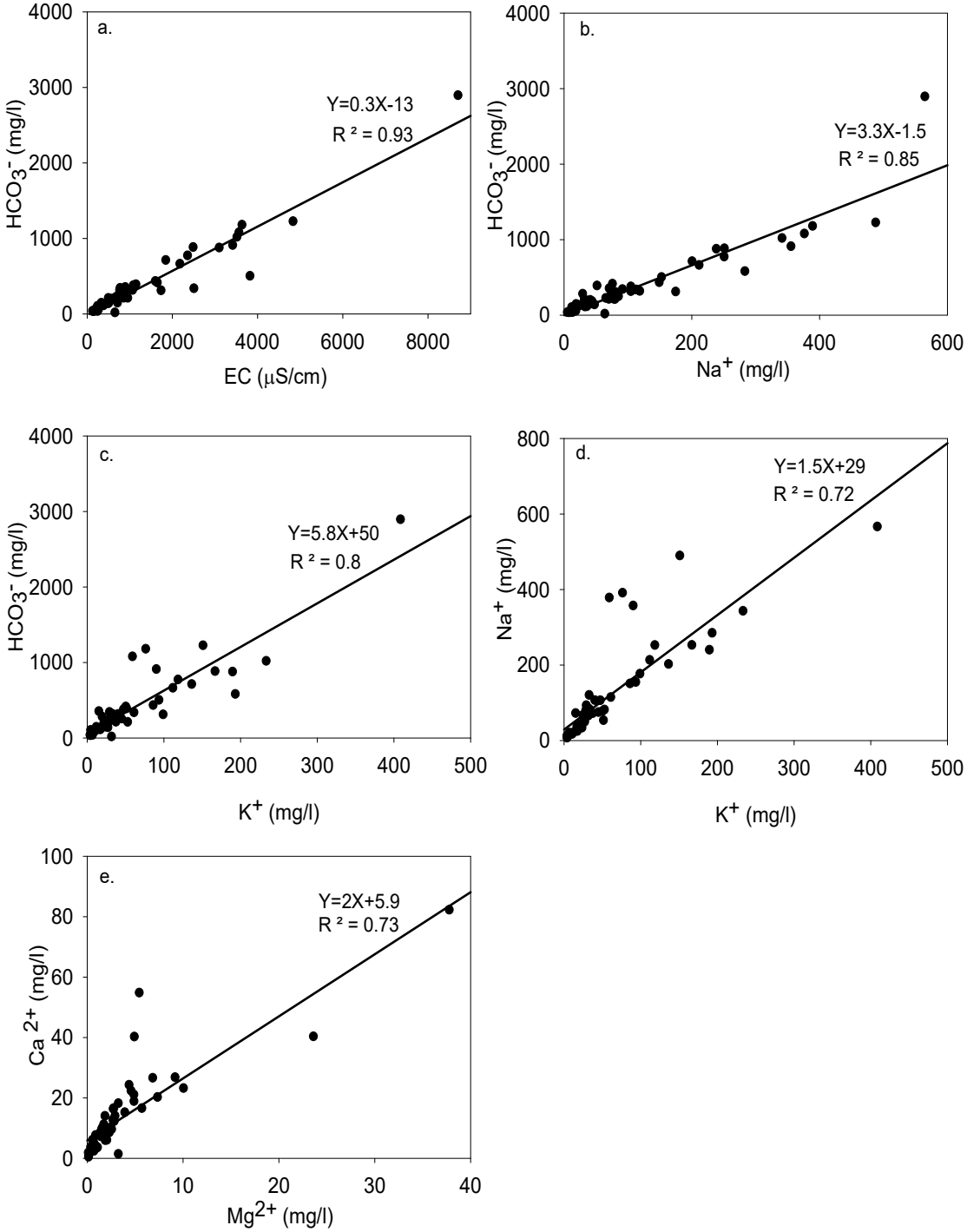

Figure 37: Positive correlations of HCO_3^- with: (a.) EC (b.) Na^+ and (c.) K^+. Other positive correlations of the paired cations are shown in (d.) Na^+ with K^+. and in (e.) Ca^{2+} with Mg^{2+}

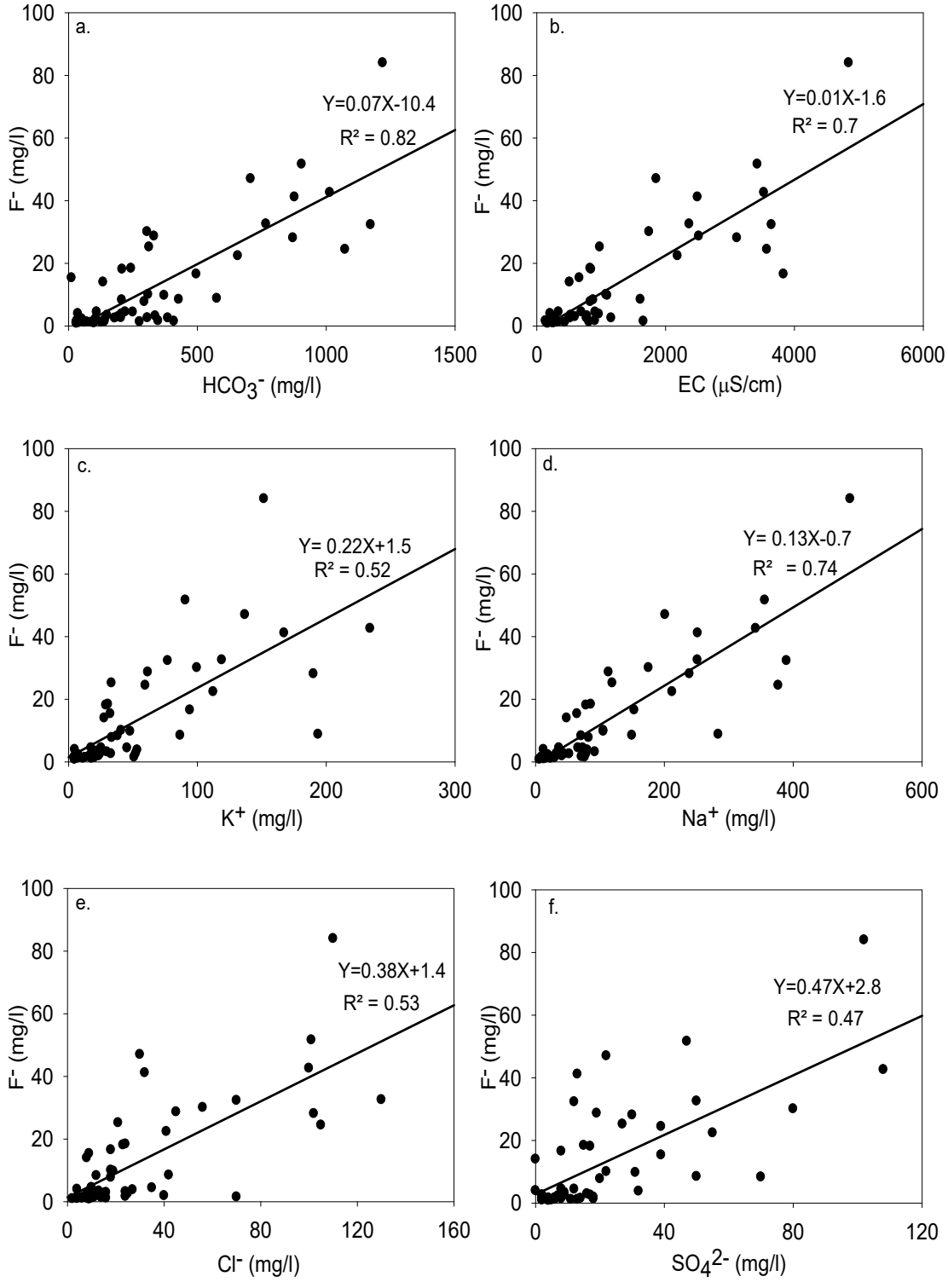

Figure 38: Positive correlation of fluoride with (a) HCO_3^-, (b). EC, (c). K^+, (d). Na^+, (e). Cl^- and (f.) SO_4^{2-}

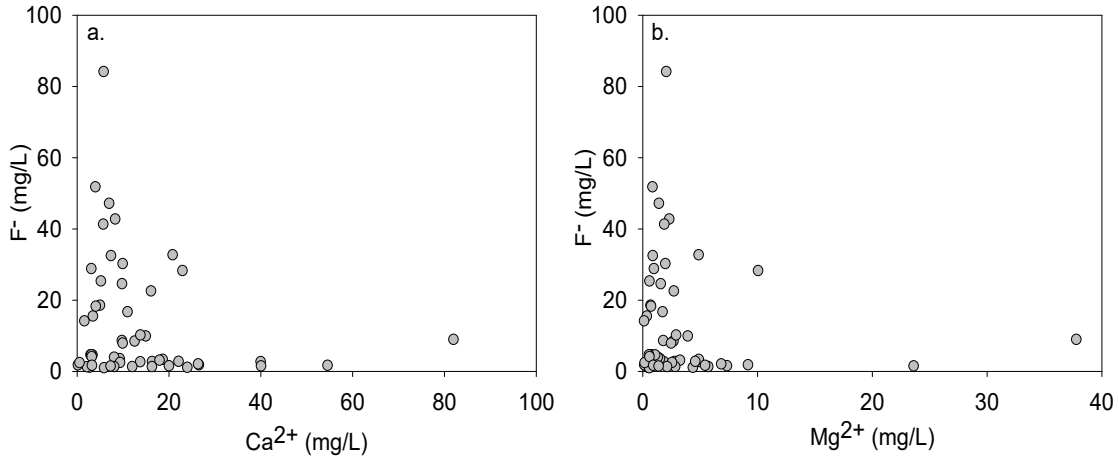

Figure 39: Relationship between Fluoride and Ca^{2+}, Mg^{2+} in Arumeru water samples

4.3.4 Major ion characteristics in specific water types

Relative abundance: The general ionic abundance pattern in all water types was Lake > Dug wells > Boreholes > Rivers/Streams > Springs (Fig. 40). Figures 41 and 42 represent water types that showed intensive/ pronounced internal variations.

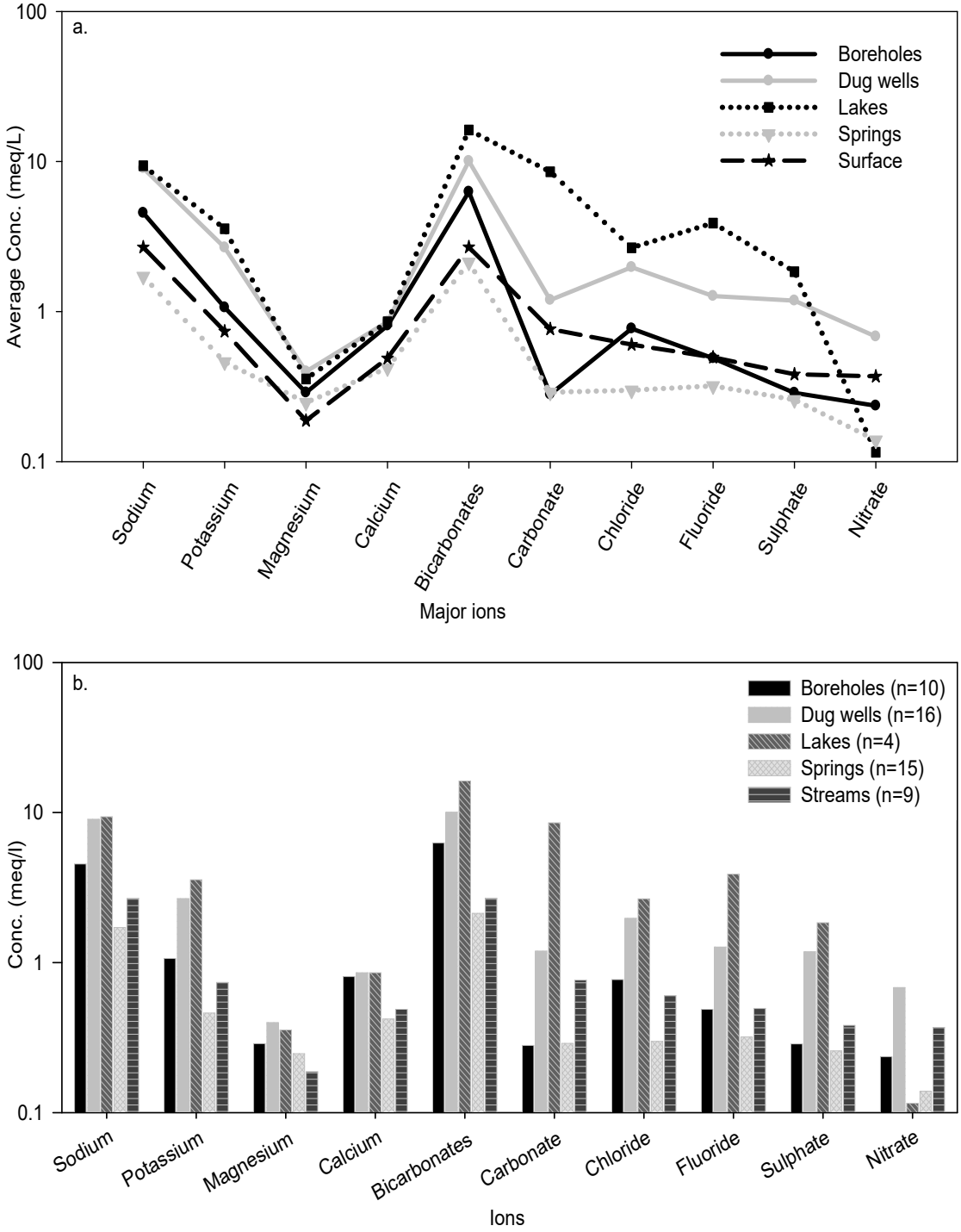

Figure 40: Major ions average concentrations for Arumeru water types a. Modified Schoeller diagram b. Equivalent histogram

Lake: The leeward lakes (Small Momella and Mlolozi) were characterized by high dissolved ions relative to the windward crater lakes (Duluti and Ngurudoto) (Fig. 41a). However, in lake Small Momella, Ca^{2+} (1.26mg/l) and Mg^{2+} (3.3 mg/l) were low relative to the values

obtained in other lakes which varied between 20 - 25 mg/l and 4.4- 4.9 mg/l respectively (Fig. 41a). Also, despite that NO_3^- values were low in all lakes within the acceptable international standard as discussed previously, Lake Duluti exhibited high NO_3^- value (12.76 mg/l) relative to other lakes where NO_3^- averaged 5.28 mg/l.

Streams: Two streams basically in the leeward side of Mt. Meru (Ngarenayuki and Kyamang'ata) showed elevated dissolved ions relative to all other sampled streams as shown in Fig. 41b. Generally, within these two streams, Ngarenanyuki river exhibited higher dissolved ions than Kyamang'ata stream with Na^+(175.5 mg/l), K^+ (99.7 mg/l), F^- (30 mg/l), Cl^- (56 mg/l), CO_3^{2-} (80 mg/l) and SO_4^{2-} (80 mg/l) as the most discerned ions (Fig. 41b). However, Kyamang'ata stream had extremely high NO_3^-(136.4 mg/l) relative to both Nganrenayuki (0.35 mg/l) and mean of other streams (9.9 mg/l) (Fig. 41b). The ions which were low in these two streams relative to the corresponding mean of the other streams were CO_3^{2-} (0.3 mg/l) in Kyamang'ata stream, Mg^{2+} (2.02 mg/l) and NO_3^- (0.35 mg/l) in Ngarenanyuki stream (Fig. 41b).

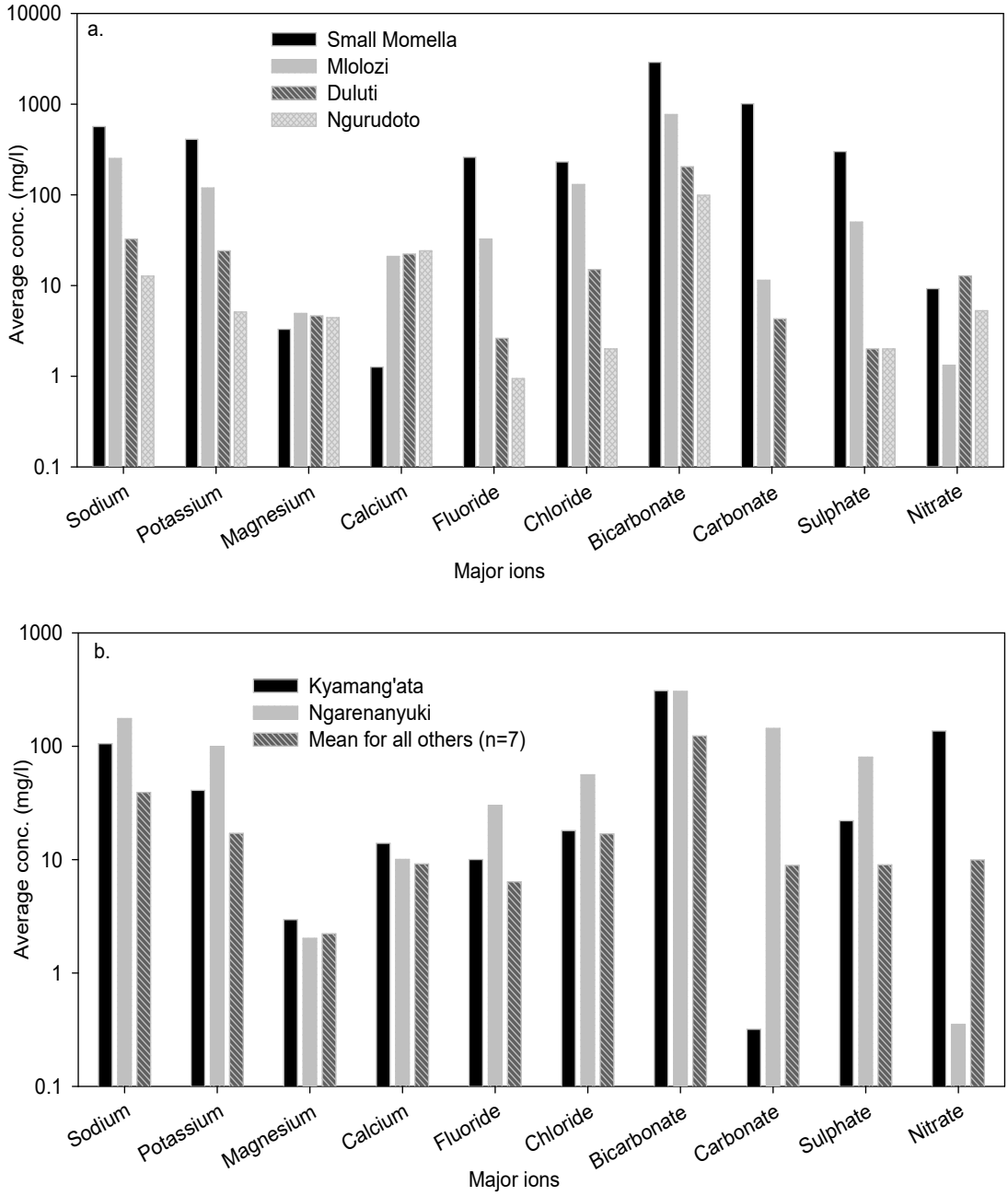

Figure 41: Major ions variation (a) in the sampled lakes (b) in two streams which showed elevated ions relative to other streams

Springs: Windward and Leeward springs showed different chemical characteristics. There were high dissolved ions in the leeward springs relative to the windward springs (Fig. 42a). However, unlike other ions, the concentrations of Mg^{2+} and Ca^{2+} were high in the windward side relative to leeward side. Furthermore, results showed that within the wind ward springs; springs generally located on the slope of Mt. Meru represented by a group of six streams (Fig.

42b) had low dissolved ions relative to springs which are not on the slope of the mountain particularly Makisolo and Nduruma flower (Fig. 42b).

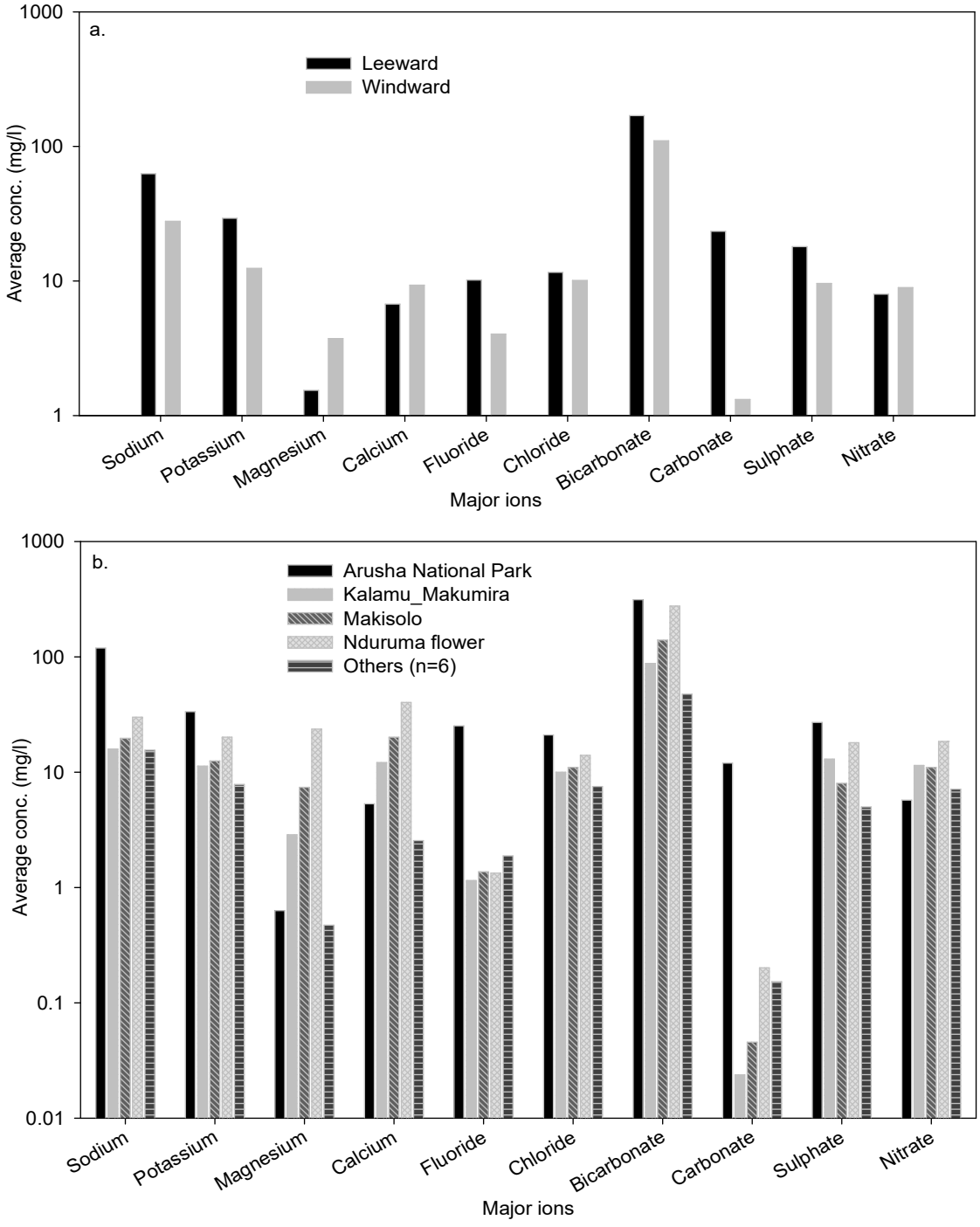

Figure 42: Major ions characterization in springs a. Leeward and windward springs b. Specific windward springs showing elevated ions relative to other windward springs.

4.3.5 Hydrogeochemical characteristics and classification

Groundwater chemistry is dynamic; being controlled by four major processes which are rainfall, weathering of rocks, precipitation (crystallization) and evaporation. Using these processes, Arumeru groundwater were characterized using piper diagram (Fig. 43), Langelier & Ludwig, 1942 (Fig. 44), Chadha's diagram (Fig. 45) and Gibb's ratios (1970) (Fig. 46 and 47). These methods have been widely used in groundwater characterization and geochemical evolution (Glover *et al.,* 2012; Narany *et al.,* 2014; Srinivas *et al.,* 2014).

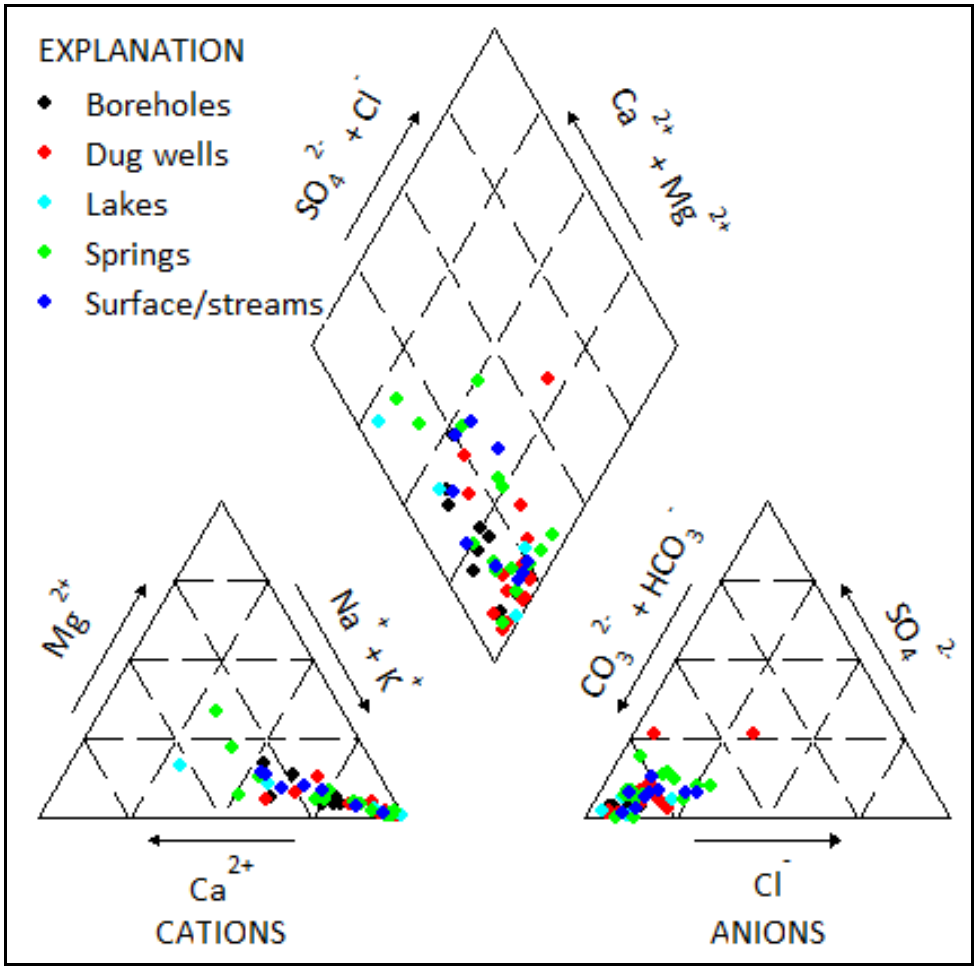

Figure 43: Piper diagram for Arumeru water samples

Based on 4 diamond quadrants of the Piper diagram (Fig. 43), > 92% of Arumeru water samples belong to Na-K-HCO_3 type. Only 4 samples plotted out of this field, with 3 samples (2 springs and 1 lake) in the fields of $CaHCO_3$ and one dug well sample in the field of Na-K-Cl type. Despite the fact that Na-K-HCO_3 is the dominant type for all samples, the springs and lakes tend to show a wide range in chemical composition compared to the borehole and

dug well samples. The leeward springs showed the dominance of Na, K and HCO_3 ions relative to the windward spring being concentrating at the bottom corner of the diamond plot.

Both Langelier & Ludwig (1942) and Chadha's diagrams (Figs. 44 and 45), showed that over 90% of all water types plot in the field of Na-K-HCO_3 hydrochemical facies. The figures showed that two springs (Nduruma and Makisolo) (Fig. 30) and one lake (Ngurudoto) belong to Ca^{2+} (Mg^{2+})-HCO_3^- hydrochemical facies. One spring at Oldonyosambu showed depletion of HCO_3^- relative to other samples (Fig. 44) and one dug well at Maji ya Chai showed depletion of HCO_3^-, belonging to Na-Cl hydrochemical facies (Fig. 45).

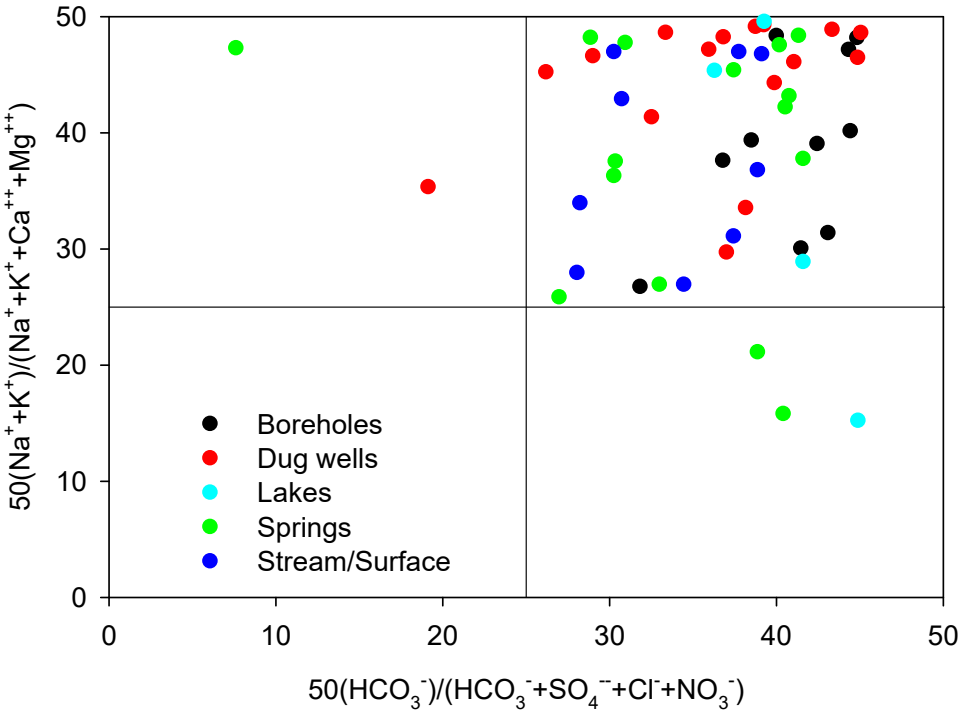

Figure 44: Compositions of different water types of Arumeru (after Langelier & Ludwig, 1942).

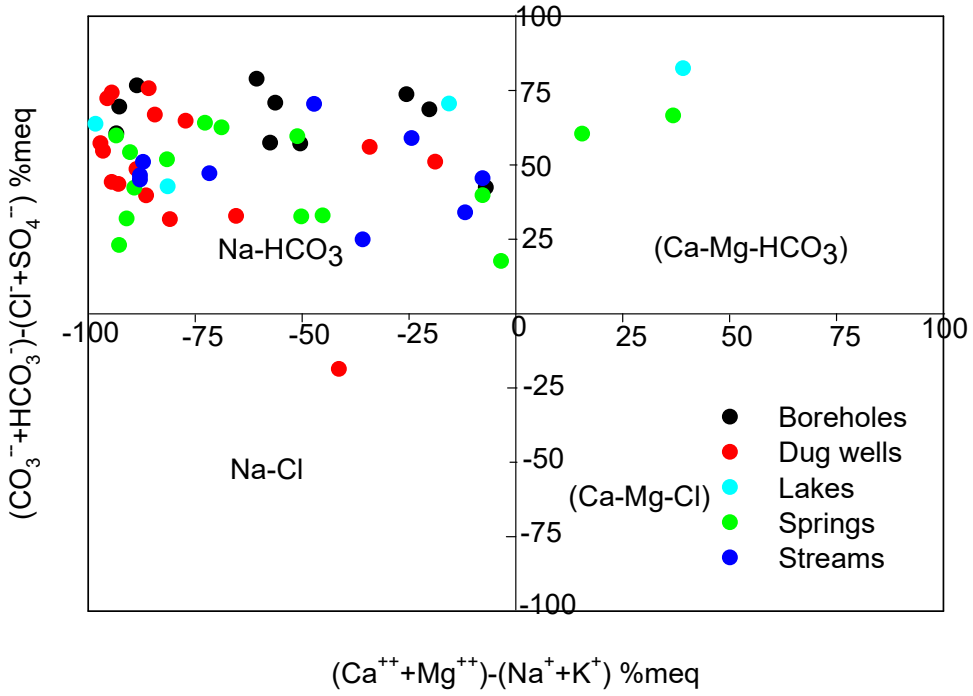

Figure 45: Chadha's diagram for hydrogeochemical classification of Arumeru groundwater

Gibb's plot (Fig. 46) indicated that weathering of rocks is the dominant process controlling water characteristics. Springs, streams and windward lakes dominated the rainfall and rock dominance fields whereas the dug wells and leeward lakes dominated the fields of rock dominance and evaporation- crystallization dominance. All boreholes plotted in the field of rock dominance (Fig. 46). Using the simplified Gibb's plot (Fig. 47A, a), where most of the water samples were characterized by high Na+K/Na+K+Ca ratio averaging at 0.8 and low $Cl/Cl+HCO_3$ averaging at 0.2, 70% of the samples plotted in the rock dominance field, 22% plotted in the field of evaporation-crystallization while 8% plotted in the field of rainfall dominance. The borehole, dug well and lake samples were plotted in the fields of rock dominance and evaporation-crystallization whereas the spring and stream samples were plotted in the fields of rock dominance and rainfall dominance. Interestingly, the samples from the dug wells are nearly equally distributed in the fields of rock dominance and evaporation-dominance whereas 90% of the borehole samples plotted in the field of rock dominance. Further characterization of spring water types using the simplified Gibb's plot (Fig. 47B, b) indicated that all leeward springs and 70% of the windward springs plotted in the field of rock dominance whereas 30% of the windward springs plotted in the field of rainfall dominance.

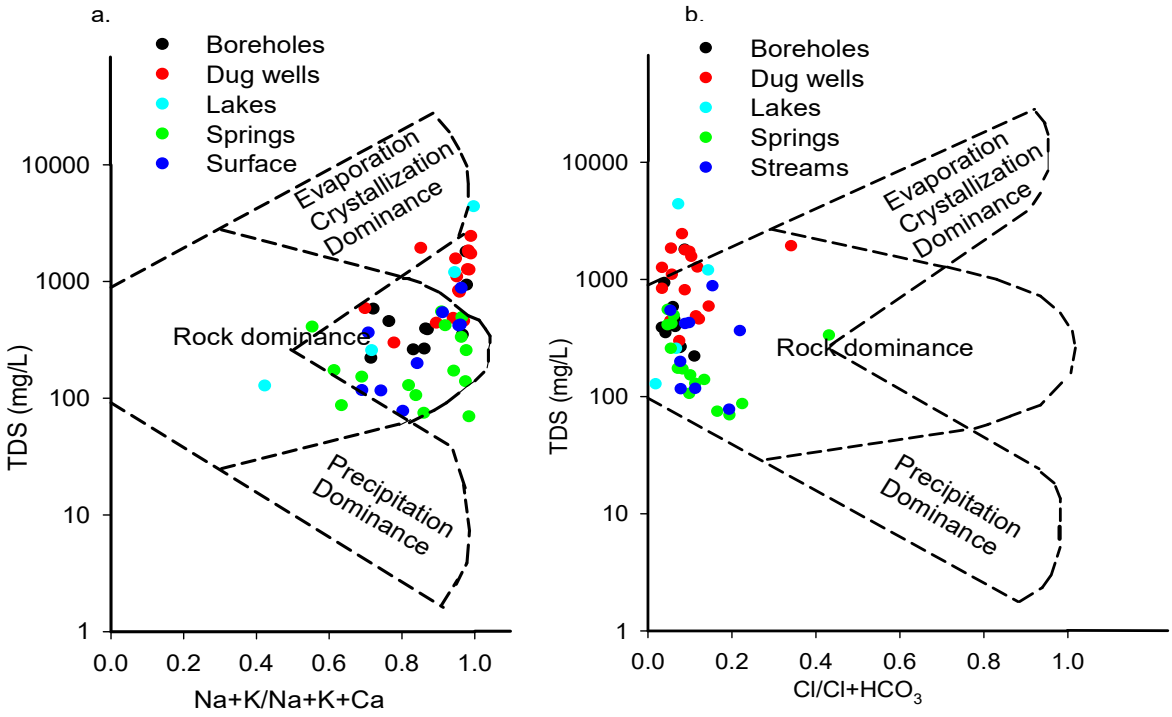

Figure 46: Modified Gibb's plot for Arumeru groundwater (After Narany *et al.,* 2014)

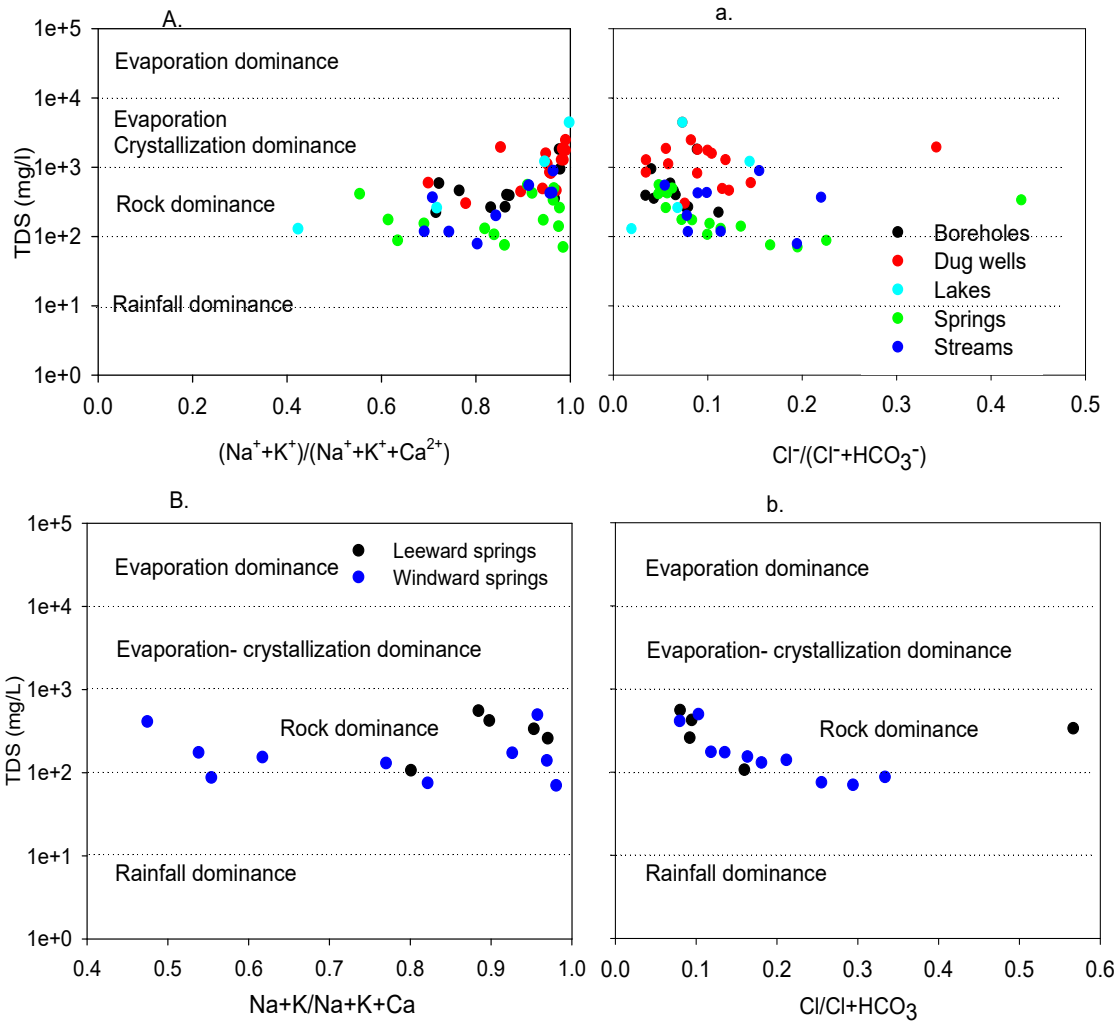

Figure 47: Simplified Gibb's plot for Arumeru groundwater (Aa). All water types (Bb.) Spring water type

4.3.6 Water Quality for Irrigation purposes

In order to assess water quality for irrigation purposes, pH, Electrical Conductivity (EC), Residual Sodium Carbonate (RSC), Sodium Adsorption Ratio (SAR), Sodium percent (%Na), Magnesium Adsorption Ration (MAR) and Kelley's ratio (KR) were considered. The results are presented in Table 8 together with the acceptable recommended standards.

pH: The suitable pH range for agriculture purposes is between 6.5 and 8.4 (Bashir *et al.,* 2013). Based on this range and Table 8, 20% of the boreholes, 56.25% of dug wells, 25% of the lakes, 33.3% of the springs and 55.6% of streams had pH beyond the recommended standard.

Residual Sodium Carbonate (RSC): Results indicated that most of the dug wells and boreholes were above the recommended minimum standard values of 2.5 (Bashir *et al.,* 2013), most of the springs were within the permissible limit while the stream and lakes had intermediate values (Table 8).

Sodium percent (%Na): Results indicated that 57% of all samples belong to unsuitable category with %Na above 80. The dug wells were totally affected with greater than 80% of the samples falling under this category and 12.5 % falling in the doubtful category (Table 8). Also, for the remaining water types (lake, stream and spring), only 26% were under the permissible limit of %Na below 60% while 47% fell in the doubtful category.

Sodium Adsorption Ratio (SAR): Results showed that springs, streams and boreholes had average SAR values of 4.4, 5.1 and 7.8 respectively. These values are within the excellent range of SAR< 8 (Bashir *et al.,* 2013). The lakes and dug wells had average SAR values of 18.8 and 16.5 respectively classified in the intermediate water quality for irrigation based on SAR (Bashir *et al.,* 2013). Only one borehole sample, one lake sample and 4 dug wells exceeded the minimum standard of SAR=26 (Bashir *et al.,* 2013).

Magnesium Adsorption Ratio (MAR): Results showed that all sample types with exception of one lake sample (Small Momella, MAR=81.2%) and one spring (Mburukuu, MAR= 50.3%) had MAR values within the acceptable range of MAR<50% (Bashir *et al.,* 2013).

Kelley's ratio (KR): Results indicated that only 18.5% of the samples had KR values less than a unity which is good for irrigation (Bashir *et al.,* 2013). For all sample types, the percentage of samples exceeding the recommended standard of a unity is high compared to all other measured irrigation parameters (Table 8).

Table 8: Arumeru water quality parameters for Irrigation purposes

Sample type	Parameters			Guidelines (Bashir et al., 2013)	
	Min-Max	Mean	%S>STD	Range	Category
		pH			
Boreholes (n=10)	6.78-8.9	8.04	20	<6.5	Not specified
Dug wells (n=16)	7.17-9.25	8.43	56.25	6.5-8.4	Suitable
Lakes (n=4)	6.84-9.57	8.24	25	>8.4	Unsuitable
Springs (n=15)	6.46-10.91	7.77	33.3		
Streams (n=9)	7.04-9.7	8.43	55.6		
		EC (µS/cm)			
Boreholes (n=10)	437-3573	1121.8	10	<250	Excellent
Dug wells (n=16)	592-4844	2335.1	50.00	250-750	Good
Lakes (n=4)	254-8715	2961.5	50	750-2250	Doubtful
Springs (n=15)	137-1094	471.5	0	>2250	Unsuitable
Streams (n=9)	154-1744	691.7	0		
		RCS			
Boreholes (n=10)	0.79-17.5	5.47	70	1.25-2.5	Medium/Marginal
Dug wells (n=16)	2.03-23.17	10	94	>2.5	Bad/Unsuitable
Lakes (n=4)	0.05-80.65	23.55	50		
Springs (n=15)	0.16-5.21	1.75	20		
Streams (n=9)	0.3-9.12	2.78	44		
		Na%			
Boreholes (n=10)	53.4-96.6	77.5	80	<20	Excellent
Dug wells (n=16)	59.3-98.5	88.5	93.75	20-40	Good
Lakes (n=4)	30.4-99.1	69.4	50	40-60	Permissible
Springs (n=15)	31.5-96.7	76.1	73.3	60-80	Doubtful
Streams (n=9)	53.8-93.9	75.5	77.8	>80	Unsuitable
		SAR			
Boreholes (n=10)	1.3-29.3	7.80	10.00	<10	Excellent
Dug wells (n=16)	2.36-44	16.50	25.00	10.0-18.0	Good
Lakes (n=4)	0.62-60.15	18.80	25.00	18-26	Doubtful
Springs (n=15)	0.61-13.02	4.40	0.00	>26	Unsuitable
Streams (n=9)	0.95-13.2	5.10	0.00		
		MAR (%)			
Boreholes (n=10)	16.94-36.6	25.90	0.00	<50	Suitable
Dug wells (n=16)	14.2-42	28.30	0.00	>50	Unsuitable
Lakes (n=4)	23.2-81.2	39.50	25.00		
Springs (n=15)	13.4-50.2	28.30	6.70		
Streams (n=9)	19.07-31.2	26.80	0.00		
		KR			
Boreholes (n=10)	0.8-26.1	7.20	80.00	>1	Suitable
Dug wells (n=16)	1.05-55.7	16.80	100.00	<1	Unsuitable
Lakes (n=4)	0.35-73.54	20.60	50.00		
Springs (n=15)	0.33-21.5	7.60	73.30		
Streams (n=9)	0.88-12.5	5.30	77.80		

%S>STD: Percentage of samples under unsuitable category

For evaluation purposes of all water types, the obtained irrigation parameter results were plotted using standard diagrams which combine different parameters as shown in Figs. 48 – 49. Integrating the 2 diagrams, results indicated that the suitability of water types for irrigation is moderate in the order of springs > streams > boreholes > lakes > dug wells.

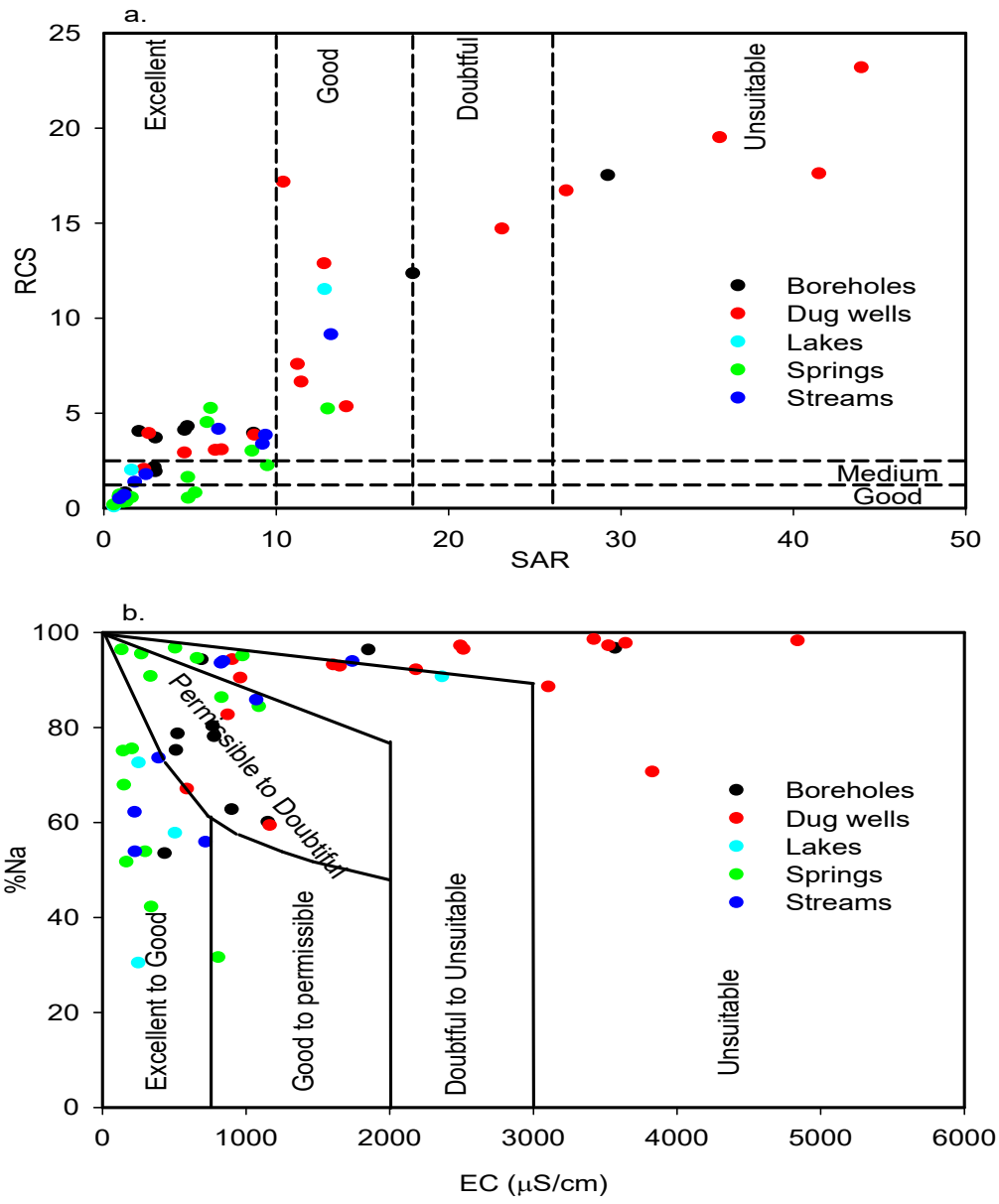

Figure 48: Arumeru groundwater classification for irrigation purposes (After Wilcox, 1955)

(a.) Classification based on RCS and SAR with exception of Lake small Momella with RCS=80.65 and SAR=60.15 (b.) Classification based on percent sodium and electrical conductivity with exception of Lake small Momella with EC=8715 and %Na = 99.06.

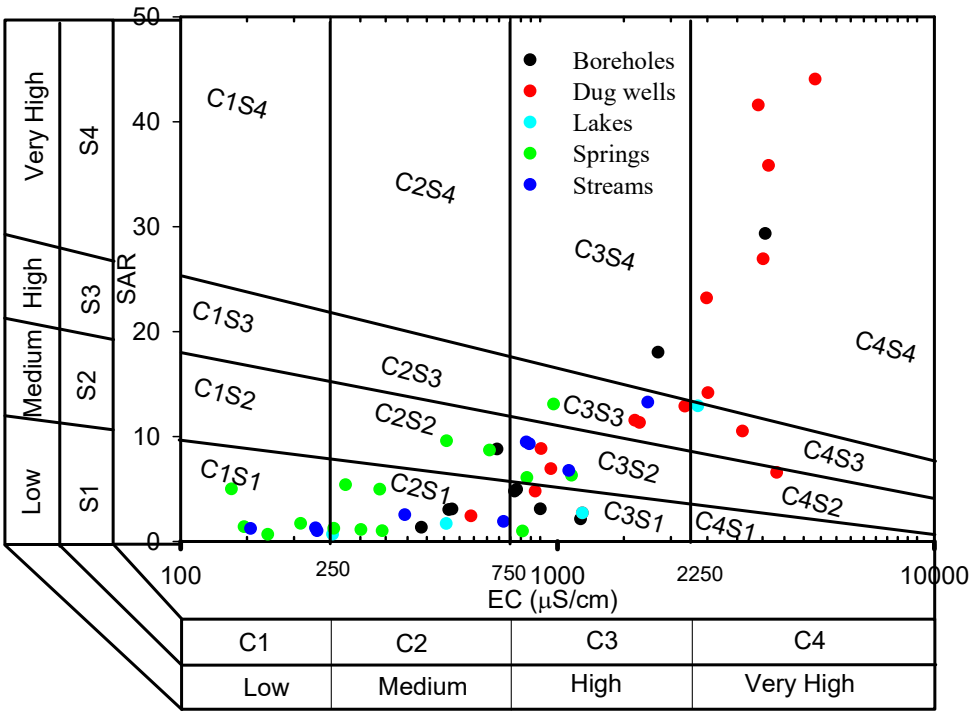

Figure 49: USSL diagram for classifying suitability of Arumeru groundwater for Irrigation

4.4 Discussion

4.4.1 Characterization of Physico-chemical parameters

The pH of the water samples indicated that waters were under nearly neutral to alkaline conditions. Nearly neutral pH values for the windward springs suggests short water interaction time/atmospheric signature. This is highly supported by the Gibb's plots where the windward springs plotted within and near the rainfall dominance field and their low dissolved ions relative to other sample types. Short water interaction time is likely to be attributed to fractured nephelinitic to phonolitic formation on the slope of Mt. Meru (Ghiglieri *et al.,* 2012) which is the main recharge zone and high hydraulic gradient. The alkaline condition for most of the springs in the leeward side could be attributed to a significant water-rock interaction time and low dilution (low rainfall) enhanced by evaporation relative to windward side. The low DO in dug wells relative to boreholes, springs and surface water types is mainly due to poor aeration, high levels of turbidity and probably organic matter. Poor aeration is due to the fact that most of the dug wells were not frequently in use because of either poor water quality for domestic purposes or the intended purposes such as seasonal irrigation and washings which do not require continuous supply of water. Most of the dug wells were shallow, constructed locally in residential areas and not protected

from surface run off. Such well's condition favored accumulation of OM and sediments leading to high turbidity and growth of oxygen consuming organisms. Low DO in Ngurudoto Crater Lake was attributed to abundance of aquatic plants as observed during the sampling campaign.

Total dissolved solids (TDS) and electrical conductivity (EC) reflect mainly the rock solubility, water-rock interaction time, precipitation and evaporation rates. More ions are dissolved as water interacts with rocks and their concentration increases with increasing evaporation rates while decreasing with increasing precipitation. Thus, as lake Small Momella is located in the leeward side of Mt. Meru, abnormal high TDS (4357 mg/l) in this lake could be attributed to low precipitation, intensive water-rock interaction time and evaporation. The studies by Dawson (2008) and Delcamp *et al*. (2013) revealed that Momella lakes were formed as a result of mass movement/collapse of Mt. Meru blocks. Therefore, it is likely that such mechanism enhanced dissolution process by generating huge loose materials leading to high dissolved ions. However, this study indicated high sulphate concentration (300 mg/l) which is not reflected in the surrounding Mt. Meru rocks suggesting the link between lake water and underground springs. As the windward side is characterized by high precipitation relative to leeward side (Oettli & Camberlin, 2005), the low TDS in crater lakes Duluti and Ngurdoto in windward side is largely the results of high precipitation and low evaporation. Geological factors such as the nature of the substrate and the susceptibility of the surrounding materials to weathering can also account for low dissolved ions in such lakes.

Slightly high TDS in streams relative to springs indicate that streams are largely gaining streams, receiving significant amount of water from the surrounding areas. This is further supported by field observation that most of the streams have developed great depths sometimes above 10 m which is likely to favor movement of water from the surroundings to streams. The significant contrast in TDS for the boreholes and dug wells is mainly attributed to their spatial distribution and evaporation-crystallization circle. Unlike the boreholes, most of the sampled dug wells were located in areas dominated by lahars (eg. Maji ya Chai-Kikatiti -Maroroni zone). Such lahars which have been documented by many researchers in the study area (Nanyaro *et al*., 1984; Decampo, 2004; Dawson, 2008; Ghiglieri *et al*., 2010, 2012) accounts for more dissolved ions in such areas due to their susceptibility to weathering through texture and high ash content. Through Gibb's plot it is revealed that evaporation - crystallization is the dominant process for dug well water type. Such processes have been known to contribute to dissolved ions in surface and groundwater (Nielsen, 1999; Kaseva,

2006) with salt crystallization in the dry season and salt dissolution in the rainy season. Therefore, such circles near the earth surface contribute to high dissolved ions in the dug well.

The temperature difference in water types is mainly a function of altitude and geographic positions in relation to Mt. Meru. For instance, the maximum temperature of 27.84 °C was observed at Lake Mlolozi in the leeward side of the mountain. The lowest temperatures generally between 17 and 13 °C were mostly observed in the springs at an altitude above 2000m a.s.l whereas elevated temperatures generally between 24-28 °C were mostly observed in the borehole and dug wells at an altitude below 1000 m a.s.l.

4.4.2 Water Quality for Domestic Purposes

The general ion dominance pattern in water types was lakes > dug wells > borehole > streams > springs with the ions showing the dominance pattern of $Na^+ > K^+ > Ca^{2+} > Mg^{2+}$ in all water types. Since the East Africa continental rift rocks including Arumeru rocks are generally alkaline (Gaciri & Davies, 1993; Peccerillo *et al.,* 2007; Ghiglieri *et al.,* 2012), high Na^+ as well as K^+ in water is basically the results of dissolution of alkaline rocks. The positive correlation of these two cations (R=0.85) suggest that they are likely to be released from the common source. For instance, the rock such as nephelinite with nepheline ($Na_3KAl_4Si_4O_{16}$) as the dominant mineral which is among the dominant rocks in the study area (Ghiglieri *et al.,* 2012) is likely to release high Na^+ and K^+ through weathering process. Furthermore, pyroclastic and ash materials which are also common in the study area (Nanyaro *et al.,* 1984; Wilkinson *et al.,* 1986; Dawson, 2008; Ghiglieri *et al.,* 2010, 2012; Malago *et al.,* 2017) are likely to have significant amount of Na^+ and K^+ because of two main reasons (a). Their association with alkaline materials in continental rift rocks (b). High Na^+ and K^+ content in water for the hand dug wells located in areas with such materials.

Therefore, the natural occurrence of Na^+ and K^+ explain their abundance in water type. High K^+ above the recommended standard of 12 mg/l (WHO, 2011) for 80% of the samples and high Na^+ above the recommended WHO threshold taste of 200 mg/l (WHO, 2011) for 50% of the dug well and two leeward lakes is attributed to water-rock interaction, susceptibility of materials to weathering, evaporation and precipitation rates as discussed previously. The low K^+ relative to Na^+ could be attributed to the dominance of Na^+ relative to K^+ bearing minerals in parent materials. The resistance of K-feldspar relative to plagioclase minerals in

weathering could be the other factor but these minerals are generally rare relative to nepheline and leucite minerals in weakly fractionated rocks.

The low Mg^{2+} and Ca^{2+} reflect their low abundance in parent rocks relative to Na^{+} and K^{+}. Their positive correlation (R=0.85) indicate that common source materials. These two cations were under the recommended drinking water quality limit of 75 and 50 mg/l respectively (WHO, 2008) with exception of one dug wells where elevated Ca^{2+} up to 82 mg/l could be attributed to the geology at that particular area. Also, as Dawson (1992) reported carbonatitic materials around Lake Ngurudoto, the elevated Ca^{2+} in this lake is likely to be attributed to carbonatite. The high concentration of Mg^{2+} and Ca^{2+} in the windward side relative to leeward side was mainly attributed to abnormal elevated concentrations of Ca^{2+} and Mg^{2+} at Nduruma spring (Ca^{2+} =40.18 mg/l; Mg^{2+} =23.65 mg/l) and Makisolo spring (Ca^{2+} =20.12 mg/l; Mg^{2+} =7.39 mg/l) at Nduruma spring and at Makisolo spring. These springs are located away from the foot of Mt. Meru relative to other springs (not on the slope of the mountain) suggesting a reasonable water-rock interaction time from the recharge to discharge point. Thus, as the geology is too erratic because of explosive eruptions along the East Africa Rift System (Rango *et al.,* 2010; Vye-Brown *et al.,* 2014), elevated Ca^{2+} and Mg^{2+} values are likely to result mainly from dissolution of Ca-Mg bearing minerals such as pyroxene being concentrated in some specific zones.

In the study area, carbonate rocks cannot justify high HCO_3^- in water systems and therefore it is strongly linked to volcanic activities. Two main factors; weathering of silicate minerals and CO_2 emission through volcanic activities explain high $HCO_3^- + CO_3^{2-}$ in Arumeru waters. It has been reported elsewhere that HCO_3^- being derived from CO_2 gas is common in active volcanic areas (Percoraino *et al.,* 2015). Along the East Africa Rift System, emission of gases such as CO_2 and SO_2 are common and recently in 2011, there was emission of strong SO_2 gas near the border between Ethiopia and Eritrea along the rift (Vye-Brown *et al.,* 2014). Therefore, with the recent eruptions at Mt. Meru, the last eruption being in 1910 (Istituto Oikos, 2011; Vye-Brown *et al.,* 2014), weathering of silicate minerals through hydrolysis under presence of the emitted CO_2 has been leading to high $HCO_3^- + CO_3^{2-}$ in water systems. Since CO_2 acts as a catalyst in water-rock interaction process (Percoraino *et al.,* 2015), its presence in volcanic materials, on the other hand, supports the obtained strong positive correlation between HCO_3^- and TDS (R=0.96). This fact together with other factors such as common source explains a strong positive correlation between HCO_3^- with other ions

particularly Na^+ (R=0.92), K^+ (R=0.90), F^-(R=0.90), Cl^- (R=0.73), CO_3^{2-} (R=0.79) and SO_4^{2-} (R=0.66) in Arumeru groundwater.

The high fluoride content along the East Africa Rift System has been reported by many researchers (Nanyaro *et al.,* 1984; Gaciri & Davies, 1993; Ghiglieri *et al.,* 2010; Rango *et al.,* 2010; Ghiglieri *et al.,* 2012). Findings from this study are in agreement with the previous researchers. The mean F^- values were found to be above the recommended standard of 1.5 mg/l (WHO, 2008) in all water sources with exception of the windward springs (mean=1.32 mg/l). The most affected areas were the leeward side of Mt. Meru (Ngarenanyuki & Oldonyosambu) and in the windward side at the foot of Mt. Meru (Maji ya Chai-Kikatiti-Makiba-Maroroni). Integrated factors leading to high fluoride in such areas include abundance of volcanic materials rich in fluoride, significant water-rock interaction time, high evaporation and low precipitation. These areas are dominated by lahars suggesting that lahars contain significant amount of fluorine and are soluble relative to lava flows as discussed previously. The local communities in such areas are strongly affected by dental and skeletal fluorosis and in some places severe effects such as crippling skeletal fluorosis are pronounced. Livestock keeping is one of the major activities in such areas with cattle consuming large amount of water with high fluoride per time. The effects of fluoride in such cattle are likely to be high but justification is still difficult because of the little attention on effects of fluoride on animals.

The high fluoride in lakes and dug wells relative to other water types follows the same mechanism that led to high TDS and ions such as Na^+, K^+ and HCO_3^- in waters. This is supported by the obtained strong positive correlation of F^- with TDS, HCO_3-, CO_3^{2-}, Na^+ and K^+. The lack of a significant correlation between F- with Ca^{2+} and Mg^{2+} is basically due to the strong affinity between $Ca^{2+,}$ Mg^{2+} with F^- relative to Na^+. That, under favorable condition, in areas with high Ca^{2+} and Mg^{2+}, CaF_2 and MgF_2 will precipitate leading to low fluoride in water system.

Chloride abundance and correlation behavior was similar to fluoride suggesting the common source. However, the correlation of Cl^- with F^- was not so strong (~0.7) (Fig. 38) suggesting that Cl^- is also likely to result from anthropogenic processes. Anthropogenic activity is further supported by a significant Cl^- contrast in boreholes and dug wells with the highest Cl^- (300 mg/l) above the recommended standard of 200 mg/l (WHO, 2008) in the dug well located about 5 m from the pit latrine.

The wide range of sulphate in dug well (8-320 mg/l, mean=56.8±77 mg/l) and Lakes (2-300 mg/l, mean=88.5±142.8 mg/l) led to high standard deviation above the mean values. Positive correlation of sulphate with TDS (R=0.76), K^+ (R=0.79), Cl^- (R=0.90), Na^+ (R=0.66), F^- (R=0.67), HCO_3^- (R=0.66) suggest SO_4^{2-} to result from water-rock interaction. A strong positive correlation between SO_4^{2-} and Cl^- suggest the common source. The low concentration of SO_4^{2-} in springs relative to other sources could be attributed to short water-rock interaction time. That high SO_4^{2-} in dug wells and lakes is related to intensive water-rock interaction time. Contrary, as SO_4^{2-} can results from anthropogenic activities particularly sewage effluent and agricultural activities (Jiang *et al.,* 2009), and most of the dug wells were located in high density areas, some close to pit latrines, high SO_4^{2-} in dug wells relative to other sources could indicate anthropogenic source. This supported by high level of SO_4^{2-} up to 320 mg/l for one hand dug well located close to pit latrine. Anthropogenic cannot explain high SO_4^{2-} in lake Small Momella (300 mg/l) because the lake is free from both human activities and surface inflow. Since there is no documented sulphide deposit surrounding the lake which could account for high SO_4^{2-} in the lake, it is suggested that there are underground springs rich in SO_4^{2-} which are feeding the lake. Therefore, with the above view, both natural and anthropogenic sources account for the obtained SO_4^{2-} values in the study area.

The levels of nitrate in groundwater have been used as an indicator of pollution (Wick *et al.,* 2012; Elisante & Muzuka, 2015) owing to the fact that there are no reported rock nitrate deposits in nature. High nitrate concentrations were obtained in dug wells, in which 12.5% of the sampled dug well had [NO_3^-] above the recommended threshold of 50 mg/l (WHO, 2008). Most of the dug wells were located in residential areas which had also high number of pit latrines, cowsheds and other sewage systems which are potential source of nitrate to surface water and groundwater systems (Wick *et al.,* 2012; Elisante & Muzuka, 2015). This suggests that the main causes of high [NO_3^-] in the study area are anthropogenic activities and not water-rock interaction processes. This is in agreement with the study by Elisante & Muzuka (2015) which revealed that high [NO_3^-] is associated with anthropogenic activities on the slope of Mt. Meru. Thus, springs, lakes and borehole water types had low nitrate concentration because of either being free from human activities or low surface input. This is well supported by the observation within the lakes; that lake Duluti, the only lake centered close to local communities had high NO_3^- (12.76 mg/l) relative to all other lakes (mean=5.3 mg/l). Elevated nitrate in one surface sample (Kyamang'ata=136.4 mg/l) could be attributed to animal excreta because it was a cow path with low water discharge. The obtained anion

dominance pattern of $HCO_3^- > CO_3^{2-} > Cl^- > SO_4^{2-} > NO_3^- > F^-$ compare well with the pattern obtained by Rango *et al.,* 2010 ($HCO_3^- > Cl^- > SO_4^{2-} > F^- > NO_3^-$) in the northern part of the same rift system in Ethiopia with exception of F^- and NO_3^- which are interchanged. The interchange of F^- and NO_3^- indicates nitrate contamination by anthropogenic activities in the study area.

4.4.3 Groundwater Evolution and Geochemical Processes

Using Gibb's plots it is clear that weathering of rocks is the major process controlling groundwater chemistry in the study area (Figs. 46 – 47).The distribution of borehole and dug well hydrogeochemical data in Gibb's plot indicated that evaporation-crystallization process dominated in the shallow part of the earth surface where dug wells are constructed (< 20 m below the surface) and weathering of the rocks dominated at great depth, generally between 20 and 150 m which is a depth range of the sampled boreholes. This is in agreement with the study by Kaseva (2006) in the study area that there is significant concentration of ions such as F^- in water resulting from crystallized salts at or near the surface.

Water-rock interaction and evaporation processes are well indicated by hydrogeochemical data of the streams and springs in Gibb's plot (Figs. 46-47)). Water sample from Ngarenanyuki river, the only perennial river in the leeward side of Mt. Meru, plots in the rock dominance field but close to evaporation-precipitation field indicating that apart from weathering of rocks, evaporation also plays a significant role in controlling water chemistry of the river. This accounts for high dissolved ions particularly Na^+, K^+, HCO_3^-, F^- and SO_4^{2-} in this river relative to other rivers. However, as SO_4^{2-} can also results from human activities (Jainag *et al.,* 2009), high [SO_4^{2-}] could have been also attributed to application of pesticides rich in sulfur on tomato plants; low scale irrigation scheme which is commonly practiced in the northern parts of the study area. Three stream samples in the windward side of the mountain; one falling in the field of rainy dominance and two falling close to the boundary of rainfall and rock dominance (Fig. 47) indicate dilution effect (high precipitation) enhanced by low evaporation for the windward streams relative to leeward streams.

It is clearly indicated that in the windward side where most of the springs and streams are located and evaporation is not intensive, stream samples showed elevated TDS relative to spring samples. It was also noted that spring samples falling in the field of rainfall dominance were typically located on the high slope of Mt. Meru and most of the springs falling in the field of rock dominance were either on the leeward side or on the lower slope/ foot of the

mountain. Such observations concur with the isotopic study by Ghiglieri *et al.,* 2012 that the slopes on Mt. Meru are the main recharge zones. Springs have undergone short water-rock interaction time relative to streams and water chemistry change progressively as water interacts with rocks.

Two different fields for the lake samples in Gibb's plot are mainly attributed to rainfall and temperature differences in the windward and leeward sides of Mt. Meru as discussed previously. Due to this fact, water chemistry of Lakes Small Momella and Mlolozi which are located in the leeward side is mainly controlled by evaporation-crystallization processes. For the crater lakes in the windward side (Duluti and Ngurudoto), water chemistry is mainly controlled by weathering process (Fig. 46-47). However, it is further noted that the intensity of these processes varies depending on other factors such as geology, geographic position relative to Mt. Meru and vegetation cover. For instance, the effect of evaporation is well reflected at lake Small Momella (plotting in the evaporation field in Fig. 46 and close to evaporation field in Fig. 47) because of its position (typically in the leeward side). The effect of rock weathering is low for lake Ngurudoto as it plots close to the rainfall dominance and this is attributed to high rainfall supported by intensive vegetation cover which reduces evaporation. For Lake Duluti, despite being in the windward side, the weathering process dominates indicating interaction of lake water with the surrounding rocks.

The dominance of weathering process is further supported by piper diagram, Langelier and Ludwig (1942) and Chadha's diagrams (Figs. 43-45), with Na-K-HCO_3 as the major water type which is a typical characteristic of groundwater in areas where weathering and ion exchange processes dominate. However, excessive evaporation and low rainfall led to elevated Na^+, K^+ and HCO_3^- ions in the leeward relative to windward water types as evidenced by springs. One sample belonging to Na-K-Cl water type is basically the effect of Cl^- contamination by anthropogenic processes and few samples belonging to Ca^{2+} (Mg^{2+})-HCO_3^- water type is probably indication of abundance of Mg^{2+} and Ca^{2+} in source materials in that particular areas. Overall, water chemistry changes progressively to more alkaline (enrichment of Na^+, K^+ and HCO_3^-) as it interacts with the rocks and atmosphere through weathering and evaporation processes.

4.4.4 Water Suitability for Irrigation Purposes

Arumeru groundwater was characterized by a wide range of suitability for irrigation purposes from excellent to poor quality. It is clearly shown that water- rock interaction degree plays a

significant role in controlling water suitability for irrigation. The dug well water types were found to be of low quality due to their high TDS relative to all water types as discussed previously. The dominance of Na^+, K^+ and HCO_3^- as reflected in the RCS, %Na and Kelley's ratio is the key factor contributing to low water quality for irrigation purposes. High RCS and %Na above the recommended standard and Kelley's ratio above the unity have effects on crop productivity particularly through soil texture. Continuous application of such water leads to soil clogging and thus lowering soil permeability (Bo *et al.,* 2013; Kumar *et al.,* 2013; Srinivas *et al.,* 2014; Nagaraju *et al.,* 2016). Effects such as crop burn in the gardens (flowers and pawpaw) which are likely to be attributed to low water quality for irrigation were observed in the study areas in some specific areas (Kikatiti-Maroroni) where crops were irrigated using dug well water with high RCS, %Na and Kelley's ratio above the unity.

Unlike Lakes Duluti and Ngurudoto in the windward side, lakes Small Momella and Mlolozi in the leeward side were found to be characterized by low water quality for irrigation. The low quality was mainly attributed to high dissolved ions as explained previously. Generally, the overall order of water quality for irrigation follows the trend of water quality for domestic purposes in the order of springs > streams > boreholes > lakes > dug wells. However, this is a general trend, the irrigation parameter diagrams (Figs. 48-49) indicate that water suitability is not a function of water type only; dug wells are generally of poor quality but there are some few dug wells with suitable water for irrigation. Other factors related to geology and water rock interaction processes might have significant contribution in controlling the water quality. Furthermore, it should be noted that apart from water chemistry, the factors like soil texture, structure and composition, local irrigation practices and types of crops are important factors in assessing water quality for irrigation purposes (Srinivas *et al.,* 2014).

4.5 Conclusions and Recommendations

Arumeru groundwater showed variation in hydrogeochemical characteristics. Despite internal variation within the particular water types, significant variation was according to water types. Geology, water-rock interaction time and climatic conditions were found to be the main factors which control hydro-geochemical characteristics of groundwater. Overall, the dominant patterns of major cation and anion in water types were $Na^+ > K^+ > Ca^{2+} > Mg^{2+}$ and $HCO_3^- > CO_3^- > Cl^- > SO_4^{2-} > NO_3^- > F^-$ respectively, with the dominant pattern of dissolved ion being in the order of lakes > dug wells > borehole > streams > springs. Springs particularly from the windward side on the slope of Mt. Meru were characterized by short-

water interaction time relative to all other water types, which is favored high hydraulic gradient on the slope of the mountain. This was evidenced by low dissolved ions and their position in water-rock interaction plots where the samples fell close to the rainfall dominance. Such observations indicate that Mt. Meru is the main recharge zone and water chemistry changes progressively to more alkaline as water interacts with the rocks towards the lowland areas. Springs in the leeward sides showed slightly high dissolved ions relative to windward springs indicating that low precipitation and excessive evaporation have great influence in controlling water chemistry. Climate effect is well observed in water-rock interaction plots where the typical leeward water types showed that weathering of rocks together with evaporation-crystallization are the dominant process whereas rainfall and weathering of rocks dominate in the leeward sides. Hydrochemical facies indicated that Na-K-HCO_3 water type dominates to about 90%. High Na^+ and K^+ is the reflection of their dominance in parent materials which are alkaline in nature. Correlation analysis indicated that HCO_3^- correlated positively with TDC, EC, Na^+, K^+, F^- and Cl^- implying that they originate from the rocks through weathering and CO_2 triggered the dissolution process.

This study revealed that more ions are dissolved close to the earth surface (0-20 m; dug well zone) particularly in areas dominated by lahars, ash and pyroclastic materials. This indicates that these materials are weak to weathering and therefore responsible for high dissolution of ions including fluoride. Salts crystallization and dissolution in dry and wet seasons respectively could be the other factor contributing to high dissolved ions in shallow groundwater as well as streams in the leeward side such as Ngarenanyuki and Kyamang'ata. Similarly, apart from intensive evaporation, high dissolved ions in the leeward lakes relative to windward lakes could also be attributed to the presence of these materials. However, high sulphate concentrations in Momella lakes which are free from surface input suggest the lakes to be fed by underground springs.

The suitability of water for domestic and agricultural purposes was found to be moderate, following the same order pattern of springs > streams > boreholes > lakes > dug wells. Fluoride was found to be the major natural pollutant lowering the water quality for domestic purposes (mean=17.6 mg/l, n=54). 78% and 52% of the samples had fluoride above the recommended WHO and Tanzanian standard respectively. Anthropogenic pollution was recognized through nitrate particularly in the dug wells located in residential areas where latrines are locally constructed. Chloride and sulphate were found to result from both natural and anthropogenic sources. High TDS, particularly in dug wells, along with abundance of

Na^+ (mean =118 mg/l) and HCO_3^- (mean=390 mg/l) in Arumeru waters were found to lower significantly the water quality for irrigation purposes.

To great extent, the effects of high fluoride in drinking water are known to the communities. However, the use of such water along with Na^+ and HCO_3^- beyond the recommended standard in irrigation and livestock purposes has been the common practice. Thus, lowering of crop productivity and consumption of agriculture products with high fluoride unknowingly is inevitable. Therefore, this study recommends (a) Intensive water quality analyses pre-utilization and effective utilization of spring water for domestic purposes. (b) More researches on fluoride mobility from soil to plants, its levels and distribution in both plants and livestock. (c) Researches on crop productivity effects resulting from of high Na^+ and HCO_3^- in water system. (d) Further geological works for intensive assessment of rocks and their spatial distribution including fluoride bearing materials. (e) Leaching experiments for assessing materials responsible for high dissolved ions in water including fluoride. (f) Geophysical works for delineation of potential groundwater zones with acceptable fluoride levels.

CHAPTER FIVE

DELINEATION OF POTENTIAL GROUNDWATER ZONES IN THE SOUTH-EASTERN PARTS OF MT. MERU, NORTHERN TANZANIA[4]

Abstract

Arumeru district is among the areas in Tanzania with water shortage and high fluoride level in water systems. The water shortage for both domestic and agricultural purposes is increasing with time due to climate change, rapid population growth and expansion of agricultural activities. In the southern part of the district, geo-electric data (resistivity) from 30 Vertical Electrical Soundings (VES) in conjunction with hydro-chemical data (Fluoride, TDS and EC) and lithological logs were used to delineate groundwater zones with contrasting quality in the fluorotic zone. Results revealed a thin upper aquifer (~25 m thick) restricted in few parts and a lower major aquifer (>100 m thick) covering about 80% of the study area. Resistivity between 35-60 Ωm represents fresh groundwater hosted in weathered and fractured mafic volcanics, tuffs and breccias. Resistivity between 25-35 Ωm represent intermediate groundwater quality whereas values between 15-25 Ωm represent low groundwater quality (TDS >1000 mg/l, F >10 mg/l) hosted in lahars. Resistivity value between 25 and 35 Ωm represent intermediate water quality whereas the resistivity less than 15 Ωm represents clay or very low water quality. Correlation analysis of the interpreted resistivity value with EC and fluoride showed a strong negative correlation (~0.9). Thus, it is generally possible to infer the quality of water and fluoride content using surface resistivity data. All data were integrated together to construct Groundwater Potential Index Map which can be used as a guide in borehole siting and further groundwater surveys.

[4] This Manuscript is under review in the Hydrological Science Journal. Manuscript ID: HSJ-2019-0487

5.1 Introduction

Economic water scarcity is the common problem among the developing countries including Tanzania (UNOCHA, 2010). Tanzania depends largely on surface water for irrigation and domestic purposes. In recent years, population growth and climate change have lowered the availability of surface water leading to rapid increase in the use of alternative water source which is groundwater (Kashaigili, 2010). For instance, since 1997, anomalous increase in new boreholes and dug wells has been reported in areas with rapid population growth such as Dar es salaam city (Mjemah *et al*., 2012). In this context, despite of having a general estimate of 5250 km^3 as total groundwater storage in the country (MacDoonald *et al*., 2012; Elisante & Muzuka, 2016), with rainfall as a major recharge (Nkotagu, 1996c; Mjemah *et al*., 2011), groundwater in the country is poorly surveyed. The groundwater potentiality in the country is further supported by the drilled boreholes. It was found that the average yield for the drilled boreholes is 11 m^3/h with the highest reported yield of 600 m^3/h from one borehole located in TPC, Moshi (GITEC & WEMA, 2011). The other reported high yield is 460 m^3/h in one borehole located in central zone, Dodoma, one among the areas receiving low rainfall in the country (Kashaigili, 2010).

In some areas with water scarcity in Tanzania, particularly central and north regions, fluoride in some of the water sources is also high above the recommended World Health Organization standards of 1.5mg/l (WHO, 2008) as well as the national standard of 4 mg/l (TBS, 2007). It is generally estimated that 30% of groundwater sources in Tanzania which are used for domestic purposes have fluoride above the recommended WHO standard (Thole, 2013). It is released from igneous rocks of various composition; granitic rocks as the main source in central zone and volcanic rocks are the source in northern Tanzania.

Arumeru district in northern Tanzania is one among the areas with water shortage as well as high level of fluoride in much of water sources above the acceptable national standard (Nanyaro *et al*., 1984; Ghiglieri *et al*., 2010, 2012; Pittalis, 2010). However, due to variation in local geology and climatic conditions within the district, low and acceptable fluoride water sources are localized in some specific areas (Ghiglieri *et al*., 2010; Malago *et al*., 2017). This creates urgent need of exploring safe water sources for domestic purposes.

Water demand in Arumeru district is increasing due to the increase in population (Vye-Brown *et al*., 2014) and climate changes. The most affected areas are the leeward side, low land areas south of Mt. Meru and eastern side of Mt. Meru. To some extent, few researches

focusing on groundwater have been conducted in the leeward side (Ghiglieri *et al*., 2010; Pittalis, 2010), the other mentioned areas remained poorly researched. These areas receive low rainfall relative to areas surrounding the mountain in the windward side which is characterized by numerous streams. Most of the spring water sources in this side exhibit low fluoride within the acceptable Tanzania standard (Ghiglieri *et al*., 2010; Malago *et al*., 2017). Due to the expansion of agricultural activities in the study area (Vye-Brown *et al*., 2014), such water sources have been also utilized for agricultural purposes through irrigation canals in upland areas leading to water shortage for domestic purposes in the low land areas. Thus, there is a need of alternative water sources which is groundwater sources in both areas surrounding the mountain and low land areas.

Under proper water management, utilization of groundwater resources in the upland areas will reduce consumption of potable surface water through irrigation canals and this in turn will lead to increase in such water in the low land areas. It is anticipated that increase in potable surface water in low land areas supplemented with the use of groundwater in such areas will completely solve water scarcity problems. Furthermore, as Tanzania is currently considering industries as one of the major sector for economic growth, availability of reliable groundwater source will be a key for local and region economic growth through industries and large scale agricultural activities.

Despite of having numerous boreholes and dug wells in Arumeru district, groundwater in the area is poorly surveyed. In most cases, local dug wells and some of the boreholes are drilled locally without groundwater survey information leading to integrated problems such as dry well, low yield, low water quality and money loss. To overcome this, scientific approaches in locating potential groundwater zones are required.

Few available geophysical survey works are localized in the northern part of Mt. Meru (Ghiglieri *et al*., 2010), one among the areas receiving low rainfall (Vye-Brown *et al*., 2014) with high fluoride above the acceptable standards in much of the water sources (Nanyaro *et al*., 1984; Ghiglieri *et al*., 2010, 2012). The geophysical work by Ghiglieri *et al*., 2010, revealed some few potential groundwater sources but could not clearly focus on characterizing aquifers in terms of water quality. Despite similarity in geology, groundwater occurrence and potentiality in the two areas (northern and southern parts of Mt. Meru) is obviously different due to differences in precipitation which accounts for groundwater recharge. Also, factors such as local geology variation, geomorphology, structures and near

surface processes (weathering, fluvial processes, sedimentation etc) may account for variation in groundwater potential in the two areas. Therefore, assessing groundwater potentiality in the south-eastern parts of Mt. Meru which is also among the areas facing water shortage, focusing on both availability and quality is essential in reducing water shortage problems.

As the study area is among the fluoritic zones in Tanzania, this research aimed to delineate potential groundwater zones in the area, emphasizing on characterization of aquifers in terms of quality and quantity and eventually development of Ground Water Potential Index Map (GWPIM) which will serve as a guide for further groundwater survey works and siting of boreholes. Such information is important for the government and Water Management Planners in both addition of new water sources through boreholes and protection/conservation of potential groundwater sources. To achieve this, Vertical Electrical Sounding (VES) method; a method which is widely used in delineation of groundwater zone (Matias *et al.,* 1993; Meju & Fontes, 1999; Maiti *et al.,* 2011; Hewaidy *et al*., 2015; Riwayat *et al*., 2018) in conjunction with hydro-geological data was employed.

5.1.1 Application of Vertical Electrical Sounding (VES) Method

Theoretical background as well as field practice of resistivity method is well documented since 1960s by Bhattacharya & Pattra (1968), Parasnis (1973), Van Zijil (1985) and Patra & Nath (1999). Since then, there is increased application of this method in Geotechnical, Civil Engineering, Environmental and Hydrogeological works. Some of these studies are Baharuddin *et al*. (2009), Hodlur *et al*. (2010), Akankpo & Igboekwe (2011), Nicaise *et al*. (2012), Anomohanran (2015), Sidhardhan *et al*. (2015), Koda *et al*. (2017) and Riwayat *et al*. (2018). However, comprehensive interpretation of resistivity data is possible if VES method is supported with other geophysical and hydrogeological information (Sonkamble, 2014; Sidhardhan *et al*., 2015; El Sayed *et al*., 2017; Koda *et al*., 2017). For instance, in hydrogeological studies, VES method is largely integrated with borehole lithological logs (Baharuddin *et al*., 2009; Sonkamble, 2014; Golshan *et al*., 2018; Kamal & Ammar, 2018), downhole electrical logs (Hodlur *et al*. 2010; Anomohanran, 2015; Jimoh *et al*., 2018), water resistivity (Hodlur *et al*., 2010), hydrochemical data (Nicaise *et al*., 2012; Ravindran *et al*., 2013; Sonkamble, 2014; Koda *et al*., 2017; Golshan *et al*., 2018), pumping test data (Anomohanran, 2015), electromagnetic (Nicaise *et al*., 2012; Golshan *et al*., 2018) for precise determination of aquifer formation, geometry and characteristics.

Lithological borehole logs are important in interpreting aquifer formation because they provide information on lithological variation within individual layer which is interpreted using VES data. Furthermore, lithological logs account for different geological formations which are characterized by the same resistivity values. Geophysical borehole logging, which is commonly applied with VES data, provides information on rock type and fluid content (Jimoh *et al*., 2018) and can also account for variation in resistivity within a single thick layer which is interpreted using VES data (Hodlur *et al*., 2010).

Vertical Electrical sounding (VES) method is widely used in delineation of aquifers with contrasting water quality. For this reason, it has been commonly employed to study saline water intrusion and other groundwater contaminations (Baharuddin *et al*., 2009; Hodlur *et al*., 2010; Sundararajan *et al*., 2011, Ravindran *et al*., 2013; Sonkamble, 2014; Sidhardhan *et al*., 2015; Koda *et al*., 2017; Jimoh *et al*., 2018). Generally, contaminated/saline water exhibits low resistivity relative to fresh groundwater formation. This is due to increase in dissolved ions which enhance conductivity (Hodlur *et al*., 2010; Sundararajan *et al*., 2012; Koda *et al*., 2017; Jimoh *et al*., 2018). Contaminated zones are well discerned by low resistivity values relative to aquifers along with elevated total dissolved solids (TDS) (eg. 4-17 Ωm, TDS > 2000 mg/l as a dump site contaminated zone (Sidhardhan *et al*., 2015). Resistivity is extremely low for saline water intrusion (~0.2-0.3 Ωm) (Baharuddin *et al*., 2009; Nicaise *et al*., 2012) along with elevated TDS sometimes as high as 10 000 – 30 000 mg/l (Ravindran *et al*., 2013; Sonkamble, 2014).

Fresh groundwater aquifers are characterized by a wide range of resistivity values but generally between 10-100s Ωm. This variation is largely attributed to differences in water quality, degree of saturation, rock/soil chemistry, porosity and permeability (Archie, 1942; Sundararajan *et al*., 2012; Koda *et al*., 2017). Due to this, various freshwater aquifer resistivity values have been obtained in different geological formation (30-300 Ωm in sands to gavels (Jimoh *et al*., 2018), 11-93 Ωm in fractured limestone (Ammar & Kamal, 2018), 70-350 Ωm in weathered and fractured gneiss (Arsène *et al*., 2018), 15-54 Ωm in clays to sands (El Sayed *et al*., 2017), 20-150 Ωm in clay sands to sandstone (Hudlur *et al*., 2010), 15-80 Ωm in fine sand (Baharuddin *et al*., 2009), 20-70 Ωm in sandy clay (Sonkamble, 2014), 25-200 Ωm in calcareous sedimentary rocks (Ravindran *et al*., 2013). The lower limits of these ranges are generally due to the increase in clay content which enhance electrical conductivity (Hudlur *et al*., 2010; El Sayed *et al*., 2017). This creates difficulties in

differentiating saline water/contaminated water and clay rich formation using resistivity values only (Sundararajan *et al*., 2011; El Sayed *et al*., 2017).

Various studies that are closely related to this study, for example Nicaise *et al*. (2012) and Ammar & Kamal (2018) indicate that there is inverse relationship between aquifer resistivity and TDS/EC of water samples collected in proximal wells. However, there is no work which specifically link surface resistivity measurement with natural contaminant such as fluoride levels in aquifers. Largely, source of fluoride in water is from dissolution of rocks (Nanyaro *et al*., 1984; Ghiglieri *et al*., 2010, 2012; Malago *et al*., 2017; Raj & Shaji, 2017). During dissociation/weathering of rocks, fluoride is released together with other ions depending on the mineralogical composition of the rock. Due to this, there is a positive correlation between fluoride with total dissolved solids (TDS) and electrical conductivity (EC) in groundwater samples (see Chapters 3 and 4). Since one of the important factors that control resistivity of the formation as summarized by Archie (1942) is water chemistry; it is possible to characterize aquifers in term of water quality using surface resistivity data supplemented with hydrogeological information. With this view, this is a new research work where groundwater is delineated within a fluorotic zone and surface resistivity data are used to establish a correlation between aquifer resistivity and fluoride levels in groundwater.

5.2 Methodology

5.2.1 Study area

The study area (~1200 Km^2) is located on the southern part of Mt. Meru (4565 m, above sea level), one of the active mountains along the East Africa Rift Valley, northern Tanzania (Fig. 50). Climate in the area varies significantly from high altitude areas (Mt. Meru) to low altitude areas (~900 m, above sea level), south of the mountain. The areas surrounding Mt. Meru in the windward side receive high rainfall averaging at about 1000 mm per annum with much of the rainfall occurring between mid-February and May (PBWB/IUCN, 2008). This amount decreases gradually to the south (Makiba-Bwawani and Mbuguni) and eastern side of the mountain (Leguruki-King'ori) within the study area (Fig. 50). In the northern side of the Mt. Meru (leeward side), it decreases to an average of 535 mm per year (Ghiglieri *et al*., 2010). The mean annual temperature within the district varies from about 20 to 29 ˚C (Ghiglieri *et al*., 2010).

Geologically, the area is studded by volcanic materials from Mt. Meru. Various groups of volcanic rocks from different volcanic eruption episodes with the latest being in 1910

(Ghiglieri *et al*., 2010; Vye-Brown *et al*., 2014) have been documented by many researchers (Wilkinson *et al*., 1986; Dawson, 2008; Ghiglieri *et al*., 2010, 2012). The dominant volcanic groups include lahars of various ages, nephelinites and phonolites, pyroclastic and ashes, basaltic lava and scoria, tuffs and breccias. Rarely, very recent alluvial sediments occur in some specific areas depending on the land morphology. The distribution of such materials together with structures and geomorphology control occurrence, distribution and quality of groundwater. For instance, fluoride which is the major natural pollutant in water systems with noticeable adverse effects such as dental and skeletal fluorosis in the community within the study area results from dissolution of volcanic rocks with fluoride bearing minerals. Such minerals include fluorite, biotite, hornblende and apatite (Chae *et al*., 2006; Ghiglieri *et al.,* 2010, 2012; Naseem *et al*., 2010).

Around Mt. Meru, the drainage network seems to be radial but patterns tend to change to dendritic towards the low land areas (Fig. 50). Significant change in hydraulic gradient after the spring zone on the slope of Mt. Meru cause most of the streams to lose large amount of water to the surroundings. Such waters are localized in specific zones and likely to contribute in groundwater recharge in such areas. The recharge in the low land area (Makiba-Bwawani and Mbuguni) (Fig. 50) is therefore a function of both precipitation in such areas and subsurface flow movement from upland areas.

5.2.2 Field methods

To assess groundwater potentiality in the study area, Vertical Electrical Sounding (VES), a method that is widely used in groundwater studies by revealing the variation of resistivity with depth (Matias *et al*., 1993; Meju & Fontes, 1999), supplemented with hydrogeological data were used. The important hydrological information used were Electrical Conductivity (EC) of water samples, Total Dissolved Solids (TDS), Fluoride, well depth and general geology. These are the data that can be integrated together with resistivity data to assess groundwater and characterize the aquifers. Such data were acquired in the dry season between January and February 2017.

Geoelectrical survey was conducted in February 2017 using the ABEM Terrameter SAS 4000 utilizing Schlumberger array with a general maximum current electrode separation (AB) of 400 m. Based on the fact that the depth of investigation is approximated to be half to one-third of the current electrode spacing (Maiti *et al*., 2011), this separation was suitable to

investigate a depth of about 130-200 m. A total of thirty VES stations (Fig. 50) were selected based on the following criteria:

(i) Existing wells: Some VES stations were located in the vicinity of the existing wells so as to aid on interpretation. Since geology differs from one area to the other, there was a need of selecting several VES stations proximal to the existing well so as to be used as a guide for interpretation in that particular area.

(ii) High water demand: Some VES stations were located in areas with serious water shortage for domestic purposes. Such areas include King'ori and Kikatiti (Fig. 50)

(iii) Fluoritic zones: Some VES were located in areas that have been demarcated as high fluoride zones. Such areas include Maji ya Chai, Maroroni, Kikatiti and USA River (Fig. 50).

(iv) Community centres: Due to population growth, water demand is increasing in community centres such as schools, market, institutions etc. Thus, there was a need of selecting VES stations in such areas for assessing groundwater potentiality and delineating the areas for siting boreholes.

(v) Space and land morphology and artificial structures: Hills and depressions were avoided by choosing a flat terrain extending to at least 400 m; placing potential electrodes in the depression could lead to high abnormal ΔV when the current electrodes are moved up the slope. The opposite is true when sounding centre is situated on a hill (Patra & Nath, 1999). The visible superficial heterogeneities such as the standing water zones were avoided because they are highly affecting resistivity measurements (Van Zijl, 1985; Weight & Sonderegger, 2001). Industrial current that could result from power sources and metals such as railway were avoided. Leakage of current into the ground from such sources leads to sudden rapid changes in measurements and are unpredictable (Van Zijl, 1985; MacDonald *et al*., 2002).

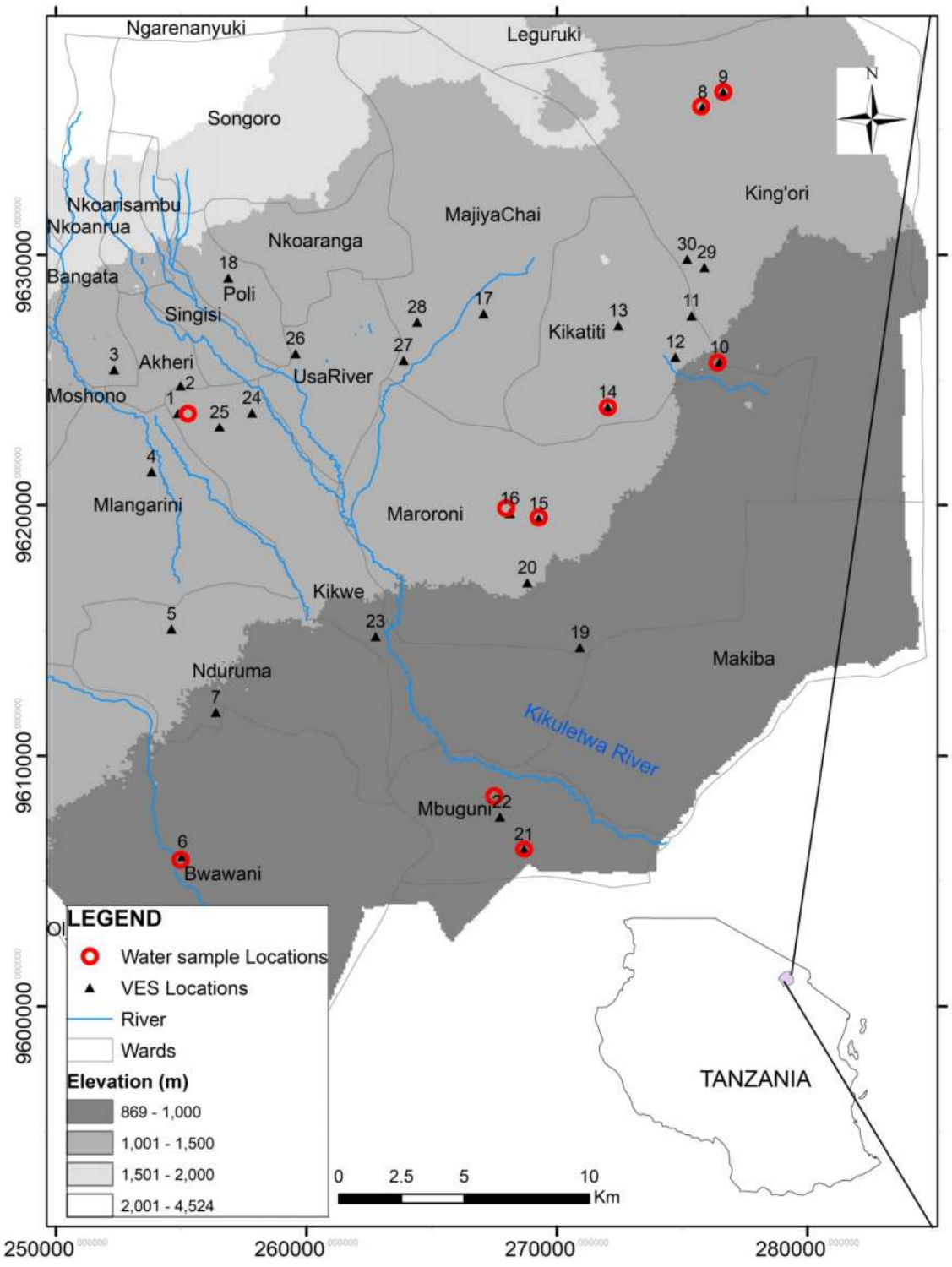

Figure 50: Vertical Electrical Sounding (VES) and water sample locations in the south eastern part of Mt. Meru

Resistivity Measurement: Schlumberger array (Fig. 51) is an array which is commonly used in resistivity survey because it saves time and minimizes the effects of lateral inhomogeneity (Mbonu *et al*., 1991; Yadav *et al*., 1997; Choudhury, 2001; Ekinci & Demirci, 2008). With this array, the electrical current I, was introduced to the outer A and B electrodes and the potential difference ΔV was measured between the inner M and N electrodes. The potential electrode distances were kept small while increasing progressively the current electrode separation until the potential difference became too low to be measured.

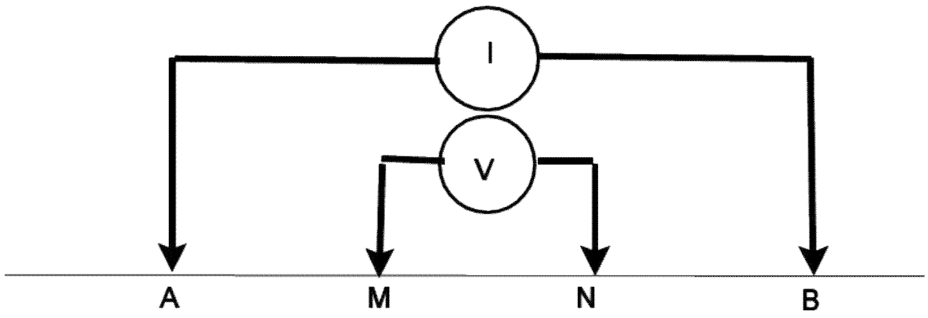

Figure 51: Schlumberger array. AB is the current dipole and MN is the potential dipole.

The terrameter SAS 4000 model displayed the resistance during measurements. The apparent resistivity was calculated using equation (5.1), by multiplying the resistance and the corresponding geometric factors:

$$\rho_a = \pi \left(\frac{\left(\frac{AB}{2}\right)^2 - \left(\frac{MN}{2}\right)^2}{MN} \right) \frac{\delta V}{I} \qquad (5.1)$$

where ρ_a : apparent resistivity (Ωm), $\delta V/I$: the resistance term (Ω), AB and MN are current electrode and potential electrode separations respectively.

For each VES station, the apparent resistivity values were plotted directly in the field on a double-logarithm graph sheet. For quality purposes and smooth transition from one potential electrode spacing to the other, there were two overlap points. Furthermore, measurements were repeated several times for apparent resistivity values that showed great divergence from the general trend of the sounding curves. However, in some few cases, especially in very dry areas at the surface, the obtained sounding curves were not so smooth despite of efforts in enhancing the signal-noise ratio (pouring water at the contact points and hammering the electrodes).

5.2.3 Modelling of Vertical Elecrical Sounding (VES) data

Modelling and inversion of resistivity data was done using a computer based program DCINV, Version 1.4 (c) of 2005 with linearization inversion based on the singular value decomposition and adaptive damping method. This method (not software) has been applied elsewhere in interpretation of Schlumberger resistivity data and various software are available (Ekinci & Demirci, 2008). The program requires good geological and hydrogeological knowledge for specification of input parameters before modelling and interpretation of model results. Therefore, initial input parameters (resistivity and thickness) for modelling purposes were obtained manually based on the raw data and field sounding curves.

The final outputs in the generated models are displayed together with the damping factors which control the convergence speed towards attaining the solution and the Root Mean Square (RMS) error which measure the quality of interpretation. The Root Mean Square error was calculated using equation (5.2) (Ekinci & Demirci, 2008):

$$RMS = \frac{\left[\sum_{i=1}^{N}(D_m - D_c)^2\right]^{1/2}}{N^{1/2}} \tag{5.2}$$

where N is a total number of data points, D_m is the measured field data and D_c is the calculated value.

After interpretation of model results, Transverse resistance (T) and longitudinal conductance (S) of the aquifers which are important in assessing groundwater potentiality were calculated using equations (5.3) and (5.4) (Patra & Nath, 1999).

$$T = \sum_{i=1}^{n} \rho_i h_i \tag{5.3}$$

$$S = \sum_{i=1}^{n} \frac{h_i}{\rho_i} \tag{5.4}$$

Finally, all VES results were used in construction of resistivity contour maps and depths to aquifer maps. In conjunction with geological and hydrogeological data, they were used to

construct cross sections for stratigraphic investigation of geoelectric units as well as construction of final groundwater potential map within the study area.

5.2.4 Water sample collection and analyses

Eleven water samples (4 boreholes and 7 dug wells) were collected in the dry season in February 2017 in some specific areas where some of the VES stations (MRVES-01, 06, 09, 10, 14, 15, 16, 17, 21 and 22) were located (Fig. 50) so as to aid on interpretation of geophysical data. The limited number of water samples was due to the lack of close groundwater sample sources in the vicinity of most of the VES stations. Unlike rain season, dry season was found to be appropriate season for obtaining samples with minimal rainfall dilution effect. Water sample collection was done carefully following standard procedures. Electrical conductivity (EC) and Total Dissolved Solids (TDS) were measured direct in the field using the Hanna - HI 9829 Multi-parameter under appropriate calibration. Fluoride analysis was done in 2 days after sample collection at the Nelson Mandela African Institution of Science and Technology (NM-AIST), Tanzania. The method used was Fluoride Ion Selective Electrode (FISE), utilizing standard Total Ionic Strength Adjustment Buffer (TISAB II) with CDTA. All quality control and assurance techniques including duplicates and the use of nearby laboratory were taken into consideration.

5.3 Results

5.3.1 Distribution of the sounding curves

Standard method of classifying sounding curves that involves grouping based on contrast in apparent resistivity into 4 fundamental types of the 3-layer cases (A, Q, K and H) was used (Patra & Nath, 1999). With this classification, A-type represents the sounding curves where the resistivity increases with depth while Q type represents sounding curves where the resistivity decreases with depth. H-type denotes the sounding curves where the intermediate layer exhibit low resistivity relative to the overlying and underlying layers, while K-type denotes the sounding curves with the intermediate layer exhibiting high resistivity relative to the underlying and overlying layers (Patra & Nath, 1999).

In this study, 3 to 5-layer cases were generally obtained (Appendix 7) and therefore, a combination of the above 4 fundamental types was used to classify the sounding curves. The curves obtained were classified into 8 types (A, H, HK, K, KH, HKH, Q and QH) as shown in Fig. 52 and Table 9. The HK-type indicates a 4-layer case where the upper three layers are

represented by the H-type and the bottom layer exhibit low resistivity relative to the third layer. The KH-type denotes the K-type for upper three layers with the bottom layer exhibiting high resistivity relative to the third layer whereas the HKH-type indicates a 5-layer case where the upper four layers are represented by the HK-types with the bottom layer exhibiting high resistivity relative to the fourth layer. The QH-type indicates a 4-layer case where the upper three layers are represented by the Q-type with the bottom layer exhibiting high resistivity relative to the third layer. Out of these 8 types, the HK, H, KH, QH, Q and K-types were the dominant comprising 93.3% of the total sounding curves (Fig. 52; Appendix 7). One sounding curve showed a 2-layer case (Appendix. 7). The distribution of types of sounding curves was generally found to be random within the surveyed area.

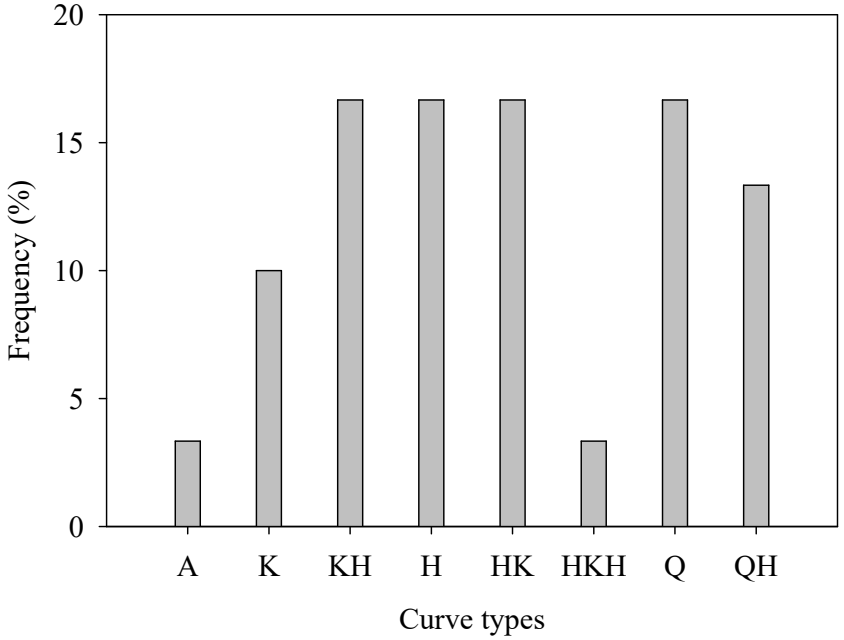

Figure 52: Frequency distribution of Vertical Electrical Sounding curves obtained in the southern parts of Mt. Meru.

5.3.2 VES Results and Interpretation

The VES raw data are presented in Appendix 6 and the corresponding models which show the number of geoelectric layers, resistivity and thicknesses are presented in Appendix 7. Figure 53 is used as an example for the models presented in Appendix 7. Overall, the obtained results showed an average RMS (root mean square) error of 2.7% for all 30 VES stations. This indicates that the generated models were in good standard with the acceptable quality for interpretation purposes.

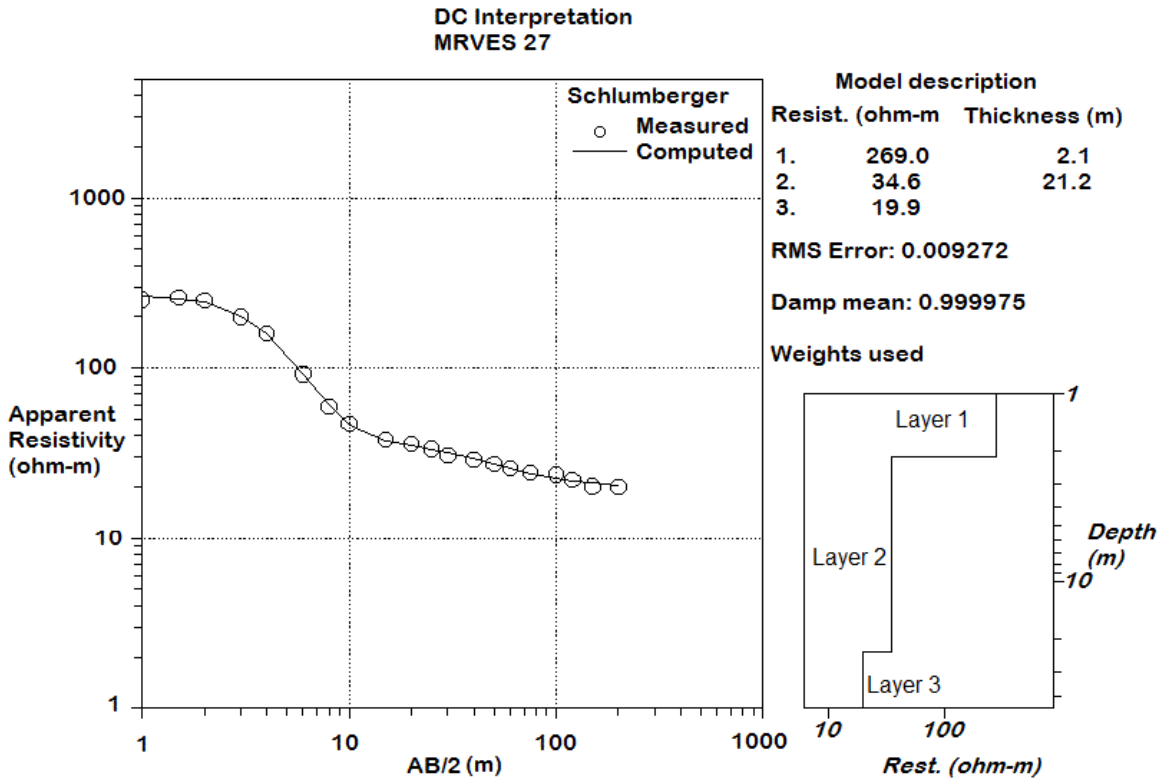

Figure 53: Model results for one sounding curve of the Q-type obtained at VES station MRVES27, USA River, southern part of Mt. Meru.

Vertical Electrical Sounding (VES) results obtained from computer modelling together with the estimated total transverse resistance (T) and the total longitudinal conductance (S) of the aquifers which play an important role in delineation of potential groundwater zones (Patra & Nath, 1999) are summarized in Table 9. Results of the water samples collected in proximal to VES stations (Table 10) and geology (surface observation, existing geological map and lithological logs for the proximal boreholes) were used in interpretation of VES data.

Table 9: Summary of the interpreted geoelectric units with aquifer parameters from the sounding curves obtained in the southern parts of Mt. Meru

MRV ES. No.	No.of Geoel. units	Curve type	Resistivity (Ωm)					Thickness (m)					Aquifer T. Rest.(Ωm^2)		Aquifer L. Cond. (Ω^{-1})	
			ρ_1	ρ_2	ρ_3	ρ_4	ρ_5	h_1	h_2	h_3	h_4	h_5	T1	T2	S1	S2
1	4	KH	58.1	271.1	5.8	49.8		0.8	2.7	2.2	134*		6673		2.69	
2	4	HK	49.4	29.5	116.3	43.3		0.5	14	7.9	117*		413	5066	0.47	2.70
3	4	QH	84	25	8.8	36.2		0.6	21.8	10.8	106*		545	3837	0.87	2.93
4	4	KH	158.6	675.3	26.4	108		0.5	8.5	37			977		1.40	
5	3	A	14.3	140.9	422			0.7	42.3							
6	4	KH	24.4	94.9	11.1	118		0.4	22	16.3			181		1.47	
7	4	HK	460.6	46.4	589	48.4		0.3	8.8	4.8	126*		6098		2.60	
8	4	QH	325.4	154	15.5	55.1		1.6	4.2	24.8	109*		384	6006	1.60	1.98
9	3	Q	505.2	56.5	21.3			0.9	9.1	130*			2769		6.10	
10	5	HKH	37.1	4.7	52.2	19.9	46.4	0.7	0.5	1.3	30.9	106*	615	4918	1.55	2.28
11	3	Q	535.1	52.4	36.7			0.8	20	119*			4367		3.24	
12	3	H	64.6	31.6	89.2			0.3	49				1548		1.55	
13	4	QH	93.5	29.9	8.1	46.8		1.2	6.9	12.6	120*		102	5616	1.56	2.56
14	3	Q	526.3	77.9	20.8			0.8	8.5	130*			2704		6.25	
15	3	K	59.3	172.5	18.4			0.6	2.8	136*			2502		7.39	
16	4	HK	34.4	12.2	104	15.2		0.5	10	6.7	123*		122	1870	0.82	8.09
17	3	H	765.7	43	42354			1.5	68.6				2950		1.60	

Table 9 Continued

MRV ES. No.	No.of Geoel. units	Curve type	Resistivity (Ωm)					Thickness (m)					Aquifer T. Rest.(Ωm^2)		Aquifer L. Cond. (Ω^{-1})	
			ρ_1	ρ_2	ρ_3	ρ_4	ρ_5	h_1	h_2	h_3	h_4	h_5	T1	T2	S1	S2
18	3	H	150.5	38	151.5			1	9							
19	4	HK	61.1	16.7	59.4	24.8		1.6	5.5	10.5	122*		624	3026	0.18	4.92
20	3	H	71.2	18.4	5608			4.4	99.3				1827		5.40	
21	3	K	49.6	398	14.5			5.5	3.7	131*			1900		9.03	
22	2		121.3	16				27.2	113*				1808		7.06	
23	3	K	7.9	2883	12.5			0.3	3	136.5*			1706		10.92	
24	4	KH	13.1	50	5.9	39.3		1.6	13.4	14.2	110*		753	4323	1.01	2.80
25	4	KH	10.1	205.4	38.8	288		0.7	0.8	140.6			5455		3.62	
26	4	HK	46.3	11.6	59.9	23.1		0.4	5.7	18.5	115*		1108	2657	0.31	4.98
27	3	Q	269	34.6	19.9			2.1	21.2	117*			734	2328	0.61	5.88
28	3	Q	305.4	52.3	21.4			3.1	22.7	114*			1187	2440	0.43	5.33
29	4	QH	111.6	10.4	6.6	36.9		0.6	7.4	25.2	106*		3911		2.87	
30	3	H	27.3	10.4	89.9			3	29							

**Thickness of the bottom layer which is approximated using the criterion that the depth of investigation is at least 140m under the current electrode spacing of 400m*

5.3.3 Relationship between Aquifer resistivity and water sample results

Water sample results (EC, TDS and F^-) together with the corresponding interpreted aquifer resistivity are presented in Table 10. The interpreted depth to aquifer and aquifer thickness (Table 9) were used to deduce the aquifer resistivity (Table 10) which is linked to the results of water samples collected from the well/borehole within the same aquifer. Results indicated that EC and F^- values vary significantly from 705 to 4940 µS/cm and 2.16 to 48 mg/l respectively (Table 10) indicating intensive variation of groundwater quality within the study area. With exception of two VES stations which were located in clay formation (MRVES No.21 and 22), integration of both aquifer resistivity values and water sample results (TDS, EC and F^-), revealed that aquifer resistivity values between 15 and 22 Ω m correspond to both high fluoride values above 20 mg/l and high TDS above 1800 mg/l (Table 10) while the aquifer resistivity between 35 and 60 Ωm corresponds to both low fluoride (<4 mg/l) and low TDS (<1000 mg/l) (Table 10).

Table 10: Relationship between aquifer resistivity, aquifer formation and water sample parameters from the proximal water sources. Note that VES No. 1, 6, 8…22 abbreviate VES stations MRVES01, 06, 08…22.

VES Results		Interpreted Aquifer formation	Vicinity Water Sample Results						
VES. No.	ρ(Ωm)		Sample No.	EC (µs/cm)	TDS (mg/l)	F (mg/l)	Well type	Depth (m)	Local Area
1	49.8	Weathered and fractured volcanics	WS88	1109	554	2.98	Borehole	130	Nelson Mandela
6	58.9	Alluvial and weathered volcanics	WS75	1640	820	2.16	Borehole	35	Bwawani
8	55.5	Lahars	WS52	1710	855	6.60	Dug well	10	King'oli
9	21.3	Lahars	WS51	3600	1800	35.00	Dug well	16	King'oli
10	46.4	Volcanic breccia and tuffs	WS54	1157	579	2.32	Borehole	150	King'oli
14	20.8	Lahars	WS61	4940	2470	48.00	Borehole	40	Kikatiti
15	18.4	Lahars	WS63	4626	2313	26.93	Dug well	15	Maroroni
16	15.2	Lahars	WS64	5412	2705	41.97	Dug well	5	Maroroni
21	14.5	Clay and weathered volcanics	WS82	768	384	3.72	Dug well	15	Mbuguni
22	16	Clay and weathered volcanics	WS83	705	352	3.36	Borehole	70	Mbugni

5.3.4 Stratigraphical results based on geoelectric layers

Vertical Electrical Sounding (VES) results presented in Table 9 were used to construct stratigraphy of the geo-electric layers. The number of geo-electric layers ranged from 2 to 5 but most of the sounding curves exhibited 3 to 4 layers (Table 9; Appendix 7). The upper layer (Layer 1) exhibited a wide range of resistivity values that varied from 8 to 800 Ωm (Fig. 54a). Resistivity values in this upper layer can be classified into three groups (Fig. 54a). Group 1, which accounts for 13% of all VES station, was characterized by resistivity values of 8-20 Ωm (mean =11.3 Ωm), while group 2 which accounts for 47% of all VES stations, had resistivity values between 20-100 Ωm (mean = 54 Ωm; Fig. 54a). The third group, which was recorded in areas with dry sediments at the surface, was characterized by resistivity values ranging from 100 to 800 Ωm (mean=353 Ωm) and accounted for 40% of all VES station (Fig. 54a). Layer 1 was thin with an averaged thickness of 1.3 m, exception for MRVES 22 that had a thickness of 27.2 m (Table 9; Appendix 7). It showed a dominance of very thin layer (0.3-1 m, mean = 0.6 m) in 66% of the VES station. The remaining percentage was equally grouped into the low thickness (1-2 m) and medium thickness (2-5.5 m) (Fig. 54b). The thickness of group 1 category of resistivity ranged from 0.3 to 1.6 m and averaged 0.8 m whereas the thickness of group 2 category of resistivity, which is the dominant group ranged from 0.3 to 5.5 m and averaged 1.5 m. The third category had the thickness ranging from 0.3 to 3.1 m and averaged 1.2 m.

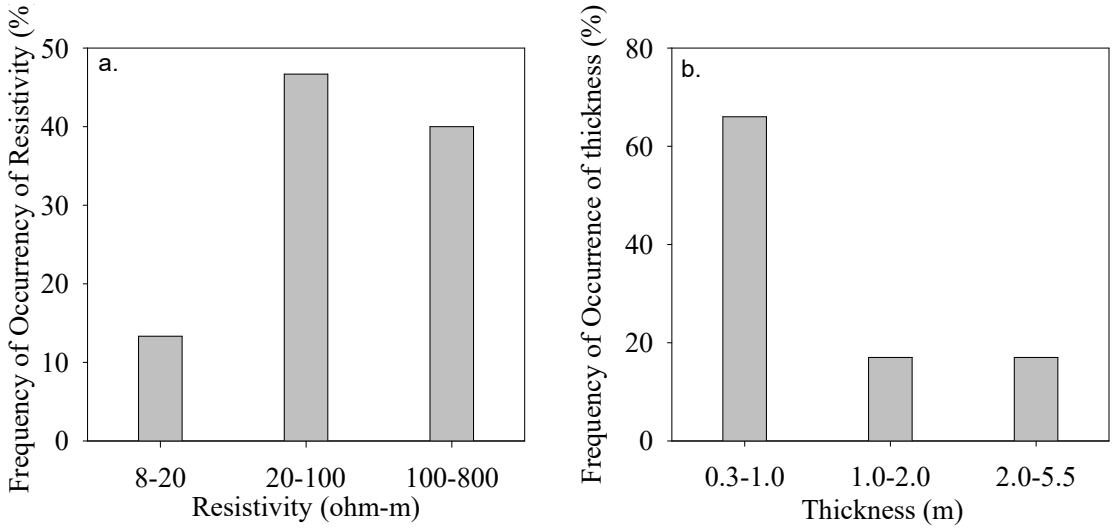

Figure 54: Frequency distribution of resistivity and thickness in the uppermost layer (a.) Resistivity and (b.) Thickness

Layer 2, which had varying thickness with the average thickness of about 18 m was thicker relative to the uppermost layer. Maroroni-Mbuguni area (MRVES 20 and 22) (Fig. 50) had the thickest layer of about 100 m. Classification of thickness of the Layer 2 showed that 50% of all VES stations exhibited the thickness between 1 and 10 m (mean = 6.4 m) whereas 33% exhibited the thickness between 10 and 50 m (mean = 25.5 m). Only 10% and 7% of VES stations fell in the group of low thickness (0.5-1, mean = 0.65 m) and high thickness (50-120, mean = 84 m) respectively (Fig. 55b). Layer 2 was characterized by a wide range of resistivity values ranging from 5 (MRVES-10) to 3000 Ωm (MRVES-23). These resistivity values were classified into low (4-20 Ωm averaging 12.5 Ωm), medium (20-100 Ωm averaging 47 Ωm), high (100-1000 Ωm averaging 288 Ωm) and very high (1000-3000 Ωm represented by one VES station with the resistivity value of 2883 Ωm) (Fig. 55a). The thickness of the low resistivity category, which comprised 27% of the VES stations, ranged from 0.5 to 120 m with a mean value of 33.8 m. The medium category, which is the dominant group comprising 47% of the VES station had a thickness that ranged from 6.9 to 68.6 m and averaged 21 m. The high category of resistivity values, which comprised 23% of VES stations had a thickness that ranged from 0.8 to 42.3 m and averaged 9.3 m. Very high resistivity category, comprising only 3% of the VES stations (1 VES station) had a thickness of 3 m.

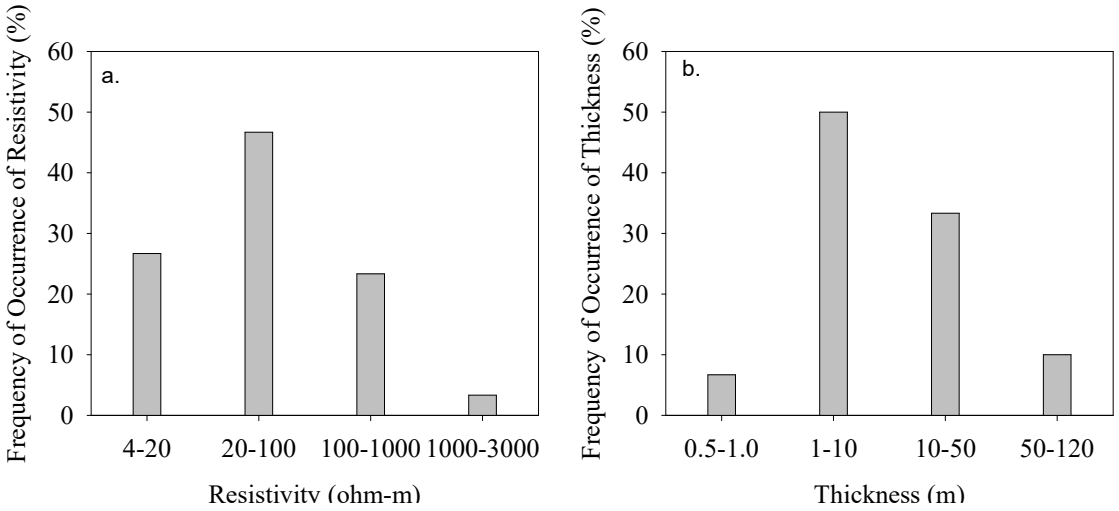

Figure 55: Frequency distribution of resistivity and thickness for the second layer (a.) Resistivity and (b.) Thickness

Layer 3 had varying thickness that can be subdivided into three major categories namely: low (1-10 m, mean = 4.6 m), medium (10-40, mean = 19 m) and high (100-150 m, mean = 128 m) (Fig. 56b and Appendix 7). It should be noted that the thickness in the last category is an estimate because of being the bottom layer for most of the sounding curves. Such estimate is based on the thickness obtained from the models of the four-layer cases (eg. MRVES-25, 140.6 m; Table 9) and the relationship between the current electrode separation and depth of investigation; that depth of investigation is about half of the current electrode spacing (Maiti *et al.,* 2011).

Layer 3 was characterized by the resistivity values that ranged from 5 to 50,000 Ωm (Table 9, Fig. 56a). These values were grouped into five resistivity categories (Table 9: Fig. 56a). Out of 29 VES stations, 17% fell in the category of low resistivity values (5-10 Ωm, mean = 7 Ωm. The dominant category (35%) was represented by the resistivity values ranging from 10 to 30 and averaged 18 Ωm. The third resistivity category, which comprised 17% of the VES stations was represented by the resistivity values between 35-60 Ωm (Fig. 56a) with the mean value of 49 Ωm. The fourth resistivity category, which accounts for 21% of VES stations was represented by the resistivity values between 60-500 Ωm (mean = 162 Ωm) whereas the last category comprising only 10% of VES stations was represented by high resistivity values ranging from 500 to 50 000 Ωm and averaged 16183 Ωm. The thickness of the low resistivity category was relatively thin, ranging from 2.2 to 25.2 m and averaged 13 m whereas the thickness of the second category of resistivity, which is largely based on estimation as discussed previously, ranged from 16 to 137 m and averaged 98 m (Fig. 56b). The third category of resistivity which corresponds to fresh groundwater (Table 10) had the thickness ranging from 1.3 to 140.6 m and averaged 58 m. However, in areas where it was thin (< 20 m; MRVES-10, 19 and 26) (Table 9), there was a thick underlying layer. The thickness for the fourth and fifth high resistivity categories could not be estimated because of being largely related to massive volcanic formation.

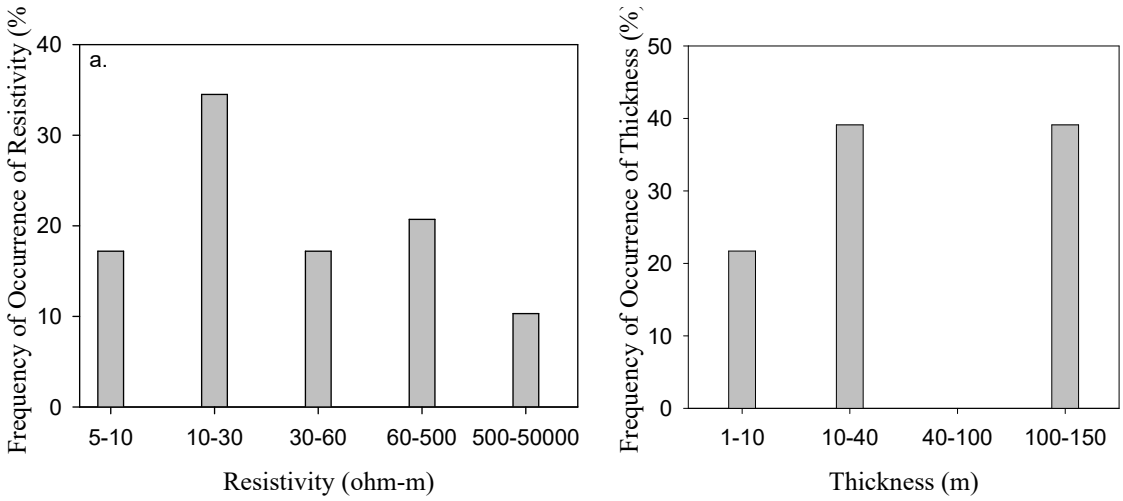

Figure 56: Frequency distribution of resistivity and thickness for the third layer (a.) Resistivity and (b.) Thickness

Half of the total sounding curves which are 15 curves showed four-layer cases (Table 9). Layer 4 was characterized by the resistivity values ranging from 15 to 300 Ωm and averaged 63.5 Ωm. These values were grouped into 3 categories (Fig. 57). The first category of resistivity was represented by the resistivity values ranging from 15-25 Ωm (mean = 21 Ωm) and comprised 27% of 15 VES stations. The second category, which is the dominant group accounting for 53% of the sounding curves was represented by the resistivity values ranging from 35 to 60 Ωm (mean = 44.5 Ωm). The third category which accounts for 20% of the sounding curves was represented by resistivity values ranging from 100 to300 Ωm (mean = 171 Ωm) (Fig. 57). Resistivity results for the fourth layer showed clear gaps in the resistivity range at 25-35 Ωm and 60-100 Ωm (Fig. 57). In this case, the thickness of the forth layer was not categorized because it was generally restricted in narrow range between 100-140 m and was obtained through estimates using geophysical consideration as explained previously.

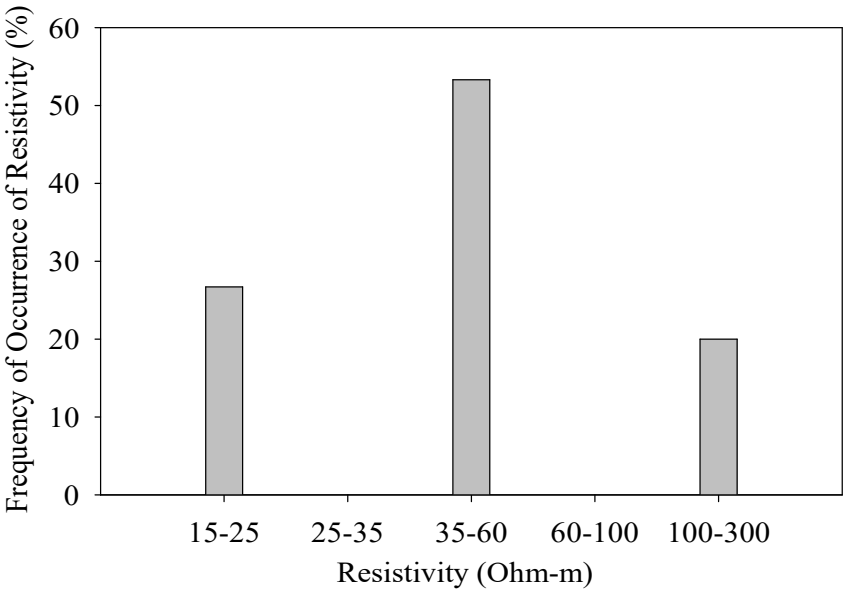

Figure 57: Frequency distribution of resistivity for the fourth layer

Overall, results showed that there was a pronounced resistivity contrast between the third and fourth layers in some of the stations (Table 9). With consideration of the sounding curves where the thickness of the 3rd layer was generally above 10 m, seven VES stations presented in Fig. 58 showed pronounced resistivity contrast. A five - layer case was obtained at one VES station only (MRVES-10). In this case, the fifth layer at a depth of about 34 m is represented by the resistivity value of 46.4 Ω m (Table 9).

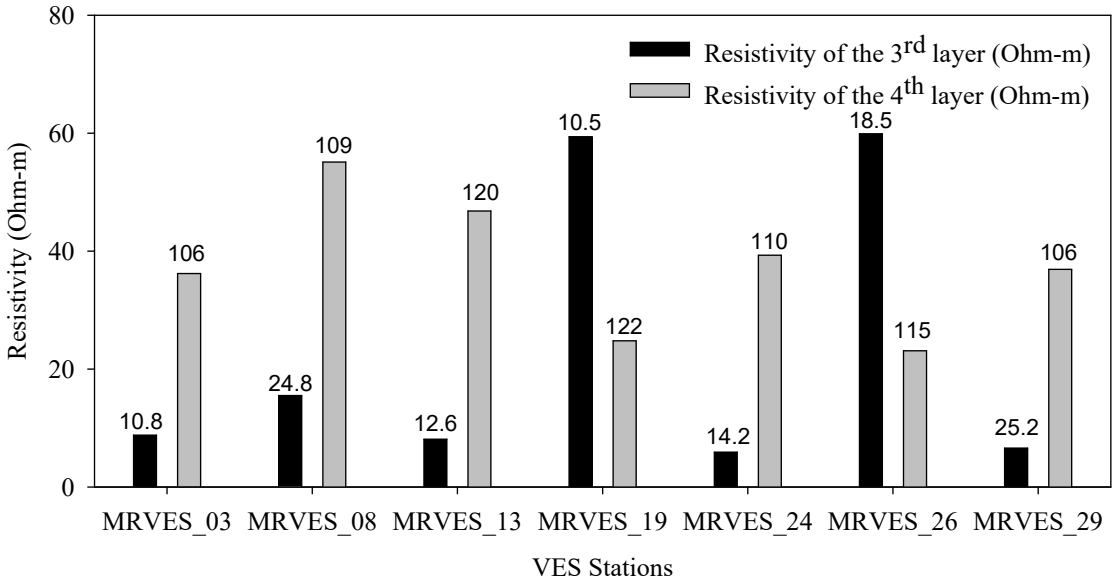

Figure 58: VES stations which showed contrast in aquifer resistivity for the 3rd and 4th layers implying stratigraphical change in either water quality or aquiferous formation. The labelled values are the aquifer thicknesses in meters.

5.3.5 Transverse resistance and longitudinal conductance of the aquifers

Based on Tables 9 and 10, the interpreted thickness and resistivity values particularly in layers 3 to 5 which are extensive forming major aquifers were used to estimate Transverse resistance (T) and longitudinal conductance (S) of the main aquifers. It was possible to estimate T and S in more than 80% of the sounding curves based on the aquifer resistivity range (10-60 Ωm) and estimated thickness (Table 9). Transverse resistance values of the main aquifer that averaged 3398 Ωm^2 were generally found to be extremely low (100-200 Ωm^2) in areas where thickness was relatively low (~15 m) and high (5000-7000 Ωm^2) in areas where the aquifer was relatively thick (100-140 m) (Table 9). The T values were grouped into low (100-1000 Ωm^2), intermediate (1000-3000 Ωm^2) and high (3000-7000 Ωm^2) categories (Fig. 59a). Distribution of T values indicated that only 8% of the sounding curves fell in the low T category and the remaining percentage was nearly equally distributed in the intermediate and high categories (Fig. 59a).

Longitudinal conductance (S) of the main aquifer ranged from 1.4 to 11 Ω^{-1} and averaged 4.6 Ω^{-1} (Table 9). Classification of these values into low (1-2 Ω^{-1}), intermediate (2-4 Ω^{-1}) and high (4-11 Ω^{-1}) categories indicated that the low S category is represented by 12% of the

sounding curves (Fig. 59b.). The dominant groups were the intermediate and high categories represented by 40 and 48% of the curves respectively (Fig. 59b).

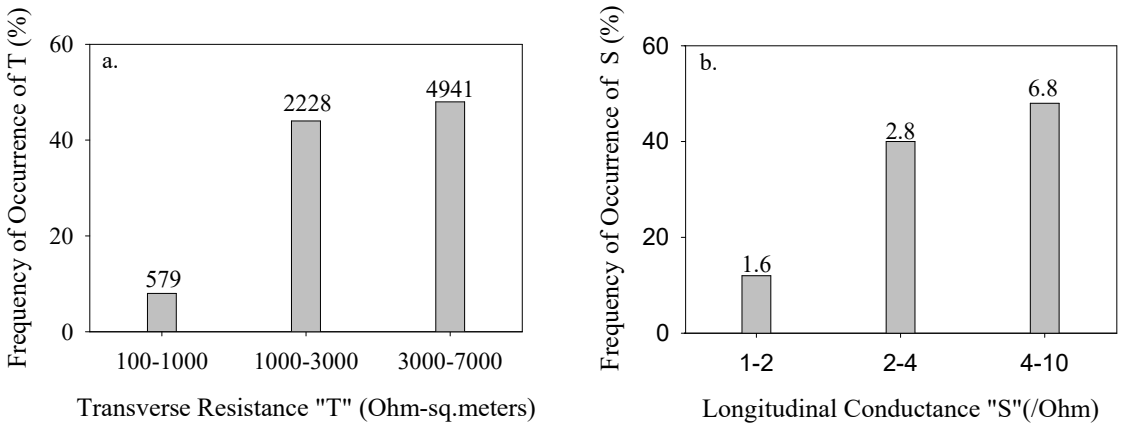

Figure 59: Frequency distribution of Transverse Resistance (T) and Longitudinal conductance (S) of the main aquifer in the surveyed Arumeru area. Labels on top of the bars are the mean values.

5.4 Discussion

Firstly, interpreted resistivity and water results were used to establish the relationship between the geophysical parameter (aquifer resistivity) and groundwater parameters (fluoride level and electrical conductivity). Thereafter, data were integrated with geology (borehole lithological logs and geological map) to construct cross-sections and aquifer maps. These maps are Transverse Resistance (T) and Longitudinal Conductance (S), depth to upper and lower aquifers and resistivity at 70 m depth. The obtained constructive information was finally used in delineation and characterization of aquifer and construction of Groundwater Potential Index Map (GWPIM) in the study area.

5.4.1 Relationship between Aquifer resistivity, lithology and groundwater parameters (F^- and EC)

When the aquifer resistivity values were integrated together with the water parameters (Fluoride and electrical conductivities), clear inverse relationships between aquifer resistivity with EC and F^- with the correlation coefficient of - 0.93 to -0.92 respectively at 95% confidence level were obtained (Figs. 60 and 61). However, such relationship is not valid in areas dominated by clay rich formation (Table 10). Therefore, it is likely to be valid at local scale particularly in volcanic provinces which are similar to Mt. Meru area where fluoride is affecting much of the water sources.

Several researchers have related resistivity of freshwater bearing formation with sea water intrusion in coastal areas (Wilson *et al.,* 2006; Kouzana *et al.,* 2010; Gupta *et al.,* 2014; Kumar *et al.,* 2015; Eissa *et al.,* 2016). Their studies mapped clearly the seawater intrusion zones being marked by low resistivity (generally < 5 Ωm) relative to that of freshwater bearing formation (generally 10-100 Ωm). However, few if any have reported relationship between fluoride concentrations and resistivity values.

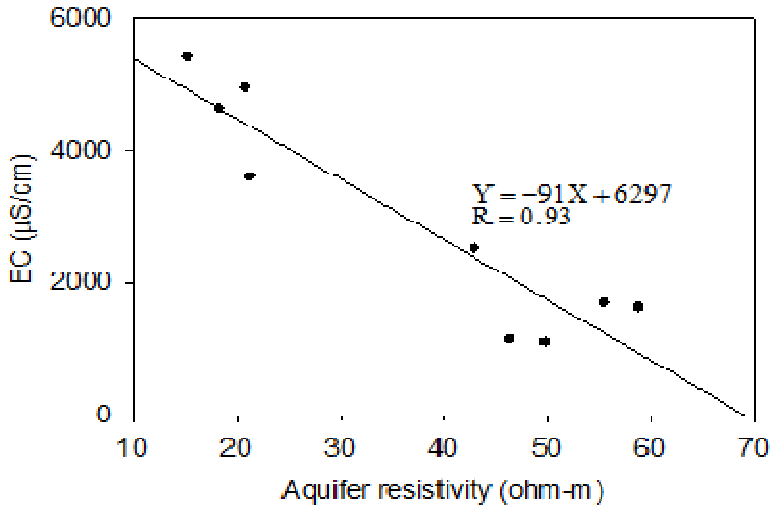

Figure 60: Relationship between aquifer resistivity and EC of the vicinity water samples

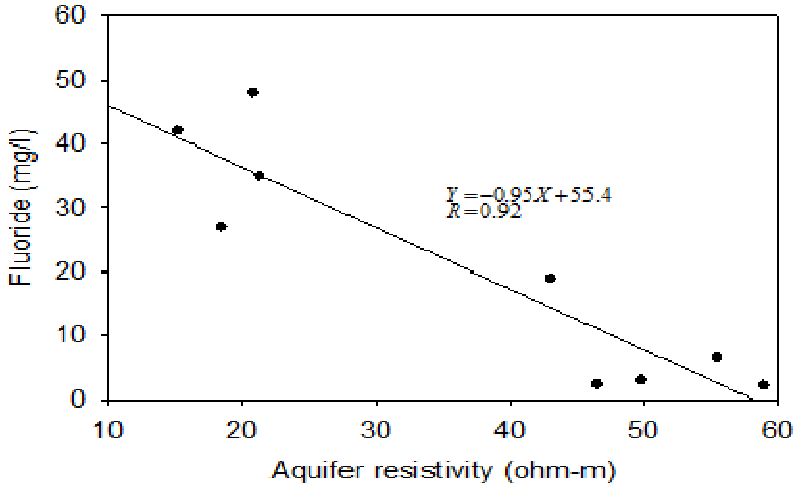

Figure 61: Relationship between aquifer resistivity and fluoride in the vicinity water

Since TDS is proportional to the conductivity of Aquifer formation and hence inverse to the resistivity of the aquifer (Patra & Nath, 1999), the obtained low resistivity values (15-22 Ωm)

which correspond to low groundwater quality (TDS >1800, F^- > 20 mg/l) (Table 10; Fig. 60 and 61) implies that more ions including F^- are dissolved from the Aquifer bearing formation. This is well supported by the geology in the sense that such low resistivity values are associated with low water quality aquifers hosted in lahar materials (Fig. 62) which are soluble relative to other rocks in the study area. This is also in agreement with other studies in Arumeru (Nanyaro *et al.,* 1984; Ghiglieri *et al.,* 2010, 2012) which revealed that lahar materials are the major source of high fluoride in Arumeru waters. Therefore, vice-versa is true for the high resistivity values (40-60 Ωm) which correspond to fresh groundwater aquifers (TDS <1000 mg/l, F<4 mg/l). Such aquifers are largely hosted in fractured and weathered volcanics (Fig. 64).

In this study, the relationship between aquifer resistivity and groundwater quality has been established using a pair of representative samples from the stations with both VES and water sample results. Therefore, through VES measurements, the developed equations can be used as a tool for estimation of fluoride level as well as water quality in terms of Electrical Conductivity (EC) and total dissolved solids (TDS) in aquifers in other areas lacking borehole/wells within the study area. However, because the data points are not uniformly distributed in the study area and some of the intermediate resistivity values (22-40 Ωm) are missing (Table 10; Figs. 60 – 62), there is a need of detailed research work to establish a clear relationship. Also, it is important to check the validity of this relationship in other related volcanic provinces.

5.4.2 Hydro-geoelectric cross sections

Four cross sections, A-A', B-B', C-C' and D-D' (Fig. 62) were used to study litho-resistivity variation with depth. A wide range of resistivity variation particularly in the upper two layers was attributed to variation in both moisture content and sediments types. This is common in areas characterized by rugged topography and different sediment types (Wilson *et al.,* 2006; Kouzana *et al.,* 2010; Abdullahi *et al.,* 2015; Eissa *et al.,* 2016; Mohamaden & Ehab, 2017). The observed variation in resistivity for the underling layers in some specific zones was largely attributed to changes in water chemistry and geology as evidenced by borehole logs and groundwater samples (Table 10). Such findings are discussed in detail using four cross sections.

For section A-A' (Fig. 63), the upper resistivity between 8-280 Ωm represented moist to dry loam soils and clays as observed at the surface. This compare well with the surface geology

which indicates variation from mantling ash (MRVES 03) through alluvium (MRVES02) to laharitic soils (MRVES01, 24 and 25) (Fig. 62). The underlying layer was wet relative to the upper layer (shallow groundwater) characterized by the resistivity between 5-30 Ωm. The low resistivity as low as 5-6 Ωm particularly at MRVES 01 and 24 (Fig. 63) indicated the dominance of clay sediments. Such low resistivity values in clay sediments are in agreements with other studies such as Mohamaden & Ehab (2017) where clay lenses in the alluvial fan of Wadi Rahada, Egypt were found to be characterized by the resistivity values between 1.3-9.1 Ωm.

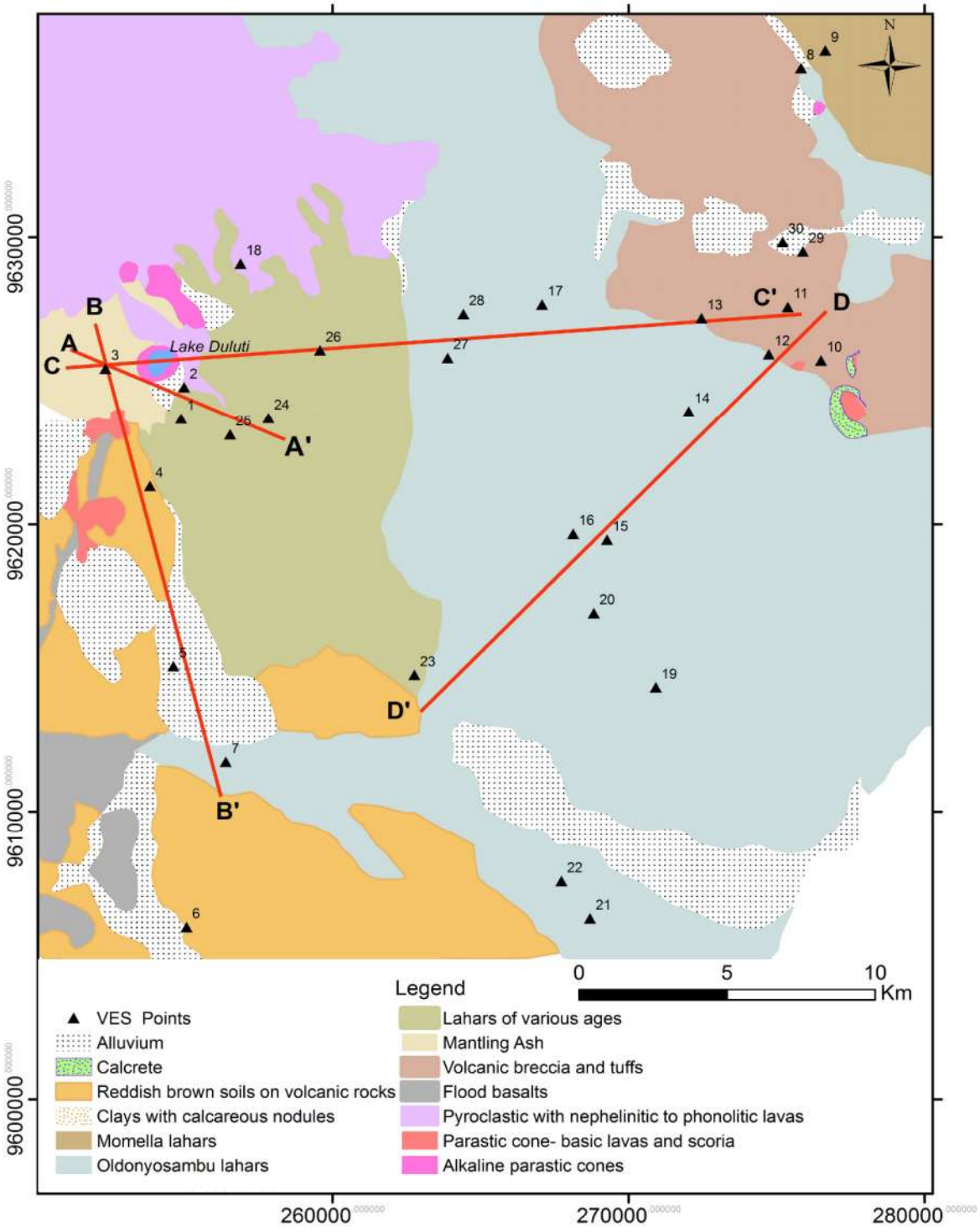

Figure 62: A simplified geological map (after Wilkinson, 1983) showing VES points and four traverses that were used in construction of hydro-geoelectric cross sections

The bottom layer in section A-A' was nearly uniform characterized by the resistivity between 36-50 Ωm representing aquifer in the weathered and fractured volcanic formation as evidenced by two boreholes near MRVES01 (Fig. 64). Such values are in close agreement with the resistivity value of 31 Ωm obtained in the northern part of Mt. Meru representing freshwater with fluoride level of 3.1 mg/l (Ghiglieri *et al.,* 2010). Weak variation in resistivity values for freshwater aquifers is well known being attributed to geology, degree of saturation, water chemistry, porosity etc. For instance, Hewaidy *et al*. (2015) reported 23-100 Ωm as freshwater aquifer resistivity in the Gulf of Suez with groundwater hosted in limestone and sandstone. Wilson *et al.* (2016) reported 80-120 Ωm as the resistivity of sands saturated with freshwater in the coast of Egypt and Mohamaden & Ehab (2017) reported the resistivity values between 38 and 100 Ωm as the resistivity of freshwater hosted in alluvial fun sediments.

Through lithological logs, it is clearly indicated that the aquifer formation is extensive and both boreholes ended on aquifer formation (Fig. 64). This aquifer is likely to be recharged through fractures and faults as noted in some potential groundwater areas in northern part of Mt. Meru (Ghiglieri *et al.,* 2010) and as indicated in the borehole lithological log (Fig. 64). Such observations concur well with resistivity data where the thickness of the underling layer which is an aquifer was found to be thick to the extent of not being determined under the applied current electrode spacing. The borehole yields were good; 33 m^3/h (Borehole No.01, drilled in 2010) and 11 m^3/h (Borehole No. 2, drilled in 2017). Periodic water sampling on borehole No.01 from 2010 to 2017 showed that water quality is good with TDS restricted between 381 and 554 mg/l and fluoride between 2.7 and 2.98 mg/l.

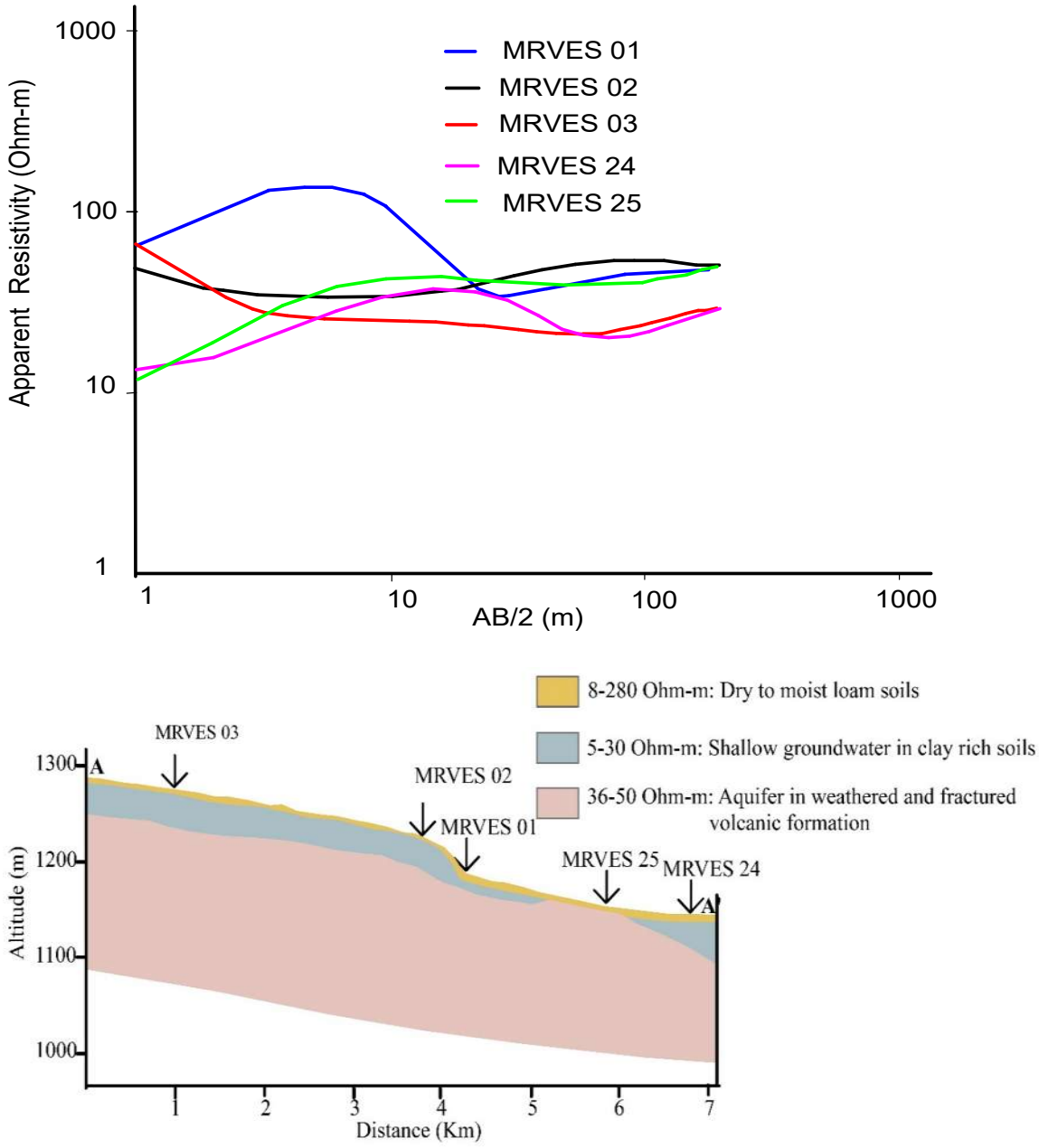

Figure 63: Hydro-geological cross section A-A' with the corresponding sounding curves

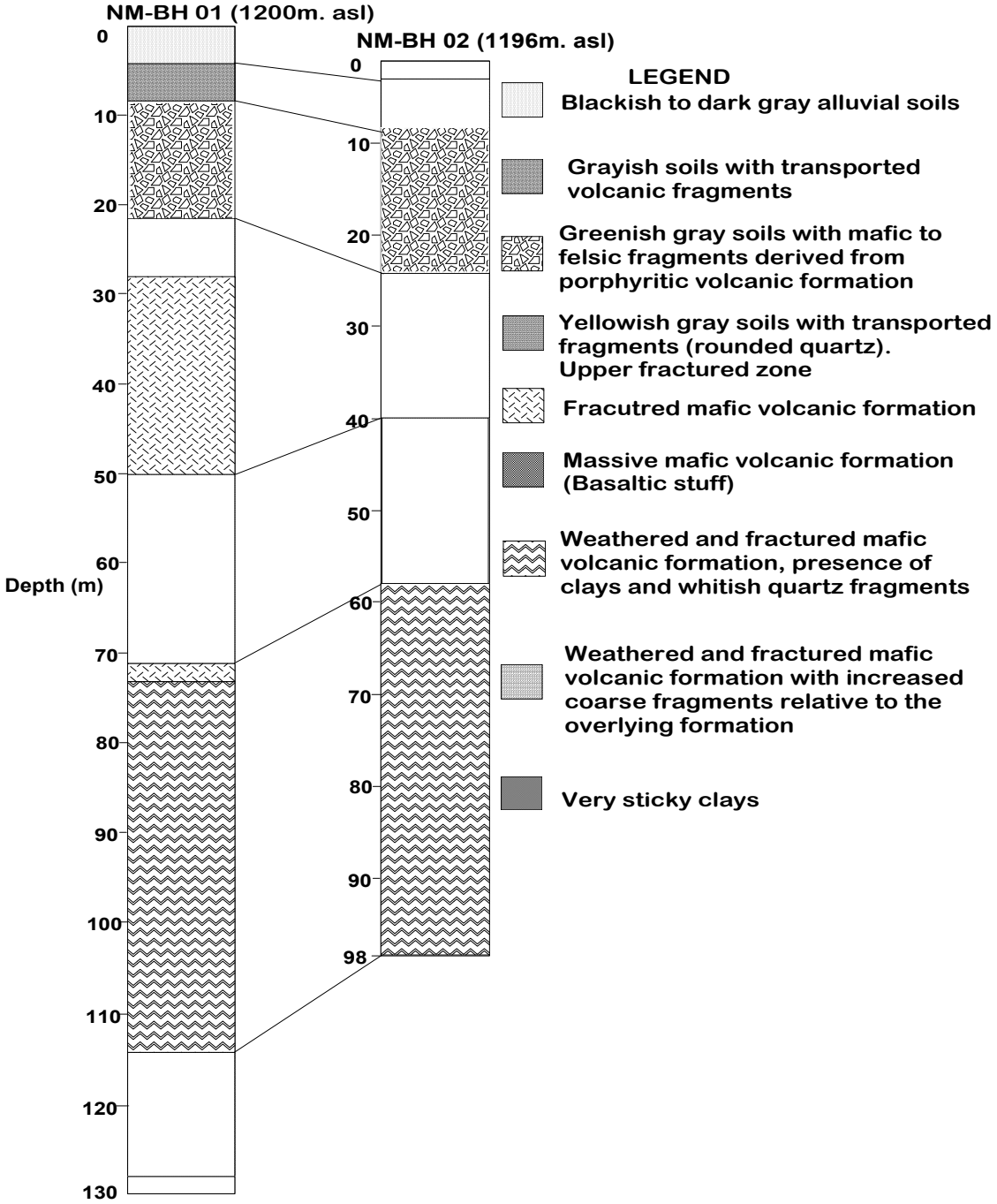

Figure 64: Lithological logs for two boreholes (~ 100 m, apart) proximal to MRVES 01 which are owned by Nelson Mandela AIST. Lithological logs on Borehole No. 1 is based on the existing borehole completion report while borehole No.02 was logged directly by the author during drilling.

Cross section B-B'

Unlike section A-A', section B-B' showed variation in geological formation as indicated in surface geology (Fig. 62). This is also reflected in sounding curves where distinctive curves were obtained (Fig. 65).

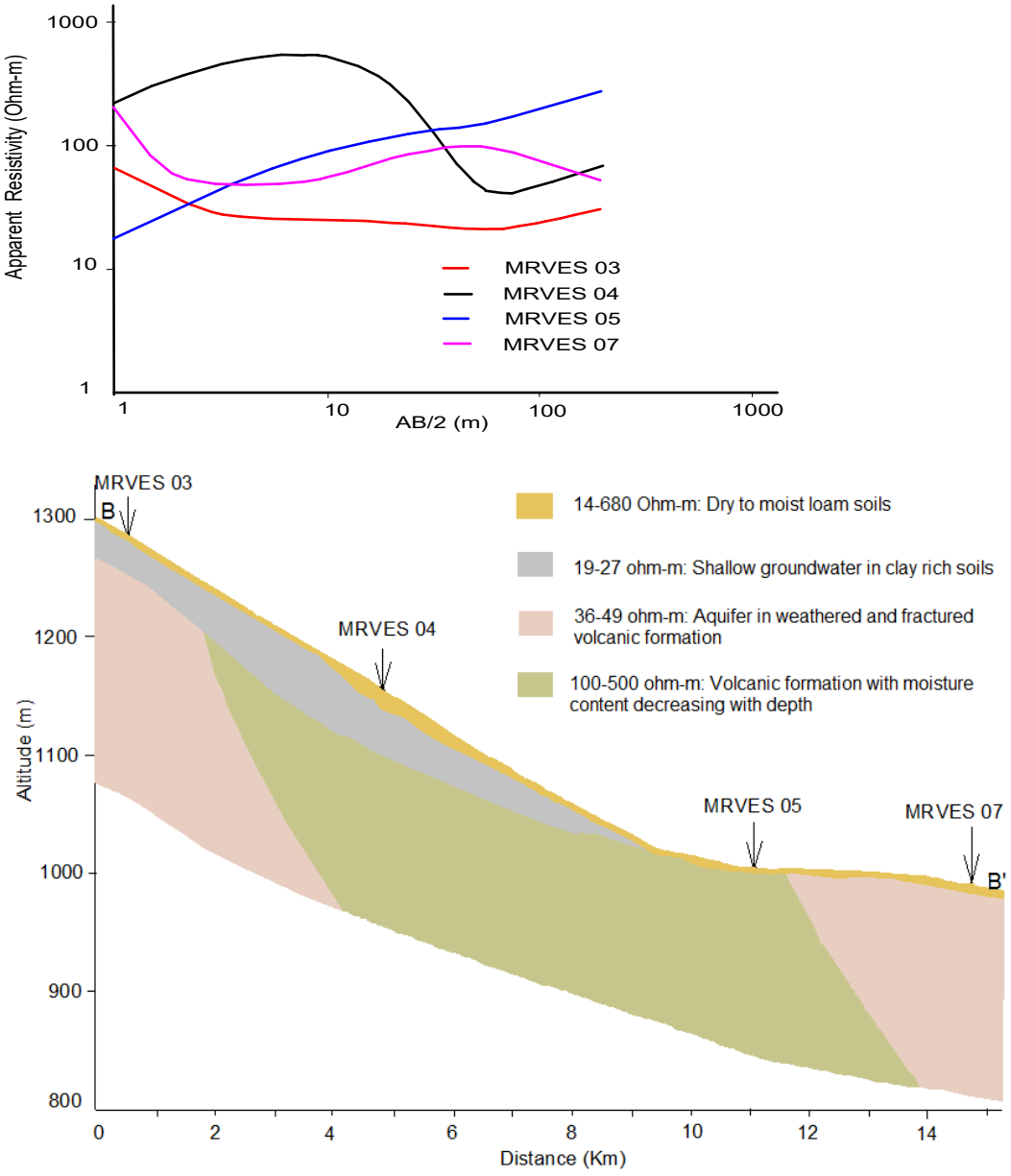

Figure 65: Cross section B-B' with the corresponding sounding curves

Shallow groundwater in clay rich formation pinching downward is underlying the top soil in the upland areas (MRVES 03 and MRVES 04). Despite of having the related uppermost layer (clays, alluvial and loam soils), the middle part of the section lacks groundwater potentiality

because of the volcanic formation close to the surface (Fig. 65). This was clearly interpreted at MRVES 05 with a A-type sounding curve showing a resistive dry formation (Fig. 65). The resistivity values between 36 and 49 Ωm for the bottom layers of the two end members (MRVES 03 and MRVES 07) (Fig. 65) is likely to represent aquifer hosted in weathered and fractured volcanic formation.

Cross section D-D'

For section D-D' (Fig. 66), a borehole centered at MRVES 10 is used as a reference to interpret the northern part of the section. Despite the fact that the data related to yields and lithological logs are missing, the yield was very good as LODHIA gypsum industry and surrounding communities depend solely on this well for domestic and cattle feeding. The water sample collected from the borehole (150 m, depth) indicated that water sample is fresh (TDS = 579 mg/l and fluoride= 2.32 mg/l) (Table 10). Unlike other areas along this profile, the upper soils at this station is reddish gray in colour, being derived from volcanic tuff and breccia (Fig. 62). Integrating water results with resistivity data, two aquifers are interpreted around this zone. The upper aquifer is a freshwater aquifer hosted in clay/silt rich formation (19-55 Ωm) and the lower aquifer (36-47 Ωm) is also a freshwater aquifer probably hosted in tuffs and breccia materials (Fig. 62 and 66). As the upper part of the borehole was sealed (~20 m) due to either high clay content or low water quality (Unpublished, local information), the lower aquifer with the resistivity value of 46.4 Ωm corresponds to freshwater (EC = 1157 µS/cm, F= 2.32 mg/l) (Table 10). The presence of fresh water aquifer (low fluoride) in breccia materials is also supported by Ghiglieri *et al*. (2010) in their study in the northern part of Mt. Meru.

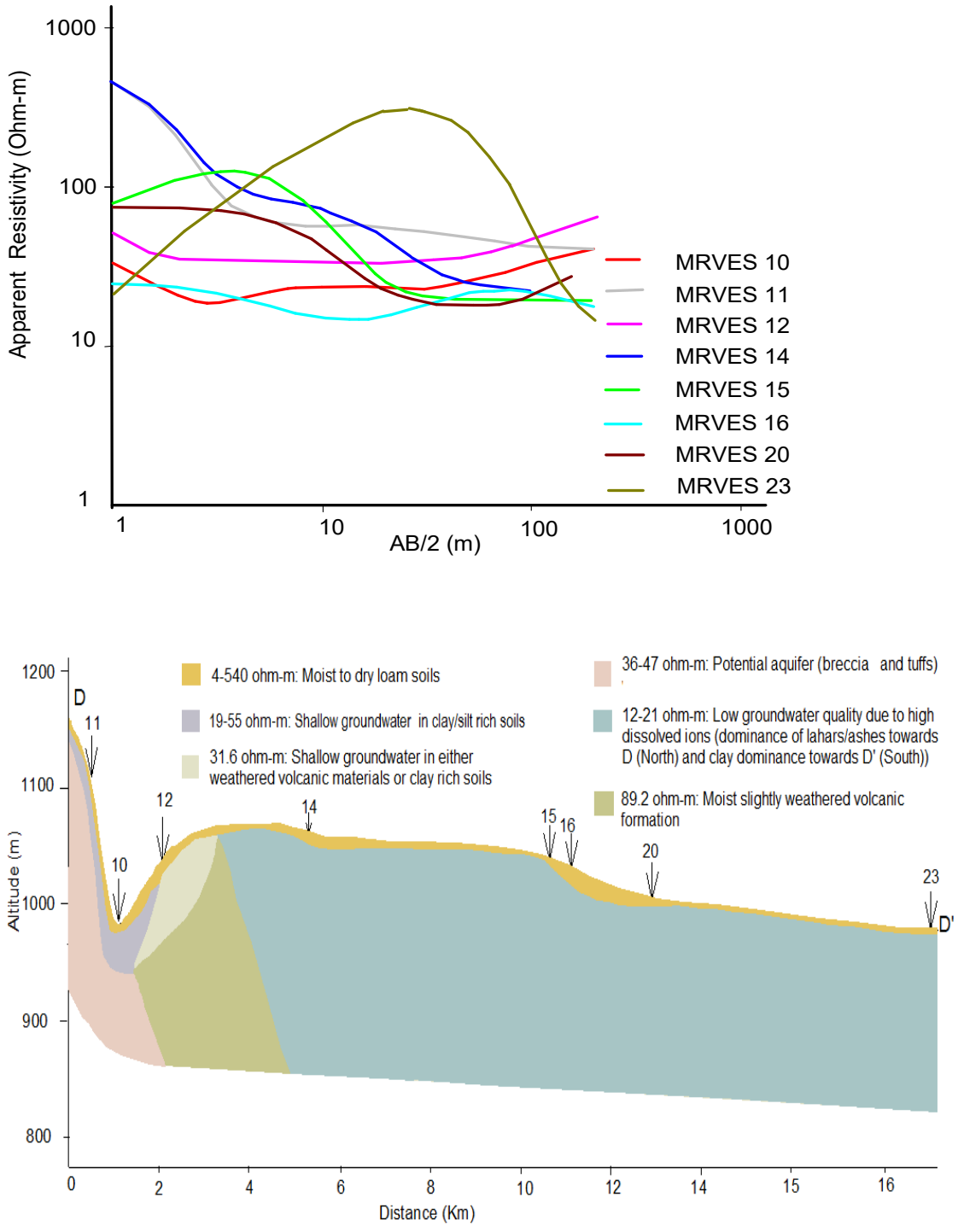

Figure 66: Cross section D-D' with the corresponding sounding curves

After MRVES 12, lahars cover the entire traverse to MRVES 23 as indicated in Figs. 62 and 66. Lithological logs of one borehole along this traverse proximal to MRVES 15 indicated that the lahar materials extend downward to more than 28 m (Fig. 67). Low water quality

aquifer was inferred from this borehole as the TDS was found to be 2313 mg/l associated with fluoride value of 26.93 mg/l (Table 10). The resistivity value of 18.4 Ωm at this point represented low water quality aquifer formation hosted in lahar materials. Similar findings were observed along the traverse and other areas covered by lahar materials. Therefore, it is interpreted with confidence that the resistivity values between 12 and 21 Ωm represent low water quality aquifer hosted in lahar materials.

The low resistivity value is the result of high dissolved ions from the readily soluble lahar materials. Such findings concur with the observation by Ghiglieri *et al*. (2010), in the northern part of Mt. Meru where water of low quality (F > 10 mg/l) was inferred from lahar materials. However, the low resistivity values generally < 15 Ωm as observed at MRVES 23 in the low land area (Fig. 66) could be attributed to high clay content derived from up-land formation. This is supported by surface observation (typical clays) as well as the water samples collected from the low land area proximal to MRVES 21 and 22 (Fig. 62) where water is fresh (TDS=332-384 mg/l, F=3.36-3.72 mg/l) while the resistivity is low between 14.5 and 16.0 Ωm. Low resistivity values for clay rich formation have been reported elsewhere (Braga *et al.,* 2006; Hewaidy *et al.,* 2015; Mohamaden & Ehab, 2017).

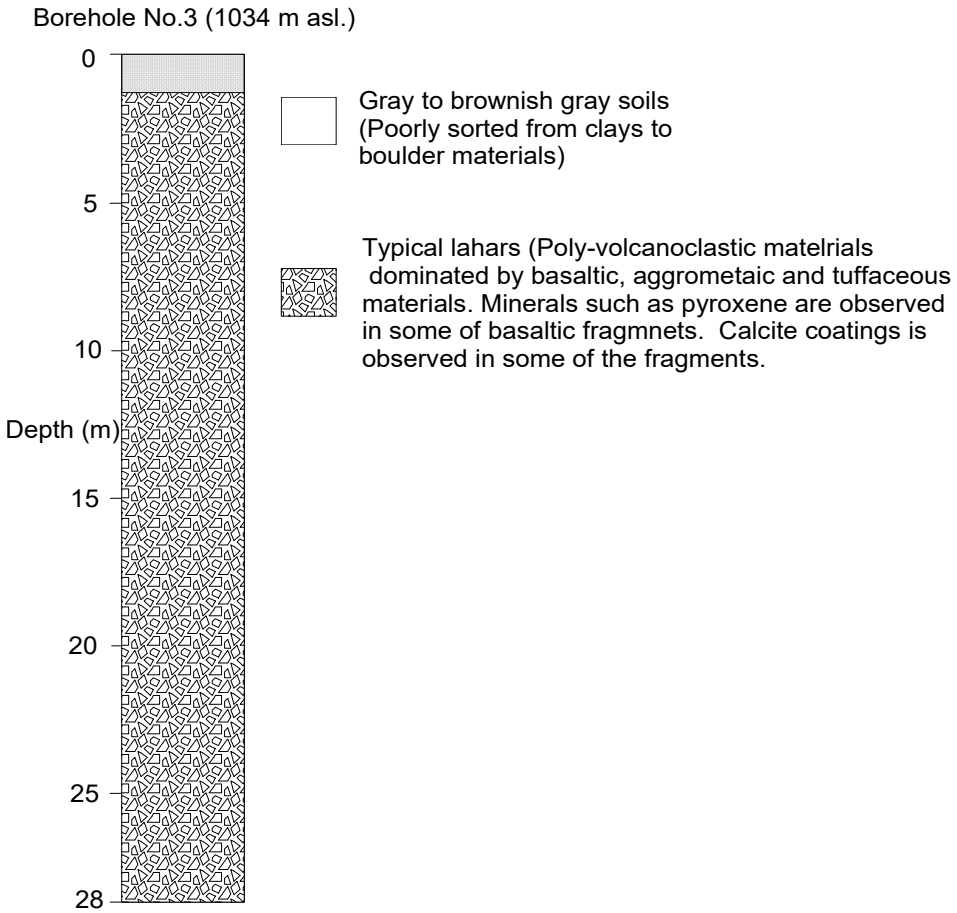

Figure 67: Lithological logs for the recently constructed dug well at Maroroni proximal to MRVES15. Logging is based on the cuttings which were not arranged systematically per interval for logging purposes

Cross section C-C'

Cross section C-C' (Fig. 68) is characterized by upper thin loam soils as other sections with varying moisture content. There was shallow freshwater in clay rich formation in western and eastern parts of the section. At the middle part, there is a massive volcanic formation as reflected at MRVES 17 acting as barrier to sediment movements. The interpreted high resistivity at this point (>1000 Ωm) is in agreement with the resistivity of the fresh bedrock elsewhere (Abdullahi *et al.,* 2015). As a result, there is fresh groundwater on top of lahar materials (MRVES 26-28) (Fig. 68) which is probably reflecting upper circulation of groundwater. Aquifers with low groundwater quality (19-23 Ωm) dominating the middle part were associated with lahar materials whereas resistivity values between 34 and 60 Ωm of the underlaying layers in the eastern and western parts represented potential aquifer hosted in weathered and fractured volcanic formation (Fig. 68). The confidence of interpretation is

based on the results of groundwater sample (Table 10), geology (Fig. 62) and cross sections A to D. Thus, the cases such as presence of shallow fresh groundwater in clay rich formation and freshwater in weathered/ fractured formation at the same station (MRVES 03, 11, 13; Fig. 68), presence of fresh water and low water quality in terms of TDS and fluoride at the same station (MRVES-26 to 28; Fig. 68) explain the observed contrast in resistivity for the third and fourth layers in some of the stations. Also, the observed resistivity gaps in the fourth layer at 25- 35 Ωm and 60 -100 Ωm mark the boundaries between zones with low water quality/clay rich in terms of fluoride and TDS (10-25 Ωm), fresh groundwater in weathered and fractured volcanic formation (35-60 Ωm and dry formation (>100 Ωm).

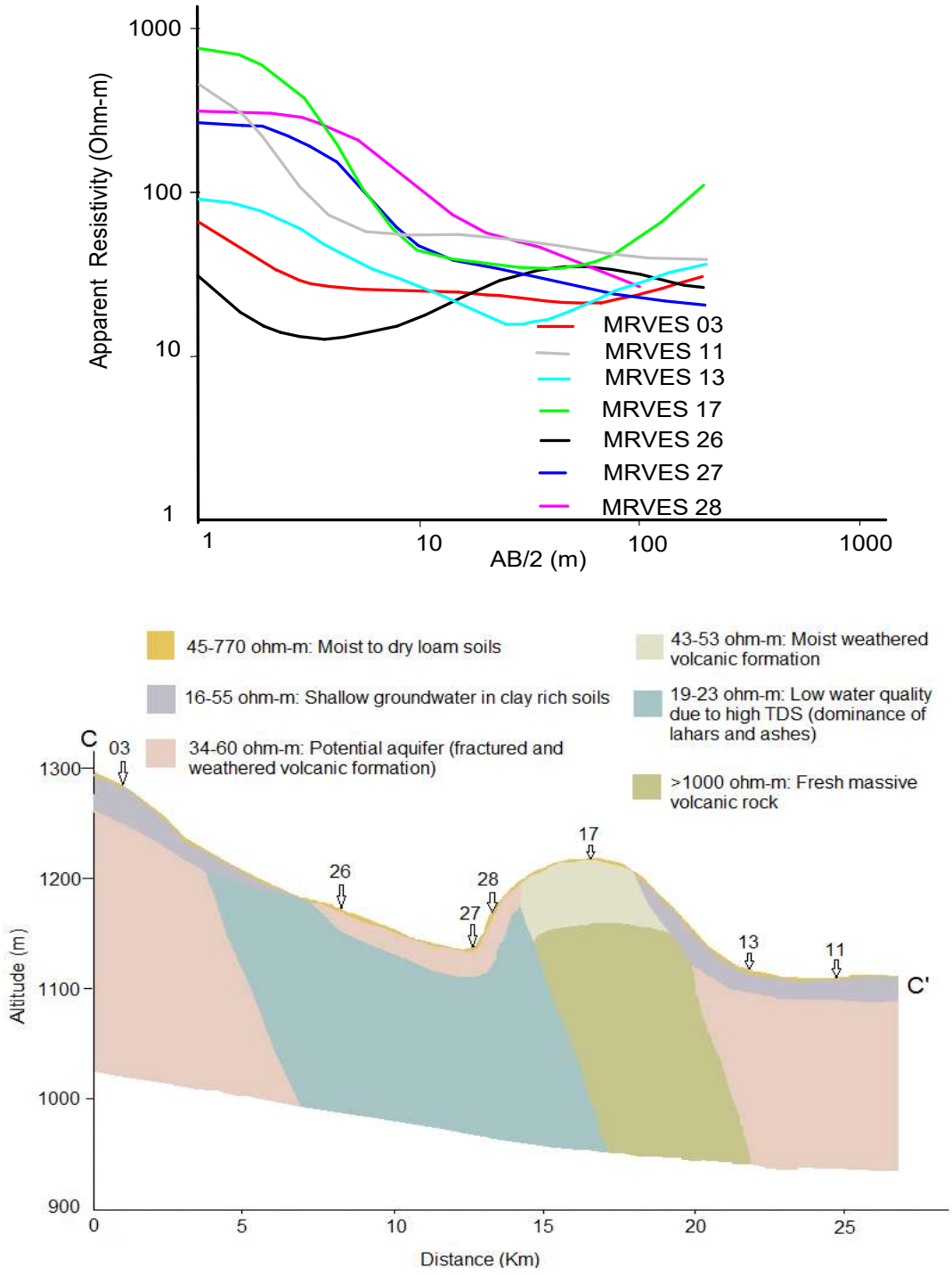

Figure 68: Cross section C-C' with the corresponding sounding curves

Overall, integration of data from geo-electric sections, lithological logs and borehole/well waters revealed that wide variation in resistivity values in the upper two thin layers (L1 and L2) is largely attributed to both variation in sediments type and moisture content. Generally, resistivity increases with increasing grainsize and decreases with increasing moisture content

(Abdullahi *et al.,* 2015; Hawaidy *et al.,* 2015; Eissa *et al.,* 2016) if other factors such as porosity and water chemistry are constant. The third and fourth layers (L3 and L4) represent aquifers that are characterized by variable water chemistry. Groundwater chemistry is largely varying from zone to zone depending on the geology but in some specific areas contrast in resistivity values in these two layers (Fig. 58) could be attributed to the presence of shallow freshwater on top of low groundwater quality or variation in geology (groundwater bearing formation). The resistivity between 10 and 25 Ωm correspond to groundwater with low quality (TDS>1000 mg/l; F^- >10 mg/l) hosted largely in lahar materials in some specific parts such Maji ya Chai, Kikatiti and Maroroni (Fig. 62). Furthermore, resistivity values ranging from 10-25 Ωm that were observed in low land areas (Bwawani and Mbuguni) represents fresh groundwater hosted in clay rich formation. Fresh groundwater hosted in weathered and fractured volcanics, tuff and breccia materials was found to be characterized by the resistivity values between 35 and 60 Ωm. Therefore, the remaining resistivity gap 25-35 Ωm is likely to represent groundwater of intermediate quality in terms of fluoride and TDS. The resistivity values generally between 60 -500 Ωm and > 500 Ωm in the layers underlying top soils (upper two layers) were interpreted as the resistivity of weathered and fresh volcanic rock respectively. Such values are in close agreement with other researchers elsewhere (Abdullahi *et al.,* 2015; Mohamaden & Ehab, 2017). The information summarized in this paragraph is important for assessing groundwater potentiality in the surveyed area.

5.4.3 Assessing Groundwater Potential

To assess groundwater potential in the study area, integrated scientific findings on Transverse Resistance (T) and Longitudinal Conductance (S) of the aquifer, variation in aquifer properties (thickness, resistivity), depth to the aquifers and groundwater quality were used. Finally, the obtained information was used to develop the Groundwater Potential Index map which serves as a guide for siting boreholes within the study area.

(i) Transverse resistance and longitudinal conductance of the Aquifer

Transverse resistance (T) and longitudinal conductance (S) of the aquifers are widely used in delineation of potential groundwater (Mbonu *et al.,* 1991; Patra & Nath, 1999; Salem, 1999; Braga *et al.,* 2006; Okiongbo & Odubo, 2012; Gupta *et al.,* 2014; Okonkwo & Ugwu, 2015). Aquifer resistivity varies depending on many factors such as rock composition, porosity and permeability, water chemistry and the degree of saturation (Patra & Nath, 1999). Thus, there is no specific resistivity value that stands for potential aquifer. Also, with consideration that

aquifer thicknesses vary from place to place depending on the geology, there is no specific values of T and S that stands for potential aquifer.

In general, high T and S values which are highly influenced by thickness of the aquifer correspond to high potential groundwater zones (Salem, 1999; Braga *et al.,* 2006; Okiongbo & Odubo, 2012; Okonkwo & Ugwu, 2015). The study area is characterized by a wide range of aquifer resistivity (10-60 Ωm) and narrow range of thickness values (Table 9). Therefore, with the defined range of aquifer resistivity (eg. 35-60 Ωm for freshwater aquifer and 15-25 Ωm for low water quality aquifer in terms of TDS and F^-), groundwater potentiality will generally increase with increasing T which is in agreement with other studies as mentioned above while decreasing with increasing S. Therefore, because of low Aquifer resistivity values around Kikatiti – Maroroni zone which are attributed to high dissolved ions from lahar materials as discussed previously, the high S between 4 and 11 Ω^{-1} represent Aquifers with low groundwater quality (Figs. 59b and 69). Also, low to intermediate S values (1 - 4 Ω^{-1}) which dominate in areas such as King'ori and Nelson Mandela (Fig. 59b and 69) indicate high aquifer resistivity values which are attributed to low dissolved ions relative to the ions which are dissolved from lahar materials. Thus, such areas represent zones with fresh groundwater (Fig. 69). The correspondence of low S with high potential zone in the study area agrees with other studies in areas with contrasting aquifer resistivity. For instance, in western India, a study by Gupta (2014) revealed that high S values correspond to saline water zones and anthropogenic pollution while low S values correspond to fresh groundwater zones. Using the stated dissolved ions-resistivity relationship, it is further revealed that high T values between 3000 and 7000 Ωm^2 (Figs. 59a and 70) in the areas such as Nelsoni Mandela, King'ori and Bwawani correspond to high groundwater potential (Fig. 70) whereas T values generally between 1800-3000 Ωm^2 mainly in the central zone (Fig. 70) correspond to aquifer of low groundwater quality.

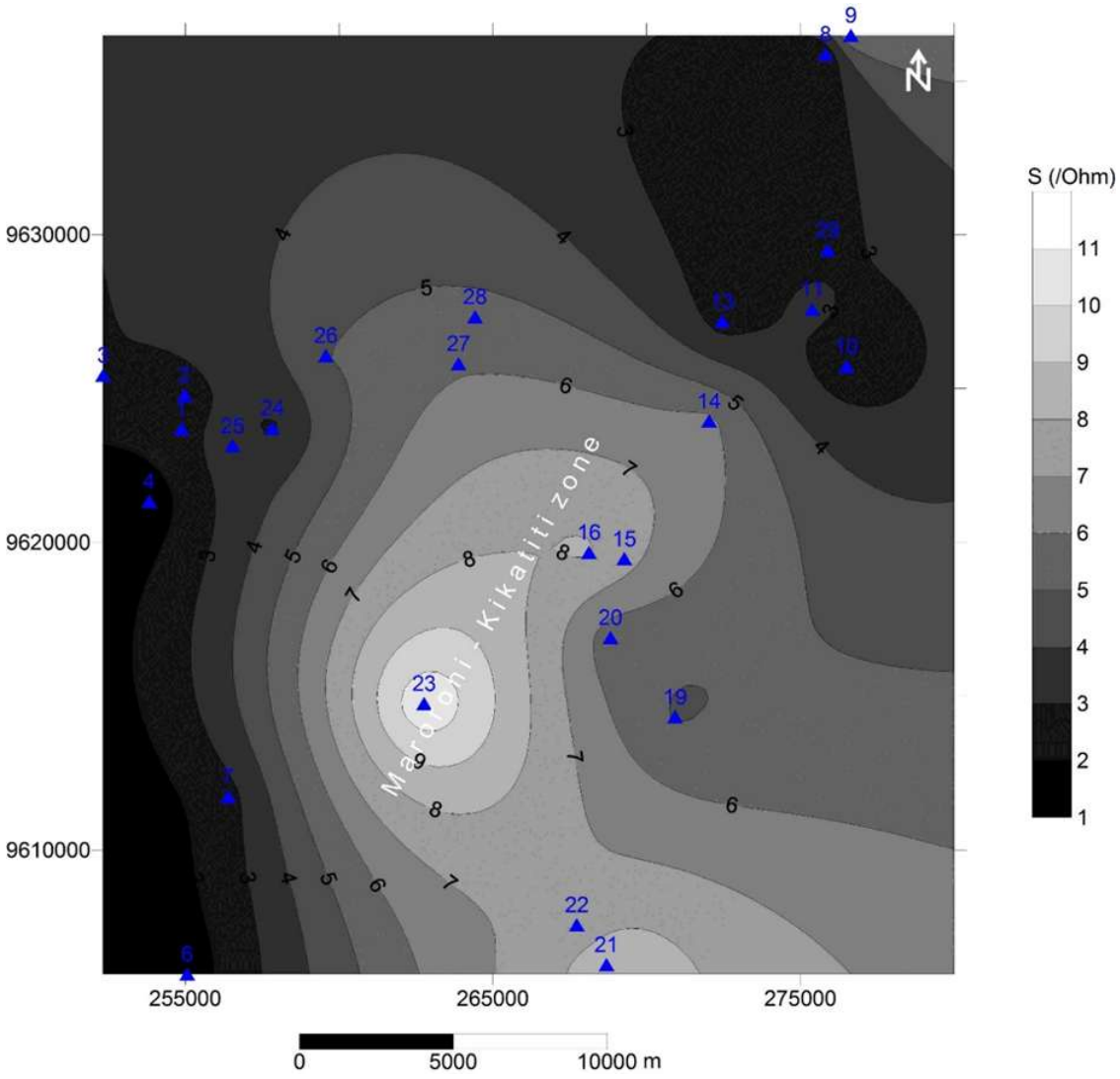

Figure 69: Longitudinal conductance (S) of the main aquifers in the surveyed area

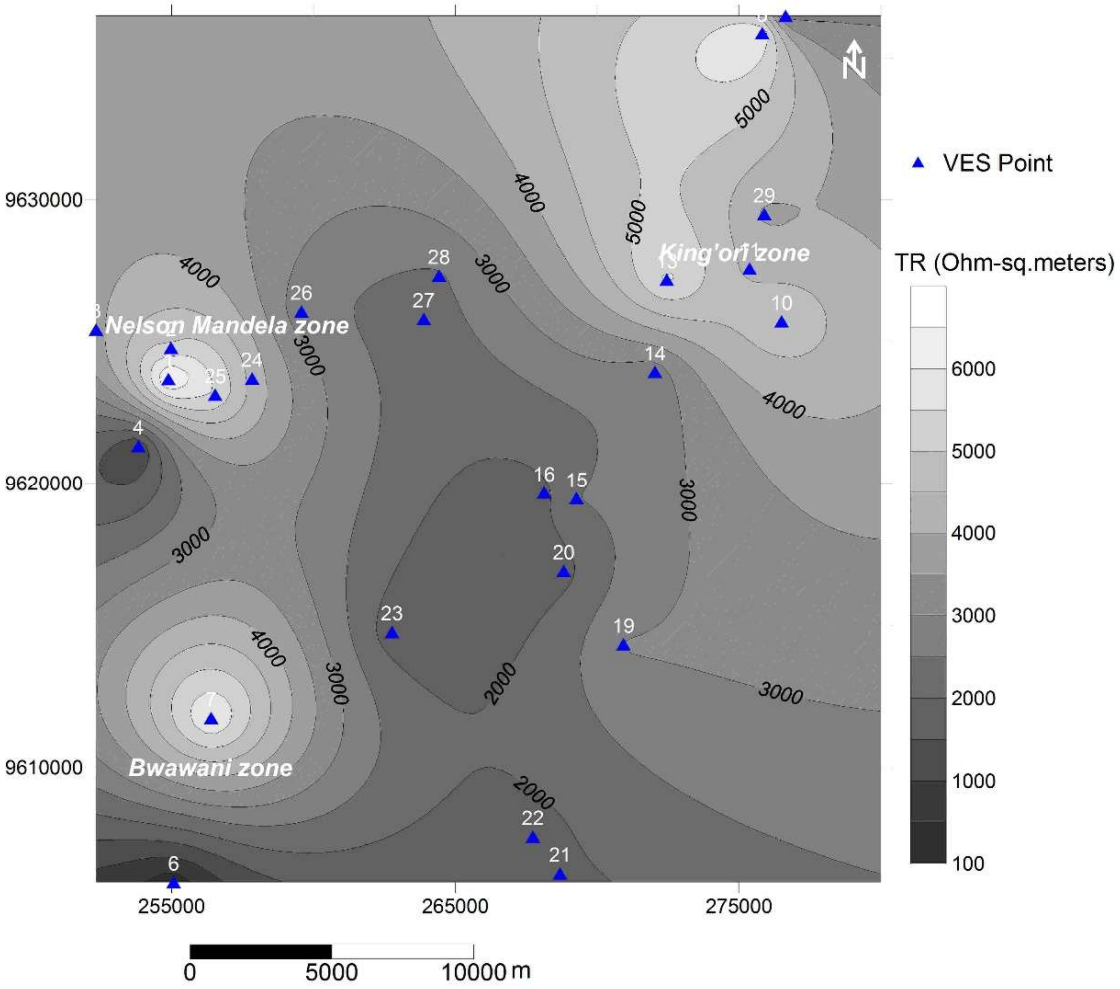

Figure 70: Transverse resistance (TR) of the main aquifers in the surveyed area

(ii) Variation in aquifer properties (depth to aquifers, thicknesses and water quality)

Stratigraphically, two main aquifer systems are defined in the study area as indicated in cross sections (Fig. 63, 65, 66 and 68). The thin upper aquifer (~25 m, average thickness) starting at a depth which is not exceeding 10 m, is restricted in some specific parts (Fig. 71). This aquifer is generally considered as the minor aquifer system because of two main reasons. First, it is associated with clays in most parts as discussed previously. Secondly, it reflects upper water circulation especially in areas where the aquifer is too shallow and thin and therefore, likely to be characterized by thickness variation depending on evaporation and precipitation intensities.

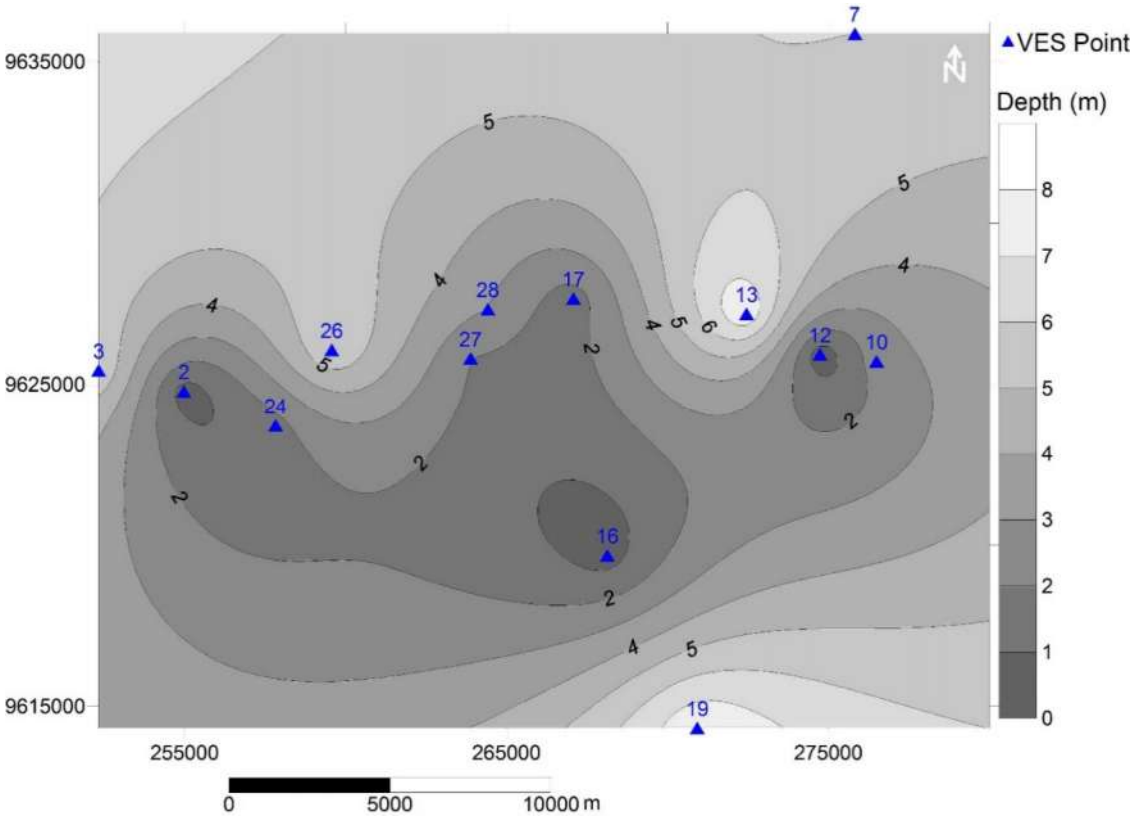

Figure 71: Depth to shallow aquifer in the surveyed area. Note that this aquifer is restricted in some specific areas.

The second aquifer system with either freshwater or low water quality in terms of fluoride and TDS is interpreted in more than 80% of the sounding curves. This is interpreted as the major aquifer because of its thickness which exceeds 100 m as determined at MRVES 20 (100 m) and MRVES 25 (140 m) (Table 9). For the other sounding curves, it was the underlying layer and therefore the thickness could not be determined rather than being estimated using the relationship between the current electrode spacing and penetration depth as explained previously. Aquifer thickness is also supported by both borehole lithological logs where the deep borehole (130 m) at Nelson Mandela (Fig. 64) ended on aquifer formation as discussed previously, and a study by Ghiglieri *et al.* (2010) in the northern part of Mt. Meru where the aquifer thickness was found to be 110 m (from 40 to 150 m). Unlike the depth to aquifer of 40 m in the northern side of Mt. Meru (Ghiglieri *et al.,* 2010), the depth to aquifer in the study area does not exceed 35 m with the shallowest parts around Nelson Mandela to central parts of Kikatiti and Maroroni (Fig. 72). This reflects high precipitation in the windward side (PBWB/IUCN, 2008; Ghiglieri *et al.,* 2010) leading to

high groundwater recharge relative to the leeward side of Mt. Meru. Overall, depth to groundwater within the surveyed area is largely controlled by the land morphology being shallow on the foot of Mt. Meru particularly in depression areas.

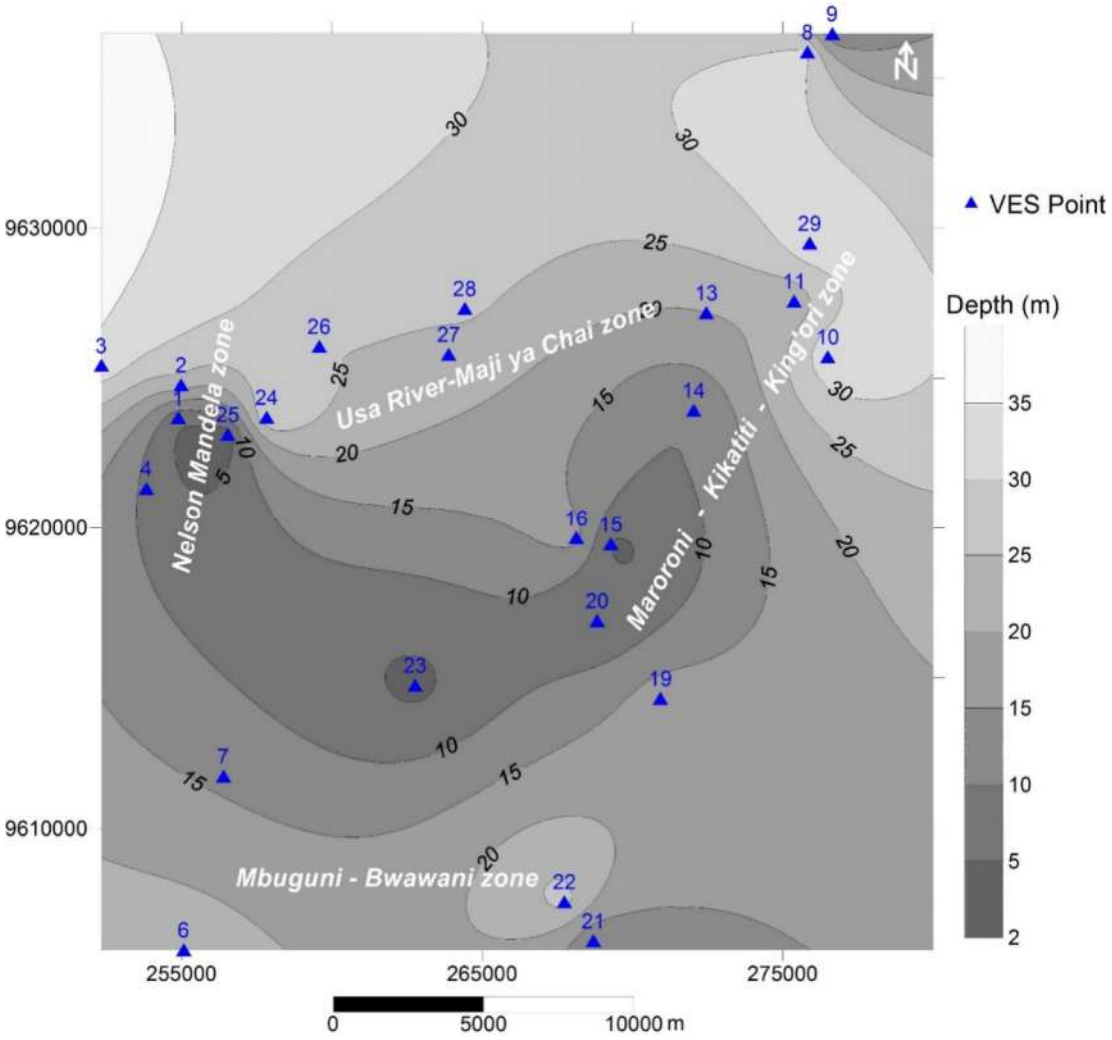

Figure 72: Depth to major aquifers in the surveyed area

Slicing of the major aquifer at a depth of 70 m below the surface showed clearly patches of freshwater aquifers (35-60 Ωm) differentiated from intermediate to low water quality aquifers (10 to 35 Ωm) (Fig. 73). Figure 5.24 depicts two major Aquifer zones which are Nelson Mandela and King'ori being connected by narrow band. The existing data in this study support well these two zones but create uncertainties on the band which is connecting two zones and the low land areas of Mbuguni-Bwawani in the southern parts (Fig. 73). It is suggested that the band is largely caused by the lack of uniformity in distribution of VES stations in the study area. Groundwater potentiality at Nelson Mandela is well supported by

both the lithological logs for two boreholes (Fig. 64) where groundwater is highly favored in weathered and fractured volcanic rocks, and the quality of the water samples (WS88) from Nelson Mandela borehole (TDS = 554 mg/l, F^- = 2.98 mg/l) (Table 10). Despite that borehole lithological logs are missing at King'ori, groundwater in this zone is favored in breccia and tuffs as reflected in the geological map (Fig. 62). Such rocks have been reported to favor groundwater in the northern part of Mt. Meru (Ghiglieri *et al.,* 2010). Groundwater potentiality in this zone is also supported by the quality of water from the borehole (150 m, WS54) owned by LODHIA Gypsum industry (WS54) where TDS and F^- were found to be 579 mg/l and 2.32 mg/l respectively (Table 10).

The central part of the surveyed area (Maroroni-Kikatiti-Maji ya Chai) centered at Maroroni (Fig. 73) and the southern low land areas (VES 21 and 22) (Fig. 73) are characterized by nearly the same geo-electric layer but different geological layer. The central part is rich in lahars where dissolution leads to low groundwater quality as discussed previously. This is well supported by the geology (Fig. 62), borehole lithological log (Fig. 67) and water sample from three existing wells where both TDS and F^- were high averaging at 2496 mg/l and 39 mg/l respectively (Table 10). Based on field observations, clay rich sediments derived from up-land areas dominate the low land areas from Makiba (VES 9) to southern parts (VES 21 and 22) (Fig. 73) and other areas around Bwawani. Since saturated clays are associated with low resistivity (Hewaidy *et al.,* 2015; Mohamaden & Ehab, 2017), the low resistivity in such areas is attributed to clay rich sediments and not the water quality. This is well supported by fresh groundwater obtained from two wells proximal to VES 21 and 22 where TDS and F^- varied from 352-384 mg/l and 3.36-3.72 mg/l respectively (Table 10).

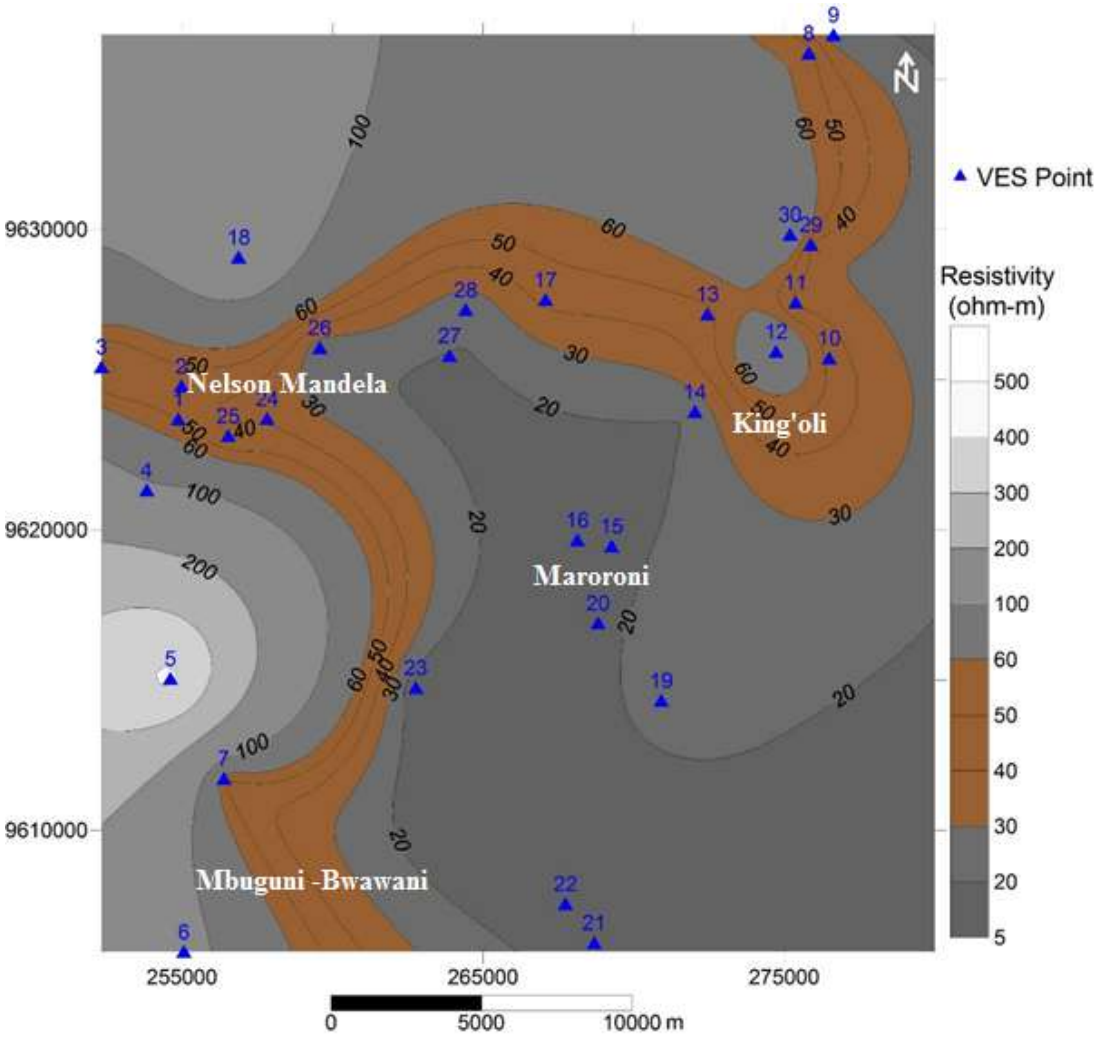

Figure 73: Resistivity contour map at a depth of 70 m below the Earth surface. Note that altitude effect is not considered.

(iii) Groundwater Potential Index Map (GWPIM)

Groundwater Potential Index Map (GWPIM) was constructed by integrating the discussed components (aquifer resistivity value, aquifer thickness, transverse resistance, longitudinal conductance, depth to aquifers, depth to water table, vicinity water chemistry in terms of TDS/EC and fluoride, borehole yields, resistivity at 70 m depth and geology). Each component was assessed separately by assigning percentages from 0-100 with 100% assigned to the most contributing factor to groundwater potentiality. Other intermediate contributing factors were assigned percentages accordingly between 0 and 100. Thereafter, the average scores were calculated for each VES stations and all VES stations were ranked with 1 as the highest groundwater potential and 6 as the lowest (Fig. 74). It is well indicated that the areas

around Nelson Mandela and King'ori are potential groundwater zones while the central zone (Maroroni - Kikatiti - Maji ya Chai) are characterized by groundwater of low quality in terms of Fluoride and TDS (Fig. 74). Thus, information from this map is essential for locating borehole sites.

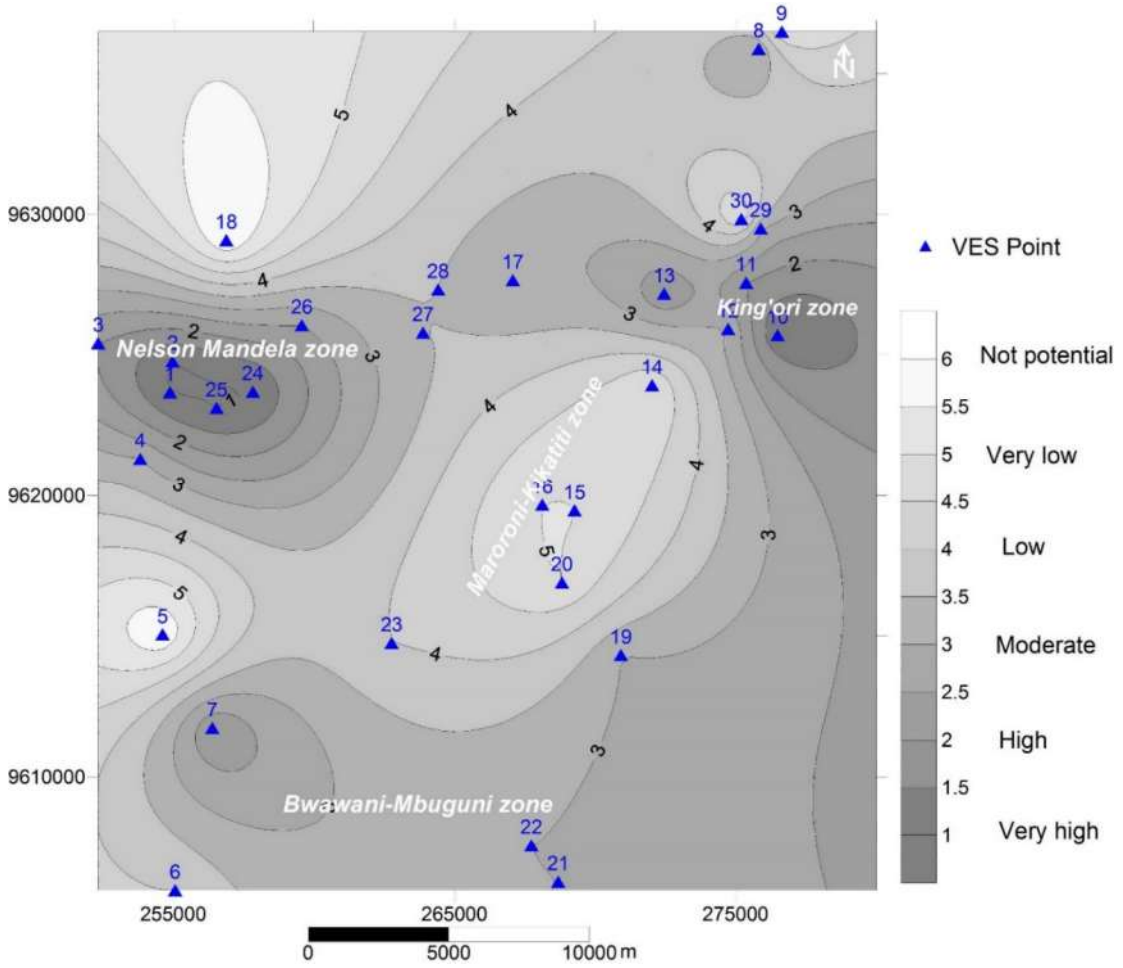

Figure 74: Developed Groundwater Potential Index Map which serves as a guide for further groundwater development.

5.5 Conclusions and Recommendations

This study revealed that the area is a potential groundwater source for domestic and industrial purposes. More than 80% of the sounding curves with HK, K, KH and Q as dominant types indicated groundwater potentiality. Stratigraphically, two major aquifers have been delineated; the upper aquifer and deep aquifer. The upper aquifer had the average thickness of 25 m starting at a depth not exceeding 10 m being restricted in some specific parts. This has been considered as a minor aquifer because it is thin, associated with clay formation in

some parts and likely to be affected by seasonal variation of rainfall and temperature especially in areas where it is too shallow (~5 m). The deep aquifer was found to be thick with the thickness exceeding 100 m. However, in most parts, the actual thickness could not be estimated because it was the last layer based on the applied electrode spacing. The depth to this aquifer does not exceed 35 m and the coverage is high (~80% of the study area). In assessing the quality of the aquifers, this study has indicated that there is a strong negative correlation (~0.9) between the aquifer resistivity with both EC and fluoride in the corresponding groundwater. Aquifer resistivity between 35-60 Ωm represents fresh groundwater hosted in weathered and fractured mafic volcanics (eg. Nelson Mandela Zone), breccia and tuffs (eg. King'ori zone) whereas the aquifer resistivity between 15 and 25 Ωm represent low groundwater quality in terms of TDS (generally >1000 mg/l) and fluoride (generally >10 mg/l) hosted mainly in lahars of various groups (Kikatiti-Maroroni zone). The aquifer resistivity between 25 and 35 Ωm represent intermediate water quality while the aquifer resistivity values generally between 10 and 15 were found to correspond to freshwater in clay rich formation particularly in the low land areas (eg. Bwawani-Mbuguni). The areas with freshwater aquifers were associated with high transverse resistance between 3000 and 7000 Ωm^2 and low longitudinal conductance between 1 and 4 Ω^{-1} whereas the areas with low groundwater quality were associated with low T between 1800-300 Ωm^2 and high S between 4 and 11 Ω^{-1}. Integrated results (VES, water samples, geology and lithological borehole logs and yields) were used to develop Groundwater Potential Index Map which serves as a guide for siting boreholes.

This study recommends proper use of the developed Groundwater Potential Index Map (GWPIM) for locating other VES stations and borehole drillings. First priority should be given to areas such as King'ori (Sakira Chini) and Makiba (Maasai territory) which are potential groundwater sources and local people particularly women are moving more than 5 km searching for water. Furthermore, as the obtained correlation coefficient (~ -0.9) between aquifer resistivity with F^- and EC/TDS was based on VES stations which are not uniformly distributed, this study recommends further VES stations at close intervals to establish the actual relationship. Further studies are also needed other volcanic provinces to see whether such correlation is valid at regional level.

CHAPTER SIX

GENERAL DISCUSSION, CONCLUSION AND RECOMMENDATIONS

6.1 General discussion

Water chemistry is dynamic being controlled by various factors including rock dissolution (Chapters 2 and 4), anthropogenic activities (Chapter 4) and climatic variability of precipitation and temperature (Varni *et al*., 2013; Lutz *et al*., 2015). Fluoride is among the natural contaminant in water systems which varies with climatic conditions (Opdyke *et al*., 1993; De Angelis & Legrand, 1994; Thompson *et al*., 2002). This agrees with this study which indicated intensive variation of fluoride in water sources from the leeward to windward sides of Mt. Meru (Chapters 3 and 4).

There is limited information on temporal variation of fluoride in water and sediments in Tanzania throughout the Holocene period. Few available data which show continuous fluoride records in the Holocene period are Kilimanjaro Ice cores (Chapter 2; Thompson *et al*., 2002). Fluoride was generally high in early Holocene (high precipitation period) relative to late Holocene (Chapter 2). The peak values were recorded during the short cool and dry periods at 8.2 ka and 4.0 ka (Chapter 2; Thompson *et al*., 2002). This suggests that in the cool and dry periods, evaporation-crystallisation circles lead to deposition of trona in lakes which are rich in fluorine (Kaseva, 2006). Thus, the high fluorine levels in the dry events are the results of deposition of dust from the lake surfaces which had trona materials. The general decrease in F from early Holocene to late Holocene (Fig. 4) suggest the decrease in availability of F rich dust which could have been attributed to the decrease in aridity periods. Therefore, variation in climatic condition in the Holocene period as discussed in Chapter 2 is the main cause of fluctuation of fluoride levels (Fig. 4). For instance, pollen and diatom records from one of windward lake which is located within the study area (Lake Duluti) indicated a short brief periods of low lake levels between ~0.41-0.37 ka (Chapter 2, Öberg *et al*., 2013). Therefore, if this is projected to the leeward lakes such as Momella, it can be hypothesized that they were nearly dry characterized by high deposition of trona which are rich in fluorine.

Integrating Chapters 2, 3 and 4, it is clear that fluoride level has been changing in water system depending on both climatic variability and susceptibility of fluorine rich materials to weathering. Peak fluoride values are well linked with the major volcanic events which generate addition F through rocks and gases (De Angelis & Legrand, 1994). In geological

context, it is suggested that periods of volcanic events around the East Africa Rift System were associated with high fluoride levels in water systems.

Precipitation and evaporation intensities are the key factors for determining economic groundwater resources. Both groundwater recharge and groundwater levels vary depending on the amount of precipitation and evaporation (Varni *et al*., 2013; Lutz *et al*., 2015). Long-term groundwater level fluctuations are linked with climatic changes and anthropogenic activities such as excessive pumping and irrigation activities (Healy & Cook, 2002). Seasonal groundwater level fluctuations are common in areas experiencing seasonal rainfall evapotranspiration and irrigation (Healy & Cook, 2002). This is the common situation in most of the areas in Tanzania (Chapter 2) including Mt. Meru areas. Around Mt. Meru, areas experiencing low precipitation and high evaporation (eg. leeward side of Mt. Meru) are characterized by low groundwater recharge with the aquifers (if present) at greater depth relative to areas with high precipitation (eg windward side). Therefore, high groundwater potential in the southern part of the study area (Chapter 5) relative to the northern side (leeward) as revealed by Ghiglieri *et al*. (2012) is a function of contrast in precipitation and evaporation in these two areas. These factors also affect rock dissolution rates and are among the factors which control the release of fluoride from rocks as well as fluoride levels in water systems (Chapters 3 and 4).

High Na^+ and K^+ in Arumeru water sources as revealed in Chapter 4 is the reflection of the abundance of these elements in continental rift rocks which are generally alkaline in nature (Chapter 3). Through petrography (Chapter 3), it is well indicated that the minerals clinopyroxene (CPX) and nepheline dominated the Arumeru rocks to more than 70%. Therefore, nepheline mineral of which Na is the major component ($Na_3KAl_4Si_4O_{16}$) and Na-rich CPX such as augite (Ca, Na) (Mg, Fe, Al, Ti) $(Si, Al)_2O_6$ and aegirine ($NaFe^{3+}SiO_6$) are the main source of Na^+ and K^+ in water systems through dissolution processes. However, K-feldspar minerals such as sanidine and microcline with the general formula $KAlSi_3O_8$ and biotite $K(Mg, Fe)_3AlSi_3O_{10}(F,OH)_2$ are likely to contribute significant amount of Na^+ in water system. Although these minerals are resistant to weathering relative to Na-feldspars and pyroxenes (Easterbrook, 1999), the replacement of biotite (and hornblende) by Fe-oxides in some of the rocks (Chapter 3) is an indication that to some extent, these minerals have been weathered; a process that accompanied with the release of constituting element such as Na and F to soils and groundwater systems. The lack of Ca and Mg in nepheline and Na-rich

clinopyroxene minerals automatically lowers their amount in parent rocks and this explains their low concentration in water system relative to K^+ and Na^+.

High fluoride in Arumeru water is discussed in detail across Chapters 3-5. In Chapter 3, it is revealed that the major fluorine bearing minerals are sphene, hornblende, apatite and biotite. Overall, a combination of these minerals leads to an increase in fluorine in a particular rock. Also, fluorine was found to increase with decreasing nepheline and clinopyroxene crystal indicating incompatibility of F in these crystals. Explosive style of volcanism is inferred through petrography (Chapter 3) and this led to emplacement of rocks with different composition at the same location. Variation of fluorine in such rocks is common (Chapter 3) due to mineralogical differences and this explains local variation of fluoride in water system (Chapter 4). However, the factors such as rocks texture, climatic condition (moisture content and temperature), soil type, land morphology and groundwater flow path play a significant role in the release, mobility and spatial distribution of fluoride in water system.

The amount of fluorine in rocks were found to be high about three times than that in equivalent soils and the values showed a linear positive relationship (R=0.77) (Chapter 3). Because this is a dominant group of soils, it can be generalized that fluorine in soils is largely an outcome of dissolution of parent materials. Its spatial distribution is governed by the amount of fluorine in parent rocks and factors that control mobility of fluorine in soils (Chapter 3). However, high fluorine content in the soils towards the top of Mt. Meru which is not reflected in rocks suggests contribution of fluorine from ashes and pyroclastic materials. High fluorine in rocks than equivalent soils could indicate that high amount of fluorine is still locked in the rocks, and fluoride is mobilized easier from soils to groundwater system. Both arguments are positively supported by data from this research as follows:

(i) In chapter 3 through petrology, it is revealed that some samples are still fresh. Also, through geochemistry in the same chapter, it is revealed that the rocks are weakly weathered as evidenced by nearly constant concentrations of trace elements As, Rb, Y and W in rocks and equivalent soils. These facts suggest that high amount of fluorine is still locked in parent materials. Considering the rock and equivalent soil fluorine data, with the assumption that there is no fluorine input on soils from ashes and pyroclastic materials and by neglecting fluorine that have been mobilized to groundwater, the amount of fluorine that have been released from rocks is estimated to be 27% only. If

this is the case, then under the current global temperature trend (Chapter 2), and water availability (Chapters 2 and 5), the rate of fluorine dissolution is expected to increase.

(ii) There is high concentration of fluoride in water sources as revealed in Chapter 4 and previous studies (Nanyaro *et al.,* 1984; Gaciri & Davies, 1993; Ghiglieri *et al.,* 2010, 2012; Malago *et al*., 2017)). This suggests that fluoride has been mobilized from rocks and soils to groundwater system. This is highly supported by geochemical data (Chapter 3) where the element F follow the similar strong depletion trends shown by mobile elements particularly Ca^{2+} and trace elements Sr, Cr, V and Cl in residual soils relative to their parent rocks.

By integrating spatial distribution of fluorine in rocks (Chapter 3), fluoride in water (Chapter 4) and aquifers (Chapter 5), it is revealed that areas with low fluoride in water sources are the areas characterized by short water-rock contact time and areas with high fluoride are areas dominated by the relatively soluble materials such as lahars. For instance, low fluoride as well as TDS in the windward spring zone where rocks had relatively high fluorine is largely an indication of short contact time. The factors such as rock type and texture might also have its contribution to low dissolution. Rocks in windward spring zone, generally lava flow (nephelinitic to phonolitic) are resistant to weathering relative to lahars which are the dominant materials in other areas within the study area.

It is also as revealed through geochemistry and petrography (Chapter 3) that, the dominance of nephelinitic materials on the slopes of Mt. Meru could lower fluorine content in nephelinitic rocks. The low groundwater quality aquifers particularly on the foot of the mountain (Chapter 5) is the results of dissolution of materials which are relatively weak to weathering (lahars) and this accounts for high TDS in very shallow dug wells located in areas rich in lahar materials. Fresh water aquifers were inferred in areas which are not dominated by lahar materials, mainly in weathered and fractured volcanics, breccia and tuffs. The relatively low fluoride content in the low land areas south of the study areas (Mbuguni-Bwawani-Makiba) as revealed in Chapter 4 could be attributed to the decrease in lahar materials as well as low hydraulic gradient connecting the foot of Mt. Meru and southern areas. Geophysical data could not characterize effectively the type of aquifers in terms of quality but generally revealed the dominance of alluvial sediments particularly clay rich sediments in such areas.

6.2 Scientific contribution

(i) Despite that fluoride in water systems has been documented widely in the study area and East Africa Rift Valley at large (Chapters 3 and 4), the source rocks and fluorine bearing minerals was poorly understood. From this study, it is revealed that compatibility of fluorine in early stages of fractional crystallization is low. That, under presence of mafic to felsic rocks, fluorine is favored in felsic rocks being increasing with increasing silica content. This explains high content of fluorine in andesitic rocks relative to foidite and basaltic rocks in the study area. Previous studies along the East Africa rift system lack information on fluorine bearing minerals (Nanyaro *et al.,* 1984; Gaciri & Davies, 1993; Dawson, 2008; Ghiglieri *et al.,* 2010, 2012; Rango *et al.,* 2010; Malago *et al.,* 2017)). Through this study it is revealed that sphene, hornblende, biotite and apatite are principal source of fluorine in water system.

(ii) It is revealed that fluorine is widely distributed in different rock types and in different concentrations. The method used in Total Fluorine Analyses is the modification of Ingram method (1970), which has been modified according to the environment. With this method, sintering involves a mixture of the sample, Na_2CO_3 and ZnO (Chapter 2). Although the method is complex and time consuming, results obtained ranging from 0.025-1.9% F which are in close agreement with the rock mineralogy as well as the fluoride level in the vicinity groundwater source indicate that the method is powerful in Total Fluorine Analyses. Therefore, this method is considered as an important part contributing to science and should be applied in total analyses of fluorine in rocks and soils elsewhere.

(iii) Concentrations of fluorine in Arumeru rocks and soils were poorly known. Overall, in terms of average, this study has revealed that there is no remarkable difference between the amount of fluorine in rocks and soils. High fluorine in soils was obtained in transported soils as well as in ashes towards the top of the mountain. This is new scientific information that pyroclastic and ash materials exhibit high fluorine content and also transported soils rich in clays and organic matter have high capacity of retaining fluorine. However, with consideration of rocks and equivalent soils, the amount of fluorine was found to be high about three times than that in equivalent soils.

(iv) Hydrogeochemical processes governing Arumeru waters were poorly known. This study has indicated that water is generally the Na-K-HCO_3 type and Mt. Meru is the main recharge zone (Chapter 3). The high Na^+ and K^+ content in waters is related to parent materials being released mainly from nepheline and clinopyroxene minerals. The water chemistry changes progressively to more alkaline as water interacts with the rocks and atmosphere (weathering and evaporation processes). Evaporation-crystallization processes dominated the leeward water types whereas rainfall and weathering of rocks dominate in the windward sides. Springs in the windward side were characterized by short water -rock interaction time.

(v) Regarding the water quality, there is addition information from this study that water quality for domestic and agriculture is moderate following the same order pattern of springs > streams > boreholes > lakes > dug wells. Fluoride and TDS (natural) along with NO_3^- (anthropogenic-in dug wells) were the main contributor in lowering the water quality for domestic purposes whereas TDS, Na^+ and K^+ were significantly lowering the water quality for irrigation.

(vi) Groundwater occurrence and distribution in the south-eastern part of the study area was not known. Through this study, two major aquifers in terms of water quality (fluoride, TDS) are inferred. These are freshwater and low groundwater quality aquifers characterized by resistivity value between 35 - 60 Ωm and 15-25 Ωm respectively. Fresh water aquifer is mainly hosted in weathered and fractured mafic volcanics, breccia and tuffs being pronounced in areas such as Nelson Mandela and King'ori. The low water quality aquifer (generally F> 10 mg/l, TDS > 1000 mg/l) is hosted mainly in lahars of various groups being pronounced in areas such as Maji ya Chai, Kikatiti and Maroroni. The aquifer resistivity between 25 and 35 Ωm represent intermediate water quality while the aquifer resistivity between 10 and 15 represent freshwater in clay rich formation (Bwawani-Mbuguni).

(vii) Stratigraphically, two major aquifers have been delineated; shallow and deep aquifers. The upper shallow aquifer with the average thickness of 25 m starts at a depth not exceeding 10 m being restricted in some specific parts. The deep aquifer covering >80% of the surveyed area was found to be extensive with average thickness exceeding 100 m. Also, the other new information is that there is a strong negative correlation (~-0.9) between aquifer resistivity with both EC and F^- in the

corresponding groundwater. Thus, one can use surface resistivity measurement to estimate fluoride level in the corresponding aquifer.

(viii) Groundwater Potential Index Map (GWPIM) has been developed by integrating geological, geophysical and hydrological data. This is the important map which serves as a guide for further groundwater development in the south-eastern part of Mt. Meru.

6.3 Conclusions

Review of Holocene climate change in Tanzania, showed fluctuation of rainfall as well as temperature which are important factors in controlling availability of groundwater resources (quantity, aquifer depth) and water chemistry through dissolution processes. Through proxies, it is suggested that the hydrological circle linking the Indian Ocean SST with the atmosphere which connects the high and low latitudes accounts for rainfall variations in Tanzania. However, the ITCZ plays its role by modifying the intensity of seasonal winds.

Through climate records, a general decrease in precipitation from the Late Holocene to present with the pronounced aridity between 3-2 ka and 1.2-0.5 ka is inferred. In the 20^{th} century, there is increased temperature, this has been causing changes in hydrological circle leading to the increase in heavy rainfall and drought periods. For instance, Tanzania experienced high precipitation in the early and late periods of the century with low precipitation in the mid of the century around 1940-1960s. Since the high rainfall of 1997/98, there is no remarkable prolonged drought in Tanzania and seasonal rainfall are pronounced. Therefore, this has created potential groundwater reservoir and increased temperature has been accelerating rock dissolution and evaporation process. Thus, fluoride level has been increasing and it is anticipated to increase under the current global trend of temperature particularly in Lakes such as Momella which are in the leeward side.

There is limited information for reconstruction of palaeoclimate in Tanzania. Few available works are concentrated in some specific zones such as major lakes, Indian Ocean and Eastern Arc Mountains. Available Holocene climatic records showed lack of information on the temporal variation of fluoride in water and sediments. It is only Mt. Kilimanjaro Glacier records which show continuous record throughout the Holocene period. From this record, it is revealed that fluoride has been varying with climate, being high during cool and dry phases (e.g. 4.0 ka and 8.2 ka), most likely derived from dried shallow lakes.

Geochemical characterization of Arumeru rocks revealed that the rocks are related to cogenetic magma. Generally, they are alkaline, poor in silica and weakly fractionated with the composition ranging from foiditic to andesitic. Petrological analysis indicated that clinopyroxene, nepheline ad plagioclase were the dominant minerals accounting to > 70% of all minerals with titanite, Fe-oxides, apatite, hornblende, biotite, sanidine, microcline, zircon as minor and accessory minerals. The high fluoride in Arumeru water sources is well linked with the high fluoride in rocks and soils. All rocks were found to have fluorine in different amount varying from 251-19,122 mg/Kg (mean=3921mg/Kg, n=68) with the contributing minerals in the decreasing order of titanite >hornblende > apatite > biotite.

Fluorine was highly concentrated in andesitic rocks relative to other rocks (mean = 0.713%, n=13) suggesting fluorine to be favored in late than early crystallization phases. Fluorine was also high in soils ranging from 637-17848 mg/Kg (mean=3526mg/Kg, n=32) being enriched in transported mbuga soils. Considering rocks and equivalent soils, this study revealed that the amount of fluorine in rocks is about three times than that in soils and they are correlated positively (R=0.77). Strong depletion of mobile elements particularly Ca^{2+} and trace elements Sr, Cr, V and Cl in residual soils relative to their parent rocks indicate that some amount of fluorine have been mobilized from the soils. However, nearly constant concentration of trace elements As, Rb, Y and W suggest that weathering was not so intensive and the rocks are young probably representing the most recent volcanic phase. The study revealed that apart from other factors such as amount of fluorine in the rocks, climatic condition (water and temperature) and rock chemistry, rock texture is the major factor controlling the release of fluorine from rocks to soils. Mobility of fluorine from soils to groundwater and within groundwater was found to be largely controlled by soil type, soil chemistry and groundwater movement. It was further observed that springs water sources, particularly from the windward side are characterized by short water-rock contact time which is largely attributed to high hydraulic gradient on the main recharge zone (slopes of Mt. Meru). Short contact time was evidenced by low fluoride which does not conform with amount of fluorine in the vicinity rocks, low TDS and their position in hydrogeochemical plots.

Hydrogeochemical characteristics of Arumeru groundwater was found to be controlled by geology, water-rock interaction time and climatic conditions. Overall, the dominant patterns of major cation and anion in water types were $Na^{+} > K^{+} > Ca^{2+} > Mg^{2+}$ and $HCO_3^{-} > CO_3^{-} > Cl^{-} > SO_4^{2-} > NO_3^{-} > F^{-}$ respectively, with the dominant pattern of dissolved ion being in the order of lakes > dug wells > borehole > streams > springs. Water chemistry changes

progressively to more alkaline as water interacts with the rocks towards the lowland areas. Climate effect is well observed in water-rock interaction plots where the typical leeward water types showed that weathering of rocks together with evaporation-crystallization are the dominant process whereas rainfall and weathering of rocks dominate in the leeward sides. Hydrochemical facies indicated that Na-K-HCO_3 water type dominates to about 90%. High Na^+ and K^+ is the reflection of their dominance in parent materials which are alkaline in nature, with large amount being released from nepheline and clinopyroxene. Also, this study indicated that lahars, ashes and pyroclastic materials contain high amount of these ions as well as fluoride as a result more ions are dissolved in dug wells constructed in areas which are rich in such materials. High HCO_3^- is linked with volcanic activities. It was correlated positively with TDC, EC, Na^+, K^+, F^- and Cl^- implying that they originate from the rocks through weathering with probably CO_2 as the main triggering agent.

The suitability of water for domestic and agricultural purposes was found to be moderate, following the same order pattern of springs > streams > boreholes > lakes > dug wells. Fluoride was found to be the major natural pollutant lowering the water quality for domestic purposes (mean=17.6 mg/l). 78% and 52% of the samples had fluoride above the recommended WHO and Tanzanian standard respectively. Anthropogenic pollution was recognized through nitrate particularly in the dug wells located in residential areas where latrines are locally constructed. Chloride and sulphate were found to result from both natural and anthropogenic sources. High Na^+ (mean =118 mg/l) and HCO_3^- (mean=390 mg/l) in Arumeru waters were found to lower significantly the water quality for irrigation purposes.

Geophysical survey in the south-eastern part of Mt. Meru indicated that the area is a potential groundwater source for domestic and industrial purposes. Stratigraphically, there are upper aquifer and deep aquifer. The upper aquifer is restricted in some specific parts and had the average thickness of 25 m. The deep aquifer was found to be thick covering about 80% of the study area with the thickness exceeding 100 m. However, in most parts, the actual thickness could not be estimated because it was the last layer based on the applied electrode spacings. The depth to this aquifer does not exceed 35m. In assessing the quality of the aquifers using resistivity values, fluoride and EC of the immediate groundwater source, this study indicated that there is a strong negative correlation (R=-0.9) between the aquifer resistivity with both EC and fluoride in the corresponding groundwater. Aquifer resistivity values between 35-60 Ωm represent fresh groundwater hosted in weathered and fractured mafic volcanics (eg. Nelson Mandela Zone), breccia and tuffs (King'ori zone) whereas the aquifer resistivity

between 15 and 25 Ωm represent low groundwater quality in terms of TDS (generally >1000 mg/l) and fluoride generally (>10 mg/l) hosted mainly in lahars of various groups (Kikatiti-Maroroni zone). The aquifer resistivity between 25 and 35 Ωm represent intermediate water quality while the aquifer resistivity between 10 and 15 Ωm represent freshwater in clay rich formation (Bwawani-Mbuguni). Groundwater Potential Index Map has been developed to serves as a guide for siting boreholes.

6.4 Recommendations

Based on the findings from this study the following are recommended:

(i) Adverse effects related to climate changes particularly periods of heavy rainfall and droughts are expected in Tanzania. There is a need of conducting more studies on climate change for predicting future climate using sediments and coral proxies of high resolution records from the lakes and Indian ocean.

(ii) It is important to study influence of climatic variability on fluoride for the purpose of predicting future level of fluoride in water systems.

(iii) Leaching experiment for all types of rocks is recommended so as to understand fluorine release mechanisms from different rocks under different conditions (texture, temperature, pH etc)

(iv) Microprobe analyses is required so as to ascertain fluorine amount in the identified fluorine bearing minerals (titanite, hornblende, apatite and biotite).

(v) Dating of volcanic rocks to account for fluoride variation in different volcanic phases.

(vi) Intensive water quality analyses pre-utilization and effective utilization of spring water for domestic purposes.

(vii) Proper knowledge dissemination to local people on water quality in their areas and the appropriate uses. This should go with conservation and protection of water resources including the identified aquifer which are susceptible to anthropogenic contamination.

(viii) Researches on fluoride mobility within the soils emphasizing on the factors such as pH, temperature and organic matter. Assessing fluoride mobility from soil to plants, its levels and distribution in both plants and livestock.

(ix) Researches on crop productivity effects resulting from the use of high Na^+ and HCO_3^- water sources in irrigation.

(x) Aquifers are extensive with the thickness above 100 m in most of the parts. The actual thicknesses of such aquifers need to be investigated.

(xi) To establish a clear relationship between aquifer resistivity and water quality (TDS, F-), studies which link them are still needed within the studied area. Such studies should also be conducted in other volcanic provinces with high fluoride in the water sources to check the validity of the relationship.

(xii) Mechanisms for enrichment of fluoride as well as Na^+ and HCO_3^- particularly in leeward lakes need to be investigated.

REFERENCES

Abbott, M. B., Finney, B. P., Edwards, M. E., & Kelts, K. R. (2000). Lake-Level Reconstructions and Paleohydrology of Birch Lake, Central Alaska, Based on Seismic Reflection Profiles and Core Transects. *Quaternary Research,* **53**: 154 –166.

Abdullahi, M. G., Toriman, M. E., & Gasim, M. B. (2015). The Application of Vertical Electrical Sounding (VES) for Groundwater Exploration in Tudun Wada Kano State, Nigeria. *Journal of Geological Geoscience,* **4**: 186. doi:10.4172/2329-6755.1000186.

Akankpo, A. O., & Igboekwe, M. U. (2011). Monitoring Groundwater Contamination Using Surface Electrical Resistivity and Geochemical Methods. *Journal of Water Resource and Protection,* **3**: 318-324. doi:10.4236/jwarp.2011.35040.

Alin, S. R., & Cohen, A. S. (2003). Lake-level history of Lake Tanganyika, East Africa, for the past 2500 years based on ostracode-inferred water-depth reconstruction. *Palaeogeography, Palaeoclimatology, Palaeoecology,* **199**: 31- 49.

Alin, S. R., & Cohen, A. S. (2004). The live, the dead, and the very dead: taphonomic calibration of the recent record of paleoecological change in Lake Tanganyika, East Africa. *Paleobiology,* **30** (1): 44–81.

Alloway, B. J. (1995). *Heavy Metals in Soils.* 2nd edn. Blackie Academic and Professional. Chapman and Hall. Glasgow. 368 pp.

Ammar, A. I., & Kamal, K. A. (2018). Resistivity method contribution in determining of fault zone and hydrogeophysical characteristics of carbonate aquifer, eastern desert, Egypt. *Applied Water Science,* **8**:1. https://doi.org/10.1007/s13201-017-0639-9.

Anomohanran, O. (2015). Hydrogeophysical and hydrogeological investigations of groundwater resources in Delta Central, Nigeria. *Journal of Taibah University for Science,* **9** (1): 57-68. doi: 10.1016/j.jtusci.2014.06.003.

Archie, G. E. (1942). The Electrical Resistivity Log as an Aid in Determining Some Reservoir Characteristics. *Transactions of the American Institute of Mining, Metallurgical and Petroleum Engineers,* **146** (01): 54–62. Doi: 10.2118/942054-g.

Arsène, M., Elvis, B. W. W., Daniel, G., Théophile, N. M., Kelian, K., & Daniel, N. J. (2018). Hydrogeophysical Investigation for Groundwater Resources from Electrical Resistivity Tomography and Self-Potential Data in the Méiganga Area, Adamawa, Cameroon. *International Journal of Geophysics,* 2018: 1-14. ID: 2697585, https://doi.org/10.1155/2018/2697585.

Baharuddin, M. F. T., Hashim, R., & Taib, S. (2009). Electrical Imaging Resistivity Study at the Coastal Area of Sungai Besar, Selangor, Malaysia. *Journal of Applied Sciences* **9** (16): 2897-2906.

Barker, P., & Gasse, F. (2003). New evidence for a reduced water balance in East Africa during the Last Glacial Maximum: Implication for model-data comparison. *Quaternary Science Reviews,* **22**: 823–837.

Barker, P., Telford, R., Gasse, F., & Thevenon, F. (2002). Late Pleistocene and Holocene palaeohydrology of Lake Rukwa, Tanzania, inferred from diatom analysis. *Palaeogeography, Palaeoclimatology, Palaeoecology,* **187**: 295-305.

Barker, P., Williamson, D., Gasse, F., & Gibert, E. (2003). Climatic and volcanic forcing revealed in a 50,000-year diatom record from Lake Massoko, Tanzania. *Quaternary Research,* **603**: 68 –376.

Barker, P. A., Leng, M. J., Gasse, F., & Huang, Y. (2007). Century-to-millennial scale climatic variability in Lake Malawi revealed by isotope records. *Earth and Planetary Science Letters,* **261**: 93–103.

Barker, P., Telford, R., Merdaci, O., Williamson, D., Taieb, M., Vincens, A., & Gibert, E. (2000). The sensitivity of a Tanzanian crater lake to catastrophic tephra input and four millennia of climate change. *The Holocene,* **10** (3): 303-310.

Barker, P. A., Hurrell, E. R., Leng, M. J., Wolff, C., Cocquyt, C., Sloane, H. J., & Verschuren, D. (2011). Seasonality in equatorial climate over the past 25 k.y. revealed by oxygen isotope records from Mount Kilimanjaro. *Geology,* **39** (12): 1111–1114. doi:10.1130/G32419.1.

Barker, P. A., Street-Perrott, F. A., Leng, M. J., Greenwood, P. B., Swain, D. L., Perrott, R. A., … Ficken, K. J. (2001). A 14,000-year oxygen isotope record from diatom silica in two alpine lakes on Mount Kenya. *Science,* **292**: 2307–2310.

Barker, P. A., Hurrell, E. R., Leng, M. J., Plessen, B., Wolff, C., Conley, D. J., … Verschuren, D. (2013). Carbon cycling within an East African lake revealed by the carbon isotope composition of diatom silica: a 25-ka record from Lake Challa, Mt. Kilimanjaro. *Quaternary Science Reviews,* **66**: 55-63.

Barry, S. L., Filippi, M. L., Talbot, M. R., & Johnson, T. C. (2002). Sedimentology and Geochronology of Late Pleistocene and Holocene sediments from Northern Lake Malawi. The East African Great Lakes: *Limnology, Palaeolimnology and Biodiversity*, 369–391.

Bashir, E., Naseem, S., Hanif, H., & Pirzada, T. (2013). Geochemical study of groundwater of Uthal and Bela areas, Balochistan and its appraisal for drinking and irrigation water quality. *International Journal of Agriculture Environment,* **2**: 1-13.

Behling, H. (2002). Late Quaternary vegetation and climate dynamics in southeastern Amazonia inferred from Lagoa da Confusao in Tocantins State, northern Brazil. *Amazoniana-Limnologia et Ocologia regionalis Systemae Fluminis Amazonas,* **17**: 27–40.

Behling, H., Pillar, V. P., Orloci, L., & Bauermann, S. G. (2004). Late Quaternary Araucaria forest, grassland (Campos), fire and climate dynamics, studied by high-resolution pollen, charcoal and multivariate analysis of the Cambara do Sul core in Southern Brazil. *Palaeogeography, Palaeoclimatology, Palaeoecology,* **203**: 277–97.

Bhattacharya, P. K., & Patra, H. P. (1968): *Direct Current Electrical Sounding*. Amsterdam Elsevier. 104pp.

Blaauw, M., Van Geel, B., Kristen, I., Plessen, B., Lyaruu, A., Engstrom, D. R., … Verschuren, D. (2011). High-resolution ^{14}C dating of a 25,000-year lake-sediment record from equatorial East Africa. *Quaternary Science Reviews,* **30**: 3043-3059.

Bo, Y., Liu, C., Jiao, P., Chen, Y., & Cao, Y. (2013). Hydrochemical characteristics and controlling factors for waters' chemical composition in the Tarim Basin, Western China. *Chemie der Erde-Geochemistry,* **73**: 343-356.

Braga, A. C., Filho, W. M., & Dourado, J. C. (2006). Resistivity (DC) Method Applied to Aquifer Protection Studies. *Brazilian Journal of Geophysics,* **24** (4): 573-581.

Brown, E. T. (2010). Lake Malawi's response to “megadrought” terminations: Sedimentary records of flooding, weathering and erosion. *Palaeogeography, Palaeoclimatology*. Article in Press (PALAEO-05263).

Burnett, A. P., Soreghan, M. J., Scholz, C. A., & Brown, E. T. (2011). Tropical East African climate change and its relation to global climate: A record from Lake Tanganyika, Tropical East Africa, over the past 90+ kyr. *Palaeogeography, Palaeoclimatology, Palaeoecology,* **303**: 155-167.

Burney, D. A. (1987a). Late Quaternary stratigraphic charcoal records from Madagascar. *Quaternary Research* **28**: 274–80.

Burney, D. A. (1987b). Late Holocene vegetational change in central Madagascar. *Quaternary Research,* **28**: 130–43.

Butzer, K. W., Isaac, G. L., Richardson, J. L., & Washbourn-Kamau, C. (1972). Radiocarbon dating of East African lake levels. *Science,* **175**: 1069–79.

Casanova J., & Hillaire-Marcel, C. (1992). Late Holocene hydrological history of Lake Tanganyika, East Africa, from isotopic data on fossil stromatolites. *Palaeogeography, Palaeoclimatology, Palaeoecology,* **91**: 35-48.

Castañeda, I. S., Werne, J. P., & Johnson, T. C. (2007). Wet and arid phases in the southeast African tropics since the Last Glacial Maximum. *Geology* **35** (9): 823–826. doi: 10.1130/G23916A.

Castañeda, I. S., Werne, J. P., Johnson, T. C., & Filley, T. R. (2009). Late Quaternary vegetation history of southeast Africa: The molecular isotopic record from Lake Malawi. *Palaeogeography, Palaeoclimatology, Palaeoecology,* **275**: 100–112.

Castañeda, I. S., Werne, J. P., Johnson, T. C., & Powers, L. A. (2011). Organic geochemical records from Lake Malawi (East Africa) of the last 700 years, part II: Biomarker evidence for recent changes in primary productivity. *Palaeogeography, Palaeoclimatology, Palaeoecology,* **303**: 140–154.

Chae, G., Yun, S., Kwon, M., Kim, Y., & Mayer, B. (2006). Batch dissolution of granite and biotite in water: Implication for fluorine geochemistry in groundwater. *Geochemical Journal,* **40**: 95 – 102.

Choudhury, K., Saha, D. K., & Chakraborty, P. (2001). Geophysical study of saline water intrusion in a coastal alluvial terrain. *Journal of Applied Geophysics,* **46**: 189-200.

Christiansen, E. H., Burt, D. M., Sheridan, M. F., & Wilson, R. T. (1983). The Petrogenesis of Topaz Rhyolites from the Western United States. *Contributions to Mineralogy and Petrology,* **83**: 16-30.

Cohen, A. S., Talbot, M. R., Awramik, S. M., Dettman, D. L., & Abell, P. (1997). Lake level and Paleoenvironmental history of Lake Tanganyika, Africa, as inferred from late Holocene and modern stromatolites. *Geological Society of America Bulletin,* **109**: 444–460.

Cohen, A. S., Lezzar, K. E., Tiercelin, J. J., & Soreghan, M. (1997). New palaeogeographic and lake-level reconstructions of Lake Tanganyika: implications for tectonic, climatic and biological evolution in a rift lake. *Basin Research,* **9**: 107-132.

Cohen, A. S., Lezzar, K. E., Cole, J., Dettman, D., Ellis, G. S., Gonneea, M. E., … Zilifi, D. (2006). Late Holocene linkages between decade–century scale climate variability and productivity at Lake Tanganyika, Africa. *Journal of Paleolimnology,* Doi: 10.1007/s10933-006-9004-y.

Cole, J. E., Dunbar, R. B., McClanahan, T. R., & Muthiga, N. A. (2000). Tropical Pacific forcing of decadal SST variability in the western Indian Ocean over the past two centuries. *Science,* **287**: 617-619.

Conway, D. (2002). Extreme rainfall events and lake level changes in east Africa: Recent events and historical precedents. The East African Great Lakes: *Limnology, Palaeolimnology and Biodiversity*, 63–92.

Crul, R. C. M. (1997). Limnology and Hydrology of Lake Tanganyika and Malawi: Intgrated Health Project (IHP-IV) M-5. In: Studies and Reports in Hydrology, 54. UNESCO, France. 111pp.

Dansgaard, W., Johnsen, S. J., Clausen, H. B., Dahl-Jensen, N. S., Gundestrup, N. S., Hammer, C. U., … Bond, G. (1993). Evidence for general instability of past climate from a 250-kyr ice-core record. *Nature,* **364**: 218 – 220.

Darbyshire, I., Lamb, H., & Umer, M. (2003). Forest clearance and regrowth in northern Ethiopia during the last 3000 years. *The Holocene,* **13**: 537–46.

De Angelis., M., & Legrand, M. (1994). Origins and variations of fluoride in Greenland precipitation. *Journal of Geophysical Research,* **99**: 1157-1172.

Dawson, J. B. (2008). The Gregory Rift Valley & Neogene – Recent Volcanoes of Northern Tanzania. *Geological Society of London*, Memoirs, 33.

DeBusk, G. H. (1997). The distribution of pollen in the surface sediments of Lake Malawi, Africa, and the transport of pollen in large lakes. *Review of Palaeobotany and Palynology,* **97**, 123-153.

DeBusk, G. H. (1998). A 37 500-year pollen record from Lake Malawi and implications for the biogeography of afromontane forests. *Journal of Biogeography,* **25**: 479-500.

Delcamp, A., Kwelwa, S., Macheyeki, A., & Kervyn, M. (2013). Multiple collapses at Mt. Meru volcano, Tanzania: remote sensing and field evidences from debris avalanche deposits, EGU General Assembly Conference Abstracts, p. 7775.

DeMenocal, P. B. (2015). End of the African Humid Period. *Nature Geoscience,* **8**: 86–87. doi: 10.1038/ngeo2355.

DeMenocal, P., Ortiz, J., Guilderson, T., Adkins, J., Sarnthein, M., Baker, L., & Yarusinsky, M. (2000). Abrupt onset and termination of the African Humid Period: rapid climate responses to gradual insolation forcing. *Quaternary Science Reviews,* **19**: 347-361.

Deocampo, D. M. (2004). Hydrogeochemistry in the Ngorongoro Crater, Tanzania, and implications for land use in a World Heritage Site. *Applied Geochemistry,* **19**: 755-767.

Deverel, S. J., Goldberg, S., & Fujii, R. (2012). Chemistry of trace elements in soils and groundwater. In: W.W Wallender and K. K. Tanji (eds.) ASCE Manual and Reports on Engineering Practice No.71, Agricultural Salinity Assessment and Management (02nd Edition). ASCE, Reston, VA. Chapter 4: 89-137.

Easterbrook, D. J. (1999). *Surface processes and Landforms*. 02nd Edition. Prentice Hall, USA. 546pp.

Edmunds, W. M., & Smedley, P. L. (2005). Fluoride in natural waters. In: Selinus, O., Alloway, B., Centeno, J. A., Finkelman, R. B., Fuge, R., Lindh, U. and Smedley, P. L. (eds.) Essentials of Medical Geology: Impacts of the natural environment on public health. *Elsevier*, pp. 301-329.

Eissa, M. A., Mahmoud, H. H., Shouakar-Stash, O., El-Shiekh, A., & Parker, B. (2016): Geophysical and geochemical studies to delineate seawater intrusion in bagoush area, northwestern coast, Egypt. *Journal of African Earth Sciences*, Doi: 10.1016/j.jafrearsci.2016.05.031.

Ekinci, Y. L., & Demirci, A. (2008): A Damped Least-Squares Inversion Program for the interpretation of Schlumberger sounding curves. *Journal of Applied Sciences* **8** (22): 4070-4078.

Elisante, E., & Muzuka, A. N. (2015). Occurrence of nitrate in Tanzanian groundwater aquifers: A review. *Applied Water Science,* **7**:71–87. Doi: 10.1007/s13201-015-0269-z.

Elisante, E., & Muzuka, A. N. (2016a). Assessment of sources and transformation of nitrate in groundwater on the slopes of Mount Meru, Tanzania. *Environmental Earth Science,* **75**:277. Doi: 10.1007/s12665-015-5015-1.

Elisante, E., & Muzuka, A. N. (2016b). Sources and seasonal variation of coliform bacteria abundance in groundwater around the slopes of Mount Meru, Arusha, Tanzania. *Environmental Monitoring Assessment*, **188**:395. Doi 10.1007/s10661-016-5384-2.

El Sayed, A. N., Barseem, M. S. M., El Deen, H. M. E., & El Din, H. A. E. (2017). Using Geo-electrical and Geochemical Techniques to Investigate the Change in Ground Water Quality-South West El Khtatbah City - Cairo-Alexandria Desert Road, Egypt. *Advanced Applied Science Research*, **8** (4):77-95.

Fawell, J., & Nieuwenhuijsen, M. J. (2003). Contaminants in drinking water. *British Medical Bulletin,* 199-208. doi: 10.1093/bmb/ldg027.

Felton, A. A., Russell, J. M., Cohen, A. S., Baker, M. E., Chesley, J. T., Lezzar, K. E., … Tiercelin, J. J. (2007). Paleolimnological evidence for the onset and termination of glacial aridity from Lake Tanganyika, Tropical East Africa. *Palaeogeography, Palaeoclimatology, Palaeoecology,* **252:** 405–423.

Finch, J., Leng, M. J., & Marchant, R. (2009). Late Quaternary Vegetation dynamics in biodiversity hotspot, the Ulugruru Mountains of Tanzania. *Quaternary Research,* **72**: 111-122.

Finch, J., Wooller, M., & Marchant, R. (2014). Tracing long term tropical montane ecosystem change in the Eastern Arc Mountains of Tanzania. *Journal of Quaternary Science,* **29** (3): 269-278.

Gaciri, S., & Davies, T. (1993). The occurrence and geochemistry of fluoride in some natural waters of Kenya. *Journal of Hydrology,* **143**: 395-412.

Garcin, Y., Williamson, D., Taieb, M., Vincens, A., Mathé, P., & Majule, A. (2006). Centennial to millennial changes in maar-lake deposition during the last 45,000 years in tropical Southern Africa (Lake Masoko, Tanzania). *Palaeogeography, Palaeoclimatology, Palaeoecology,* **239**: 334–354.

Garcin, Y., Vincens A., Williamson, D., Guiot J., & Buchet G. (2006). Wet phases in tropical southern Africa during the last glacial period. *Geophysical Research Letter*, **33**: L07703. Doi:10.1029/2005GL025531.

Gasse, F. (2000). Hydrological changes in the African tropics since the Last Glacial Maximum. *Quaternary Science Reviews,* **19**: 189–211.

Gasse, F., Barker, P., Gell, P. A., Fritz, S. C., & Chalie, F. (1997). Diatom inferred salinity in palaeolakes: an indirect tracer of climate change. *Quaternary Science Reviews* **16**: 547–63.

Ghiglieri, G., Balia, R., Oggiano, G., & Pittalis, D. (2010). Prospecting for safe (low fluoride) groundwater in the Eastern African Rift: the Arumeru District (Northern Tanzania). *Hydrology and Earth System Sciences,* **14**: 1081-1091.

Ghiglieri, G., Pittalis, D., Cerri, G., & Oggiano, G. (2012). Hydrogeology and hydrogeochemistry of an alkaline volcanic area: the NE Mt. Meru slope (East African Rift–Northern Tanzania). *Hydrology and Earth System Sciences,* **16**: 529-541.

GITEC, & WEMA (2011). Groundwater Assessment of the Pangani Basin, Tanzania. The Pangani Basin Water Board (PBWB) and the International Union for Conservation of Nature (IUCN) Report.

Glover, E., Akiti, T., & Osae, S. (2012). Major ion chemistry and identification of hydrogeochemical processes of ground water in the Accra Plains. *Geoscience* **50**: 10279-10288.

Golshan, M., Colombani, N., & Mastrocicco, M. (2018). Assessing Aquifer Salinization with Multiple Techniques along the Southern Caspian Sea Shore (Iran). *Water* **10**: 348. Doi:10.3390/w10040348.

Grumet, N. S., Dunbar, R. B., & Cole, J. E. (2000). Multisite Record of Climate Change from Indian Ocean Corals. Proceedings 9th International Coral Reef Symposium, Bali, Indonesia 23-27 October 2000, Vol. 1.

Gupta, G., Maiti, S., & Erram, V. C. (2014). Analysis of Electrical Resistivity Data in Resolving the Saline and Fresh Water Aquifers in West Coast Maharashtra. *Journal Geological Society of India,* **84**: 555-568.

Hallett, B. M. (EngD thesis) (2012). The Mineralogy of Fluoride Mobilisation to Groundwater from the Peninsular Granite, Andhra Pradesh, India.

Hallett, B. M., Dharmagunawardhane, H. A., Atal, S., Valsami-Jones, E., Ahmed S., & Burgess, W. G. (2015). Mineralogical sources of groundwater fluoride in Archaen bedrock/regolith aquifers: Mass balances from southern India and north-central Sri Lanka. *Journal of Hydrology: Regional Studies.* http://dx.doi.org/10.1016/j.ejrh. 2014.10.003.

Healy, R. W., & Cook, P. G. (2002). Using groundwater levels to estimate recharge. *Hydrogeology Journal,* **10**: 91–109.

Hewaidy, A. G. A., El-Motaal, E. A., Sultan, S. A., Ramdan, T. M., El khafif, A. A., & Soliman, S. A. (2015). Groundwater exploration using resistivity and magnetic data at the northwestern part of the Gulf of Suez, Egypt. *Egyptian Journal of Petroleum,* **24:** 255-263.

Hillaire-Marcel, C., Carro, O., & Casanova, J. (1986): ^{14}C and Th/U Dating of Pleistocene and Holocene Stromatolites from East African Paleolakes. *Quaternary Research,* **25**: 312-329.

Hodlur, G. K., Dhakate, R., Sirisha, T., & Panaskar, D. B. (2010): Resolution of freshwater and saline water aquifers by composite geophysical data analysismethods. *Hydrological Sciences Journal,* **55** (3): 414-434. Doi: 10.1080/02626661003738217.

Ingram, B. L., (1970). Determination of fluoride in silicate rocks without separation of aluminium using a specific ion electrode. *Analytical Chemistry,* **42**: 1825–1827.

Intergovernmental Panel on Climate Change (IPCC) (2007). The physical science basis. Contribution of working group I to the fourth assessment report of the Intergovernmental Panel on Climate Change (edited by: Solomon, S., Qin, D., Manning, M., Chen, Z., Marquis, M., Averyt, K. B., Tignor, M., & Miller, H.L.). Cambridge University Press. Cambridge and New York. 996 pp.

Istituto Oikos (2011). *The Mt. Meru Challenges.* Integrating Conservation and Development in Northern Tanzania. Ancora Libri, Milano (Italy). 70pp.

Jiang, Y., Wu, Y., Groves, C., Yuan, D., & Kambesis, P. (2009). Natural and anthropogenic factors affecting the groundwater quality in the Nandong karst underground river system in Yunan, China.*Journal of Contaminant Hydrology,* **109**: 49–61.

Jianwu, L. I., Ganlin, Z., & Zitong, G. (2014). Mobilization and redistribution of elements in soils developed from extreme weathering basalt on Hainan Island. Chin. *Journal of Geochemistry*, **33**: 262–271.

Jimoh, R. A., Bankole, O. M., Ahmed, K., Christopher, O. A., Adeniji, M. A., Ebhodaghe, J., … Ezima, E. A. (2018). Use of geophysical logs in hydrogeological studies and borehole designs: A case study of Apapa coastal area, Lagos, Nigeria. *Applied Water Science,* **8**:191. https://doi.org/10. 1007/s13201-018-0804-9.

Johnson, T. C., Barry, S. L., Chan, Y., & Wilkinson, P. (2001). Decadal record of climate variability spanning the past 700 yr in the Southern Tropics of East Africa. *Geology* **29** (1): 83–86.

Jouzel, J., Masson-Delmotte, V., Cattani, O., Dreyfus, G., Falourd, S., Hoffmann, G., … Wolff, E. W. (2007). Orbital and Millennial Antarctic Climate Variability over the Past 800 000 Years. *Science,* **317**: 793-796.

Kappelman, J. (1986). Plio-Pleistocene Marine-Continental Correlation Using Habitat Indicators from Olduvai Gorge, Tanzania. *Quaternary Research,* **25**: 141 -149.

Kaser, G., Mölg, T., Cullen, N. J., Hardy, D. R., & Winkler, M. (2010). Is the decline of ice on Kilimanjaro unprecedented in the Holocene? *The Holocene,* **20** (7): 1079–109.

Kaseva, M. (2006). Contribution of trona (magadi) into excessive fluorosis—A case study in Maji ya Chai ward, northern Tanzania. *Science of the Total Environment,* **366** (1): 92–100. Doi: 10.1016/j.scitotenv.2005.08.049.

Kashaigili, J. J. (2010). Assessment of groundwater availability and its current and potential use and impacts in Tanzania. Unpublished Report Prepared for the International Water Management Institute (IWMI). 97pp.

Kayanne, H., Iijima, H., Nakamura, N., McClanahan, T. R., Behera, S., & Yamagata, T. (2006). Indian Ocean Dipole index recorded in Kenyan coral annual density bands. *Geophysical Research Letters,* **33**: l19709. Doi:10.1029/2006gl027168.

Kiage, L. M., & Liu, K. (2006). Late Quaternary paleoenvironmental changes in East Africa: A review of multiproxy evidence from palynology, lake sediments, and associated records. *Progress in Physical Geography,* **30**: 633–658.

Koda, E., Tkaczyk, A., Lech, M., & Osinski, P. (2017). Application of Electrical Resistivity Data Sets for the Evaluation of the Pollution Concentration Level within Landfill Subsoil. *Applied Science,* **7**: 262. Doi:10.3390/app7030262.

Kouzana, L., Benassi, R., Ben mammou, A., & Sfar felfoul, M. (2010). Geophysical and hydrochemical study of the seawater intrusion in Mediterranean semi arid zones. A case of the Korba coastal aquifer (Cap-Bon, Tunisia). *Journal of African Earth Sciences,* **58**: 242–254.

Kuhnert, H., Kuhlmann, H., Mohtadi, M., Meggers, H., Baumann, K. H., & Pätzold, J. (2014). Holocene tropical western Indian Ocean sea surface temperatures in covariation with climatic changes in the Indonesian region. *Paleoceanography,* **29**: 423–437. Doi: 10.1002/2013PA002555.

Kumar, K. S. A., Prijub, C. P., & Prasad, N. B. N. (2015). Study on Saline Water intrusion into the Shallow Coastal Aquifers of Periyar River Basin, Kerala using Hydrochemical and Electrical Resistivity Methods. *Aquatic Procedia,* **4**:32–40. Doi: 10.1016/j.aqpro.2015.02.006.

Kumar, X. R. A., Giridharan, L., Shyamala, J., Velmurugan, P., & Jayaprakash, M. (2013). Urbanisation impact of groundwater quality in Cuddalore District, East Coast of India. *Journal of Environmental Chemistry and Ecotoxicology,* **5**: 63-73.

Lærdal, T., Talbot, M. R., & Russell, J. M. (2002). Late Quaternary Sedimentation and Climate in the Lakes Edward and George Area, Uganda – Congo. In the East African Great Lakes: *Limnology, Palaeolimnology and Biodiversity*, 415–428.

Lamb, H., Darbyshire, L., & Verschuren, D. (2003). Vegetation response to rainfall variation and human impact in central Kenya during the past 1100 years. *The Holocene,* **13**: 285–292.

Liu, K. B., & Colinvaux, P. A. (1988). A 5200-year history of Amazon rain forest. *Journal of Biogeography,* **15**: 231–248.

Long, C. J., Whitlock, C., Bartlein, P. J., & Millspaugh, S. H. (1998). A 9000-year fire history from the Oregon Coast Range based on high-resolution charcoal study. *Canadian Journal of Forest Research,* **28**: 774–787.

Lukiko, K., Machunda, R. L., & Ijumba, J. N. (2016). Regeneration of Fluoride-Saturated Bone Char by Means of Wood Ash and Heat. *Fluoride,* **49** (4 Pt 2): 549-559.

Lundblad, K., & Holmgren, K. (2005): Palaeoclimatological survey of stalagmites from coastal areas in Tanzania. *Geogarafisca Annaler. Series A, Physical Geography*, **87A** (1): 125–140.

Lutz, A., Minyila, S., Saga, B., Diarra, S., Apambire, B., & Thomas, J. (2015). Fluctuation of Groundwater Levels and Recharge Patterns in Northern Ghana. *Climate,* **3**: 1-15. Doi:10.3390/cli3010001.

Lyons, R. P., Scholz, C. A., Buoniconti, M. R., & Martin, M. R. (2011). Late Quaternary stratigraphic analysis of the Lake Malawi Rift, East Africa: An integration of drill-core and seismic-reflection data. *Palaeogeography, Palaeoclimatology, Palaeoecology,* **303**: 20–37.

MacDonald, A. M., Davies, J., & Ó Dochartaigh, B. É. (2002). Simple methods for assessing groundwater resources in low permeability areas of Africa. British Geological Survey Commissioned Report, CR/01/168N. 71pp.

MacDonald, A. M., Bonsor, H. C., Dochartaigh, B. E. O., & Taylor, R. G. (2012): Quantitative maps of groundwater resources in Africa. *Environmental Research Letter,* **7**:024009.

Machiwa, J. F. (2010). Stable carbon and nitrogen isotopic signatures of organic matter sources in near-shore areas of Lake Victoria, East Africa. *Journal of Great Lakes Research,* **36**: 1–8.

Maiti, S., Gupta, G., Erram, V. C., & Tiwari R. K. (2011). Inversion of Schlumberger resistivity sounding data from the critically dynamic Koyna region using the Hybrid Monte Carlo-based neural network approach. Nonlin. *Processes Geophysics,* **18**: 179–192.

Malago, J., Makoba, E., & Muzuka, A. N. N. (2017). Fluoride Levels in Surface and Groundwater in Africa: A Review. *American Journal of Water Science and Engineering,* **3** (1): 1-17. Doi: 10.11648/j.ajwse.20170301.11.

Maley, J., & Brenac, C. (1998). Vegetation dynamics, palaeoenvironments and climate change in the forests of western Cameroon during the last 28,000 years BP. *Review of Palaeobotany and Palynology,* **99**: 157–187.

Mann, M. E. (2007). Climate Over the Past Two Millennia. *Annual Review of Earth and Planetary Sciences,* **35**:111-136.

Mann, M. E., Zhang, Z., Hughes, M. K., Bradley, R. S., Miller, S. K., Rutherford, S., & Ni, F. (2008): Proxy-based reconstructions of hemispheric and global surface temperature variations over the past two millennia. *PNAS* **105** (36): 13252-13257.

Matias, M. S., Marques da Silva, M., Ferreira, P., & Ramalho, E. (1993). A geophysical and hydrogeological study of aquifers contamination by landfill. *Journal of Applied Geophysics*, **32**: 155-162.

Mbonu, P. D. C., Ebeniro, J. O., Ofoegbu C. O., & Ekine A. O. (1991). Geo-electric sounding for the determination of aquifer characteristics in parts of the Umuahia area of Nigeria. *Geophysics,* **56**: 284-291.

McCaffrey, L. P. (1998): Distribution and causes of high fluoride groundwater in the Western Bushveld area of South Africa. A thesis submitted in fulfillment of the requirements for the degree of Doctor of Philosophy, Department of Geological Sciences, Faculty of Science, University of Cape Town. 278 pp.

Meju, M. A., & Fontes, S. L. (1999). Regional aquifer mapping using combined VES-TEM-AMT/EMAP methods in the semi-arid eastern margin of Parnaiba basin, Brazil. *Geophysics,* **64** (2): 337-356.

Mjemah, I. C., Van Camp, M., Martens, K., & Walraevens, K. (2011). Groundwater exploitation and recharge rate estimation of a quaternary sand aquifer in Dar-es-Salaam area, Tanzania. *Environmental Earth Science,* **63**:559–569.

Mjemah I. C., Mtoni Y., Elisante E., Tungaraza C. T., Mtakwa P. W., & Walraevens K., (2012). Sources of salinity in the Quaternary sand aquifer of Dar-es-Salaam, Tanzania. In: da Silva GC Jr, and Montenegro SMGL (eds). Proceedings of the 22nd Saltwater Intrusion Meeting (SWIM), Buzios, Brazil, 17–21 June 2012, META: Buzios, Brazil, pp 264–267.

Miller, R. W., & Donahue, R. L. (1990). An introduction to soils and plant growth. 06th Edition. Prentice Hall Inc. USA.

Mohamaden, M. I. I., & Ehab, D. (2017). Application of electrical resistivity for groundwater exploration in Wadi Rahaba, Shalateen, Egypt. *NRIAG Journal of Astronomy and Geophysics,* **6**: 201–209.

Mohammed, S. M. (2002). A review of water quality and pollution studies in Tanzania. *Journal of the Human Environment,* **31**: 617-620.

Moernaut, J., Verschuren, D., Charlet, F., Kristen, I., Fagot, M., & De Batist, M. (2010). The seismic-stratigraphic record of lake-level fluctuations in Lake Challa. Hydrological stability and change in equatorial East Africa over the last 140 kyr. *Earth and Planetary Science Letters,* **290**: 214–223.

Moy, C. M., Seltzer, G. O., Rodbell, D. T., & Anderson, D. M. (2002). Variability of El Niño/Southern Oscillation activity at millennial timescales during the Holocene epoch. *Nature,* **420**: 162-165. Doi:10.1038/nature01194.

Mumbi, C. T., Marchant, R., Hooghiemstra, H., & Wooller, M. J. (2008). Late Quaternary Vegetation reconstruction from the Eastern Arc Mountains, Tanzania. *Quaternary Research,* **69**: 326-341.

Muzuka, A. N. N. (2006). Stable isotope compositions of organic carbon and contents of organic carbon and nitrogen of lacustrine sediments from sub-arid northern Tanzania. *Tanzania Journal of Science,* **32** (1).

Muzuka, A. N., & Nyandwi, N. (2002). Lake Tanganyika Holocene Record on Variability in Precipitation in the Malagarasi Catchment Basin. In the East African Great Lakes: *Limnology, Palaeolimnology and Biodiversity*, 415–428.

Muzuka, A. N. N., Ryner, M., & Holmgren, K. (2004). 12,000-Year, preliminary results of the stable nitrogen and carbon isotope record from the Empakai Crater lake sediments, Northern Tanzania. *Journal of African Earth Sciences,* **40**: 293–303.

Mwakabona, H. T., Said, M., Machunda, R. L., & Njau, K. N. (2014). Plant Biomasses for Defluoridation Appropriateness: Unlocking their Potentials. *Research Journal in Engineering and Applied Sciences,* **3**(3): 167-174.

Mworia-Maitima, J. (1991). Vegetation response to climate change in central Rift Valley. *Quaternary Research,* **35**: 234–245.

Nagaraju, A., Muralidhar, P., & Sreedhar, Y. (2016). Hydrogeochemistry and Groundwater Quality Assessment of Rapur Area, Andhra Pradesh, South India. *Journal of Geoscience and Environment Protection,* **4**, 88.

Nanyaro, J., Aswathanarayana, U., Mungure, J., & Lahermo, P. (1984). A geochemical model for the abnormal fluoride concentrations in waters in parts of northern Tanzania. *Journal of African Earth Sciences,* **2**: 129-140.

Narany, S. T., Ramli, M. F., Aris, A. Z., Sulaiman, W. N. A., Juahir, H., & Fakharian, K. (2014). Identification of the hydrogeochemical processes in groundwater using classic integrated geochemical methods and geostatistical techniques, in Amol-Babol Plain, Iran. *The Scientific World Journal, 2014* (1-16). ID: 419058. http://dx.doi.org/10. 1155/ 2014/419058.

Naseem, S., Rafique, T., Bashir, E., Bhanger, M. I., Laghari, A., & Usmani, T. H. (2010). Lithological influences on occurrence of high-fluoride groundwater in Nagar Parkar area, Thar Desert, Pakistan. *Chemosphere,* **78**: 1313–1321.

Nelson, D. M., Verschuren, D., Urban, M. A., & Hu, F. S. (2012). Long-term variability and rainfall control of savanna fire regimes in equatorial East Africa. *Global Change Biology,* **18**: 3160–3170.

Nicaise, Y., Marc, D., Abdoukarim, A., Daouda, M., & Moussa, B. (2012). Environmental Geophysical Study of the Groundwater Mineralization in a Plot of the Cotonou Littoral Zone (South Benin). *Hindawi Publishing Corporation, International Journal of Geophysics*. Article ID 329827. Doi:10.1155/2012/329827.

Nicholson, S. E. (1998). Historical fluctuations of Lake Victoria and other lakes in the northern Rift Valley of East Africa. J. T. Lehman (ed.). *Environmental Change and Response in East African Lakes,* 7-35.

Nicholson, S. E. (1998). Fluctuations of Rift Valley Lakes Malawi and Chilwa during historical times: A synthesis of Geological, Archaeological and historical information. J.T. Lehman (ed.), *Environmental Change and Response in East African Lakes,* 207-231.

Nicholson, S. E. (1999). Historical and modern fluctuations of lakes Tanganyika and Rukwa and their relationship to rainfall variability. *Climatic Change,* **41**: 53–71.

Nicholson, S. E., & Yin, X. (2001). Rainfall conditions in Equatorial East Africa during the nineteenth century as inferred from the record of Lake Victoria. *Climatic Change* **48**: 387–398.

Nielsen, J. M. (1999). East African magadi (trona): fluoride concentration and mineralogical composition. *Journal of African Earth Sciences,* **29**: 423–428. Doi:10.1016/s0899-5362(99)00107-4.

Nkotagu, H. (1996c). Application of environmental isotopes to groundwater recharge studies in a semi-arid fractured crystalline basement area of Dodoma, Tanzania. *Journal of African Earth Sciences,* **22**: 443–457.

Oettli, P., & Camberlin, P. (2005). Influence of topography on monthly rainfall distribution over East Africa. *Climate Research*, **28**: 199-212. Doi: 10.3354/cr028199.

Öberg, H., Norström, E., Ryner, M. M., Holmgren K., Westerberg, L. O., Risberg, J., … Muzuka, A. N. (2013). Environmental variability in northern Tanzania from AD 1000 to 1800, as inferred from diatoms and pollen in Lake Duluti *Palaeogeography, Palaeoclimatology, Palaeoecology,* **374**: 230-241.

Okiongbo, K. S., & Odubo, E. (2012): Geoelectric Sounding for the Determination of Aquifer Transmissivity in Parts of Bayelsa State, South South Nigeria. *Journal of Water Resource and Protection* **4**: 346-353.

Okonkwo, A. C., & Ugwu, G. Z. (2015). Determination of Dar-zarrouk parameters for prediction of Aquifer protective capacity: A case of Agbani Sandstone Aquifer, Enugu State, Southeastern Nigeria. *International Research Journal of Geology and Mining (IRJGM), (2276-6618)* **5**(2): 12-19. Doi: http://dx.doi.org/10.14303/irjgm. 2015.107.

Opdyke, B. N., Walter, L. M., & Huston, T. J. (1993). Fluoride content of foraminiferal calcite: Relations to life habitat, oxygen isotope composition, and minor element chemistry. *Geology,* **21**: 169-172.

Pangani Basin Water Board (PBWB)/International Union for Conservation of Nature (IUCN) (2008). Basin Delineation Report. Pangani Basin Water Board, Moshi and IUCN Eastern and Southern Africa Regional Programme, Nairobi, Kenya. 57 pp.

Parasinis, D. S. (1973). *Principles of Applied Geophysics*. Fifth Edition, Chapman and Hall, London. 291pp.

Patra, P. H., & Nath, S. K. (1999): Schlumberger geoelectric sounding in groundwater: principles, interpretation and application. A.A. Balkema publishers, Old post road, U.S.A. 208pp.

Peccerillo, A., Donati, C., Santo, A. P., Orlando A., Yirgu G., & Ayalew, D. (2007). Petrogenesis of silicic peralkaline rocks in the Ethiopian rift: Geochemical evidence and volcanological implications. *Journal of African Earth Sciences,* **48**: 161–173.

Pecoraino, G., D'Alessandro, W., & Inguaggiato, S. (2015). The Other Side of the Coin: Geochemistry of Alkaline Lakes in Volcanic Areas. Volcanic Lakes Chapter, Part of the series Advances in Volcanology, 219-237.

Petit J. R., Jouzel, J., Raynaud, D., Barkov N. I., Barnola, J. M., Basile, I., … Stievenard, M. (1999). Climate and atmospheric history of the past 420,000 years from the Vostok ice core, Antarctica. *Nature,* **399**: 429-436.

Peyron, O., Jolly, D., Bonnefille, R., Vincens, A., & Guiot, J. (2000). Climate of East Africa 6000 14C yr BP. as inferred from pollen data. *Quaternary Research,* **54**: 90–101.

Piperno, D. R. (1988). Phytolith analysis: an archaeological and geological perspective. San Diego: Academic Press.

Piperno, D. R., & Pearsall, D. M. (1998). The silica bodies of tropical American grasses: morphology, taxonomy and implications for grass systematics and fossil phytolith identification. *Annals of the Smithsonian Institution,* **85**: 1–40.

Pittalis, D. (2010). Interdisciplinary studies for the knowledge of the groundwater fluoride contamination in the eastern African rift: Meru District–North Tanzania. Doctoral dissertation, University of Sassari.

Powers, L. A., Johnson, T. C., Werne, J. P., Castan˜eda, I. S., Hopmans, E. C., Sinninghe Damste´ J. S., … Schouten, S. (2005). Large temperature variability in the southern African tropics since the Last Glacial Maximum. *Geophysical Research Letter,* **32**. L08706. Doi:10.1029/ 2004GL022014.

Raj, D., & Shaji, E. (2017). Fluoride contamination in groundwater resources of Alleppey, southern India. *Geoscience Frontiers,* **8**: 117-124.

Rango, T., Bianchini, G., Beccaluva, L., & Tassinari, R. (2010). Geochemistry and water quality assessment of central Main Ethiopian Rift natural waters with emphasis on source and occurrence of fluoride and arsenic. *Journal of African Earth Sciences,* **57**: 479-491.

Ravindran, A. A., Ramanujam, N., & Sudarsan, R. (2013). Delineation of Saltwater and Freshwater Interface in Beach Groundwater Study Using 2D ERI Technique in the Northern Sector of the Gulf of Mannar Coast, Tamilnadu. *Water*, **5**:1-11. Doi: 10.14294/WATER.2013.2.

Rieuwerts, J. S. (2007): The mobility and bioavailability of trace metals in tropical soils: a review. *Chemical Speciation and Bioavailability,* **19** (2): 75-85. Doi: 10.3184/ 095422907X21191.

Riwayat, A. I., Nazri, M. A. A., & Abidin, M. H. Z. (2018). Application of Electrical Resistivity Method (ERM) in Groundwater Exploration. IOP Conf. Series: *Journal of Physics:* Conf. Series 995, 012094; doi:10.1088/1742-6596/995/1/012094.

Roberts, M. A. (2002). The Geochemical and Volcanological Evolution of the Mt. Meru Region, Northern Tanzania. A dissertation submitted for the degree of Doctor of Philosophy (PhD) at the University of Cambridge, United Kingdom. 276pp.

Rohling, E. J., & Pälike, H. (2005). Centennial-scale climate cooling with a sudden cold event around 8,200 years ago. *Nature,* **434**: 975-979.

Romahn, S., Mackensen, A., Groeneveld, J., & Pätzold, J. (2014). Deglacial intermediate water reorganization: new evidence from the Indian Ocean. *Climate of the Past,* **10**: 293–303.

Ryner, M., Gasse, F., Rumes, B., & Verschuren, D. (2007). Climatic and hydrological instability in semi-arid equatorial East Africa during the late Glacial to Holocene transition: A multi-proxy reconstruction of aquatic ecosystem response in northern Tanzania. *Palaeogeography, Palaeoclimatology, Palaeoecology,* **248**: 440–458.

Said, M., & Machunda, R. L. (2014). Defluoridation of Water Supplies Using Coconut Shells Activated Carbon: Batch Studies. *International Journal of Science and Research (IJSR),* **3** (7): 2327-2331.

Salem, H. S. (1999). Detrmination of fluid transmissivity and electric transverse resistance for shallow aquifers and deep resevoirs from surface and well-log measurements. *Hydrology and Earth System Sciences,* **3** (3): 421-427.

Salzmann, U. (2000). Are savannas degraded forests? A Holocene pollen record from the Sudanian zone of NE-Nigeria. *Vegetation History and Archaeobotany,* **9**: 1–15.

Salzmann, U., Hoelzmann, P., & Morczinek, I. (2002). Late Quaternary climate and vegetation of the Sudanian zone of northeast Nigeria. *Quaternary Research,* **58**: 73–83.

Scholz, C., Johnson T. C., Cattaneo P., Malinga H., & Shana S. (1998). Initial Results of 1995 IDEAL Seismic Reflection Survey of Lake Victoria, Uganda and Tanzanian, in Lehman, J. T. (ed.), Environmental Change and Response in East African Lakes, Kluwer Academic Press.

Scholz, C. A., Cohen, A. S., Johnson, T. C., King J., Talbot M. R., & Brown, E. T. (2011). Scientific drilling in the Great Rift Valley: The 2005 Lake Malawi Scientific Drilling Project — An overview of the past 145,000 years of climate variability in Southern Hemisphere East Africa. *Palaeogeography, Palaeoclimatology, Palaeoecology,* **303**: 3–19.

Scholz, C. A., Talbot, M. R., Brown, E. T., & Lyons, R. P. (2011). Lithostratigraphy, physical properties and organic matter variability in Lake Malawi drill core sediments over the past 145 000 years. *Palaeogeography, Palaeoclimatology, Palaeoecology,* **303**: 38–50.

Schüler, L., Hemp, A., & Behling, H. (2014). Relationship between vegetation and modern pollen-rain along an elevational gradient on Kilimanjaro, Tanzania. *The Holocene,* **24** (6): 702 –713.

Senior, L. A., & Sloto, R. A. (2006). Arsenic, boron, and fluoride in ground water in and near diabase intrusions, Newark Basin, southeastern Pennsylvania: U.S. Geological Survey Scientific Investigations Report 2006-5261. 105 pp.

Shanahan, T. M., McKay, N. P., Hughen, K. A., Overpeck, J. T., Otto-Bliesner, B., Heil, C. W., … Peck, J. (2015): The time-transgressive termination of the African Humid Period. *Nature Geoscience,* **8**: 140–144. Doi: 10.1038/NGEO2329.

Sidhardhan, S., Adishkumar, S., & Jayganesh, D. (2015). A Geophysical Investigation of Resistivity and Groundwater Quality near a Corporate Solid Waste Dump. *Polish Journal of Environmental Studies,* **24** (6): 2761-2766. Doi: 10.15244/pjoes/59239.

Smedley, P. L., & Kinniburgh, D. G. (2002). A review of the source, behaviour and distribution of arsenic in natural waters. *Applied Geochemistry,* **17**: 517–568.

Sonkamble, S. (2014). Electrical Resistivity and Hydrochemical Indicators Distinguishing Chemical Characteristics of Subsurface Pollution at Cuddalore Coast, Tamil Nadu. *Journal of Geological Society of India,* **83**: 535-548.

Srinivas, Y., Hudson, O. D., Stanley, R. A., & Chandrasekar, N. (2014). Quality assessment and hydrogeochemical characteristics of groundwater in Agastheeswaram taluk, Kanyakumari district, Tamil Nadu, India. *Chinese Journal of Geochemistry* **33**: 221-235.

Ssemmanda, I., & Vincens, A. (2002). Vegetation changes and their climatic implications for the Lake Victoria region during the late Holocene. The East African Great Lakes: *Limnology, Palaeolimnology and Biodiversity*, 509–523.

Stager, J. C., Cumming, B. F., & Meeker, L. D. (1997). A 17 400-year, high resolution diatom record from Lake Victoria, East Africa. *Quaternary Research,* **47**: 81–89.

Stager, J. C., Ryves, D., Cumming, B. F., Meeker, L. D., & Beer, J. (2005). Solar variability and the levels of Lake Victoria, East Africa, during the last Millennium. *Journal of Paleolimnology,* **33**: 243–251.

Stager, J. C., Cocquyt, C., Bonnefille, R., Weyhenmeyer, C., & Bowerman, N. (2009). A late Holocene paleoclimatic history of Lake Tanganyika, East Africa. *Quaternary Research,* **72**: 47–56.

Stone J. R., Westover K. S., & Cohen A. S. (2011). Late Pleistocene paleohydrography and diatom paleoecology of the central basin of Lake Malawi, Africa. *Palaeogeography, Palaeoclimatology, Palaeoecology,* **303**: 51–70.

Sultan, S. A., Essa, K. S. A. T., Khalil, M. H., El-Nahry, A. E. H., & Galal, A. N. H. (2017). Evaluation of groundwater potentiality survey in south Ataqa-northwestern part of Gulf of Suez by using resistivity data and site-selection modeling. *NRIAG Journal of Astronomy and Geophysics,* **6**: 230–243.

Sundararajan, N., Sankaran, S., & Al-Hosni, T. K. (2012). Vertical electrical sounding (VES) and multi-electroderesistivity in environmental impact assessment studies over some selected lakes: a case study. *Environtal Earth Science,* **65**:881–895. Doi:10.1007/s12665-011-1132-7.

Talbot, M. R., & Lærdal, T. (2000): The late Pleistocene-Holocene palaeolimnology of Lake Victoria, East Africa, based upon elemental and isotopic analyses of sedimentary organic matter. *Journal of Palaeolimnology,* **23**: 141-164.

Tanzania Bureau of Standards (TBS), (2007). Environmental Management (Water Quality Standards) Regulations. 28pp.

Thevenon, F., Williamson, D., Vincens, A., Taieb, M., Merdaci, O., Decobert, M., & Buchet, G. (2003). A late-Holocene charcoal record from Lake Massoko, SW Tanzania: climatic and anthropologic implications. *The Holocene,* **13**: 785-792.

Thole, B. (2013). Ground water contamination with fluoride and potential fluoride removal technologies for east and Southern Africa. INTECH Open Access Publisher.

Thompson, L. G., Mosley-Thompson, E., Davis, M. E., & Mountaina, K. (2011). Paleoclimatic perspective on the 21st-century glacier loss on Kilimanjaro, Tanzania. *Annals of Glaciology,* **52** (59).

Thompson, L. G., Mosley-Thompson, E., Davis, M. E., Henderson, K. A., Brecher, H. H., Zagorodnov, V. S., … Beer, J. (2002). Kilimanjaro Ice Core Records: Evidence of Holocene Climate Change in Tropical Africa. *Science, **298*** (5593):589-593.

Tiepolo, M., Oberti, R., & Vannucci, R. (2002). Trace-element incorporation in titanite: constraints from experimentally determined solid/liquid partition coefficients. *Chemical Geology,* **191** (Issues 1–3): 105-119.

Tierney, J. E., Russell, J. M., Damsté, J.S., Huang, Y., & Verschuren, D. (2011). Late Quaternary behavior of the East African monsoon and the importance of the Congo Air Boundary. *Quaternary Science Reviews,* **30**: 798-807.

Tierney, J. E., Russel, J. M., Huang, Y., Sinninghe Damsite, J. S., Hopmans, E. C., & Cohen, A.S. (2008). Northern Hemisphere Controls on Tropical Southeast African climate during the past 60,000 yrs. *Science,* **322**: 252-255.

Tierney, J. E., Mayes, M. T., Meyer, N., Johnson, C., Swarzenski, P. W., Cohen, A. S., & Russel, J. M. (2010). Late-twentieth-century warming in Lake Tanganyika unprecedented since AD 500. *Nature Geoscience,* **3**: 422-425.

Tiwari, M., & Ramesh, R. (2007). Solar Variability in the Past and Paleoclimate Data Pertaining to the Southwest Monsoon. *Current Science,* **93** (4): 477-487.

Trauth, M. H., Maslin, M. A., Deino, A., & Strecker, M. R. (2005). Late Cenozoic Moisture History of East Africa. *Science,* **309**: 2051-2053.

UNICEF, (2015). Progress on sanitation and drinking water. 2015 Update and MDG assessment. United State of America. 90pp.

UNICEF, (2017). Progress on Drinking Water, Sanitation and Hygiene, Update and SDG Baselines. Geneva: World Health Organization (WHO) and the United Nations Children's Fund (UNICEF). Licence: CC BY-NC-SA 3.0 IGO.

United Nation Office for the Coordination of Humanitarian Affairs (UNOCHA), (2010). Water Scarcity and Humanitarian Action: Key Emerging Trends and Challenges. Policy Development and Studies Branch, OCHA Occasional Policy Briefing Series – No. 4. 15 pp.

United Nations Office for the coordination of Humanitarian Affairs (UNOCHA) (2016). El Niño Report in East Africa. 56pp.

Van Zijl, J. S. V. (1985). *A practical manual on the resistivity method:* National Physical Research Laboratory, Council for Scientific and Industrial Research (CSIR), Pretoria, South Africa. 135pp.

Varni, M., Comas, R., Weinzettel, P., & Dietrich, S. (2013). Application of water table fluctuation method to characterize the groundwater recharge in the Pampa plain, Argentina. *Hydrological Sciences Journal,* **58** (7): 1445–1455.

Verschuren, D., Cocquyt, C., Tibby, J., Roberts, C. N., & Leavitt, P. R. (1999). Long-term dynamics of algal and invertebrate communities in a small, fluctuating tropical soda lake. *Limnology and Oceanography*, **44** (5): 1216–1231.

Verschuren, D., Johnson, T. C., Kling, H. J., Edgington, D. N., Leavitt, P. R., Brown, E. T., … Hecky, R. E. (2002). History and timing of human impact on Lake Victoria, East Africa. *Proceedings of the Royal Society of London,* **269**: 289–294. Doi 10.1098/rspb.2001. 1850.

Verschuren, D., Damste´, J. S. S., Moernaut, J., Kristen, I., Blaauw, M., Fagot, M., & Haug, G. H. (2009). Half-precessional dynamics of monsoon rainfall near the East African Equator. *Nature,* **462**. Doi:10.1038/nature 08520.

Vincens, A., Williamson, D., Thevenon, F., Taieb, M., Buchet, G., Decobert, M., & Thouveny, N. (2003). Pollen-based vegetation changes in southern Tanzania during the last 4200 years: Climate change and/or human impact. *Palaeogeography, Palaeoclimatology, Palaeoecology,* **198**: 321-334.

Vye-Brown, C., Crummy, J., Smith, K., Mruma, A., & Kabelwa, H. (2014). Volcanic hazards in Tanzania.

Wang, W., Li, R., Tan, J., Luo, K., Yang, L., Li, H., & Li, Y. (2002). Adsorption and leaching of fluoride in soils of China. *Fluoride,* **35** (2): 122-129.

Weight, D. W., & Sonderegger, L. J. (2001). *Manual of Applied Field Hydrogeology*, McGraw-Hill, U.S.A. 56pp.

Weldeab, S., Menke, V., & Schmiedl, G. (2014). The pace of East African monsoon evolution during the Holocene. *Geophysical Research Letters,* **41**: 1724–1731, doi:10.1002/ 2014GL059361.

Whitlock, C., & Millspaugh, S. H. (1996). Testing the assumptions of fire history studies: an examination of modern charcoal accumulation in Yellowstone National Park, USA. *The Holocene,* **6**: 7–15.

Wick, K., Heumesser, C., & Schmid, E. (2012). Groundwater nitrate contamination: Factors and indicators. *Journal of Environmental Management,* **111** (3): 178–186.

Wilcox, L. V. (1955). *Classification and use of irrigation water*. Washington: USDA, Circular 969, Wash., U.S. Department of Agriculture, DC.19pp.

Wilkinson C., Downie C., & Cattermole P. J. (1983). Geological map of Arusha, Tanzania, Quarter Degree Sheet 55, with brief geological explanation. A map under Geological Survey of Tanzania. United Kingdom Directorate of Overseas Survey, UK.

Wilkinson, P., Mitchell, J., Cattermole, P., & Downie, C. (1986). Volcanic chronology of the Meru-Kilimanjaro region, northern Tanzania: *Journal of the Geological Society of London,* **143 (**10): 601-605.

Wilson, S. R., Inghamb, M., & McConchiea, J. A. (2006). The applicability of earth resistivity methods for saline interface definition. Journal of Hydrology **316**: 301–312.

Wolff, C., Haug, G. H., Timmermann, A., Damsté, J. S. S., Brauer, A., Sigman, D. M., Cane, M. A., & Verschuren, D. (2011). Reduced Interannual Rainfall Variability in East Africa During the Last Ice Age. *Science,* **333**: 743-747. Doi: 10.1126/science. 1203724.

Wolff, C., Jenny, I. K., Schettler, G., Plessen, B., Meyer, H., Dulski, P., … Haug, G. H. (2014). Modern seasonality in Lake Challa (Kenya/Tanzania) and its sedimentary documentation in recent lake sediments. *Limnology and Oceanography,* **59** (5): 1621–1636.

Wooller, M. J., Street-Perrott, F. A., & Agnew, A. D. Q. (2000). Late Quaternary fires and grassland palaeoecology of Mount Kenya, East Africa: evidence from charred grass cuticles in lake sediments. *Palaeogeography, Palaeoclimatology, Palaeoecology,* **164**: 207–30.

World Health Organization (WHO), (2008). *Guidelines for drinking water quality.* Third Edition, incorporating the first and second addenda, Volume 1, Recommendations. WHO, Geneva. 515 pp.

World Health Organization (WHO), (2011). *Guidelines for drinking water quality*. Fourth Edition. 564pp.

World Health Organization Sustainable Development and Healthy Environments (WHO-SDE) (1999): El Niño and Health. Protection of the Human Environment Task Force on Climate and Health, Geneva. 108pp.

Yadav, G. S., Singh, P. N., & Srivastava, K. M. (1997). Fast method of resistivity sounding for shallow groundwater investigations. *Journal of Applied Geophysics,* **36**: 45-52.

Zalasiewicz, J., & Williams, M. (2009). A Geological History of Climate Change. In: Letcher, T. M (Ed.), Climate Change: Observed Impacts on Planet Earth, Chapter 6. Elsevier Science; First edition: 127-142.

Zinke, J., Pfeiffer, M., Timm, O., Dullo, W. C., & Davies, G. R. (2005). Atmosphere–ocean dynamics in the Western Indian Ocean recorded in corals. *Philosophical Transactions of the Royal Society A,* **363**: 121–142.

Zinke, J., Pfeiffer, M., Timm, O., Dullo, W., & Brummer, G. J. A. (2009). Western Indian Ocean marine and terrestrial records of climate variability: a review and new concepts on land–ocean interactions since AD 1660. *International Journal of Earth Science, (Geol Rundsch),* **98**:115–133.

APPENDICES

Appendix 1: Major element composition (%) in Arumeru rocks

R_ID	R-Name	SiO_2	K_2O	CaO	TiO_2	Fe_2O_3	Al_2O_3	MnO	ZnO	MgO	BaO	Na_2O	P_2O_5	F	L.O.I
MR-02	Andesite	57.30	0.65	5.80	2.17	11.80	17.00	0.30	0.03	0.65	0.58	1.97	0.00	0.317	1.34
MR-03	Andesite	57.20	0.94	4.67	1.56	11.40	17.00	0.33	0.04	0.64	0.47	3.65	0.00	0.483	0.68
MR-22	Andesite	62.10	1.27	1.94	0.73	9.72	18.00	0.37	0.05	0.24	0.12	3.44	0.00	0.621	0.86
MR-45	Andesite	59.60	1.41	7.89	2.89	18.30	0.00	0.51	0.05	0.84	0.55	3.91	0.00	0.025	2.26
MR-46	Andesite	58.40	0.80	5.87	1.90	11.70	16.00	0.31	0.03	0.51	0.47	2.83	0.00	0.036	0.42
MR-48B	Andesite	59.50	0.75	5.81	1.84	11.30	16.00	0.31	0.03	0.54	0.46	2.83	0.00	1.263	0.41
MR-51	Andesite	57.60	0.74	6.21	2.43	13.20	15.00	0.33	0.03	0.58	0.47	1.99	0.00	1.187	1.10
MR-12	Basalt	49.30	0.88	9.08	3.57	16.54	15.00	0.38	0.03	0.76	0.00	2.19	0.00	0.077	1.39
MR-30	Basalt	50.40	1.43	13.00	4.74	22.93	0.00	0.63	0.06	1.31	0.00	3.46	0.00	0.193	1.24
MR-38	Basalt	49.00	1.32	8.92	3.33	15.40	15.00	0.43	0.03	0.76	0.00	3.31	0.00	0.319	0.82
MR-49	Basalt	48.20	1.09	9.86	3.63	17.47	13.00	0.42	0.03	0.59	0.00	2.80	0.00	0.596	1.25
MR-62	Basalt	46.30	1.26	8.57	3.39	15.85	16.00	0.49	0.04	0.88	0.00	3.30	0.00	0.035	3.27
MR-01	Basaltic Andesite	56.30	0.63	4.99	1.84	12.00	17.00	0.37	0.04	0.60	0.65	1.50	0.00	1.471	3.55
MR-33B	Basaltic Andesite	52.20	1.11	12.90	4.71	22.74	0.00	0.62	0.05	1.11	0.00	3.55	0.00	0.711	1.29
MR-36	Basaltic Andesite	56.10	0.89	7.14	1.91	11.50	16.00	0.30	0.03	0.58	0.47	2.13	0.00	0.530	1.70
MR-47	Basaltic Andesite	55.90	1.09	3.21	0.84	9.80	18.00	0.26	0.04	0.19	0.33	4.28	0.00	0.033	4.81
MR-05	Basaltic trachandesit	54.40	1.37	5.05	1.77	12.40	17.00	0.34	0.03	0.65	0.50	4.41	0.00	1.604	1.39
MR-48	Basaltic trachy andes	54.30	1.14	5.58	1.78	10.80	17.00	0.30	0.03	0.48	0.45	4.54	0.00	0.990	2.15
MR-32	Calcareous mudstone	31.60	2.52	10.50	4.51	22.16	15.00	0.43	0.04	0.75	0.00	3.98	0.00	0.301	9.34
MR-39	Dacite	63.20	0.85	3.55	0.91	8.62	17.00	0.42	0.05	0.18	0.38	2.87	0.00	0.093	1.56
MR-13	Foidite	38.40	3.09	11.10	4.04	17.91	13.00	0.37	0.04	1.14	0.00	4.06	1.10	0.311	7.62

Appendix 1 continued

R_ID	R-Name	SiO_2	K_2O	CaO	TiO_2	Fe_2O_3	Al_2O_3	MnO	ZnO	MgO	BaO	Na_2O	P_2O_5	F	L.O.I
MR-20	Foidite	38.72	2.54	9.93	3.89	19.67	15.00	0.45	0.04	0.74	0.00	5.40	0.00	0.283	3.79
MR-04	Foidite	40.50	1.66	13.70	4.66	20.04	14.00	0.51	0.04	0.85	0.00	0.55	0.00	0.414	2.82
MR-07	Foidite	30.70	1.67	11.90	6.13	26.58	11.00	0.46	0.03	0.42	0.00	1.31	0.00	0.181	9.92
MR-08	Foidite	37.70	2.16	13.00	5.77	25.57	10.00	0.46	0.03	0.49	0.00	2.37	0.00	0.250	4.13
MR-09	Foidite	30.90	1.45	11.50	6.10	26.94	11.00	0.47	0.04	0.40	0.00	0.96	0.00	0.189	9.91
MR-10	Foidite	38.10	1.88	13.40	4.27	18.74	15.00	0.49	0.04	0.86	0.00	3.51	1.30	0.091	2.58
MR-11	Foidite	38.70	1.86	13.20	4.61	19.48	14.00	0.44	0.03	0.72	0.00	4.35	1.20	0.121	2.24
MR-15	Foidite	30.30	3.24	10.20	4.01	19.90	14.00	0.42	0.04	0.75	0.00	3.33	0.00	0.697	12.84
MR-16	Foidite	27.30	2.14	16.20	4.77	28.50	0.00	0.71	0.08	2.35	1.30	12.58	1.30	0.489	2.84
MR-17	Foidite	42.50	3.42	14.60	5.42	26.02	0.00	0.62	0.05	0.97	0.00	5.45	0.00	1.912	0.95
MR-18	Foidite	36.80	1.63	15.20	5.40	24.47	11.00	0.47	0.03	0.55	0.00	4.39	0.00	0.154	0.00
MR-19	Foidite	37.90	2.13	13.60	5.00	20.31	14.00	0.47	0.04	0.64	0.00	4.84	1.20	0.182	0.80
MR-25	Foidite	39.90	1.14	13.80	5.29	22.18	12.00	0.45	0.03	0.59	0.00	3.17	1.20	0.787	0.00
MR-27	Foidite	39.10	1.16	12.90	4.75	20.07	13.00	0.44	0.03	0.65	0.00	2.92	1.30	0.259	0.30
MR-28	Foidite	39.10	1.12	18.30	6.43	28.10	0.00	0.56	0.04	0.66	0.00	3.19	1.60	0.275	0.19
MR-29	Foidite	42.10	2.18	10.60	4.16	18.67	14.00	0.45	0.04	0.75	0.00	6.26	0.00	0.227	1.44
MR-33A	Foidite	39.80	2.99	12.20	3.86	15.90	15.00	0.42	0.03	0.84	0.00	1.63	0.00	0.206	7.86
MR-34	Foidite	42.10	2.44	9.62	3.52	17.03	14.00	0.47	0.04	0.84	0.00	5.35	0.00	0.581	5.21
MR-37	Foidite	35.20	3.59	12.80	4.20	17.57	14.00	0.41	0.03	0.70	0.00	1.83	0.00	0.583	10.24
MR-40	Foidite	42.70	2.30	9.56	3.07	16.50	15.00	0.50	0.05	1.01	0.77	6.24	0.00	0.062	2.69
MR-42	Foidite	39.10	2.45	10.90	3.34	17.66	15.00	0.52	0.05	1.01	0.72	6.78	0.00	0.147	2.95
MR-52	Foidite	36.60	1.43	14.40	5.48	24.35	11.00	0.47	0.04	0.52	0.00	3.46	1.20	1.207	0.38
MR-53	Foidite	40.20	1.23	14.20	4.96	21.61	13.00	0.46	0.03	0.61	0.00	2.77	0.00	0.257	0.88
MR-56	Foidite	39.70	1.10	13.20	5.11	22.11	12.00	0.43	0.03	0.57	0.00	3.24	1.30	0.408	0.56

Appendix 1 continued

R_ID	R-Name	SiO_2	K_2O	CaO	TiO_2	Fe_2O_3	Al_2O_3	MnO	ZnO	MgO	BaO	Na_2O	P_2O_5	F	L.O.I
MR-57	Foidite	32.50	1.55	11.90	5.97	26.33	11.00	0.46	0.04	0.42	0.00	0.92	0.00	0.378	9.84
MR-58	Foidite	30.00	1.69	13.50	4.46	20.03	15.00	0.52	0.04	1.01	0.00	5.88	1.20	0.146	6.68
MR-50	Picro basalt	41.50	1.07	17.80	6.32	28.62	0.00	0.58	0.04	0.74	0.00	1.35	1.40	0.085	1.02
MR-06	Tephrite Basanite	43.50	1.18	9.82	2.92	16.60	16.00	0.50	0.05	1.01	0.72	4.57	0.00	0.095	2.29
MR-14	Tephrite Basanite	43.90	1.15	12.60	4.74	20.08	12.00	0.41	0.03	0.57	0.00	3.50	0.00	0.601	0.05
MR-23	Tephrite Basanite	43.20	1.14	12.40	4.66	20.28	13.00	0.45	0.03	0.62	0.00	3.16	0.00	0.537	0.48
MR-24	Tephrite Basanite	41.20	0.93	11.80	4.37	18.10	14.00	0.46	0.04	0.84	0.00	2.95	0.90	0.635	4.09
MR-26	Tephrite Basanite	44.90	1.75	7.47	2.15	14.90	17.00	0.42	0.04	0.96	0.69	5.12	0.00	0.279	5.19
MR-31	Tephrite Basanite	41.80	2.64	10.30	3.63	17.11	15.00	0.49	0.04	1.00	0.00	4.40	0.95	0.207	2.86
MR-35	Tephrite Basanite	44.40	1.39	9.25	2.23	15.10	16.00	0.49	0.06	1.15	0.78	4.16	0.00	0.187	4.08
MR-41	Tephrite Basanite	44.20	1.86	9.48	3.31	16.49	16.00	0.49	0.05	0.96	0.00	4.70	0.00	0.133	2.27
MR-52B	Tephrite Basanite	41.30	1.71	12.70	4.11	18.86	15.00	0.46	0.04	0.81	0.00	3.80	0.00	0.881	4.55
MR-54	Tephrite Basanite	42.20	1.22	11.10	4.03	18.15	14.00	0.41	0.03	0.67	0.00	2.73	1.10	0.212	1.23
MR-55	Tephrite Basanite	42.60	1.13	13.30	4.92	21.32	12.00	0.43	0.03	0.57	0.00	3.43	1.40	0.237	0.75
MR-59	Tephrite Basanite	42.20	1.33	10.70	3.72	17.28	15.00	0.51	0.05	1.00	0.00	3.73	0.00	0.079	4.12
MR-60	Tephrite Basanite	44.30	1.37	10.60	4.08	17.75	14.00	0.42	0.03	0.63	0.00	4.53	0.00	0.238	0.59
MR-61	Tephrite Basanite	43.00	0.94	12.80	5.09	21.14	13.00	0.39	0.03	0.52	0.00	2.26	1.30	0.092	0.00
MR-64	Tephrite Basanite	44.60	0.82	7.30	3.54	16.80	16.00	0.53	0.04	0.71	0.00	6.93	0.00	0.055	3.61
MR-21	Trachyandesite	57.50	2.31	3.14	0.84	10.10	17.00	0.46	0.05	0.41	0.20	4.69	0.00	0.159	2.62
MR-44	Trachyandesite	58.70	1.48	4.15	1.20	10.30	16.00	0.33	0.04	0.61	0.48	5.83	0.00	0.102	0.99
MR-43	Trachybasalt	47.40	1.41	12.60	4.39	23.04	0.00	0.74	0.08	1.60	0.00	4.17	0.00	0.067	4.30
MR-63	Trachy-basalt	49.70	4.30	12.20	4.96	23.30	0.00	0.66	0.06	1.21	0.00	2.93	0.00	0.072	0.32
MR-65	Trachy-basalt	47.70	1.19	8.92	3.27	14.96	16.00	0.45	0.04	0.80	0.00	3.84	0.00	0.025	2.08

Appendix 2: Trace element composition (ppm) in Arumeru rocks

R_ID	R-Name	S	V	W	Sr	Rb	Cu	Cr	Y	U	Pb	As	Ni	Nb	Ag	Cl
MR-02	Andesite	0	697	141	1404	114	13.0	33.2	20.0	0.0	32.9	15.0	0.0	2.0	0.0	723
MR-03	Andesite	388	453	126	1232	141	12.7	26.0	14.0	0.0	34.6	7.0	0.0	2.0	0.0	1753
MR-22	Andesite	468	181	163	460	162	45.2	10.7	14.0	0.0	37.4	7.0	0.0	2.0	0.0	2472
MR-45	Andesite	404	540	145	1142	124	11.9	12.0	18.0	0.0	32.8	11.0	0.0	2.0	0.0	447
MR-46	Andesite	421	500	96	1032	130	12.2	16.2	19.0	0.0	28.7	13.0	0.0	2.0	0.0	1727
MR-48B	Andesite	452	520	136	1069	146	25.4	18.1	20.0	0.0	31.6	10.0	0.0	2.0	0.0	2076
MR-51	Andesite	364	590	119	1170	95	12.2	20.5	20.0	0.0	29.6	14.0	0.0	2.0	0.0	1152
MR-12	Basalt	806	654	117	1563	75	28.0	12.6	20.0	0.0	30.9	16.0	0.0	2.0	0.0	325
MR-30	Basalt	827	876	175	1965	89	52.2	19.2	26.0	0.0	33.3	22.0	0.0	3.0	0.0	1232
MR-38	Basalt	434	710	104	1514	83	22.4	15.8	21.0	0.0	28.4	15.0	15.0	2.0	0.0	812
MR-49	Basalt	513	754	160	1243	69	13.0	11.2	22.0	0.0	25.1	16.0	0.0	2.0	0.0	249
MR-62	Basalt	696	774	135	1747	101	59.7	11.5	23.0	0.0	30.1	15.0	13.0	3.0	0.0	305
MR-01	Basaltic Andesite	328	646	228	1129	97	8.7	17.5	15.0	0.0	34.0	13.0	0.0	2.0	0.0	464
MR-33B	Basaltic Andesite	848	753	140	1635	81	30.6	19.2	22.0	0.0	33.1	19.0	0.0	3.0	17.0	1185
MR-36	Basaltic Andesite	401	519	177	0	124	12.0	9.5	18.0	0.0	28.7	13.0	0.0	2.0	0.0	1770
MR-47	Basaltic Andesite	397	262	174	396	149	26.2	8.5	11.0	0.0	35.1	6.0	0.0	2.0	0.0	0
MR-05	Basaltic trachandesit	396	533	209	1270	141	12.2	17.3	14.0	0.0	34.2	12.0	0.0	2.0	0.0	1387
MR-48	Basaltic trachy andes	538	456	121	1026	136	33.1	14.9	18.0	0.0	46.4	10.0	0.0	2.0	0.0	590
MR-32	Calcareous mudstone	518	781	131	1453	79	52.8	21.5	26.0	0.0	37.8	27.0	22.0	3.0	0.0	451
MR-39	Dacite	350	365	206	320	121	3.3	12.3	20.0	0.0	26.3	0.0	0.0	3.0	0.0	286
MR-13	Foidite	719	799	73	2418	154	22.1	16.1	20.0	0.0	30.8	22.0	0.0	2.0	16.0	240

Appendix 2 Continued

R_ID	R-Name	S	V	W	Sr	Rb	Cu	Cr	Y	U	Pb	As	Ni	Nb	Ag	Cl
MR-20	Foidite	673	842	149	1507	57	16.5	21.3	23.0	0.0	34.0	25.0	14.0	2.0	0.0	967
MR-04	Foidite	896	1030	125	1818	71	54.6	14.4	27.0	0.0	32.5	25.0	14.0	3.0	0.0	434
MR-07	Foidite	601	723	69	886	29	28.4	27.9	22.0	0.0	30.9	33.0	37.0	2.0	0.0	277
MR-08	Foidite	741	724	164	1017	45	55.9	32.0	23.0	0.0	34.7	29.0	26.0	2.0	0.0	386
MR-09	Foidite	820	708	144	795	32	53.1	25.6	21.0	0.0	33.3	31.0	33.0	2.0	0.0	358
MR-10	Foidite	532	962	160	1891	82	30.9	15.5	24.0	0.0	29.8	25.0	13.0	3.0	22.0	0
MR-11	Foidite	471	865	116	1649	80	43.9	19.4	26.0	0.0	32.0	23.0	18.0	2.0	20.0	934
MR-15	Foidite	690	635	88	1419	121	39.1	17.1	20.0	0.0	34.1	19.0	13.0	2.0	16.0	599
MR-16	Foidite	797	872	145	2247	82	32.1	21.9	22.0	0.0	41.1	16.0	0.0	2.0	0.0	546
MR-17	Foidite	855	773	81	1415	126	31.5	30.7	20.0	0.0	40.6	21.0	11.0	2.0	18.0	1392
MR-18	Foidite	539	877	80	1205	44	49.4	30.5	24.0	0.0	29.7	29.0	22.0	2.0	18.0	837
MR-19	Foidite	1160	792	166	1388	78	40.9	23.3	25.0	0.0	32.1	27.0	11.0	3.0	0.0	876
MR-25	Foidite	926	783	149	1283	48	44.4	15.4	24.0	0.0	27.0	30.0	19.0	2.0	19.0	1026
MR-27	Foidite	1234	989	214	1460	74	24.1	18.5	27.0	0.0	31.0	24.0	0.0	2.0	17.0	1272
MR-28	Foidite	560	986	230	1241	46	65.0	27.8	27.0	0.0	30.4	34.0	22.0	2.0	20.0	1178
MR-29	Foidite	926	771	184	1654	72	27.2	17.1	27.0	0.0	30.8	27.0	0.0	0.0	0.0	241
MR-33A	Foidite	457	887	116	1822	205	17.9	12.9	26.0	0.0	30.7	17.0	0.0	2.0	20.0	0
MR-34	Foidite	525	763	89	1637	92	27.7	14.1	23.0	0.0	34.4	17.0	11.0	3.0	0.0	442
MR-37	Foidite	504	791	202	1686	89	61.0	12.1	25.0	0.0	33.3	25.0	15.0	2.0	0.0	0
MR-40	Foidite	586	1020	182	2075	108	23.6	10.8	24.0	0.0	31.7	20.0	14.0	3.0	0.0	511
MR-42	Foidite	710	919	182	2155	86	26.1	16.1	28.0	0.0	34.6	19.0	16.0	3.0	0.0	916
MR-52	Foidite	778	893	184	1205	42	59.1	32.7	28.0	0.0	29.9	39.0	0.0	2.0	0.0	942
MR-53	Foidite	660	897	144	1364	78	58.2	30.3	25.0	0.0	27.2	26.0	0.0	2.0	0.0	932
MR-56	Foidite	687	1013	178	1225	29	37.0	17.3	23.0	0.0	29.3	25.0	12.0	2.0	0.0	342

Appendix 2 continued

R_ID	R-Name	S	V	W	Sr	Rb	Cu	Cr	Y	U	Pb	As	Ni	Nb	Ag	Cl
MR-57	Foidite	688	780	194	869	32	52.3	31.5	24.0	0.0	34.6	30.0	27.0	2.0	0.0	0
MR-58	Foidite	625	927	97	2088	94	47.4	13.2	27.0	0.0	26.2	25.0	12.0	3.0	0.0	0
MR-50	Picro basalt	3155	834	116	1327	53	56.1	15.0	28.0	0.0	28.2	30.0	15.0	2.0	0.0	865
MR-06	Tephrite Basanite	1024	850	101	2054	104	24.7	17.4	24.0	0.0	34.0	16.0	0.0	3.0	0.0	1286
MR-14	Tephrite Basanite	1126	830	168	1348	72	43.3	26.0	25.0	0.0	27.1	31.0	17.0	2.0	19.0	1082
MR-23	Tephrite Basanite	1040	781	141	1411	78	36.8	15.2	26.0	0.0	29.0	24.0	11.0	2.0	15.0	0
MR-24	Tephrite Basanite	1256	820	90	1821	82	7.0	15.6	22.0	0.0	33.3	19.0	0.0	2.0	0.0	0
MR-26	Tephrite Basanite	639	771	116	1915	102	26.0	18.9	20.0	0.0	31.3	13.0	11.0	2.0	0.0	0
MR-31	Tephrite Basanite	754	1012	222	2018	84	27.6	12.2	25.0	0.0	33.8	19.0	12.0	3.0	0.0	439
MR-35	Tephrite Basanite	536	859	127	2230	117	15.3	14.8	25.0	0.0	51.5	13.0	0.0	3.0	0.0	841
MR-41	Tephrite Basanite	497	893	165	2037	118	102.7	21.7	24.0	0.0	38.3	18.0	0.0	3.0	0.0	1550
MR-52B	Tephrite Basanite	426	1049	145	1741	48	53.2	15.0	28.0	0.0	29.9	24.0	15.0	3.0	0.0	233
MR-54	Tephrite Basanite	2223	727	125	92	90	34.5	16.6	22.0	0.0	29.5	23.0	18.0	2.0	0.0	0
MR-55	Tephrite Basanite	555	862	104	1314	67	49.5	21.1	27.0	0.0	28.7	27.0	12.0	2.0	0.0	431
MR-59	Tephrite Basanite	538	964	98	471	83	26.3	13.0	21.0	0.0	29.9	17.0	0.0	3.0	0.0	247
MR-60	Tephrite Basanite	409	748	199	1395	88	34.0	22.8	24.0	0.0	30.6	23.0	14.0	2.0	0.0	509
MR-61	Tephrite Basanite	1350	871	130	1212	69	1005.6	22.4	25.0	0.0	25.4	27.0	15.0	2.0	0.0	812
MR-64	Tephrite Basanite	653	754	143	493	109	19.1	11.6	24.0	0.0	53.2	19.0	0.0	3.0	0.0	0
MR-21	Trachyandesite	461	212	149	685	211	52.2	11.8	14.0	0.0	45.2	6.0	0.0	2.0	0.0	1226
MR-44	Trachyandesite	447	481	103	1191	146	25.0	21.5	10.0	0.0	39.7	0.0	0.0	2.0	0.0	1830
MR-43	Trachybasalt	574	979	118	2228	84	23.5	15.0	23.0	0.0	36.3	17.0	10.0	3.0	0.0	469
MR-63	Trachy-basalt	656	790	129	1649	100	77.1	21.3	24.0	0.0	46.9	17.0	0.0	3.0	0.0	1468
MR-65	Trachy-basalt	724	759	161	1713	104	26.7	17.2	22.0	0.0	28.4	16.0	0.0	3.0	0.0	543

Appendix 3: Chemical composition of the soils from Arumeru area

SL_ID	ARS-10	ARS-21	ARS-08	ARS-31	ARS-02	ARS-03	ARS-04	ARS-06	ARS-07	ARS-11	ARS-12	ARS-13	ARS-14	ARS-15	ARS-16
S_type	AL	AL	LC	LC	RESD	RESD	RESD	RESD	RESD	RESD	RESD	RESD	RESD	RESD	RESD
Comp (%)															
SiO_2	28.8	30.2	33.7	27.35	30.6	25.8	30.15	34.09	29.7	44.4	24.4	29.3	25	31.5	32.7
K_2O	1.74	1.10	2.67	2.29	1.21	2.66	1.23	1.54	1.64	1.67	0.86	2.19	1.09	1.18	1.77
CaO	4.23	3.89	3.42	4.36	3.28	3.62	3.87	3.38	3.99	2.85	4	3.04	3.48	3.47	3.37
TiO2	4.54	4.99	4.82	5.99	4.05	4.73	3.96	4.27	4.88	3.07	4.89	4.17	6.25	4.41	4.27
Fe_2O_3	14.57	17.19	12.31	17.7	12.28	13.23	13.39	11.84	14.99	9.44	15.73	9.27	13.52	16.18	13.94
Al_2O_3	30.94	30.48	26.84	29.03	26.64	29.83	29.71	24.27	28.75	25.44	29.22	17.66	29.76	28.46	27.88
MnO	0.542	0.482	0.478	0.621	0.531	0.509	0.558	0.445	0.471	0.32	0.532	0.519	0.749	0.574	0.451
ZnO	0.054	0.044	0.04	0.045	0.035	0.035	0.033	0.043	0.036	0.039	0.032	0.065	0.077	0.036	0.044
SrO	0.74	0.546	0.651	1.05	0.722	0.718	0.736	0.68	0.671	0.551	0.63	0.832	1.05	0.643	0.585
BaO	0	0	0	0	0	0	0	0	0	0	0	0	0	0	0
Na_2O	3.59	2.87	5.31	4.79	1.00	6.51	2.71	2.21	5.03	2.66	1.38	3.19	1.25	1.97	1.32
P2O5	0	0	1.2	0	0	1.2	0	0	1.1	0	0	1.5	1.5	1.2	1.2
F	0.08	0.16	0.15	0.77	0.20	0.24	0.21	0.21	0.21	0.06	0.39	0.15	0.10	0.18	0.19
L.O.I	10.24	8.34	9.23	6.62	19.29	12.34	11.93	17.74	8.2	9.82	17.42	27.69	15.73	9.37	11.64
Comp (ppm)															
S	1422	1175	1383	2420	1231	1607	763	1486	2398	828	1221	2054	955	1584	1209
V	807	931	824	819	769	718	739	773	836	653	845	683	678	811	828
W	93	151	150	140	187	174	155	162	179	163	154	134	49	210	183
Sr	1343	1213	1248	1740	1303	1260	1455	1242	1307	1120	1292	1322	1176	1303	1217
Rb	74	49	66	58	58	66	73	74	71	84	43	49	72	82	72
Cu	27.7	45.2	135.5	50.3	22.1	80.6	16.7	28.3	45.6	63.5	33.0	77.0	40.4	44.7	68.8
Cr	12.6	14.3	15.6	12.1	14.4	19.7	24.7	16.5	11.9	7.8	16.8	19.5	9.0	16.6	19.8
Y	23	27	25	23	22	26	22	23	25	22	29	24	27	28	26
U	0	0	0	0	0	0	0	0	0	0	0	0	0	0	0
Pb	25.87	30.81	38.60	27.25	30.44	35.17	26.77	26.24	22.32	24.84	27.02	32.29	26.54	29.26	25.48
As	21	36	29	35	22	26	26	20	28	21	32	24	23	29	28
Ni	17	19	17	15	18	18	20	14	17	0	0	15	18	16	22
Nb	2	2	2	2	2	2	2	2	2	2	2	2	2	3	2
Ag	0	0	0	0	0	0	0	0	0	0	0	0	0	0	0
Cl	327	247	258	294	302	385	0	1036	0	0	0	0	0	295	0

AL: Alluvial soils, LC: Lacustrine soils, RESD: Residual soils, TRANS: Transported soils (mbuga)

Appendix 3 continued

SL_ID	ARS-17	ARS-18	ARS-20	ARS-22	ARS-24	ARS-27	ARS-28B	ARS-29	ARS-29B	ARS-30	ARS-31B	ARS-32	ARS-33	ARS-01	ARS-25	ARS-05	ARS-23
S_type	RESD	RESD	RESD	RESD	RESD	RESD	RESD	RESD	RESD	RESD	RESD	RESD	RESD	RSD	TRANS	TRANS	TRANS
Comp (%)																	
SiO_2	25.01	30.2	31.2	44.4	31.9	13.9	47.1	32.7	31.79	31.1	30.63	31.04	35.3	25.8	30.29	29.1	37.1
K_2O	1.48	1.26	0.71	1.92	0.81	0.51	0.93	0.42	0.08	1.21	0.99	2.09	1.84	1.50	1.25	2.54	1.51
CaO	3.63	3.62	2.74	2.99	3.18	3.12	2.36	2.73	3.56	3.76	3.15	3.91	4.22	3.22	2.99	4.03	3.8
TiO2	6.86	4.55	4.08	3.69	4.59	6.02	2.29	6.07	5.27	4.63	4.83	4.76	5.43	2	3.91	3.81	4.5
Fe_2O_3	14.05	13.6	10.95	10.5	13.62	13.61	9.41	15.71	14.37	14.83	14.79	14.84	17.98	9.19	12.82	14.16	14.85
Al_2O_3	26.12	24.64	27.46	22.48	28	23.85	24.14	24.7	24.78	28.18	27.66	29.74	27.35	22.17	30.72	30.54	26.04
MnO	0.753	0.474	0.552	0.46	0.537	0.812	0.399	0.24	0.563	0.513	0.629	0.565	0.493	0.256	0.44	0.469	0.48
ZnO	0.077	0.04	0.032	0.046	0.043	0.1	0.046	0.039	0.044	0.035	0.044	0.046	0.031	0.021	0.041	0.035	0.036
SrO	1.45	0.69	0.565	0.757	0.699	0.449	0.656	0.34	0.763	0.58	0.662	0.727	0.522	0.385	0.623	0.666	0.623
BaO	0	0	0	0	0	0	0.46	0	0	0	0	0	0	0	0	0	0
Na_2O	2.65	1.56	1.39	4.24	1.51	1.45	2.05	1.35	3.12	3.18	1.33	5.68	5.10	1.42	3.44	5.53	3.62
P2O5	1.5	1.3	0	0	0	1.9	0	0.87	1.4	0.96	0	0	0	0.87	1.2	0	0
F	0.13	0.10	0.10	0.16	0.11	1.48	0.47	0.53	0.39	0.55	0.33	0.48	0.72	0.22	1.78	0.29	0.14
L.O.I	15.75	17.08	19.42	8.57	14.24	34.86	9.87	14.13	14.39	9.84	14.76	6.83	1.73	31.39	10.4	7.28	7.87
Comp (ppm)																	
S	962	1400	865	7.5	917	2040	529	623	1622	917	953	1097	1112	1894	704	1378	835
V	842	758	680	676	923	713	533	848	773	825	995	732	752	670	802	662	887
W	135	141	173	157	102	127	176	159	138	112	164	192	106	68	153	125	224
Sr	1547	1307	1068	1479	1328	630	1285	668	1331	1224	1286	1393	1168	1539	1343	1489	1351
Rb	113	79	30	89	61	11	140	31	65	58	53	74	54	77	100	87	70
Cu	40.5	64.3	32.0	25.4	44.5	52.2	54.5	36.5	39.2	40.4	128.5	51.6	73.4	34.5	34.0	41.8	198.5
Cr	12.9	12.4	9.7	20.9	8.0	12.0	10.7	32.0	8.4	11.5	18.7	19.2	19.6	16.8	13.3	14.1	12.4
Y	26	24	28	24	28	29	19	23	27	24	30	26	25	20	27	21	26
U	0	0	0	0	0	0	0	0	0	0	0	0	0	0	0	0	0
Pb	22.96	22.01	27.05	40.82	25.16	32.03	43.39	25.80	22.77	23.03	43.11	28.11	27.30	31.17	28.51	27.73	29.13
As	25	28	25	21	27	31	17	35	29	26	34	28	36	17	24	23	29
Ni	12	23	16	16	17	20	17	40	14	0	14	20	20	11	22	21	20
Nb	2	2	3	2	2	2	2	2	2	2	3	2	2	2	2	2	2
Ag	18	0	0	0	0	0	0	20	0	0	0	0	20	0	0	0	0
Cl	0	0	295	493	0	0	0	0	0	233	0	0	378	206	0	354	0

Appendix 4: Physical parameters and major ions in various Arumeru water types

Sample_ID	W-type	pH	Temp	EC	TDS	DO	Na	K	Mg	Ca	F^-	Cl^-	HCO_3^-	CO_3^{-2}	SO_4^{-2}	NO_3^-
			˚C	µS/cm	(mg/l)											
ARW_03	Spring	8.3	22.2	1094	547	3.4	105.26	47.87	3.97	15.08	9.73	19	371.4	7.0	31.0	14.52
ARW_04	Surface	7.04	22.28	1076	538	3.84	105.36	40.81	2.95	13.91	10.02	18	309.0	0.3	22.0	136.4
ARW_05	Spring	8.62	20.36	833	416	4.01	82.47	33.52	2.52	10.05	7.75	18	294.0	11.5	20.0	10.12
ARW_07	Surface	9.7	22.2	1744	872	5.43	175.46	99.67	2.02	10.04	30.07	56	305.0	143.7	80.0	0.352
ARW_08	Lake	8.2	27.84	2368	1188	3.74	251.39	119.01	4.92	20.94	32.53	130	766.7	11.4	50.0	1.32
ARW_09	Borehole	8.9	24.87	694	347	5.05	66.06	25.32	0.79	3.04	4.45	10	220.0	16.4	8.0	0.572
ARW_11	Spring	10.91	17.52	663	331	5.68	64.46	32.4	0.41	3.55	15.33	9	11.8	90.2	39.0	0.3916
ARW_13	Spring	9.16	18	209	105	5.75	12.47	4.82	0.63	3.3	3.94	4	36.0	4.9	0.0	0.352
ARW_14	Spring	8.45	13.76	510	255	5.72	48.45	27.7	0.16	1.7	14.00	8	134.3	3.6	0.0	14.52
ARW_18	Dug Well	8.74	22.64	876	438	2.57	70.86	38.06	2.72	12.63	8.31	12	207.0	10.7	70.0	1.32
ARW_19	Dug Well	9.18	24.2	2187	1093	3.21	212.1	112.36	2.76	16.21	22.40	41	657.2	93.5	55.0	2.2
ARW_21	Dug Well	8.28	23.24	1611	805	3.1	149.72	86.69	1.83	9.87	8.48	42	428.0	7.7	50.0	176
ARW_22	Dug Well	8.5	23.84	964	482	4.53	80.49	53.39	1.35	8.19	3.77	27	206.0	6.1	32.0	101.2
ARW_24	Dug Well	8.65	22.36	3832	1914	2.71	283.82	193.76	37.82	82.11	8.80	300	575.6	24.2	320.0	3.08
ARW_25	Dug Well	9.25	22.72	3109	1554	2.75	239.03	190.15	10.1	23.07	28.10	102	871.0	145.6	30.0	6.6
ARW_27	Spring	7.85	17.94	339	170	6.14	36.47	17.49	0.59	3.21	4.48	10	109.1	0.7	8.0	9.24
ARW_28	Spring	6.87	17.33	256	128	7.28	8.22	4.8	0.48	2.86	0.99	4	31.0	0.0	5.0	7.04
ARW_33	Dug Well	7.58	24.39	592	296	4.52	41.6	22.31	3.3	18.06	2.93	16	194.0	0.7	16.0	12.32
ARW_34	Borehole	7.86	25.54	517	259	5.35	44.44	24.5	1.9	13.86	2.50	15	179.2	1.2	9.0	27.28
ARW_35	Borehole	8.02	25.58	527	263	6.12	37.93	21.23	1.55	9.39	3.37	13	150.0	1.5	9.0	11
ARW_36	Surface	9.33	21.26	395	197	6.93	33.43	17.58	2.6	9.47	2.29	9	105.7	21.2	2.0	12.32
ARW_38	Spring	6.89	22.54	811	405	4.33	29.99	20.1	23.65	40.18	1.33	14	275.8	0.2	18.0	18.48
ARW_39	Surface	8.41	18.6	231	116	6.52	11.86	6.52	2.16	8.19	1.13	8	62.0	1.5	6.0	6.6
ARW_40	Dug well	8.49	26.44	1169	584	4.17	76.61	50.98	5.48	54.66	1.50	70	409.0	11.9	14.0	4.84
ARW_42	Surface	9.32	22.01	722	361	5.25	41.05	23.4	6.88	26.46	1.89	40	141.3	27.8	18.0	18.92
ARW_44	Borehole	8	26.33	1156	578	4.47	52.45	52.14	4.96	40.11	2.52	25	385.3	3.6	17.0	14.52

Appendix 4 continued

Sample_ID	W-type	pH	Temp	EC	TDS	DO	Na	K	Mg	Ca	F^-	Cl^-	HCO_3^-	CO_3^{-2}	SO_4^{-2}	NO_3^-
			°C	µS/cm	(mg/l)											
ARW_46	Borehole	8.2	25.93	3573	1786	4.42	376.97	59.59	1.62	9.9	24.43	105	1073.5	16.0	39.0	37.4
ARW_48	Dug Well	9.03	25.02	3426	1714	2.52	356.04	90.72	0.9	4.09	51.63	101	905.0	91.2	47.0	13.64
ARW_50	Borehole	8.1	25.38	772	385	5.69	78.82	32.96	2.83	16.44	2.59	11	306.3	3.6	9.0	7.92
ARW_52	Dug Well	8.98	25.91	4844	2422	3.2	488.52	151.67	2.1	5.89	84.00	110	1219.5	109.5	102.0	34.32
ARW_53	Dug Well	8.29	27.06	3646	1823	4.44	389.77	76.98	0.92	7.49	32.30	70	1172.9	21.5	12.0	44
ARW_55	Dug Well	8.33	24.56	3527	1762	3.77	341.99	234.12	2.36	8.4	42.60	100	1014.3	20.4	108.0	198
ARW_56	Dug Well	8.09	24.13	2517	1258	3.21	113.43	61.6	1.02	3.22	28.67	45	332.0	3.8	19.0	17.16
ARW_57	Dug Well	7.9	24.17	1657	829	3.16	153.39	94.22	1.78	11.11	16.53	18	496.3	3.7	8.0	15.4
ARW_59	Dug Well	8.44	25.9	2497	1248	4.01	251.81	167.34	1.92	5.82	41.13	32	877.2	22.7	13.0	24.2
ARW_60	Borehole	8.74	24.47	1856	928	5.01	201.18	136.89	1.46	7.1	46.97	30	707.0	36.5	22.0	1.32
ARW_62	Borehole	7.8	25.98	904	452	5.48	71.34	15.85	9.22	26.65	1.65	24	347.9	2.1	6.0	6.6
ARW_65	Borehole	7.99	24.68	782	391	5.45	92.08	29.67	4.93	18.76	3.19	24	336.9	3.1	8.0	8.36
ARW_66	Surface	7.5	16.46	154	77	5.76	9.34	4.4	0.96	3.35	1.5	8	33.0	0.1	3.0	7.92
ARW_68	Spring	6.57	14.32	148	74	4.77	9.08	5.07	0.75	2.27	1.12	6	30.0	0.0	2.0	6.6
ARW_70	Spring	7.29	16.67	137	69	5.38	14.16	7.51	0.19	0.31	1.63	8	32.9	0.1	4.0	5.28
ARW_71	spring	7.44	17.61	171	86	4.6	5.89	4.55	0.61	5.99	0.807	9	30.8	0.1	4.0	5.72
ARW_75	Spring	6.58	19.48	275	138	4	19.34	7.57	0.21	0.65	2.25	8	51.0	0.0	7.0	8.8
ARW_78	Spring	6.46	19.95	302	151	4.45	15.88	11.28	2.87	12.13	1.15	10	87.5	0.0	13.0	11.44
ARW_79	Dug Well	7.17	22.46	908	454	0.62	73.69	45.44	1.13	3.48	4.43	35	249.5	0.3	12.0	22
ARW_82	Spring	6.54	21.33	344	172	2.65	19.64	12.53	7.39	20.12	1.37	11	140.0	0.0	8.0	11
ARW_84	surface	8.33	17.76	830	415	5.32	85.9	30.66	0.73	5.11	18.4	24	242.8	4.9	15.0	7.04
ARW_86	surface	8.52	17.83	845	422	5.44	78.41	28.98	0.77	4.19	18.1	23	208.1	6.5	17.0	6.16
ARW_87	Spring	8.61	19.48	980	489	2.59	119.17	33.42	0.63	5.31	25.2	21	312.8	12.0	27.0	5.72
ARW_88	Lake	6.84	19	254	127	0	12.71	5.1	4.42	24.14	0.942	2	98.9	0.1	2.0	5.28
ARW_89	Lake	9.57	20.89	8715	4357	5.37	565.43	409.24	3.3	1.26	259	230	2889.0	1009.0	300.0	9.24
ARW_91	Lake	8.35	20.85	509	255	1.5	32.53	24.08	4.62	22.2	2.62	15	203.6	4.3	2.0	12.76
ARW_92	Borehole	6.78	21.85	437	219	2.56	23.52	17.9	5.75	16.41	1.14	16	126.9	0.1	11.0	31.24
ARW_94	surface	7.7	19.63	229	115	3.75	13.82	7.68	1.43	7.4	1.31	6	69.5	0.3	2.0	10.56

Appendix 5: Fluoride data from various water sources in the study area (After Malago, 2017)

Sample_ID	Water_type	F^-(mg/l)	Sample_ID	Water_type	F^-(mg/l)
ARW_01	Spring	4.12	ARW_58	Well	41.80
ARW_02	Spring	5.19	ARW_61	Borehole	28.25
ARW_06	Spring	4.66	ARW_64	Borehole	1.17
ARW_10	Surface	4.04	ARW_67	Spring	0.921
ARW_12	Surface	2.25	ARW_69	Spring	0.67
ARW_15	Spring	0.92	ARW_72	Surface	1.24
ARW_16	Well	3.10	ARW_73	Surface	1.26
ARW_17	Well	0.58	ARW_74	Spring	2
ARW_20	Well	0.35	ARW_76	Spring	1.13
ARW_23	Well	3.55	ARW_77	Well	0.958
ARW_26	Spring	2.27	ARW_80	Surface	1.61
ARW_29	Spring	1.04	ARW_81	Surface	1.83
ARW_30	Spring	1.04	ARW_83	Spring	1.22
ARW_31	Spring	1.03	ARW_85	surface	8.52
ARW_32	Well	2.13	ARW_90	Lake	1410
ARW_37	Borehole	2.00	ARW_93	Borehole	3.52
ARW_41	Well	2.15	ARW_95	Tape water	0.44
ARW_43	Well	1.45	ARW_96	Spring	0.41
ARW_45	Well	3.30	ARW_97	Spring	0.51
ARW_47	Well	23.67	ARW_98	Surface	34.88
ARW_49	Borehole	3.90	ARW-99	surface	43.87
ARW_51	Well	4.17	ARW-100	Surface	14.82
ARW_54	Surface	1.70	ARW_101	Surface	38.88

Appendix 6: Apparent resistivity data from the southern part of Mt. Meru

AB/2	MN/2	ρ_1	ρ_2	ρ_3	ρ_4	ρ_5	ρ_6	ρ_7	ρ_8	ρ_9	ρ_{10}	ρ_{11}	ρ_{12}	ρ_{13}	ρ_{14}	ρ_{15}
1	0.5	66.3	42.6	64.9	222.0	17.5	39.0	201.6	306.8	522.8	31.8	411.8	50.0	90.1	442.0	80.0
1.5	0.5	89.4	36.8	49.3	302.0	24.5	49.8	92.0	321.8	310.1	24.2	308.0	39.4	85.4	282.0	91.0
2	0.5	101.6	33.0	35.3	359.0	31.0	58.2	52.3	302.2	234.9	19.9	194.4	31.9	71.1	190.0	101.0
3	0.5	114.2	30.5	28.3	441.0	44.7	73.2	49.5	250.8	132.5	17.0	97.2	32.3	56.8	124.2	114.9
4	0.5	127.4	31.7	27.2	490.0	51.4	84.2	51.5	207.7	94.5	18.0	70.0	30.2	44.9	91.9	121.5
6	0.5	135.0	30.9	25.6	522.0	65.2	91.1	53.9	165.2	63.8	21.3	51.9	28.9	33.8	81.9	106.5
8	0.5	118.2	31.0	25.2	531.0	74.1	82.2	57.5	122.7	54.3	21.8	53.9	28.8	28.6	80.1	76.4
8	2	136.4		24.5		79.4	82.6	46.6	132.2	61.2	22.2	46.7	40.0	30.4	70.3	83.1
10	0.5	95.9	30.0	25.8	534.7	83.8	84.0	63.4	87.8	51.7	22.1	57.7	27.2	25.6	71.8	59.3
10	2	112.3	30.2	24.6	528.3	91.5	84.9	43.0	92.8	41.8	22.7	50.6	36.7	26.9	65.4	65.1
15	2	56.4	29.3	24.3	449.2	103.7	82.8	53.2	50.3	32.1	21.6	53.9	36.6	20.3	54.5	33.7
20	2	38.4	33.0	23.7	315.2	114.5	87.1	67.4	29.7	40.0	21.4	54.6	32.0	17.3	49.7	24.4
20	5	41.5	35.1	25.8	332.9	115.9	86.2	70.8	28.5	27.0	21.1	53.4	30.6	17.5	44.8	27.8
25	2	34.8	36.4	22.6	218.3	121.4	85.5	80.1	24.5	37.7	21.6	54.6	33.6	15.8	39.9	20.7
25	5	35.5	38.7	24.6	230.8	124.3	85.3	85.8	23.4	36.5	21.5	53.2	32.6	15.9	37.0	22.6
30	5	34.9	41.8	23.4	147.4	127.7	79.2	98.4	21.7	31.1	21.6	49.2	33.5	15.4	30.7	20.6
40	5	38.3	43.0	21.7	77.3	146.3	63.8	113.0	19.7	21.2	23.0	47.3	34.7	16.6	24.8	18.1
50	5	41.0	44.9	20.4	51.0	159.5	51.4	113.8	22.3	22.8	24.4	43.5	29.1	18.7	24.9	18.4
50	10	43.6	45.0	22.2	54.9	151.1	55.8	116.2	23.5	25.0	24.3	43.6	37.3	18.2	25.2	18.6
60	5	42.6	45.5	20.2	40.0	161.8	46.3	100.6	24.4	21.5	25.5	41.9	31.9	21.4	25.7	19.4
60	10	46.1	46.0	21.5	41.7	153.7	49.5	102.8	25.1	21.8	25.7	41.7	35.1	20.8	25.6	19.2
75	10	46.0	48.0	21.7	41.6	165.1	45.0	78.2	28.8		26.2	39.7	38.2	24.4	21.1	19.0
100	10	47.9	48.4	24.5	47.8	194.3	46.0	64.1			29.2	39.1	46.0	27.3	20.2	19.4
100	20	47.9	46.5	24.3	49.2	196.7	45.5	59.7	34.0		31.4	39.6	43.0	27.5		
120	10		48.5	25.0	52.0	214.9	47.9	62.0	35.9		31.1	38.4	49.0	33.0	45.7	19.3
120	20	44.9	47.0	26.7	53.7	217.3	47.7	57.9	35.9		33.4	39.1	53.0	31.3	36.4	
150	20	46.0	45.1	28.4	60.5	237.8	52.3	62.2	38.4		35.2	39.6	58.7	34.0	44.2	
175	20	46.1	45.3	28.5	62.3	254.4	59.0	58.5	40.6		37.2	34.8	51.1	33.1	46.3	16.4
200	20	46.2	45.7	28.9	69.0	281.0	65.0	65.0	42.0		39.1	40.0	60.0	34.0	48.0	16.0

Appendix 6 continued

AB/2	MN/2	ρ_{16}	ρ_{17}	ρ_{18}	ρ_{19}	ρ_{20}	ρ_{21}	ρ_{22}	ρ_{23}	ρ_{24}	ρ_{25}	ρ_{26}	ρ_{27}	ρ_{28}	ρ_{29}	ρ_{30}
1	0.5	30.0	700.0	150.4	61.0	75.0	55.0	131.0	22.0	13.3	12.1	31.0	252.3	347.9	86.7	27.5
1.5	0.5	24.5	756.6	115.2	58.9	70.0	53.0	119.6	33.0	13.9	15.0	19.2	259.6	325.0	50.5	26.4
2	0.5	22.3	501.0	91.0	52.1	67.0	50.7	115.2	41.4	16.4	18.2	15.1	248.5	308.0	29.2	28.0
3	0.5	18.9	299.6	69.2	44.5	69.7	53.5	117.7	63.4	19.7	27.1	12.4	199.6	275.0	16.1	24.4
4	0.5	17.7	207.0	54.0	32.0	66.3	52.0	129.9	82.5	21.5	33.2	12.5	159.4	217.7	12.2	24.0
6	0.5	16.9	95.3	43.8	26.5	54.4	53.6	130.3	115.6	26.5	41.5	13.9	92.0	169.8	9.9	18.8
8	0.5	15.3	53.5	43.2	22.7	45.0	58.7	126.0	156.3	29.9	40.0	15.3	61.9	126.8	10.2	15.8
8	2	16.1	61.1	42.7	23.3	47.0	59.9	113.0	154.9	31.5	37.3	15.5	57.4	147.3	10.1	18.1
10	0.5	14.3	44.7	45.4	22.7	39.9	66.5	121.5	193.1	33.6	41.5	16.8	49.5	101.9	10.0	13.5
10	2	14.9	49.4	44.5	23.0	41.4	67.8	109.6	197.2	35.5	39.5	17.1	44.9	114.5	9.8	15.3
15	2	14.0	37.2	51.2	27.3	27.1	86.9	109.4	253.6	36.9	41.5	21.1	37.9	68.6	9.1	12.3
20	2	13.1	34.3	58.1	31.1	21.8	91.5	108.3	285.2	34.9	45.4	24.9	35.7	56.8	8.5	11.5
20	5	13.9	36.0	62.0	29.4		90.1	114.1	300.9	36.2	40.5	24.1	35.9	59.9	8.6	12.3
25	2	14.3	33.7	66.0	33.7		82.2	104.0	289.4	33.3	48.5	27.5	33.4	47.5	8.5	11.3
25	5	14.9	35.1	70.8	32.1		81.6	108.8	311.5	34.9	44.3	27.1	33.5	48.4	8.5	12.1
30	5	16.4	32.3	77.1	32.9	17.4	67.6	104.5	293.1	32.9	41.6	30.2	30.5	47.7	8.4	12.3
40	5	18.6	32.7	87.4	33.1	17.6	53.5	93.5	261.7	23.8	38.3	33.7	28.9	40.3	8.9	13.5
50	5		33.6	94.1	32.1	17.1	43.9	76.3	223.5	22.5	37.7	34.8	27.3	37.1	9.5	15.6
50	10	20.4	36.7	90.6			44.3	73.7	229.1	21.1	43.4	34.4	27.3	39.8	9.7	15.4
60	5	22.3	34.5	102.5	32.7	17.0	36.3	61.6	165.3	22.3	36.4	34.8	25.3	34.7	10.5	18.0
60	10	21.4	36.5	99.4	30.6	18.3	36.4	59.4		20.8	40.8	34.6	26.2	36.9	10.6	20.2
75	10	21.6	42.9	109.3	30.7	19.3	25.5	42.1	106.6	19.2	39.7	34.7	24.4	30.5	12.4	20.9
100	10	20.2	54.0	125.6	29.5	19.3	17.8	27.1	53.0	21.4	40.2	30.1	22.9	25.3	14.9	21.9
100	20		48.6	126.0			21.6	27.0	59.3	21.4	38.4		24.4		14.7	26.6
120	10	17.9		133.0	29.5	20.6	16.2	23.7	26.9	23.2	46.5	29.3	22.1		18.2	31.4
120	20			132.9	26.5	24.4	18.8	23.5	30.6	21.9	44.1	25.9			16.9	31.3
150	20	16.7		140.3	25.1	26.9	15.2	19.5	22.0	24.6	45.2	26.8	20.2			33.9
175	20	19.0		134.6	26.2		14.2		16.0	27.6		28.0			19.8	38.8
200	20	18.0		126.0	24.0		13.7	19.0	14.0	29.0		29.0	20.0		22.0	

AB/2: Current electrode separation (m), MN/2: Potential electrode separation (m), $\rho_{1,2,3...:}$ Resistivity (Ωm)

Appendix 7: Model results of 30 VES stations from southern eastern part of Mt. Meru

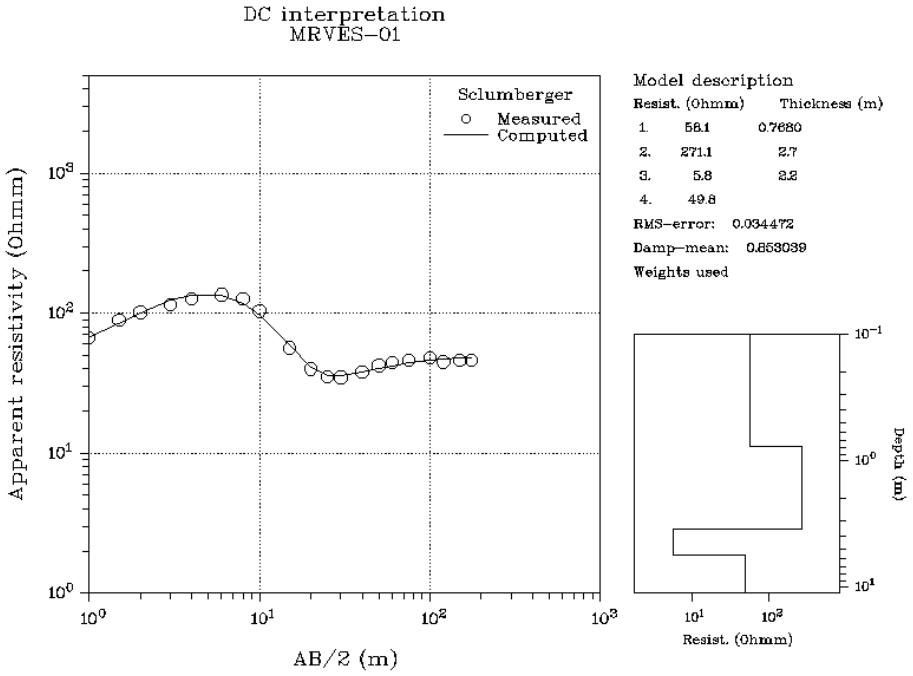

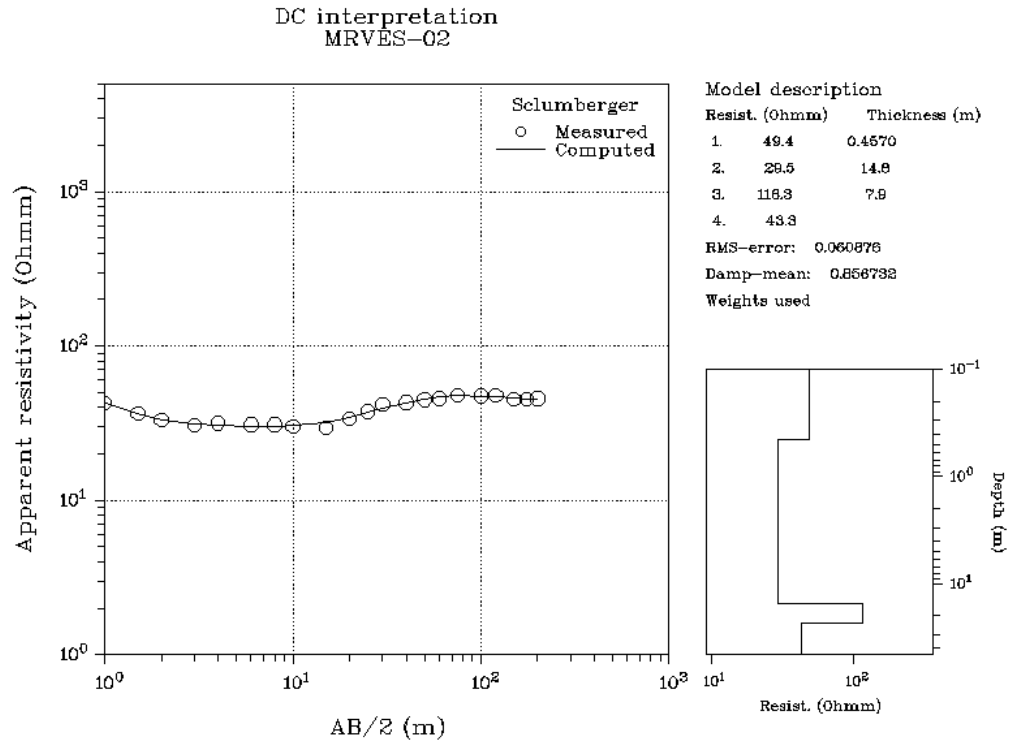

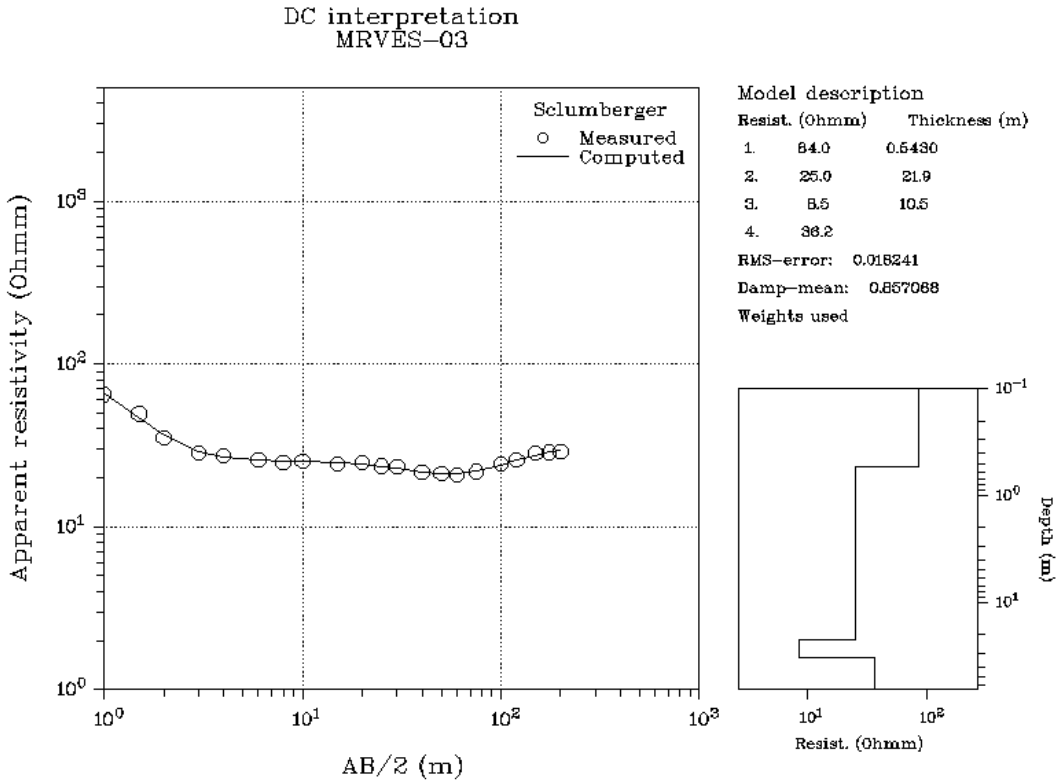
DC interpretation
MRVES-03
Sclumberger
Measured
Computed
Apparent resistivity (Ohmm)
AB/2 (m)
Model description
Resist. (Ohmm) Thickness (m)
1. 84.0 0.5430
2. 25.0 21.9
3. 8.5 10.5
4. 36.2
RMS-error: 0.018241
Damp-mean: 0.857068
Weights used
Depth (m)
Resist. (Ohmm)

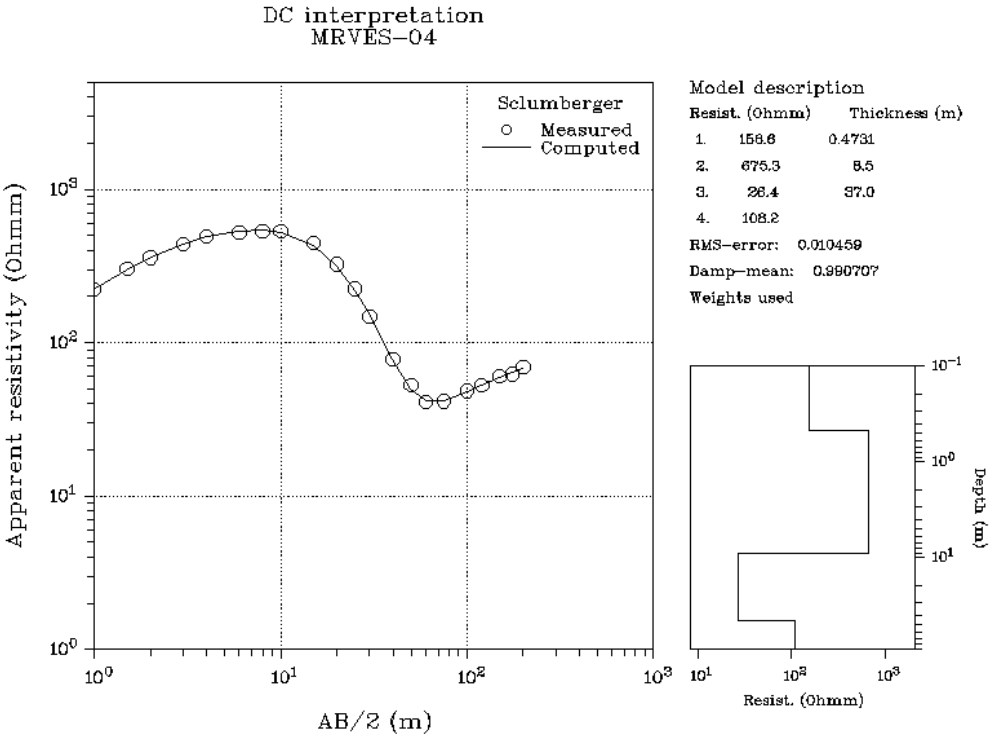
DC interpretation
MRVES-04
Sclumberger
Measured
Computed
Apparent resistivity (Ohmm)
AB/2 (m)
Model description
Resist. (Ohmm) Thickness (m)
1. 158.6 0.4731
2. 675.3 8.5
3. 26.4 37.0
4. 108.2
RMS-error: 0.010459
Damp-mean: 0.990707
Weights used
Depth (m)
Resist. (Ohmm)

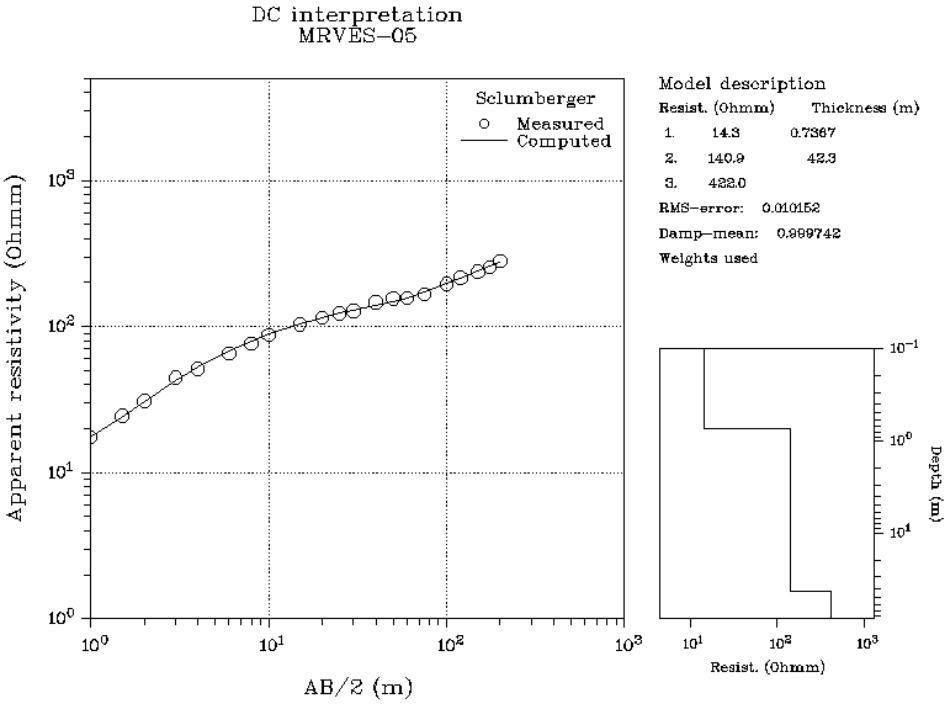
DC interpretation
MRVES-05
Schlumberger
Measured
Computed
Apparent resistivity (Ohmm)
AB/2 (m)
Model description
Resist. (Ohmm) Thickness (m)
1. 14.3 0.7367
2. 140.9 42.3
3. 422.0
RMS-error: 0.010152
Damp-mean: 0.999742
Weights used
Depth (m)
Resist. (Ohmm)

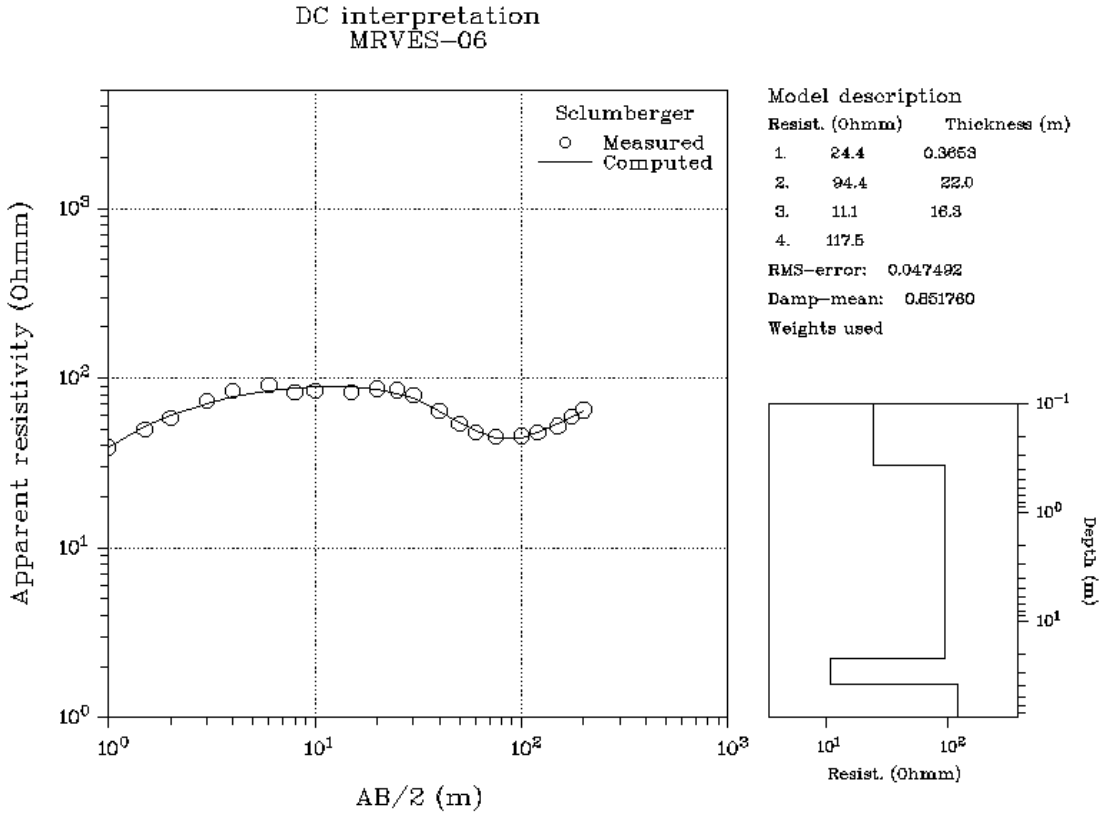
DC interpretation
MRVES-06
Schlumberger
Measured
Computed
Apparent resistivity (Ohmm)
AB/2 (m)
Model description
Resist. (Ohmm) Thickness (m)
1. 24.4 0.3653
2. 94.4 22.0
3. 11.1 16.3
4. 117.5
RMS-error: 0.047492
Damp-mean: 0.851760
Weights used
Depth (m)
Resist. (Ohmm)

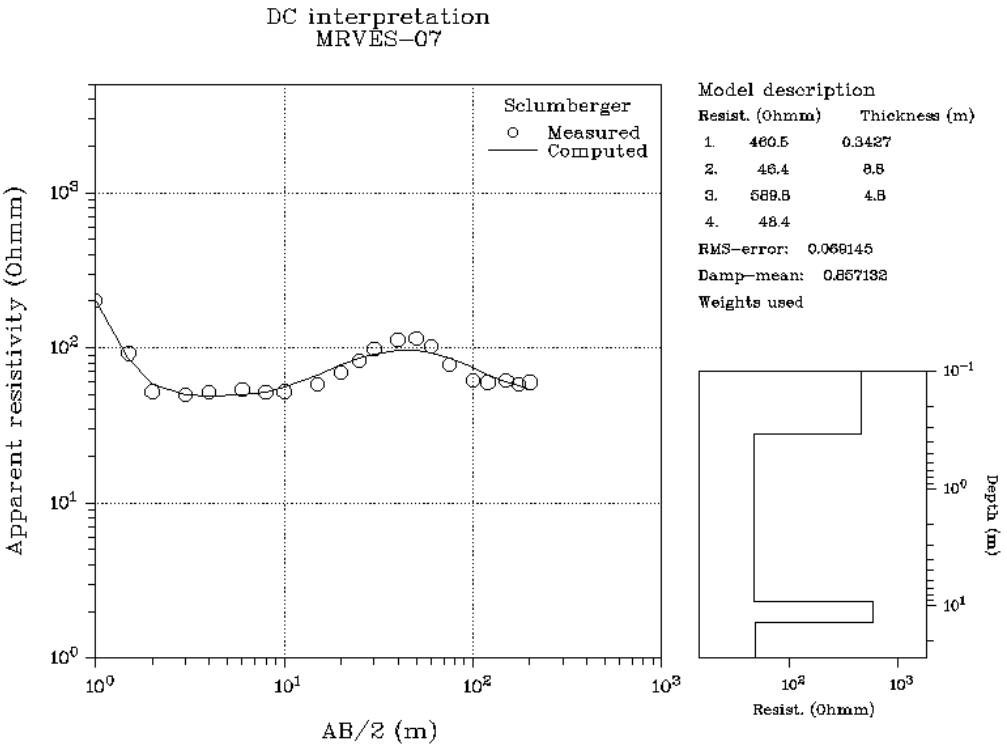
DC interpretation
MRVES-07
Schlumberger
Measured
Computed
Apparent resistivity (Ohmm)
AB/2 (m)
Model description
Resist. (Ohmm) Thickness (m)
1. 460.5 0.3427
2. 46.4 8.5
3. 589.5 4.5
4. 48.4
RMS-error: 0.069145
Damp-mean: 0.857132
Weights used
Resist. (Ohmm)
Depth (m)

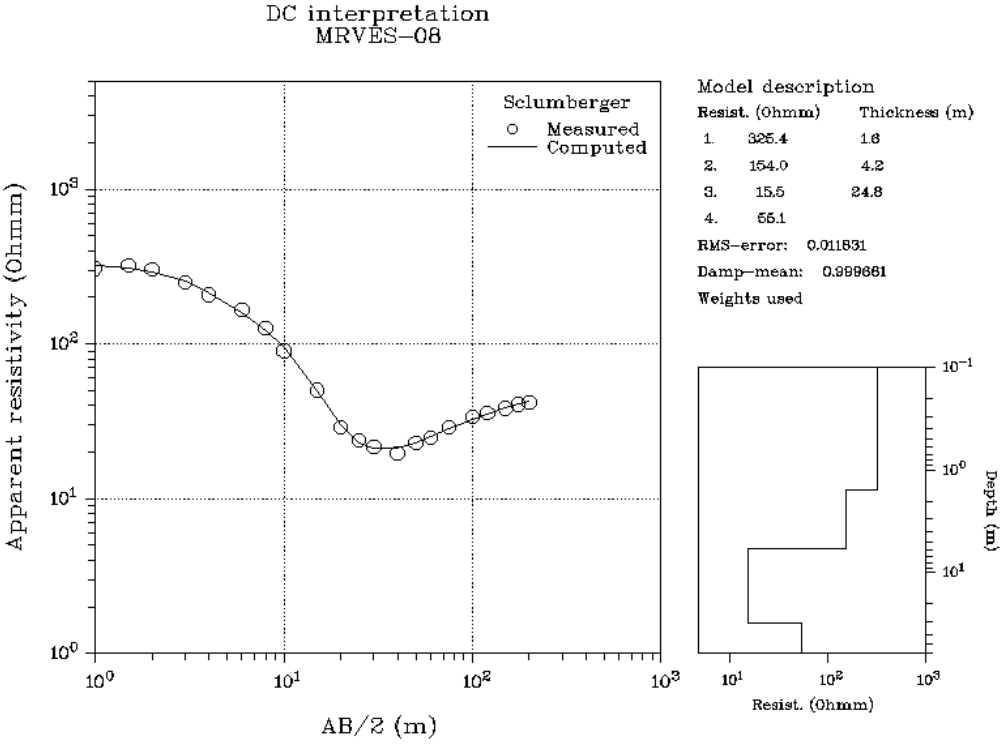
DC interpretation
MRVES-08
Schlumberger
Measured
Computed
Apparent resistivity (Ohmm)
AB/2 (m)
Model description
Resist. (Ohmm) Thickness (m)
1. 325.4 1.6
2. 154.0 4.2
3. 15.5 24.8
4. 55.1
RMS-error: 0.011831
Damp-mean: 0.999661
Weights used
Resist. (Ohmm)
Depth (m)

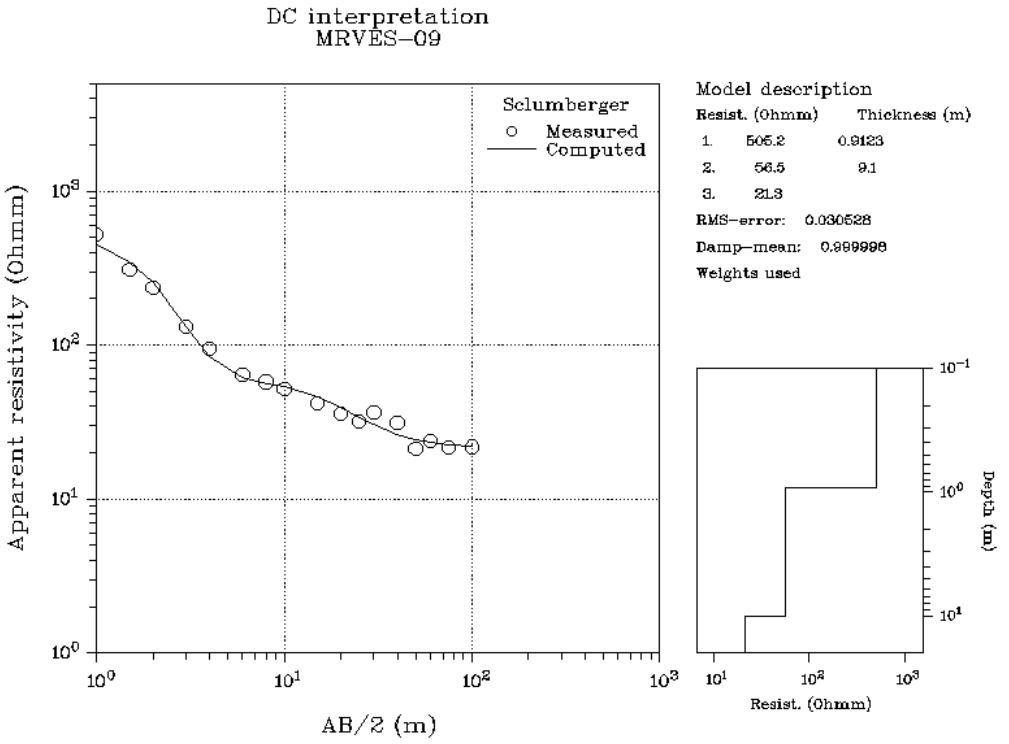
DC interpretation
MRVES-09
Schlumberger
Measured
Computed
Apparent resistivity (Ohmm)
AB/2 (m)
Model description
Resist. (Ohmm) Thickness (m)
1. 505.2 0.9123
2. 56.5 9.1
3. 21.3
RMS-error: 0.030528
Damp-mean: 0.999998
Weights used
Resist. (Ohmm)
Depth (m)

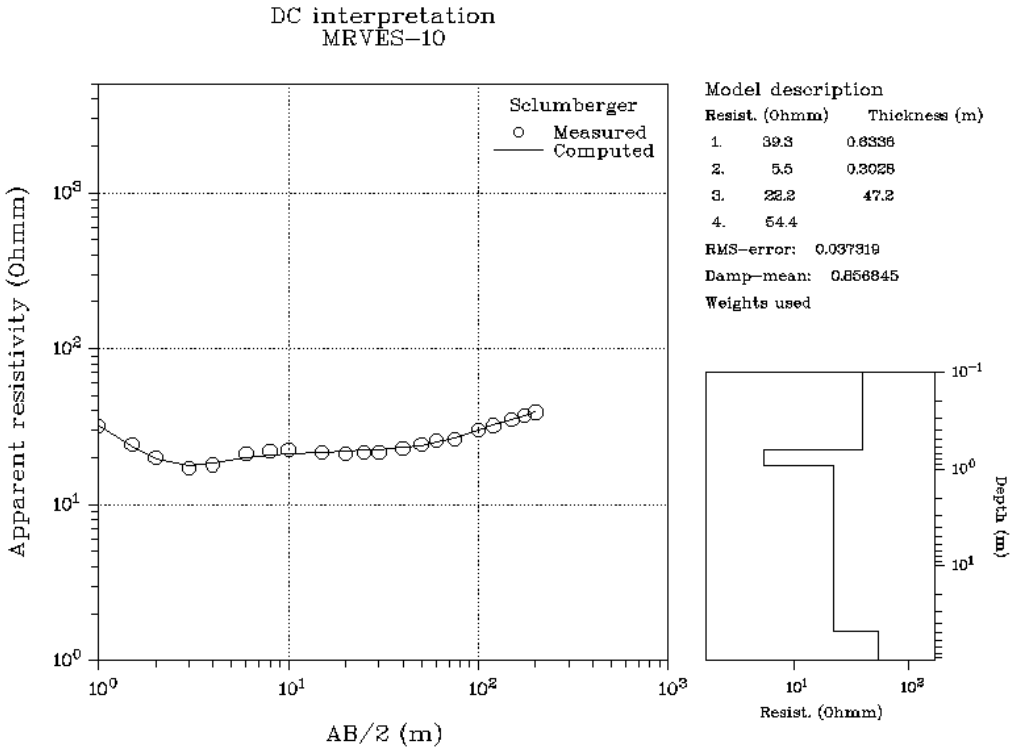
DC interpretation
MRVES-10
Schlumberger
Measured
Computed
Apparent resistivity (Ohmm)
AB/2 (m)
Model description
Resist. (Ohmm) Thickness (m)
1. 39.3 0.6336
2. 5.5 0.3028
3. 22.2 47.2
4. 54.4
RMS-error: 0.037319
Damp-mean: 0.856845
Weights used
Resist. (Ohmm)
Depth (m)

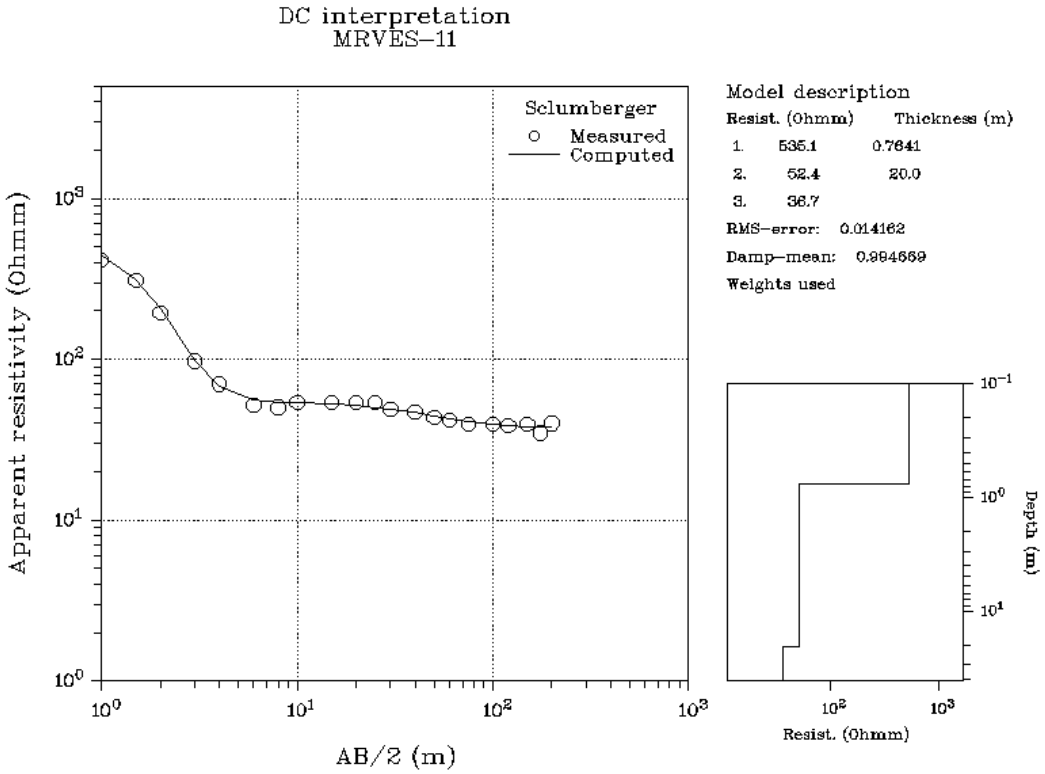
DC interpretation
MRVES-11
Schlumberger
Measured
Computed
Apparent resistivity (Ohmm)
AB/2 (m)
Model description
Resist. (Ohmm) Thickness (m)
1. 535.1 0.7641
2. 52.4 20.0
3. 36.7
RMS-error: 0.014162
Damp-mean: 0.994669
Weights used
Depth (m)
Resist. (Ohmm)

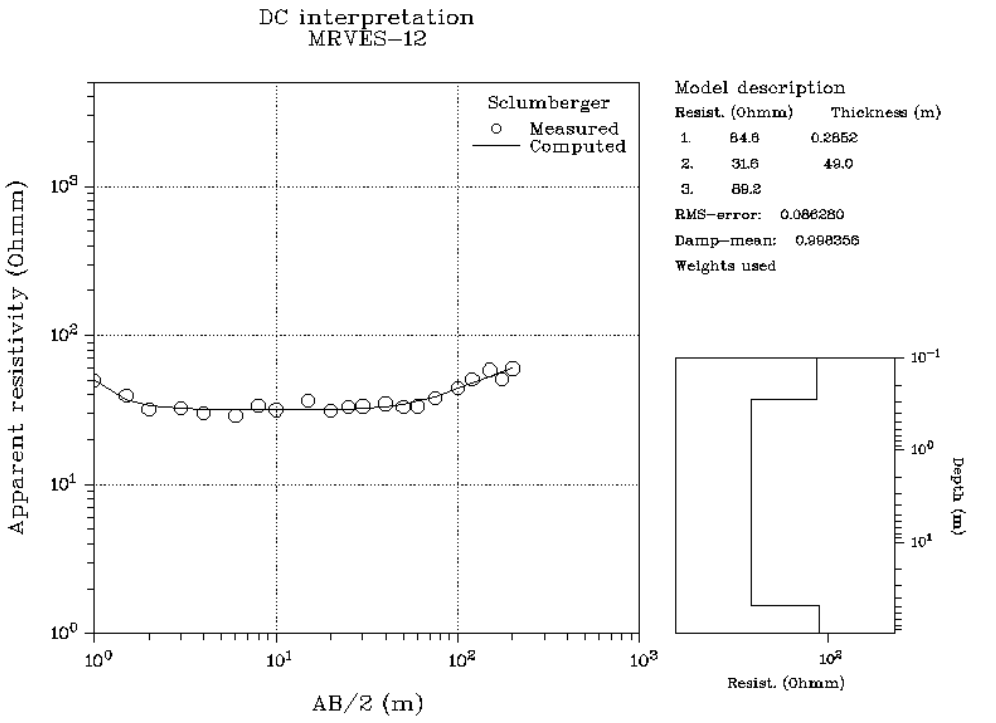
DC interpretation
MRVES-12
Schlumberger
Measured
Computed
Apparent resistivity (Ohmm)
AB/2 (m)
Model description
Resist. (Ohmm) Thickness (m)
1. 84.6 0.2852
2. 31.6 49.0
3. 89.2
RMS-error: 0.086280
Damp-mean: 0.998356
Weights used
Depth (m)
Resist. (Ohmm)

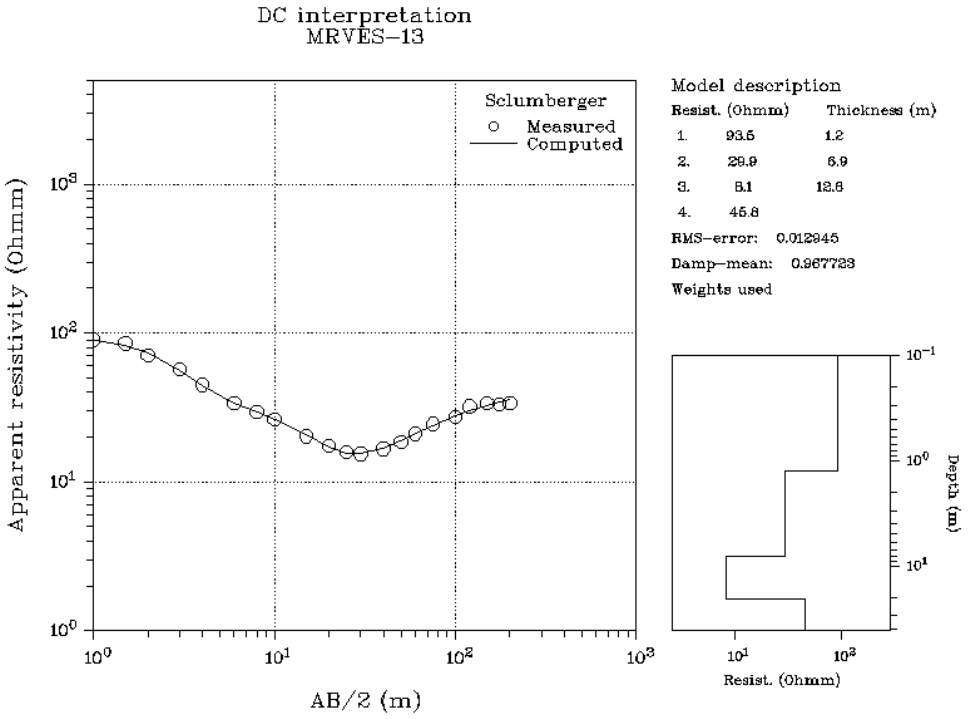
DC interpretation
MRVES-13
Schlumberger
Measured
Computed
Apparent resistivity (Ohmm)
AB/2 (m)
Model description
Resist. (Ohmm) Thickness (m)
1. 93.5 1.2
2. 29.9 6.9
3. 8.1 13.6
4. 45.8
RMS-error: 0.012945
Damp-mean: 0.967723
Weights used
Depth (m)
Resist. (Ohmm)

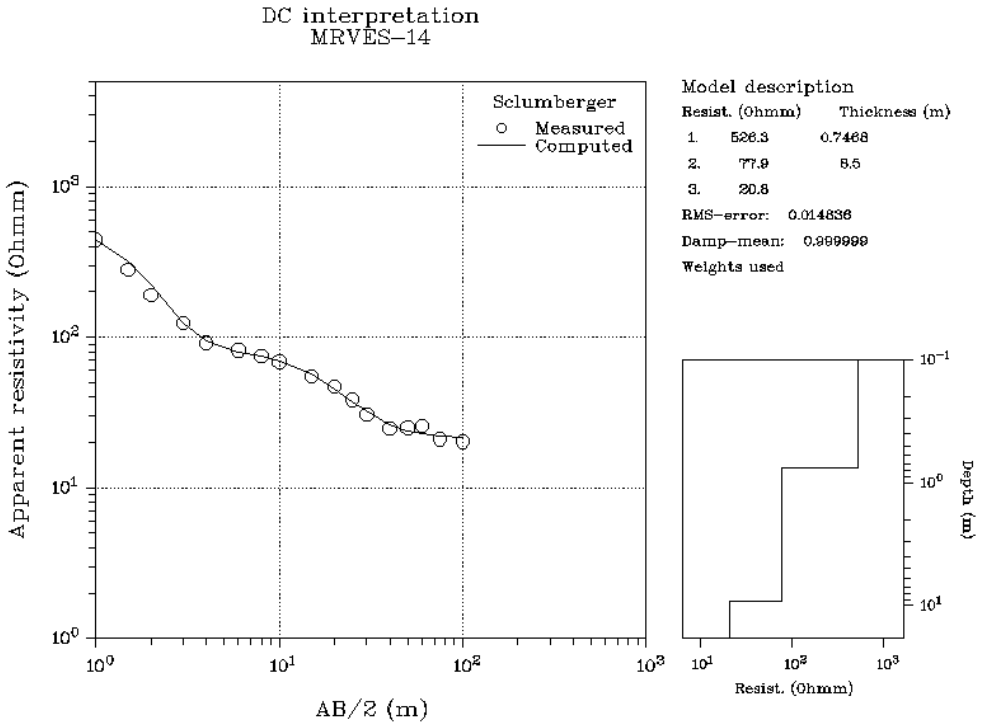
DC interpretation
MRVES-14
Schlumberger
Measured
Computed
Apparent resistivity (Ohmm)
AB/2 (m)
Model description
Resist. (Ohmm) Thickness (m)
1. 526.3 0.7468
2. 77.9 8.5
3. 20.8
RMS-error: 0.014836
Damp-mean: 0.999999
Weights used
Depth (m)
Resist. (Ohmm)

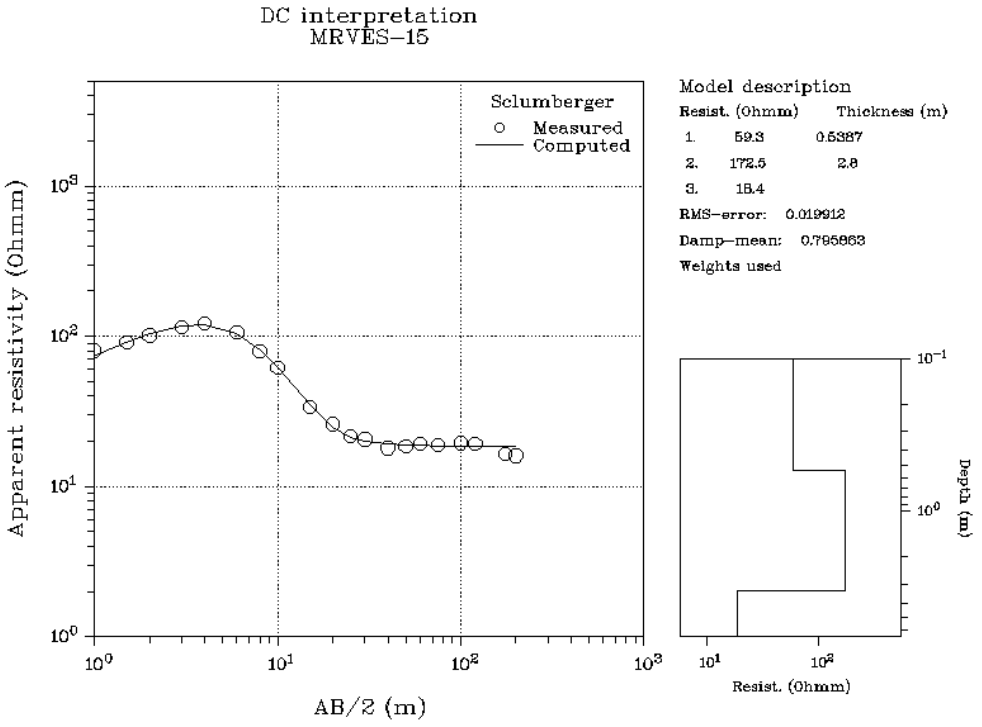
DC interpretation
MRVES-15
Schlumberger
Measured
Computed
Apparent resistivity (Ohmm)
AB/2 (m)
Model description
Resist. (Ohmm) Thickness (m)
1. 59.3 0.5387
2. 172.5 2.8
3. 15.4
RMS-error: 0.019912
Damp-mean: 0.795863
Weights used
Depth (m)
Resist. (Ohmm)

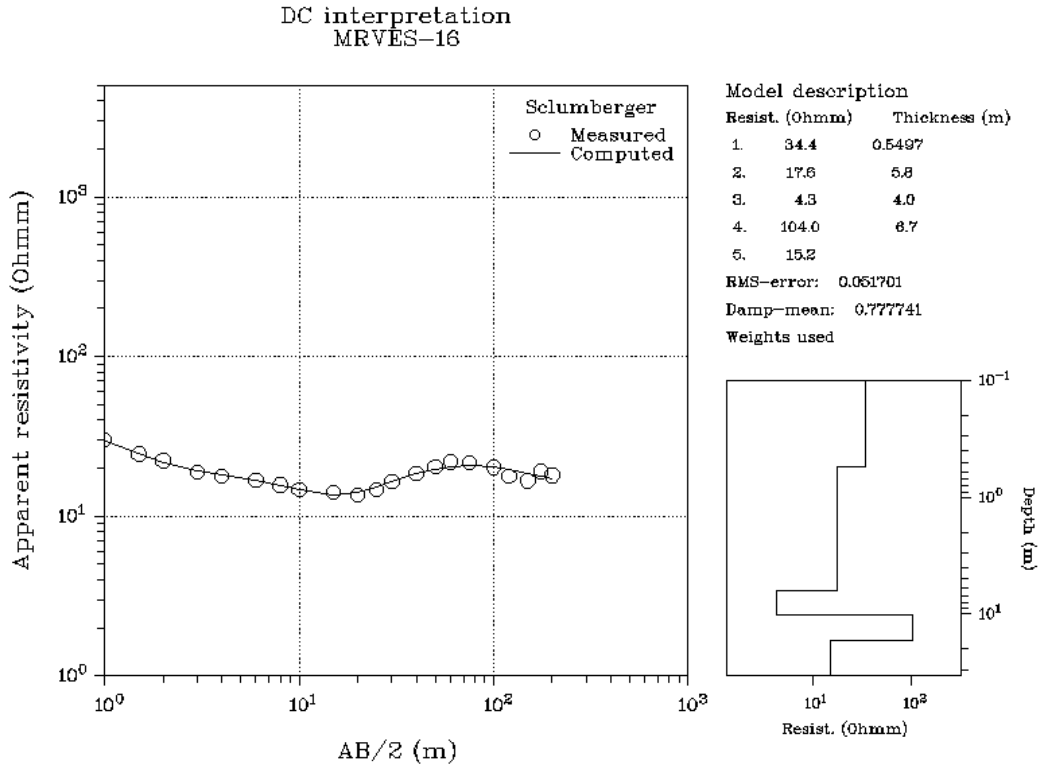
DC interpretation
MRVES-16
Schlumberger
Measured
Computed
Apparent resistivity (Ohmm)
AB/2 (m)
Model description
Resist. (Ohmm) Thickness (m)
1. 34.4 0.5497
2. 17.6 5.8
3. 4.3 4.0
4. 104.0 6.7
5. 15.2
RMS-error: 0.051701
Damp-mean: 0.777741
Weights used
Depth (m)
Resist. (Ohmm)

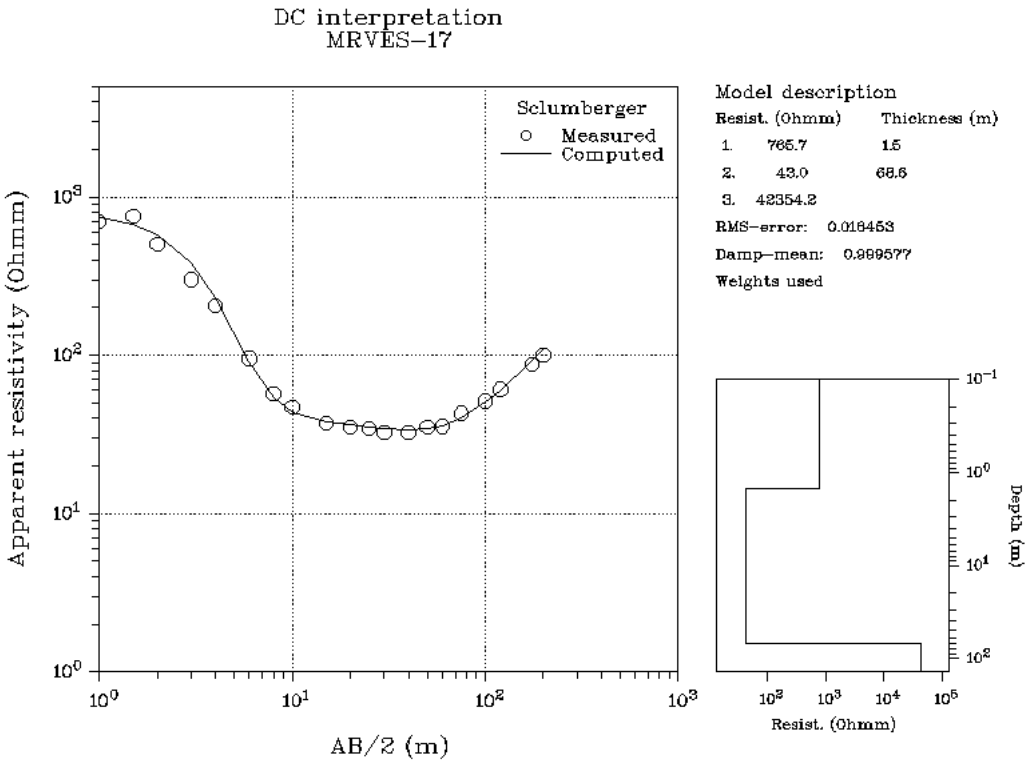
DC interpretation
MRVES-17
Schlumberger
Measured
Computed
Apparent resistivity (Ohmm)
AB/2 (m)
Model description
Resist. (Ohmm) Thickness (m)
1. 765.7 1.5
2. 43.0 66.6
3. 42354.2
RMS-error: 0.018453
Damp-mean: 0.999577
Weights used
Resist. (Ohmm)
Depth (m)

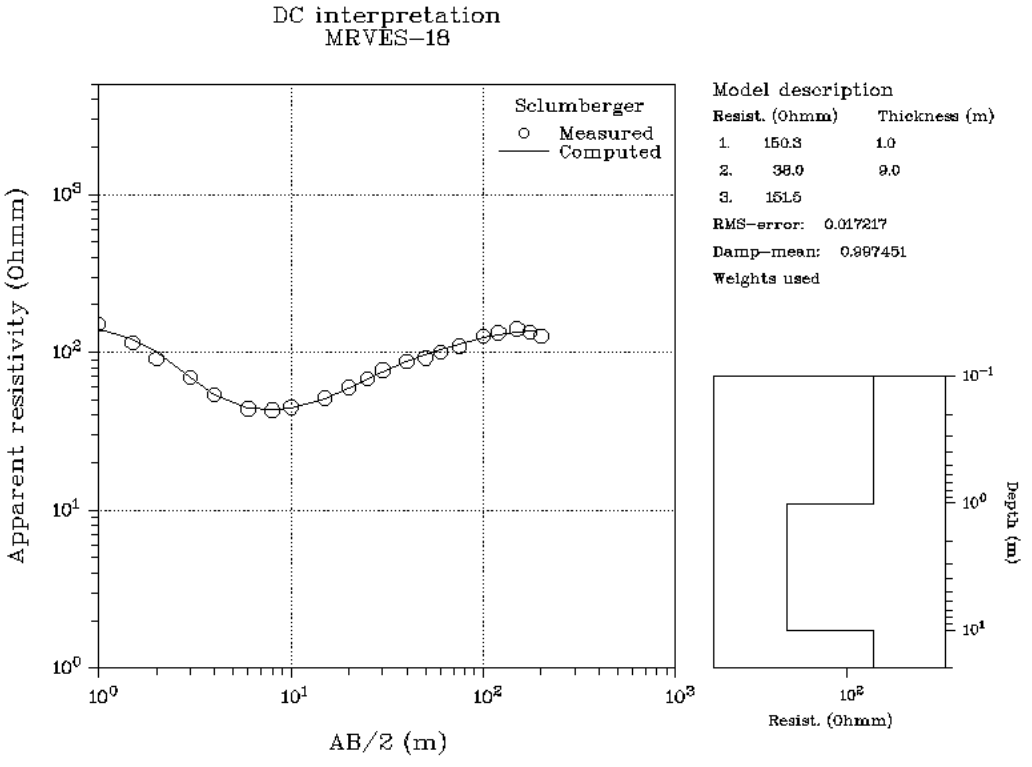
DC interpretation
MRVES-18
Schlumberger
Measured
Computed
Apparent resistivity (Ohmm)
AB/2 (m)
Model description
Resist. (Ohmm) Thickness (m)
1. 150.3 1.0
2. 38.0 9.0
3. 151.5
RMS-error: 0.017217
Damp-mean: 0.997451
Weights used
Resist. (Ohmm)
Depth (m)

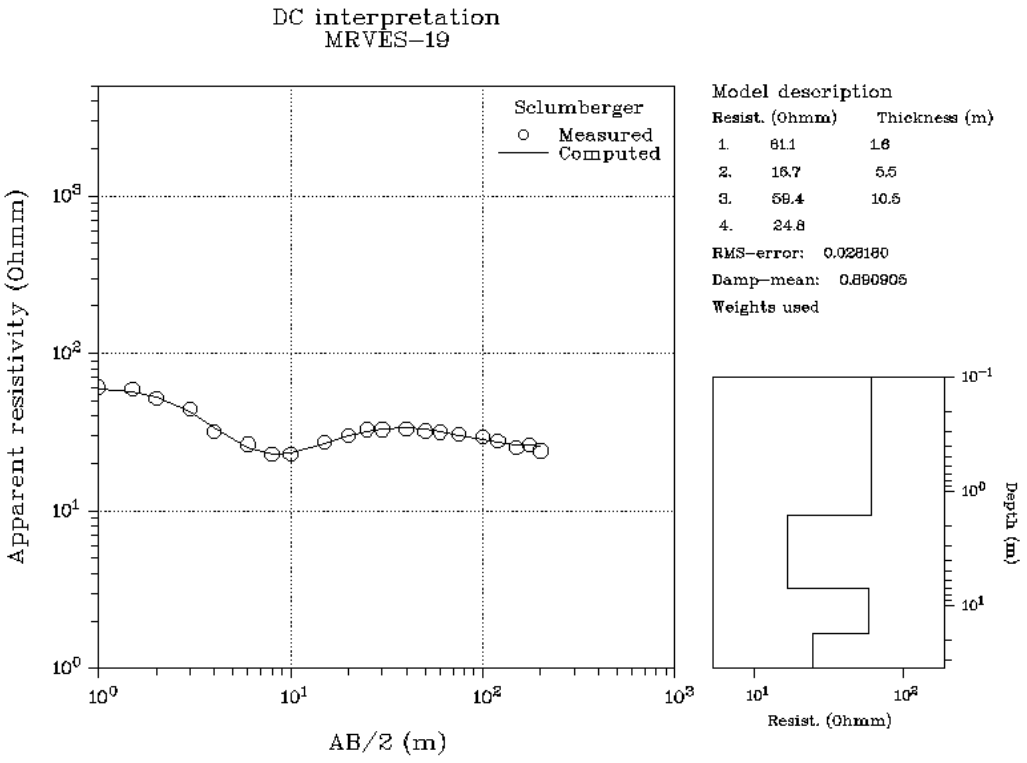
DC interpretation
MRVES-19
Schlumberger
Measured
Computed
Apparent resistivity (Ohmm)
AB/2 (m)
Model description
Resist. (Ohmm) Thickness (m)
1. 61.1 1.6
2. 15.7 5.5
3. 59.4 10.5
4. 24.8
RMS-error: 0.028160
Damp-mean: 0.890905
Weights used
Depth (m)
Resist. (Ohmm)

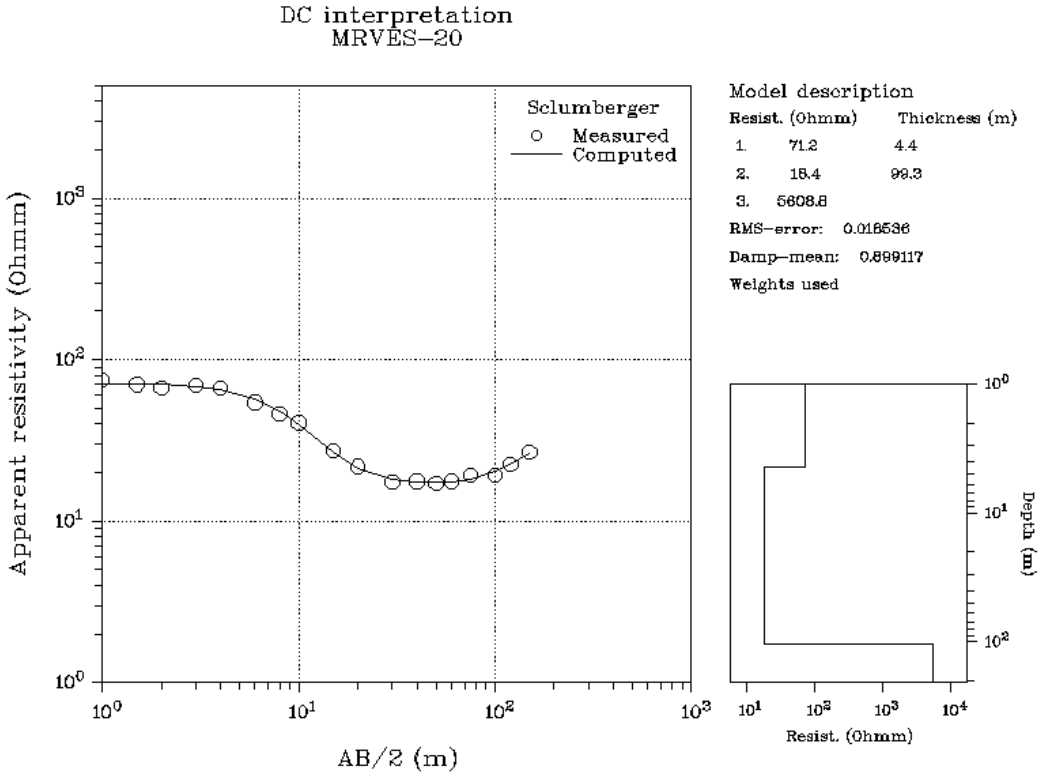
DC interpretation
MRVES-20
Schlumberger
Measured
Computed
Apparent resistivity (Ohmm)
AB/2 (m)
Model description
Resist. (Ohmm) Thickness (m)
1. 71.2 4.4
2. 18.4 99.3
3. 5608.8
RMS-error: 0.016536
Damp-mean: 0.899117
Weights used
Depth (m)
Resist. (Ohmm)

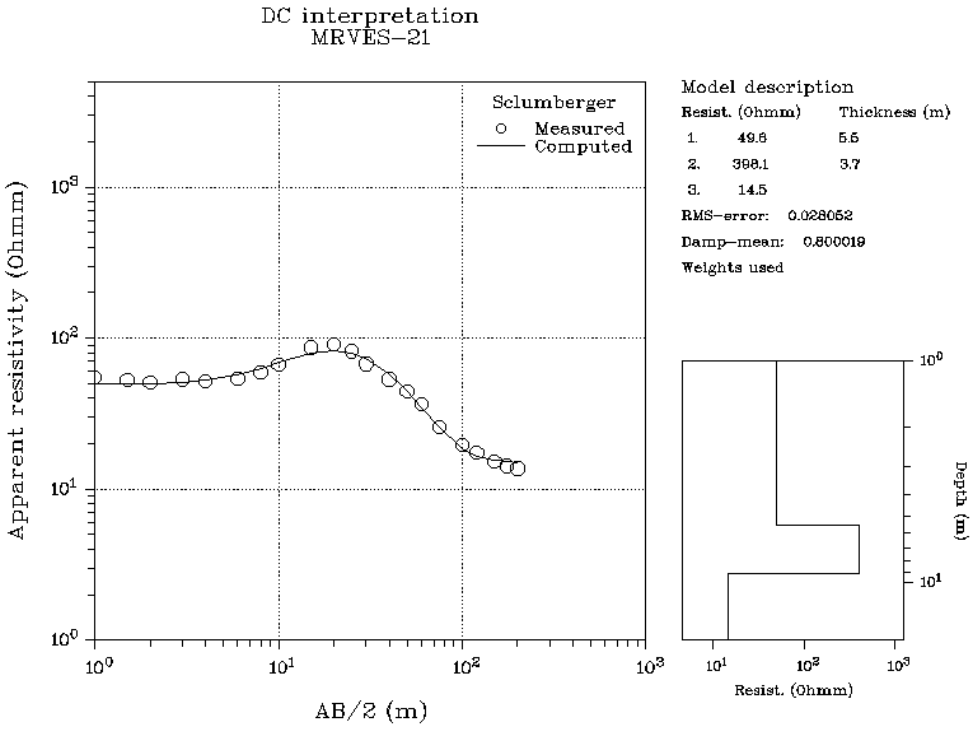
DC interpretation
MRVES-21
Sclumberger
Measured
Computed
Apparent resistivity (Ohmm)
AB/2 (m)
Model description
Resist. (Ohmm) Thickness (m)
1. 49.6 5.5
2. 398.1 3.7
3. 14.5
RMS-error: 0.028052
Damp-mean: 0.800019
Weights used
Depth (m)
Resist. (Ohmm)

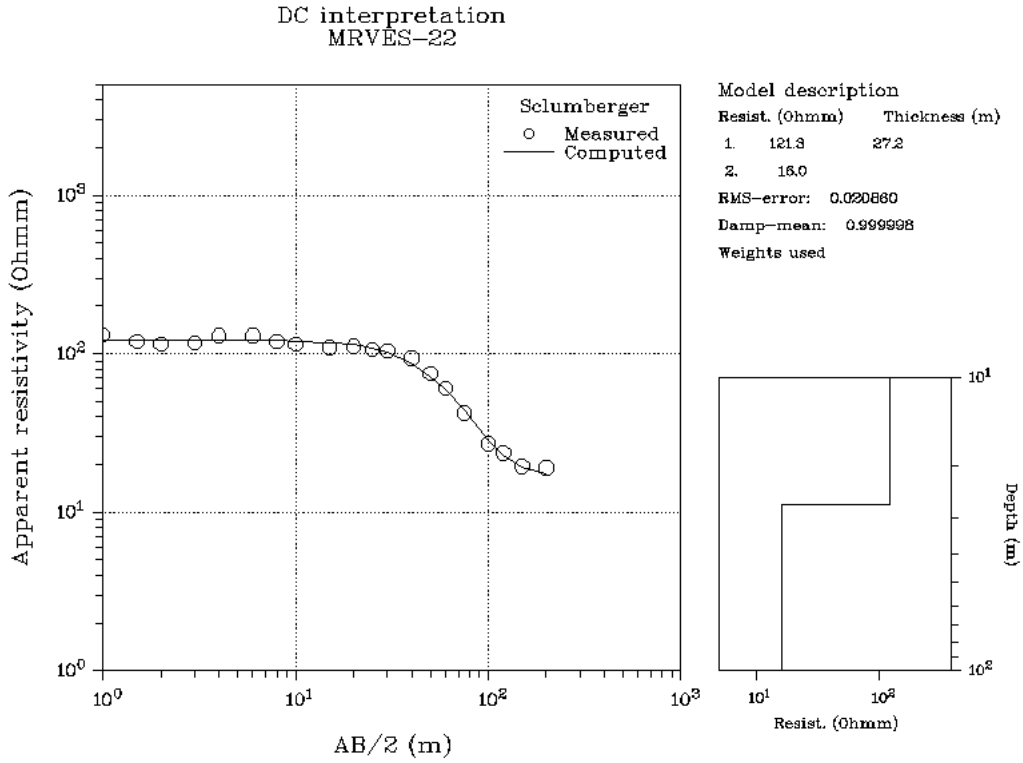
DC interpretation
MRVES-22
Sclumberger
Measured
Computed
Apparent resistivity (Ohmm)
AB/2 (m)
Model description
Resist. (Ohmm) Thickness (m)
1. 121.3 27.2
2. 16.0
RMS-error: 0.020860
Damp-mean: 0.999998
Weights used
Depth (m)
Resist. (Ohmm)

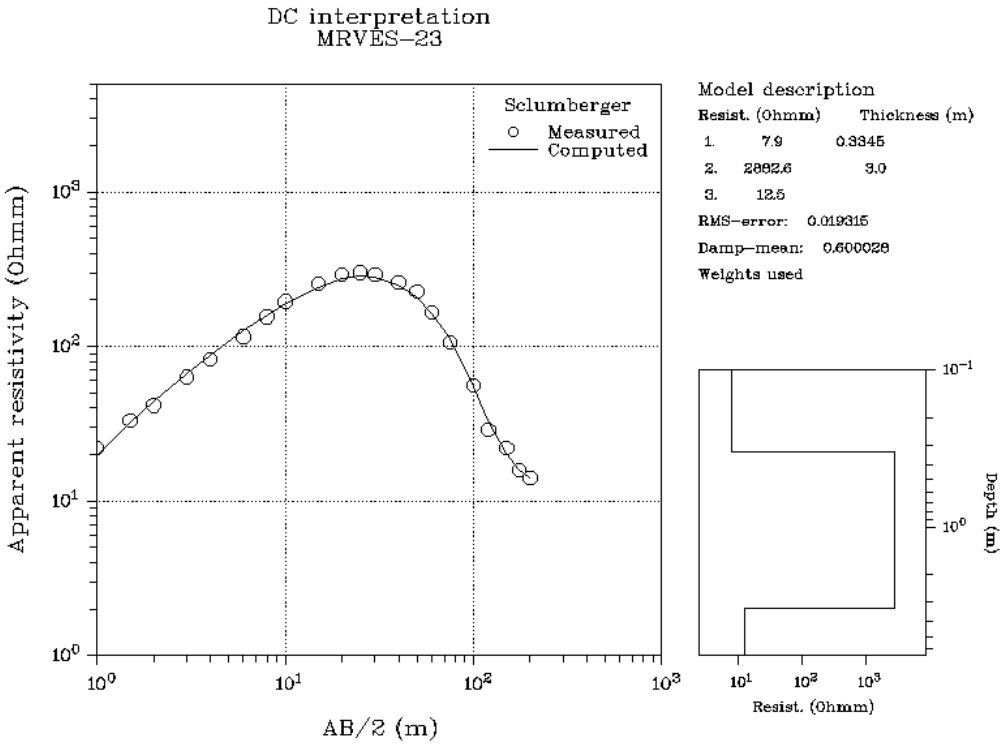
DC interpretation
MRVES-23
Sclumberger
Measured
Computed
Apparent resistivity (Ohmm)
AB/2 (m)
Model description
Resist. (Ohmm) Thickness (m)
1. 7.9 0.3345
2. 2882.6 3.0
3. 12.5
RMS-error: 0.019315
Damp-mean: 0.600028
Weights used
Resist. (Ohmm)
Depth (m)

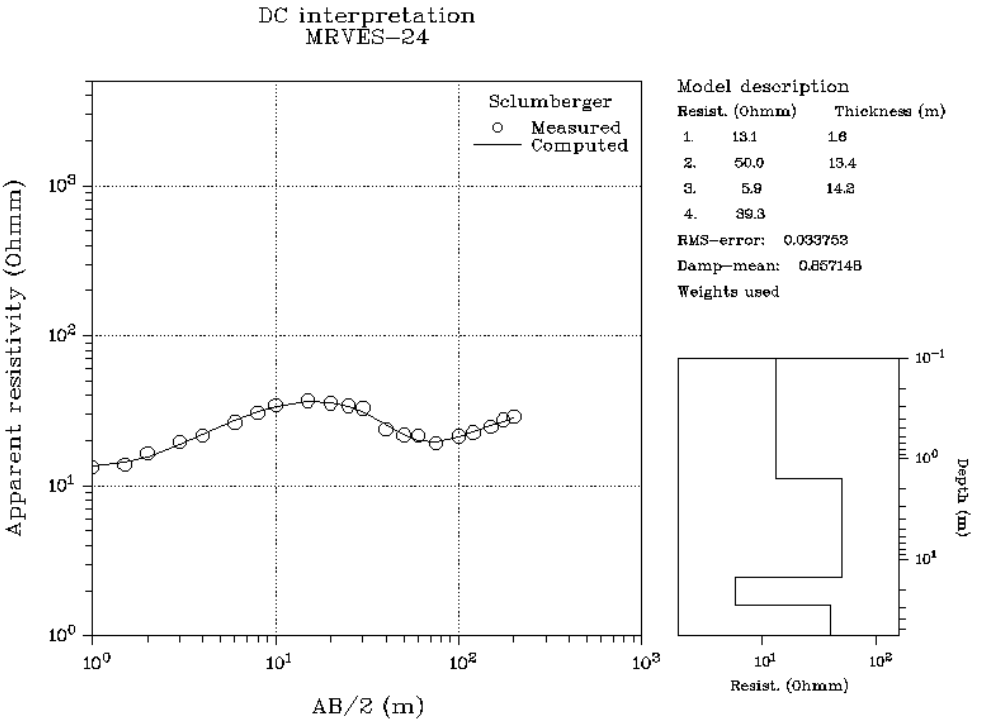
DC interpretation
MRVES-24
Sclumberger
Measured
Computed
Apparent resistivity (Ohmm)
AB/2 (m)
Model description
Resist. (Ohmm) Thickness (m)
1. 13.1 1.6
2. 50.0 13.4
3. 5.9 14.2
4. 39.3
RMS-error: 0.033753
Damp-mean: 0.857148
Weights used
Resist. (Ohmm)
Depth (m)

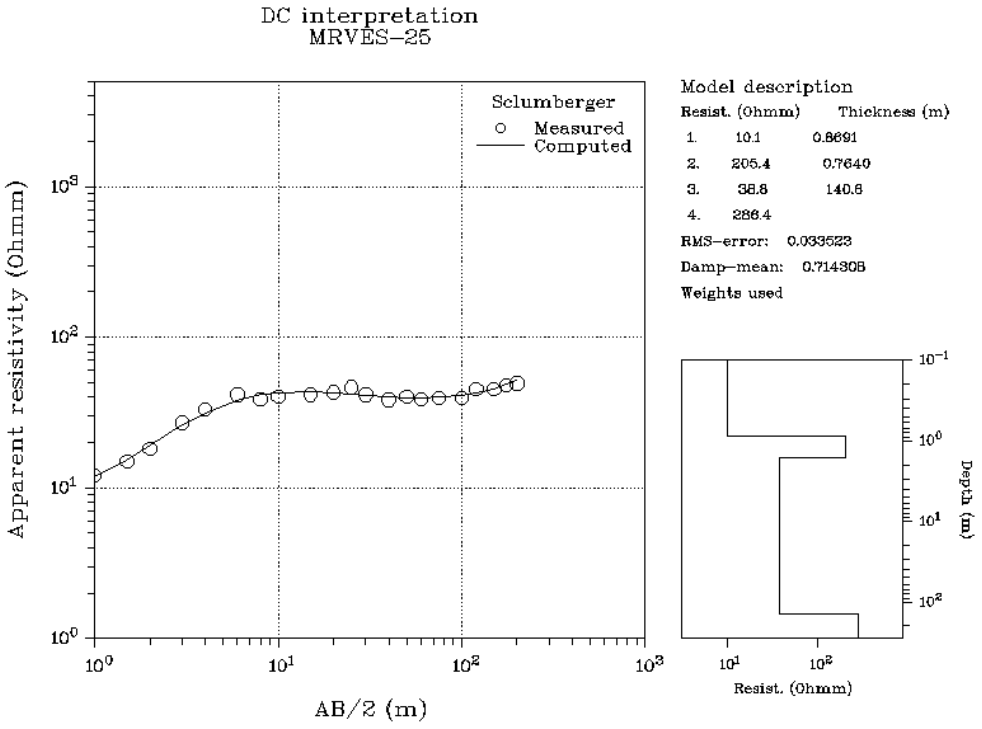
DC interpretation
MRVES-25
Sclumberger
Measured
Computed
Apparent resistivity (Ohmm)
AB/2 (m)
Model description
Resist. (Ohmm) Thickness (m)
1. 10.1 0.8691
2. 205.4 0.7640
3. 38.8 140.6
4. 286.4
RMS-error: 0.033523
Damp-mean: 0.714308
Weights used
Depth (m)
Resist. (Ohmm)

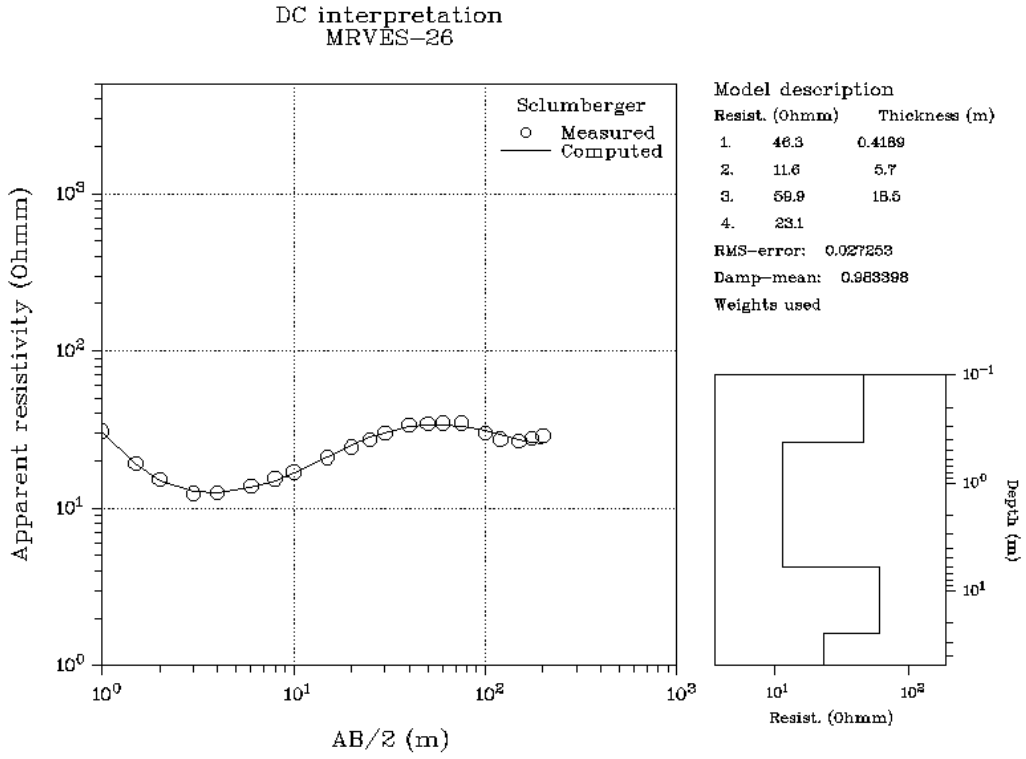
DC interpretation
MRVES-26
Sclumberger
Measured
Computed
Apparent resistivity (Ohmm)
AB/2 (m)
Model description
Resist. (Ohmm) Thickness (m)
1. 46.3 0.4189
2. 11.6 5.7
3. 59.9 15.5
4. 23.1
RMS-error: 0.027253
Damp-mean: 0.983398
Weights used
Depth (m)
Resist. (Ohmm)

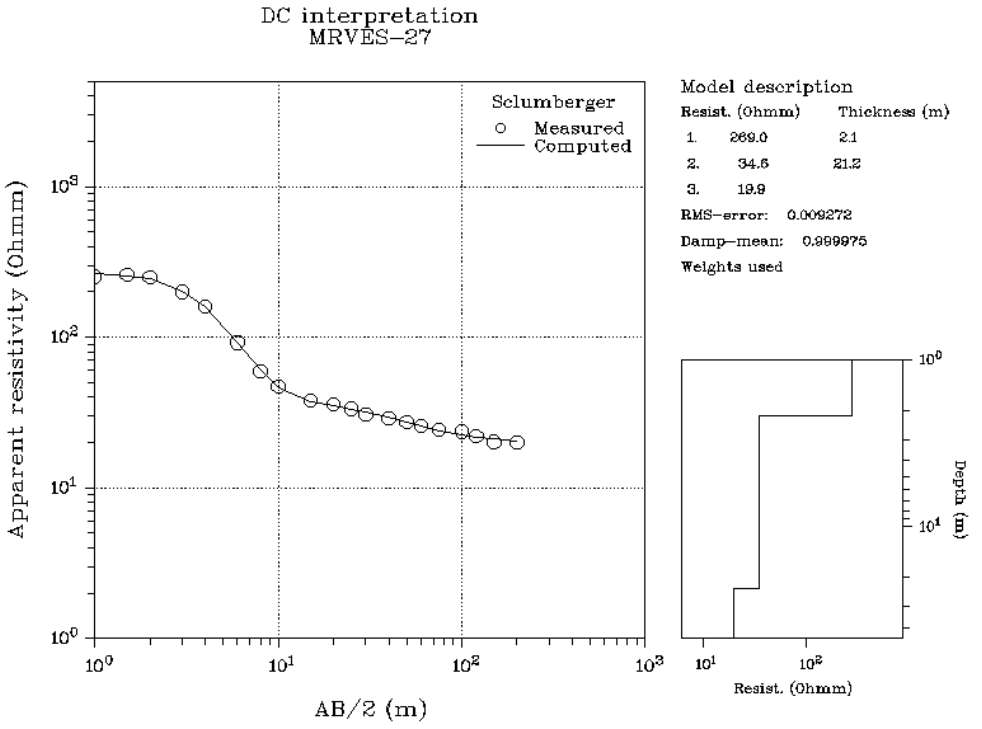
DC interpretation
MRVES-27
Schlumberger
Measured
Computed
Apparent resistivity (Ohmm)
AB/2 (m)
Model description
Resist. (Ohmm) Thickness (m)
1. 269.0 2.1
2. 34.6 21.2
3. 19.9
RMS-error: 0.009272
Damp-mean: 0.999975
Weights used
Depth (m)
Resist. (Ohmm)

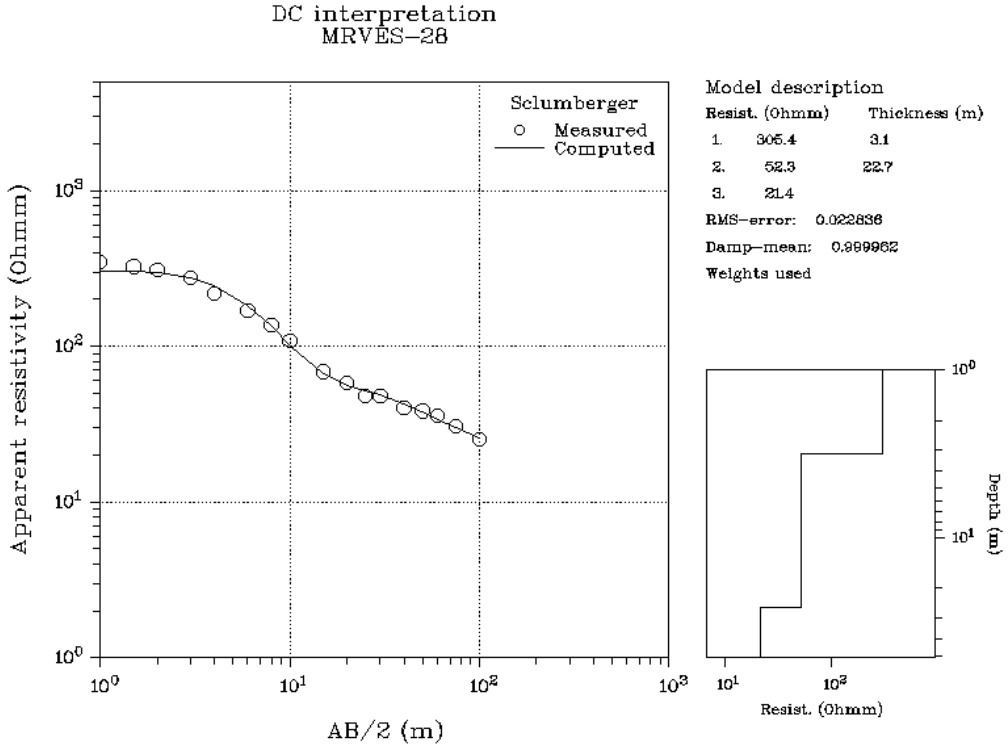
DC interpretation
MRVES-28
Schlumberger
Measured
Computed
Apparent resistivity (Ohmm)
AB/2 (m)
Model description
Resist. (Ohmm) Thickness (m)
1. 305.4 3.1
2. 52.3 22.7
3. 21.4
RMS-error: 0.022836
Damp-mean: 0.999962
Weights used
Depth (m)
Resist. (Ohmm)

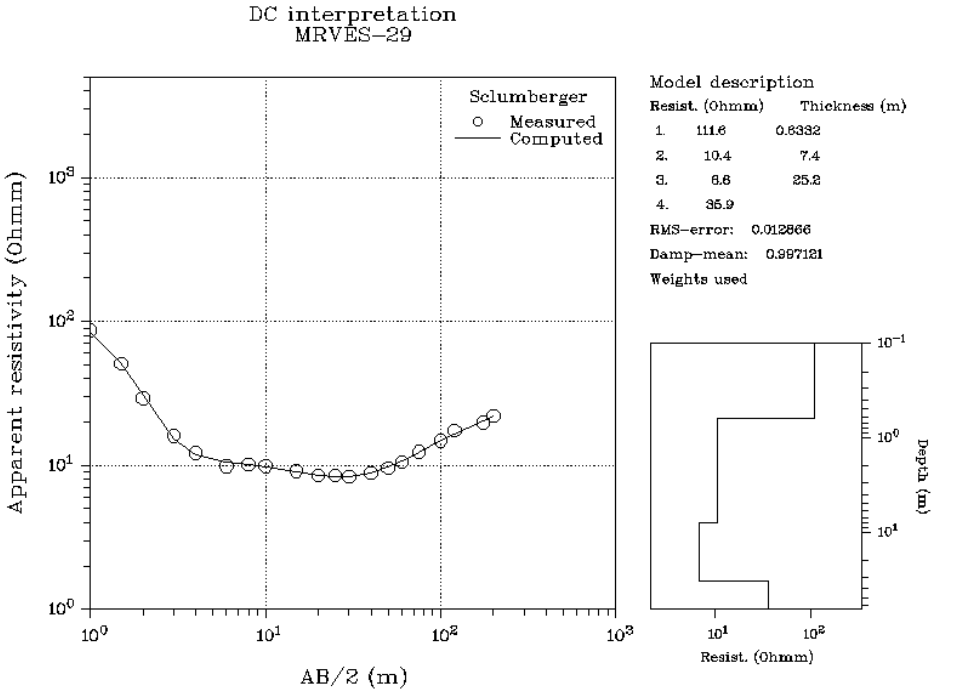
DC interpretation
MRVES-29
Schlumberger
Measured
Computed
Apparent resistivity (Ohmm)
AB/2 (m)
Model description
Resist. (Ohmm) Thickness (m)
1. 111.6 0.8332
2. 10.4 7.4
3. 6.6 25.2
4. 35.9
RMS-error: 0.012866
Damp-mean: 0.997121
Weights used
Depth (m)
Resist. (Ohmm)

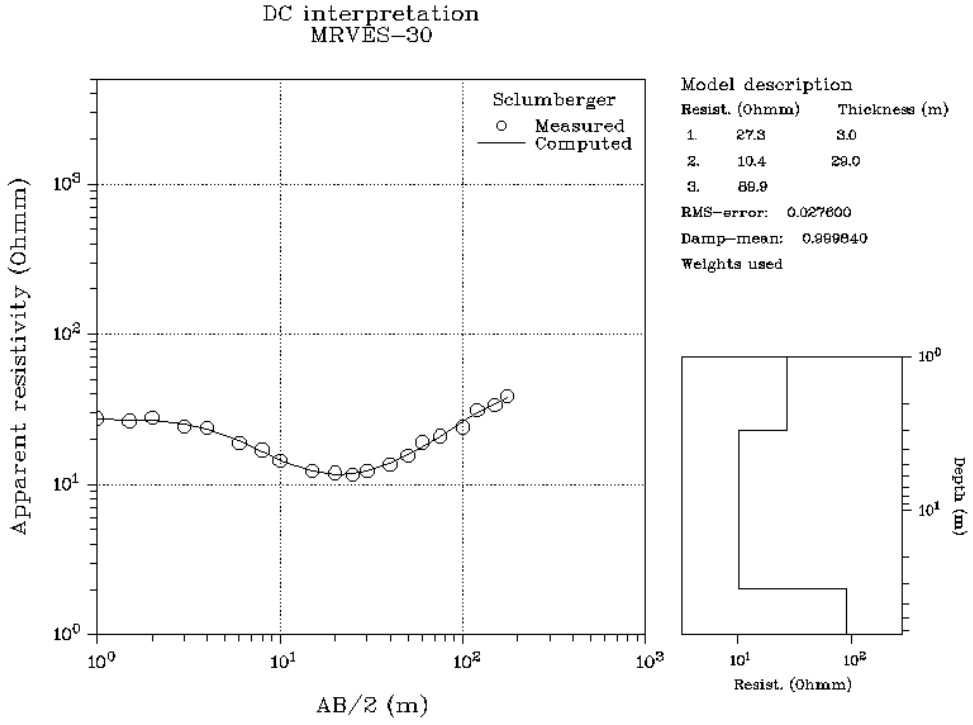
DC interpretation
MRVES-30
Schlumberger
Measured
Computed
Apparent resistivity (Ohmm)
AB/2 (m)
Model description
Resist. (Ohmm) Thickness (m)
1. 27.3 3.0
2. 10.4 29.0
3. 89.9
RMS-error: 0.027600
Damp-mean: 0.999640
Weights used
Depth (m)
Resist. (Ohmm)